



HAL
open science

From skeletal muscle stem cells to tissue atlases: new tools to investigate and circumvent dissociation-induced stress

Léo Machado

► **To cite this version:**

Léo Machado. From skeletal muscle stem cells to tissue atlases: new tools to investigate and circumvent dissociation-induced stress. Cellular Biology. Université Paris-Est, 2019. English. NNT : 2019PESC0080 . tel-03471274

HAL Id: tel-03471274

<https://theses.hal.science/tel-03471274>

Submitted on 8 Dec 2021

HAL is a multi-disciplinary open access archive for the deposit and dissemination of scientific research documents, whether they are published or not. The documents may come from teaching and research institutions in France or abroad, or from public or private research centers.

L'archive ouverte pluridisciplinaire **HAL**, est destinée au dépôt et à la diffusion de documents scientifiques de niveau recherche, publiés ou non, émanant des établissements d'enseignement et de recherche français ou étrangers, des laboratoires publics ou privés.

Université Paris XII Créteil

Ecole doctorale SVS ED402 : Sciences de la Vie et de la Santé

**From skeletal muscle stem cells to tissue atlases:
new tools to investigate and circumvent
dissociation-induced stress**

Léo Machado

PhD thesis supervised by Pr. Frédéric Relaix and Dr. Philippos Mourikis

Publically presented and defended November 8th, 2019

PhD Jury:

Pr. Frédéric Relaix – Directeur de thèse

Dr. Philippos Mourikis – Co-directeur de thèse

Dr. Bénédicte Chazaud – Rapporteur

Pr. Piotr Topilko – Rapporteur

Pr. Thomas Rando – Examineur

Pr. Carmen Birschmeier – Examineur

“Questions you cannot answer are usually far better for you than answers you cannot question.”

— Yuval Noah Harari

Acknowledgements

First and foremost, I wish to respectfully thank the jury members for their time and presence. Dr. Bénédicte Chauzaud, Pr. Piotr Topilko, thank you for evaluating the manuscript. Pr. Carmen Birschmeier and Pr. Thomas Rando, thank you for travelling from abroad to grant me the opportunity to defend my thesis. I hope the present work will be of great value for you and justify the time you kindly donated me.

I wish to thank my supervisor Pr. Frédéric Relaix for the tremendous trust you put in me – for reasons I still cannot explain – and for your invaluable scientific guidance and work ethic. With your help and guidance I always felt in the right track to maximize my professional and personal well-being. I still need to learn your astounding human skills and capacity to interact with people with such kindness and goodwill. I hope the future will yields more opportunity for me to keep learning from you if you can forgive me one day for all the sequencing experiment you generously have been forced to pay.

I wish to thank my – other – supervisor Dr. Philippos Mourikis. I wish for every student to have a mentor like you and for every human to have a friend like you. I was 19 when I first started working with you, thus you shaped my scientific mind and adult personality... I hope you did a good job! You taught me to do the hard thing when it is the right thing to do and I will stay true to it. You also unknowingly taught me not to do a thing when I don't feel like it and I will far more easily stay true to it. A significant portion of this thesis has been generated with the aim to make you proud and I will keep trying.

I wish to thank again Pr. Thomas Rando for the intense and fruitful learning experience that interning in your laboratory is. You gave me total freedom and the tools and technics I learned in this environment permitted most of the discoveries presented in the present thesis.

I wish to thank Pr. Romain Gherardi for kickstarting my scientific career and believing in me against all odds. I regret only not having had more opportunity to be exposed to your wisdom, insightful advises and cheerfulness.

I wish to thank all the people that participated in the present work, especially Matthieu Dos Santos, Jordi Camps and Jens Van Herck which initiated me to new technics and friendships.

I wish to thank all the members of the Relaix laboratory, among which Perla, Reem and Zeynab which provided me much needed Lebanon-induced calories and emotional support, Stamatia for being a true great friend and creator of entertaining dramaturgy, Joana for your experimental help and *chouchou*-ness, Matthew and Despoina for your cakes, manuscript proofing and sometimes laughing at my jokes.

I wish to thank David Hardy for b'hulking and our adventure in Caen. I wish to thank Meryem Baghdadi for your camaraderie under the Mourikis reign and for setting the bar so high. I wish to thank Daniel Benjamin for your transoceanic friendship and scientific companionship.

Je souhaite remercier ma sœur, mes parents, mes grands-parents et le reste de ma famille pour leur soutien inconditionnel au quotidien et plus particulièrement durant ces études étonnamment interminables. J'espère pouvoir un jour vous rendre une fraction de ce que vous m'avez apporté.

Abstract

Every cell in a multicellular organism is dynamically interacting with its microenvironment, which acts as a major regulator of its properties and gene-expression profile. However, most modern high-throughput molecular assays such as RNA-sequencing require the isolation of cells from their microenvironment. Such isolation procedures are often an order of magnitude longer than the time it takes for a cell to alter its molecular state – such as their gene-expression profile - in response to a stimulus.

We developed a new procedure relying on aldehyde-fixation to preserve the *in vivo* transcriptome of isolated cells. Using quiescent skeletal muscle stem cells (MuSCs), we demonstrated that during dissociation they undergo unexpectedly broad transcriptional changes that initiate a cell fate transition from quiescence to activation. Moreover, we uncovered that MuSCs cell-cycle entry is mediated through MAPK ERK1/2 signalling, and uncoupled from MuSCs differentiation, which requires Notch signalling silencing. We also confirmed with complementary time-course strategies that MuSCs initiate a conserved transcriptional response to diverse stimuli as the signatures of *ex vivo* dissociation and *in vivo* activation were very similar, down to the single-cell level.

To investigate the ubiquity of such dissociation-response we used single nuclei RNA-sequencing to generate transcriptional organ atlases from intact and dissociated skeletal muscle and liver and found - consistently with MuSCs - strong alterations across cell types and tissues. The majority of the modifications were cell type specific, yet we defined a core dissociation signature that revealed a high degree of distortion in published datasets, in a dissociation-time dependent manner. Overall, our study proposes that during isolation cells execute specialized genetic programs, which lead to cellular state alterations. Therefore, by using cells isolated with conventional methods the initiating events of cell transitions, like quiescence exit, are overlooked, and reference cell maps, like cell atlases, are fundamentally distorted.

Key words: RNA-sequencing ; Transcriptomics ; Single-cell ; Single-nuclei ; Quiescence ; Activation ; Stem cells ; Atlas ; Epigenetics ; Dissociation ; Stress

Résumé

Chaque cellule d'un organisme multicellulaire interagit dynamiquement avec son microenvironnement, ce dernier étant un régulateur majeur de ses fonctions et de son profil d'expression génique. Cependant, la plupart des analyses moléculaires à haut débit modernes comme le séquençage d'ARN nécessitent l'isolation des cellules de leur microenvironnement. Ces procédures d'isolation sont souvent un ordre de grandeur plus longues que le temps qu'il faut à une cellule pour altérer son état moléculaire - tel que son profil d'expression génique - en réponse à un stimulus.

Nous avons développé une nouvelle procédure utilisant la fixation par aldéhyde pour préserver le transcriptome *in vivo* de cellules isolées. En utilisant les cellules souches du muscle strié squelettique (MuSCs), nous avons démontré que lors de la dissociation, ces dernières subissent des modifications transcriptionnelles d'une ampleur inattendue qui initient une transition de leur état cellulaire de la quiescence vers l'activation. De plus, nous avons découvert que l'entrée du cycle cellulaire des MuSCs est médiée par la signalisation MAPK ERK1/2 et découplée de la différenciation des MuSCs, qui nécessite l'extinction de la voie de signalisation Notch. Nous avons également confirmé par des stratégies complémentaires de cinétique temporelle que les MuSCs initient une réponse transcriptionnelle inchangée face à différents stimuli. En effet, les signatures de dissociation *ex vivo* et d'activation *in vivo* observées sont très similaires, même en séquençage de cellule unique.

Pour étudier l'omniprésence d'une telle réponse à la dissociation, nous avons utilisé le séquençage d'ARN de noyau unique pour générer des atlas cellulaires à partir de muscle strié squelettique et de foie - intacts et dissociés - et avons trouvé, conformément aux MuSCs, de fortes et ubiquitaires modifications transcriptionnelles, au niveau cellulaire et tissulaire. La plupart des modifications étaient spécifiques pour chaque type cellulaire, mais nous avons cependant pu définir une signature de dissociation commune qui révèle un degré élevé de distorsion dans les jeux de données publiés dans la littérature, d'une manière corrélée au temps de dissociation de ladite cellule ou dudit tissu. Dans l'ensemble, notre étude propose ainsi que, pendant l'isolation, les cellules exécutent des programmes génétiques spécialisés qui entraînent des modifications de leur état cellulaire. Par conséquent, en utilisant des cellules isolées par des méthodes conventionnelles, les événements initiateurs des transitions d'état cellulaires, tels que la sortie de quiescence, sont ignorés et les jeux de données transcriptomiques de référence, comme les atlas cellulaires, sont fondamentalement déformés.

Mots clés: Séquençage d'ARN ; Transcriptomique ; Cellule unique ; Noyau unique ; Quiescence ; Activation ; Cellules souches ; Atlas ; Epigénétique ; Dissociation ; Stress

Table of Contents

ACKNOWLEDGEMENTS	4
ABSTRACT	5
RESUME	6
TABLE OF CONTENTS	7
ABBREVIATIONS	9
STATE OF THE ART	10
CHAPTER 1: THE TRANSCRIPTOME AS A DETERMINANT OF CELLULAR IDENTITY	10
PAST AND CURRENT PARADIGMS	10
THE EMERGENCE OF RNA-SEQUENCING	10
THE SINGLE-CELL ERA	12
MAPPING THE CELLULAR LANDSCAPE	14
EPIGENETIC COMPONENTS OF CELLULAR IDENTITY	15
CHAPTER 2: PROTOCOLS AND KINETICS OF CELLULAR ISOLATION	17
THE CELLULAR MICRO-ENVIRONMENT	17
CELLULAR DISSOCIATION	18
EARLY RESPONSE TO STIMULATION	19
EARLY RESPONSE TO DISSOCIATION	21
METHODS TO PRESERVE CELLULAR TRANSCRIPTOME	22
CHAPTER 3: THE SKELETAL MUSCLE STEM CELLS IN HOMEOSTASIS AND REGENERATION	25
ANATOMY OF THE SKELETAL MUSCLE TISSUE	25
TRANSCRIPTOMIC CHARACTERIZATION OF THE SKELETAL MUSCLE POPULATIONS	26
THE SKELETAL MUSCLE STEM CELLS	27
EXPERIMENTAL TOOLS	29
INTRINSIC FACTORS FOR QUIESCENCE MAINTENANCE	29
EXTRINSIC FACTORS FOR QUIESCENCE MAINTENANCE	30
ACTIVATION OF MuSCs	32
THE MYOGENIC PROGRAM	33
MUSCLE INJURY: DIFFERENT MODELS AND CELL TYPES THAT DRIVE TISSUE REGENERATION	34
HETEROGENEITY	39
MOLECULAR PROFILING OF SKELETAL MUSCLE STEM CELLS	41

RESULTS	43
PART I: <i>IN SITU</i> FIXATION REDEFINES QUIESCENCE AND EARLY ACTIVATION OF SKELETAL MUSCLE STEM CELLS	44
PART II: DISSOCIATION DISTORTS THE PROFILE OF ISOLATED CELLS AND DRIVES QUIESCENT MUSCLE STEM CELLS TO AN ACTIVATED STATE	70
DISCUSSION	128
I – SUMMARY	128
II – THE IMPACT OF DISSOCIATION	129
III – LITERATURE CONTAMINATION	132
IV - METHODS TO PRESERVE THE TRANSCRIPTOME	133
V – CONSIDERATIONS FOR MUSCs QUIESCENCE	136
VI – CONCLUDING REMARKS	138
REFERENCES	139
APPENDIX	155
PART I: RECIPROCAL SIGNALLING BY NOTCH-COLLAGEN V-CALCR RETAINS MUSCLE STEM CELLS IN THEIR NICHE	156
PART II: WAKING UP MUSCLE STEM CELLS: PI3K SIGNALLING IS RINGING	174

Abbreviations

3'-UTR: 3'-Untranslated Region

ATAC-seq: Assay for Transposase-Accessible Chromatin using sequencing

bHLH: basic Helix-Loop-Helix

ChIP-seq: Chromatin Immunoprecipitation and sequencing

DEGs: Differentially-Expressed Genes

EDU: 5-ethynyl-2'-deoxyuridine

EU: 5-ethynyl uridine

iSiFi: *in situ* fixation

DNase-seq: DNase-sequencing

ECM: Extra-Cellular Matrix

FACS: Fluorescent Associated Cell Sorting

FFPE: Formalin-Fixed Paraffin-Embedded

IEGs: Immediate Early Genes

miRNA: Micro-RNA

MuSCs: Muscle Stem Cells

MRFs: Myogenic Regulatory Factors

PFA: Paraformaldehyde

RNA-seq: RNA-sequencing

RRBS: Reduced Representation Bisulfite Sequencing

RT-qPCR: Real-Time quantitative Polymerase Chain Reaction

RTK: Receptor Tyrosine Kinase

UMI: Unique Molecular Identifier

Chapter 1: The transcriptome as a determinant of cellular identity

Past and current paradigms

Since the first description of a cell (Hooke, 1665) and the formulation of its theory (Schwann, 1839), many cellular attributes have been employed to define cell types in multi-cellular organisms such as shape, anatomical location or function. With the emergence of biology's central dogma (Crick, 1958, 1970), the macro-molecular content of a cell (e.g. its RNA or protein composition) became preponderantly used for cellular ontology segregation. The current paradigm to define cellular identity is to consider the intricacy of several comprehensive macro-molecular layers such as its proteome, its transcriptome or its epigenome. This holistic vision of cellular biology - consistent with the concept of systems biology - define the "multi-omic" era (reviewed in Ge *et al*, 2003). However, it remains illusory for a scientist today to totally embrace the multi-omic world, as none of the methods developed to study these biological layers captures the entire complexity of them nor can be performed in combination at single cell level and/or with an acceptable cost and accessibility. Such methods are reviewed in Macaulay *et al*, 2017.

If one of these layers were intuitively to be chosen as a method of choice to describe a cell's ontology, the proteomic layer would appear the most informative as proteins are the molecular effectors of the majority of cellular behaviors. Surprisingly, however, the transcriptomic layer is the one that has received most attention from modern cellular biologist, for reasons that will be developed in this chapter.

The emergence of RNA-sequencing

Transcriptomic methods became more quantitative with time and increasingly covered larger part of the transcriptome from northern blot to RT-qPCR to microarrays. Born at the beginning of this millennium in the wake of next generation sequencing (Margulies *et al*, 2005; Shendure *et al*, 2005), RNA-sequencing quickly surpassed the other method of choice for transcriptomic analysis, which was at the time the microarrays (Figure 1). To paraphrase a recent review (Weber, 2015), RNA-sequencing can allow larger scale experiments at lower cost due to multiplexing. RNA-sequencing is also independent of transcriptome knowledge, and provides direct measurement of RNA abundance with a

dynamic range at least 2 orders of magnitudes greater than microarrays. Consequently, it also allows the detection of low-abundance transcripts, splice-isoforms, and sequence variants.

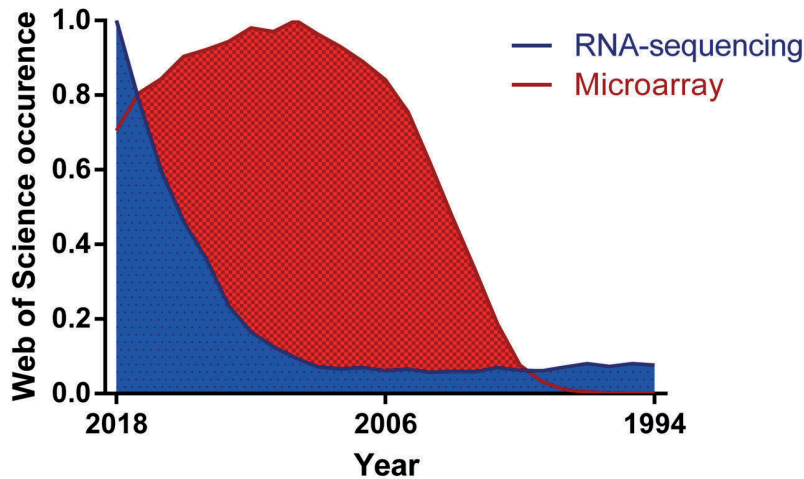


Figure 1: Analysis of the occurrence of the terms “RNA-sequencing” and “Microarray” in the Web of Science corpus from 1994 to 2018, normalized to the maximal occurrence for each term.

These factors, associated to the democratization of Illumina-based next generation sequencing and library preparation methods, fueled many years of biological research. Despite the variable RNA to protein correlations (Edfors *et al*, 2016), the transcriptome of a cell is a very convenient proxy of its proteome and has been studied extensively – notably via RNA-sequencing - to infer active biochemical pathways and cellular functions. Such inferences permitted researchers to match physiological and pathological states with the activity of specific genes and pathways. Therefore, RNA-sequencing correlated gene expression to cellular function and generated many testable hypothesis with often a very good predictive value. Moreover, differences in transcription is one way for a multi-cellular organism to exhibit cellular diversity from an identical genetic material. Indeed, the study of differential gene expression within an organism or a tissue permitted the segregation of cells in extremely well defined subgroups by virtue of the 20-40.000 features (e.g transcripts) that generally constitute a RNA-sequencing dataset.

It is almost an epistemological question to wonder how many cell types hosts a multi-cellular organism. All cells are unique by virtue of their spatial position and developmental history and none of the discussed multi-omic layers – disregarding the combination of them – could be identical between two cells. From these premises, the only possible conclusion is that the number of different cell types in a multi-cellular organism is the total number of cells that compose it. The human body is estimated to

contain 37.2 trillion cells (Bianconi *et al*, 2013). Therefore not much more can be learned from such a conclusion and, as stated before, scientists usually define cell types based on an empiric combination of active biochemical pathways, cellular function, anatomical location and developmental history that creates cohesive and consistent subgroups. In practical terms, cellular identity in the biomedical sciences has a very context-dependent definition and the boundaries between cell types are flexibly refined whenever they contradict a sufficient amount of new research. One of the prevalent issues in cellular biology is that until recently, most of these studies were performed on cellular populations composed of mixtures of cells of unknown heterogeneity. This conundrum was recently been solved with the advent of single-cell RNA-sequencing.

The single-cell era

Cellular populations in traditional bulk RNA-sequencing experiments were often defined via the combination of a handful of surface protein markers that would allow their separation from a mixture of different cellular populations. Subsequently the cells were considered homogeneous and the expression profiles obtained from the analysis was considered as the true transcriptome of the population of interest. It became clearer with time, however, that heterogeneity within most cell populations was not negligible and that the expression profiles obtained from such experiments represented more of an average of the true transcriptomes of distinct cell subpopulations. One approach to investigate this heterogeneity would be to refine the populations by the adjunction of more surface proteins or separation markers. However, a more powerful method to answer this question would be to study heterogeneity from the irreducible unit of cell biology –a single-cell –and to infer populations from the bottom-up.

The study of single-cell gene activity dates back to almost thirty years ago with the amplification of a handful of transcripts from single-cells (Brady *et al*, 1990; Finnell *et al*, 1992), and was latter associated with microarrays to study single-cell gene expression in a more complex format (Klein *et al*, 2002; Tietjen *et al*, 2003; Kurimoto *et al*, 2006). However, the efficiency and sensitivity of these methods was insufficient to allow a wide-spread adoption. Single-cell transcriptome analysis really emerged when combined with next generation-sequencing, for the first time a decade ago (Tang *et al*, 2009). Akin to Moore's law for the number of transistors on a chip, the number of single-cell sequenced per individual experiment appears to follow an exponential growth (**Figure 2**). This growth is partly due to the exponential drop in next generation sequencing costs and partly due to the incrementally improved single-cell library preparation methods that appear almost on a monthly basis.

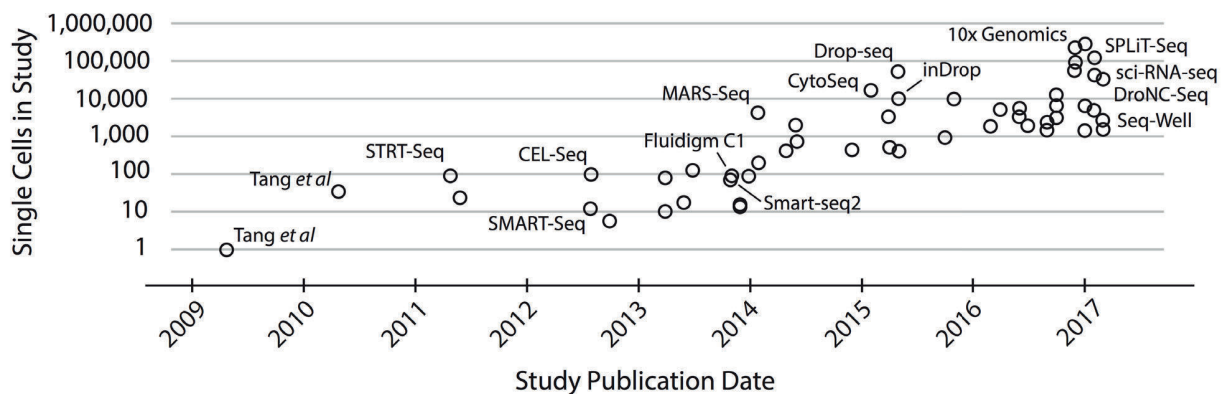


Figure 2: Chronological analysis of milestone publications on single-cell RNA-sequencing – adapted from Svensson *et al*, 2018.

Lastly, two methods became increasingly considered as leader in the field due to their accessibility and reproducibility in many different experimental settings. The first one, SMARTseq2 (Picelli *et al*, 2014) allows the sequencing of relatively low number of cells with a great sensitivity. The second one, GemCode/10X Genomics (Zheng *et al*, 2017) permits the sequencing of large number of cells at the expense of a relatively low sensitivity (these two methods are compared in Baran-gale *et al*, 2018). The main difference between these methods is due to the use of barcode – also called UMI, for Unique Molecular Identifier – which is a feature of GemCode/10X Genomics and permits the multiplexing of many cells within the same sample. Another difference is the coverage of the transcripts which is 3' enriched for GemCode/10X Genomics while it is full length for SMARTseq2, which allows a more precise coverage of transcripts dynamics, such as the detection of splicing events for the latter. Many more methods are currently used but are often a variation of the two mentioned above. Most experimental contexts are covered by these methods, from the deep characterization of splicing events in a rare cellular populations which is most suited to SMART-Seq2 and similar methods, unlike the large scale analysis of hundreds of thousands of cells from an entire organism which require UMI-based methods such as Gemcode/10X Genomics.

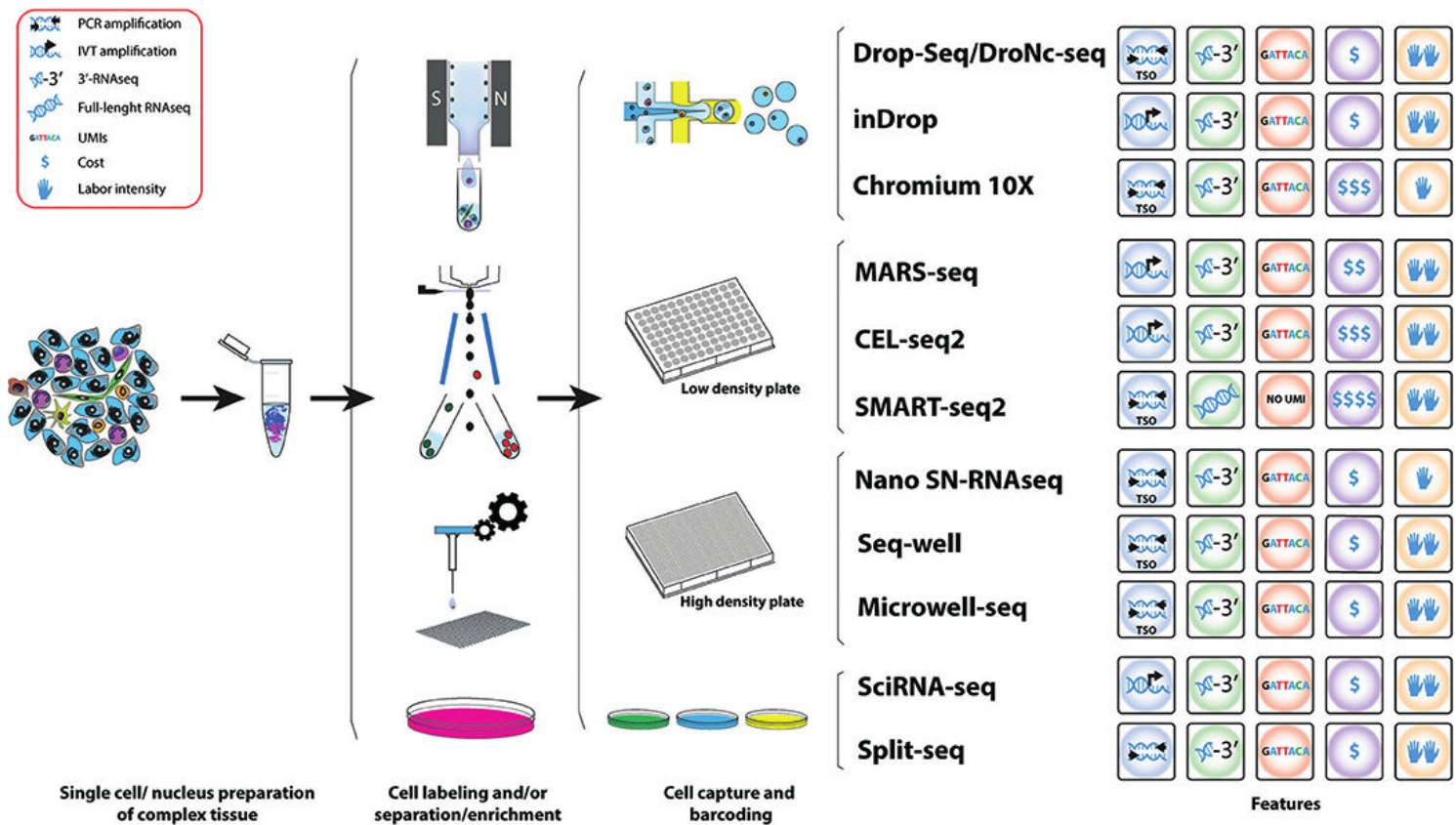


Figure 3: Comparison between varying single-cell RNA-seq protocols (Valdes-Mora *et al*, 2018).

Mapping the cellular landscape

Applying the high-throughput methods described above permit researchers to discover new cellular (sub)-populations and biological phenomena of interest from high-throughput screens of entire tissues, organs or organisms. This process allowing the emergence of biological insights from the data can be described under the term *reverse cellular biology* – referring to the concept of reverse genetics – and the production of such cellular atlases has been the strategy of choice for many recent biological endeavors. This trend culminated in the publication of many high-profile atlases from the planarian *Schmidtea mediterranea* (Fincher *et al*, 2018) to the *Drosophila* optic lobe (Konstantinides *et al*, 2018) to an entire developing (Cao *et al*, 2019) or adult mouse (Han *et al*, 2018; Schaum *et al*, 2018). This list is far from exhaustive and many high-profile projects are expected in the coming years such as the Human Cell Atlas (Regev *et al*, 2017) which aims to define all human cell types.

Epigenetic components of cellular identity

Despite the supremacy of transcriptomic analyses for cellular states characterizations, the study of epigenetics states also became an important area of research. Epigenetic – as initially defined (Waddington, 1942) – designated phenotypic changes not mediated through genetic alterations. It is contemporarily endorsed as the propagation – from cells to organisms - of gene expression through chromatin organization without genetic changes (Allis & Jenuwein, 2016). The epigenetic modifications can be impinged on the nucleotides themselves most notably through the addition of a methyl group on cytosines to form 5-methylcytosine (5mC) which leads to genetic repression (Razin & Riggs, 1980). Additionally, the epigenetic modifications can be imposed on the structural unit that organize DNA topological organization: the nucleosomes. Indeed, some of the most studied epigenetic modifications are histone modifications: covalent adjunctions of methyl or acetyl groups – among others - on the histones, the core proteins of the nucleosome, which induce or label functional elements of the chromatin. Among such, Histone3 lysine (K) 4 trimethylation (H3K4me3) (Barski *et al*, 2007), H3K27 acetylation (Rada-Iglesias *et al*, 2010) and H3K27me3 (Cao *et al*, 2002) are critical and mark active promoters, active regulatory regions and facultative repressed chromatin region, respectively. More generally, chromatin can be described by its degree of accessibility by biological macromolecules, with technics often measuring the cutting frequency of DNA cleaving agents such as DNase-seq (Boyle *et al*, 2008) or ATAC-seq (Buenrostro *et al*, 2013). Active loci such as regulatory regions, promoters or sites of active transcription are generally more accessible than repressed loci that form constitutive or facultative chromatin. These loci tend to cluster with similar regions and form segregated chromatin compartments along different levels of topological organizations often called *euchromatin* for more accessible regions and *heterochromatin* for inaccessible ones. This segregation is mediated through contact and repulsion of chromatin loci and recently the study of genome-wide chromatin topology - notably through the invention of chromosome conformation captures technologies such as Hi-C (Lieberman-Aiden *et al*, 2009) - helped to systematically map such interactions. Altogether, these regulatory layers intricately govern the recruitment of biological macromolecules such as transcription-factors, co-activators and the replication machinery to the chromatin, ultimately determining gene expression, cellular states and enforcing cellular identities.

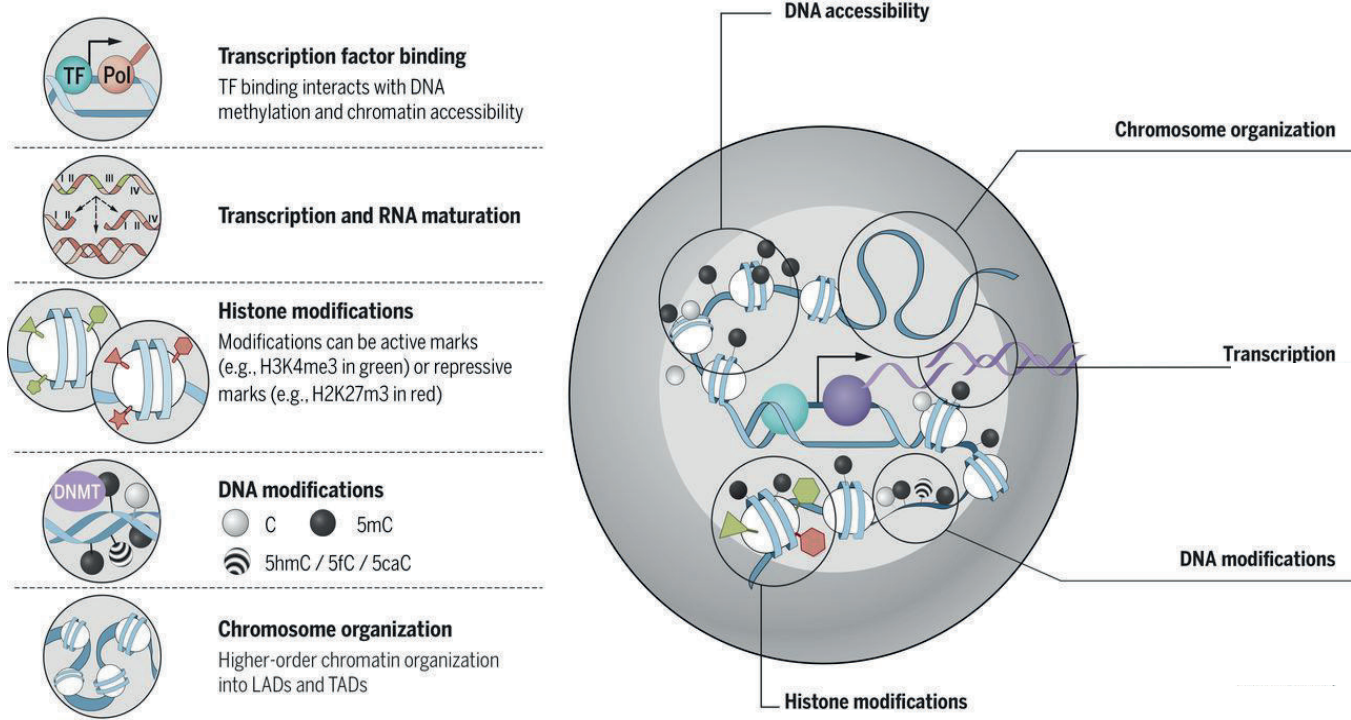


Figure 4: Common epigenetic layers. C: Cytosine; 5mC: 5-Methylcytosine; 5hmC: 5-Hydroxymethylcytosine, 5fC: 5-Formylcytosine; 5caC: 5-Carboxycytosine. LADs: Lamina-associated domains; TADs: Topologically associating domain. Adapted from Kelsey *et al*, 2017.

Chapter 2: Protocols and kinetics of cellular isolation

The cellular micro-environment

The micro-environment of a eukaryotic cell has a critical influence on its function and identity. It is essential for a cell's capacity to survive, communicate, and move and is at the basis of tissue organization. It has a cellular component: the neighboring cells, a molecular one: the extra-cellular matrix (ECM) with secreted factors, and a mechanical one: physical forces, like blood flow. Cell-cell interactions are mostly mediated through cadherins while cell-matrix adhesions occur principally via integrins. Cell-cell interactions are important to maintain tissue cohesiveness and resistance to mechanical forces but also are primordial to tissues function such as the barrier function of epithelium or endothelium through adherens junctions, the electrical coupling of cardiomyocytes through gap-junctions or the electro-chemical coupling of neurons through synaptic junctions. The ECM is mainly composed of collagens, glycosaminoglycans and proteoglycans as well as diverse signaling molecules. The ECM functions are multiple, it provides a scaffold for cells anchorage or movement, biophysical properties of tissues and organs such as stiffness, elasticity or tensile strength as well as an organization center for growth-factors and signaling molecules distribution (Frantz *et al*, 2010). Both cell-cell and cell-matrix interactions are coupled with the cytoskeleton and intra-cellular signaling pathways which can transduce micro-environment properties to influence virtually any cellular internal process. The ECM of a cell is a highly dynamic entity, constantly synthesized, degraded and remodeled, notably with the help of proteolytic enzymes. Such enzymes are the method of choice to isolate viable cells from entire tissues.

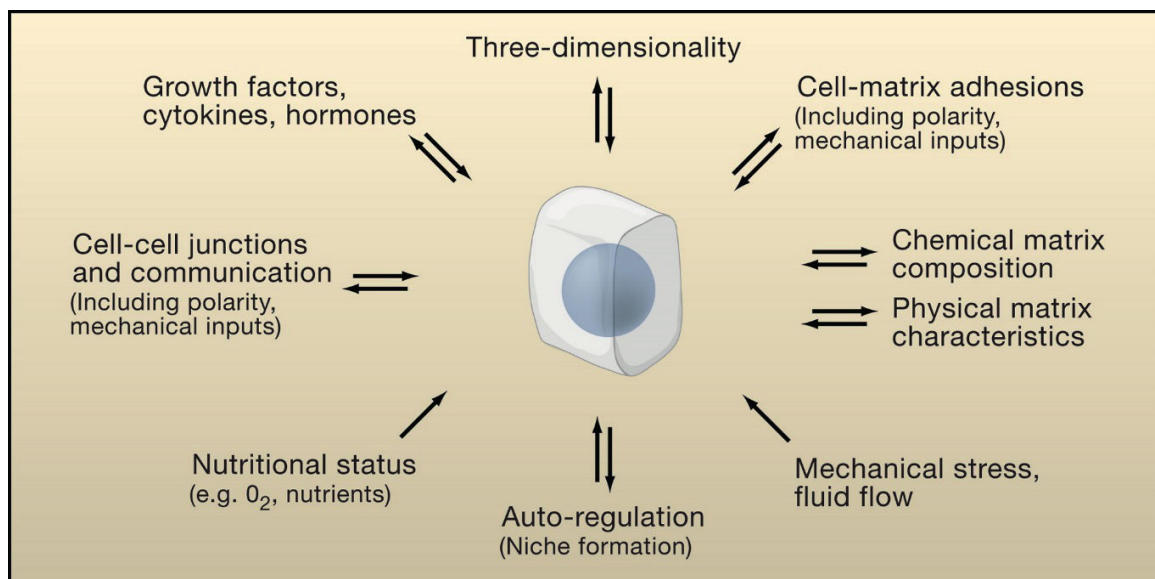


Figure 5: Overview of the different environmental factors governing the molecular state of a cell (Yamada & Cukierman, 2007).

Cellular dissociation

Except from circulating cells, eukaryotic cells are rarely dissociated from their micro-environment in physiological conditions. To study a cell of interest however, isolating it from its surroundings is often necessary, especially to apply the technics described in **Chapter 1**. Most protocols used to isolate cells from tissues require a combination of mechanical and enzymatic dissociation steps. Mechanical dissociation steps include tissue mincing, homogenization, trituration, or shaking. Enzymatic dissociation steps rely on the activity of proteolytic enzymes such as collagenase, dispase or trypsin to digest the micro-environment ECM components of a cell, in order to liberate it. Trypsin is a pancreatic serine protease discovered by Wilhelm Kühne in the 19th century (Kühne, 1877) and is still the method of choice to dissociate cultured cells or for proteomics studies (Vandermarliere *et al*, 2013). The discovery of metalloproteases such as dispase (Fukumoto, 1951) or collagenase (Mandl *et al*, 1953) which digest elements of the extra-cellular matrix, permitted the isolation of intact cells from tissues. These enzymes are frequently most active at 37 °C and many dissociation protocols take hours to be completed from tissue dissection to cellular isolation for downstream analysis, in addition to the time required for the cells to be sorted through a flow cytometer. An excerpt of such protocols can be found in **Table 1**.

Tissue	Enzyme	Time 37°C	Mechanical
Heart	Trypsin-EDTA ; Collagenase A/B	30	Minced ; triturated
Aorta	Collagenase II	10	Minced
Lung	Liberase (Collagenase I, II and thermolysin)	30	Minced ; homogenized
Trachea	Collagenase I ; Dispase	66	Cut
Tongue	Dispase ; Collagenase IV ; TrypLE ; DNase I	100	Perfused ; peeled
Liver	Liver Perfusion Medium ; Collagenase IV	16	Perfused
Pancreas	Collagenase XI ; Accumax ; Dispase	10	
Large Intestine	EDTA	22	Cut
Kidney	Liberase	32.5	Minced
Bladder	Collagenase IV ; DNaseI ; TrypLE	90	Minced
Limb Muscles	Collagenase II ; Dispase	90	Minced ; Needle homogenized
Diaphragm	Collagenase II ; Dispase	55	Minced ; Needle homogenized
Skin	Trypsin	35	Scrapped
Mammary Gland	Collagenase ; Hyaluronidase ; Dispase ; DNase	120	Minced
Fat	Collagenase II ; Dispase II	30	Agitated
Bone Marrow	DNase I	2	Crushed
Thymus	Collagenase II	40	Crushed ; Agitated
Spleen	No dissociation?	2.5	Minced
Brain	DNase I	8	Minced ; Dounced

Table 1: Dissociation methods from a state-of-the-art organismal atlas (Schaum *et al*, 2018). A ratio of 0.5 and 0.2 was applied to discount dissociation time at room temperature and on ice, respectively.

Early response to stimulation

Cells have evolved complex mechanisms to maintain homeostasis in response to external or internal disturbances (reviewed in Alway *et al*, 2014). Cellular stress was first described when chromosomal puffs – a hallmark of active transcription – were readily observed in response to heat in *Drosophila* salivary glands (Ritossa, 1962). Besides heat (Gomez-Pastor *et al*, 2017), many cellular stressors have been identified since then, such as oxidative stress (Liguori *et al*, 2018), unfolded proteins (Walter & Ron, 2011) or hypoxia (Majmundar *et al*, 2010). For example, upon heat-shock on mammalian cells, several hundred genes are rapidly induced and several thousand swiftly repressed through RNA polymerase II displacement (Mahat *et al*, 2016). Part of this heat-shock response is dependent on the heat shock factors HSF1 and HSF2 (Sarge *et al*, 1991) which induce the expression of the heat shock protein families such as HSP60, HSP70 or HSP90. Interestingly, upon heat-shock, part of the transcriptional response is independent of HSF1 and HSF2 and mediated through the serum response

factor SRF for the transient induction of cytoskeletal genes (Mahat *et al*, 2016). SRF is a transcription factor responsible of the transient induction of *immediate early genes* (IEGs) or primary response genes, mainly upon serum – e.g growth-factors – exposure. IEGs are a family of genes regulated by extra-cellular signals whose induction does not require protein synthesis. Some of the IEGs have been identified as mitogenic factors in the 1980s from seminal cloning experiments (Kelly *et al*, 1983; Greenberg & Ziff, 1984; Cochran *et al*, 1984) and the field rapidly expanded this family and uncovered its ubiquity (reviewed in Herschman, 1991). Examples of IEGs include the transcription factors *Jun*, *Fos*, *Junb*, *Fosb*, *Egr1*, *Ier5* among many others (Lee *et al*, 2010). These genes are induced by SRF through the MAPK cascade (Janknecht *et al*, 1993; Buchwalter *et al*, 2004), notably through ERK1/2 phosphorylation. These inductions are rapid, precise and transient in about 20-60 minutes upon stimulation and form self-inhibitory mechanisms to restrain their activity (Amit *et al*, 2007). Interestingly, these IEGs have been found induced by seizures or sensory stimuli in the brain (Spangrude *et al*, 1988; Saffen *et al*, 1988; Kaufmann *et al*, 1995; Link *et al*, 1995) and by behavioral tasks in different regions such as the hippocampus or the amygdala (Rosen *et al*, 1998; Guzowski *et al*, 1999; Vann *et al*, 2000; Hall *et al*, 2001; Ramírez-Amaya *et al*, 2005). More than markers of neuronal activity, these genes have been linked to synaptic plasticity and the generation of memories (Minatohara *et al*, 2016).

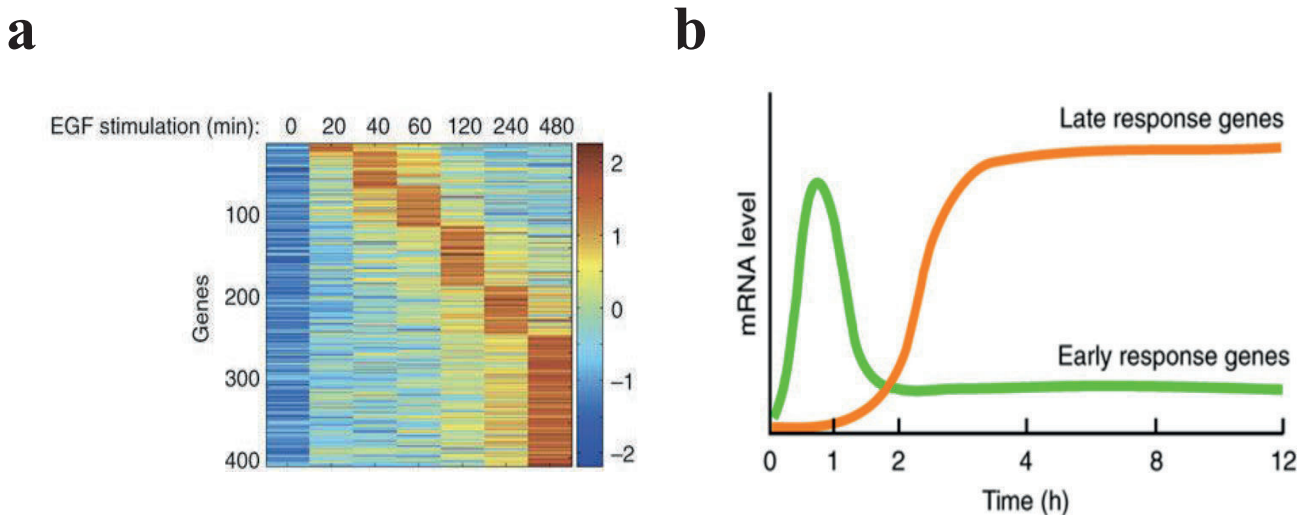


Figure 6: Kinetics of transcriptional inductions after stimuli (a) EGF treatment (Amit *et al*, 2007) on HeLa cells, heatmap displaying EGF-induced genes on microarrays (b) Graphical representation of the effect of serum treatment (Shah & Tyagi, 2013)

Early response to dissociation

It is striking that the duration of the dissociation methods presented In **Chapter 2**. are frequently an order of magnitude longer than the time it takes for isolated cells to induce the expression of early-response genes and stress-response genes. Considering the importance of the micro-environment for a cell as stated in **Chapter 2.X**, it appears explicit that removing a cell from its surroundings will significantly alter its molecular properties, notably its transcriptome. One commentary first reported reproducibility difficulties in FACS profiles and organoids formation efficiency from human breast cellular preparations, using the same reagents. After carefully comparing the protocols used, the authors found that length and agitation frequency of the collagenase digestion step explained the experimental heterogeneity (Hines *et al*, 2014). Later, it was reported that dissociated neurons exhibited large amounts of IEGs expression such as *Jun*, *Egr1* and *Arc*, masking the expected effect of seizure-inducing agents or behavioral tasks on these genes (Lacar *et al*, 2016). Such induction of IEGs in dissociated cells was soon detected in the kidney (Adam *et al*, 2017; Wu *et al*, 2019), the skeletal muscle (van den Brink *et al*, 2017; Machado *et al*, 2017; van Velthoven *et al*, 2017) and confirmed in the brain (Wu *et al*, 2017; Bakken *et al*, 2018). More than inducing IEGs, it has been shown on multiple tissues and cell-types that dissociation significantly distorted the molecular profile of freshly-isolated cells, altering the expression of thousands of genes with cell-specific and ubiquitous modifications, in a time-dependent manner (Machado et al. 2019, in preparation). By looking at state-of-the-art cellular atlases, traces of IEGs inductions are ubiquitous and appear to correlate with a cells' dissociation time as shown in **Figure 7**. Methods that abrogate the effect of dissociation on the molecular state of a cell must be exploited to improve the accuracy of transcriptomic studies.

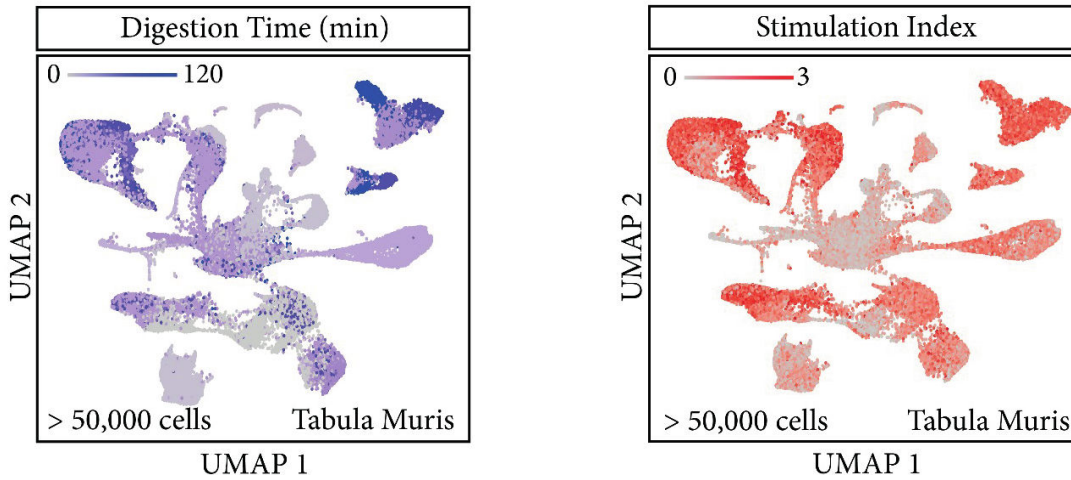
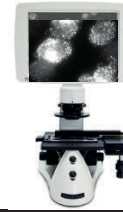
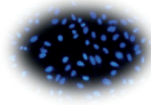
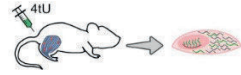


Figure 7: Correlation between dissociation-time (left) and stimulation index (right) in > 50,000 cells extracted from the Tabula Muris Smart-Seq2 dataset over 20 different tissues. The stimulation index approximates the average expression of ubiquitous IEGs induced during dissociation (Machado *et al.* 2019, in preparation)

Methods to preserve cellular transcriptome

Aldehydes such as formaldehyde or paraformaldehyde (PFA) have been used for more than a century to preserve biological samples through the process of fixation (reviewed in Fox *et al.*, 1985). Fixation is needed to harden biological samples and prevent their decomposition and is mediated - for formaldehyde - through biological macromolecules cross-linking (Thavarajah *et al.*, 2012). All fixative distort the original biological samples and induce technical artefacts, for example, high-concentration formaldehyde can impact RNA quality on Formalin-Fixed Paraffin-Embedded (FFPE) samples (von Ahlfen *et al.*, 2007). Nevertheless, low-concentration (0.5%) PFA has been shown to accurately preserve RNA integrity and composition upon bulk and single-cell RNA-seq (Thomsen *et al.*, 2016; Machado *et al.*, 2017). Using 0.5% PFA fixation on intact tissue pieces can preserve the nascent transcriptome of isolated cells and abrogate the impact of dissociation (Machado *et al.*, 2017; van Velthoven *et al.*, 2017). Moreover, molecular tagging technologies can be used to label nascent mRNA and compare *in vivo* nascent transcriptome with freshly isolated cells' transcriptome to infer the effect of dissociation (van Velthoven *et al.*, 2017). Different methods attempted to remove the dissociation-induced artefact through transcriptional inhibitors such as α -amanitin (van Velthoven *et al.*, 2017) or actinomycin-D (Wu *et al.*, 2017) supplementation during dissociation. However, these methods only targeted modifications impinged by neo-transcription and spared other transcriptomic alterations (for example, transcript down-regulation). A more drastic approach was to lower

temperature during dissociation by using cold-digesting enzymes such as psychrophilic proteases that can digest tissues on ice thus lowering intra-cellular metabolism and slowing transcription, and this protocol successfully inhibited IEGs induction (Adam *et al*, 2017). An alternative obvious strategy to avoid the impact of dissociation is to avoid dissociation. In that spirit, single nuclei RNA-seq which rely on the immediate lysis of intact tissues and the individual barcoding of single nuclei (Grindberg *et al*, 2013; Habib *et al*, 2016; Lake *et al*, 2016) is a method of choice for large-scale projects, as nuclear transcriptome largely reflects its cytoplasmic counterpart (Gaidatzis *et al*, 2015). Comparison between RNA-seq from digestion-isolated whole cells and single-nuclei from intact tissue confirmed the absence of IEGs in the latter (Lacar *et al*, 2016; Wu *et al*, 2017; Bakken *et al*, 2018; Wu *et al*, 2019). Finally, spatial transcriptomic methods are constantly improving in depth, sensitivity and complexity and can increasingly compete with illumine-based methods (Lee *et al*, 2015; Wang *et al*, 2018a; Rodriques *et al*, 2019; Eng *et al*, 2019). Despite not having systematically studied IEGs expression with these methods, it is explicit that spatial transcriptomics methods, by studying *in situ* gene expression and conserving tissue topography will preserve the cells of interest from dissociation-induced artefacts.



Method Properties	Aldehyde Fixation	Nascent mRNA labeling	Single nuclei RNA-seq	Spatial Transcriptomics	Cold digestion
Preserve cell	no	yes	no	no	yes
Tissue topology	no	no	no	yes	no
FACS compatible	yes	yes	Yes (only nuclear)	no	yes
Full-transcriptome	Yes	Yes	No (only nuclear)	Partially limited in depth	yes
Accessibility	++	-	++	-	+

Table 2: Comparison of the different methods used to preserve transcriptomes from dissociation-induced effects. Nascent mRNA labeling icon adapted from Velthoven et al. 2017.

Chapter 3: The skeletal muscle stem cells in homeostasis and regeneration

Anatomy of the skeletal muscle tissue

The skeletal muscle tissue allows vertebrates to create motion from contraction which helps them to move and interact with their environment. The main component of the skeletal muscle is the skeletal muscle fiber or myofiber, a syncytium originating from the fusion of muscle progenitor cells. Muscle fibers contain differing numbers of nuclei - from a few dozens to thousands - according to the muscle and organism of origin (Frontera & Ochala, 2015). There is a striking heterogeneity in muscle fiber types according to their color, contractile properties, fatigability and metabolism. There is a continuum of muscle fiber types which can be simplified in four categories in mammalian species (Schiaffino & Reggiani, 2011): I (slow, fatigue-resistant, oxidative), IIA (intermediate) and IIX (intermediate) and IIB (fast, fatigable, glycolytic). Each muscle contains varying proportions of each fiber type. Each muscle fiber is connected to the central nervous system via the neuro-muscular junction which transduce central electrical signals into mechanical force. A muscle fiber is innervated by one unique motoneuron which itself innervates many muscle fibers. The sum of a motoneuron and its innervated fiber is called a muscle unit. When the motoneuron action potential reaches the neuromuscular junction, acetylcholine is released in the synapse that triggers the depolarization of the fiber cytoplasmic membrane: the sarcolemma. This depolarization triggers the release of Ca^{2+} into the muscle fiber cytosol that in turn triggers the contraction of the muscle fiber motor unit: the myofibril. The myofibril is composed mainly of myosin and actin that are aligned in a highly ordered architecture called a sarcomere. The release of Ca^{2+} permits the sliding of myosin molecules onto the actin filaments, shrinking the sarcomeres and allowing the conversion of chemical energy into mechanical force, which results in muscle contraction.

Moreover, the skeletal muscle tissue is also composed of several mononucleated cell-types such as fibroblasts, mesenchymal cells and immune cells, which can be found in the space between individual fibers (the endomysium) or in the space between fiber bundles (the perimysium). The muscle tissue is highly vascularized and endothelial cells can be found between individual fibers. Finally, each single fiber is enclosed by a basal lamina beneath which are found the muscle stem cells – also called satellite cells - which will be described latter.

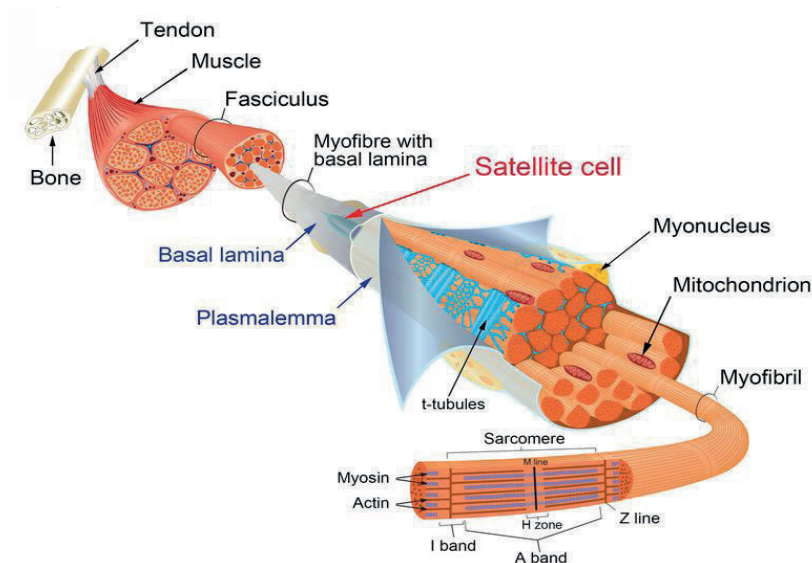


Figure 8: Anatomical representation of the skeletal muscle tissue and its contractile apparatus (adapted from Tajbakhsh, 2009).

Transcriptomic characterization of the skeletal muscle populations

The comprehensive characterization of all the cell types present within the skeletal muscle tissue was first attempted through lengthy marker-gene based methods such as immunostainings or *in situ* hybridization. However, as described in **Chapter 1**, high-throughput single-cell RNA-sequencing methods can help to categorize the many populations within the skeletal muscle. Recently, many groups performed such experiments using different technologies, all based on early-barcoding procedures to unbiasedly characterize high number of cells without prior knowledge of the existing populations (Schaum *et al*, 2018; Dell'Orso *et al*, 2019; Giordani *et al*, 2019). These reports present similar results and the most sensitive report describe 10 different populations within the mononucleated fraction of the skeletal muscle tissue: skeletal muscle stem cells, mesenchymal cells, smooth muscle cells, macrophages, neutrophils, endothelial cells, glial cells, B cells, T cells and tenocytes. The caveat of these studies is their reliance on the enzymatic dissociation of single mononucleated cells: in such protocols, damaged myofibers are discarded. Therefore, the syncytial nature of the muscle fiber prevents its inclusion in such analysis, therefore depleting such datasets from the most abundant cell type – in term of nuclei - from the tissue of interest.

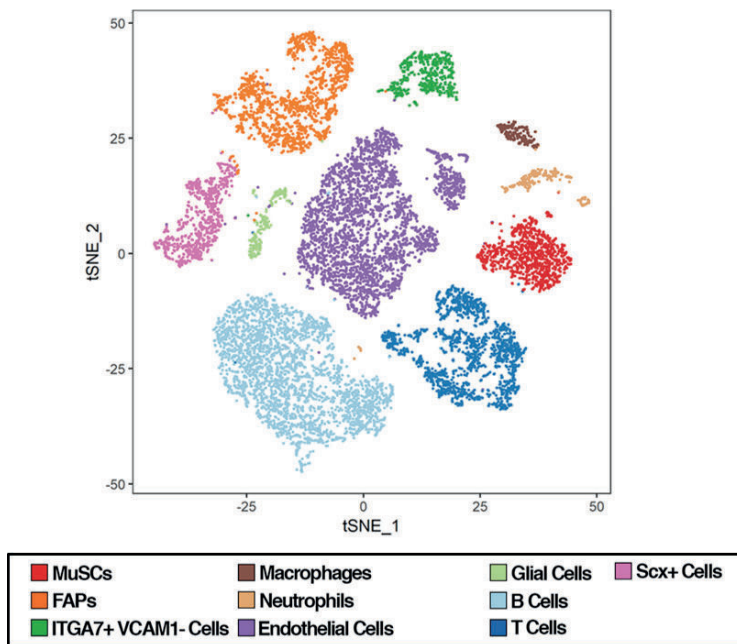


Figure 9: Transcriptional atlas of the skeletal muscle tissue depicting 10 different cell types (Giordani *et al*, 2019).

The skeletal muscle stem cells

The skeletal muscle stem cells (MuSCs) are the indispensable stem cell population responsible for the homeostasis and regeneration of the skeletal muscle tissue. Originally, MuSCs were identified – and named - by their anatomical position, at the periphery of muscle fibers, under the basal lamina. These cells have first been described in 1961 via electron microscopy in frog muscles (Katz, 1961) and immediately confirmed in rat muscles (Mauro, 1961). Simultaneously, it was shown that mononucleated cells in the muscle tissue – myoblasts - proliferate (Bintliff & Walker, 1960) during muscle regeneration. It was later discovered that MuSCs were capable of proliferation in response to muscle injury *in vivo* (Mintz & Baker, 1967). These discoveries initiated a new era in the study of myogenesis, continuing a century-long debate about the origin of muscle regeneration (Scharner & Zammit, 2011). Definite proof that MuSCs had a myogenic potential came from studies with isolated myofibers (Moss & Leblond, 1971; Bischoff, 1975, 1986a) and transplanted MuSCs (Collins *et al*, 2005; Montarras *et al*, 2005) which demonstrated the ability of these cells to form new muscle tissue in specific environment. MuSCs were initially described based on their anatomical location using electron-microscopy and it took many years before molecular markers were discovered to accurately identify these cells using classical microscopy. The paired-box transcription factor PAX7 emerged as the most

accepted marker of quiescent MuSCs *in vivo* (Seale *et al*, 2000). This transcription factor is critical for the specification of the muscle lineage from pre-somitic mesoderm during embryogenesis (Relaix *et al*, 2005) and for the regenerative function of adult MuSCs (von Maltzahn *et al*, 2013). The ablation of PAX7 expressing cells using genetic models ultimately demonstrated that satellites cells were crucial: without MuSCs, muscle tissue lost its ability to regenerate (Lepper *et al*, 2011; Sambasivan *et al*, 2011; Murphy *et al*, 2011) or to respond properly to hypertrophy-inducing stimuli (McCarthy *et al*, 2011). Researchers also demonstrated the ability of MuSCs to self-renew after proliferation, in single-cell (Sacco *et al*, 2008) or sequential (Rocheteau *et al*, 2012) transplantation experiments which is a property of adult stem cells. Hence, the aforementioned experiments explain why the satellite cells is also called the skeletal muscle stem cell.

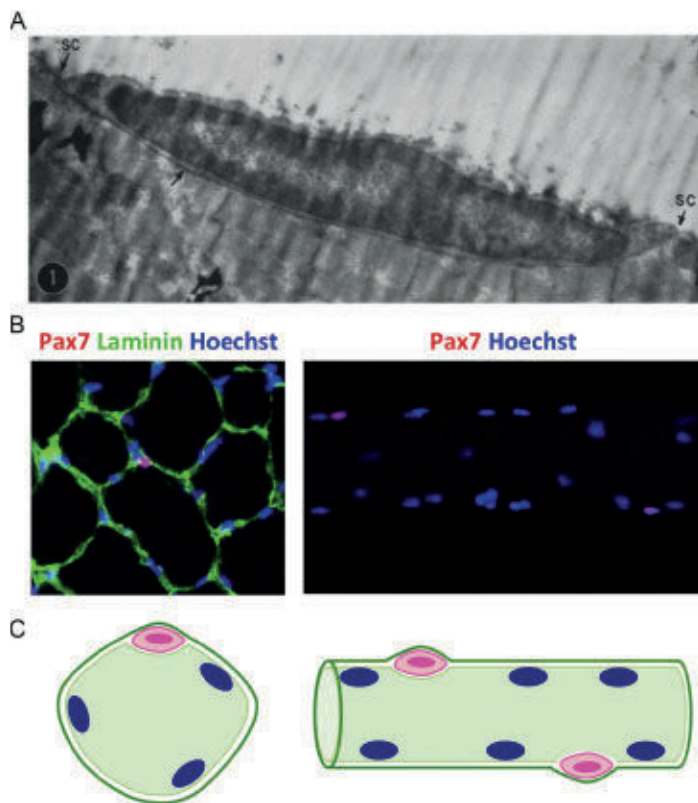


Figure 10: MuSCs anatomical localization (Giordani *et al*, 2018) (a) Electron micrograph of a MuSC along a myofiber and under the basal lamina (b) Immunostaining depicting a MuSC (PAX7+) under the basal lamina (LAMININ) of a myofiber c) Graphical representation of MuSCs (pink) along a myofiber and under the basal lamina on transversal (left) and longitudinal (right) sections.

Experimental tools

Quiescence is a state of replicative and metabolic dormancy that is a hallmark of some adult stem cells (Cho *et al*, 2019). In homeostatic conditions, almost all MuSCs are outside of the cell cycle, in a state of G0-arrest. Such state is influenced by many intrinsic and extrinsic factors. The development of lineage tracing tools permitted the precise identification of MuSCs and the dissections of the mechanisms that regulate their quiescence. Among these tools were mouse lines that put a fluorescent reporter under the control of *Pax7* expression (Bosnakovski *et al*, 2008; Sambasivan *et al*, 2009; Tichy *et al*, 2018; Kitajima & Ono, 2018) and conditional lines allowing the targeted temporal recombination of a genetic locus of interest through *Pax7* expression with the Cre-lox system (Lepper *et al*, 2009; Nishijo *et al*, 2009; Murphy *et al*, 2011; Mourikis *et al*, 2012).

Intrinsic factors for quiescence maintenance

As described in **Chapter 1**, the epigenetic state of a cell is a critical determinant of its identity and functions. Quiescence does not escape this rule, as demonstrated by the role of facultative heterochromatin, notably at the *Myod1* locus, into the maintenance of MuSCs quiescence. Such data have been obtained by the deletion of the H4K20 dimethyltransferase SUV4-20h1 (Boonsanay *et al*, 2016).

Besides the elucidation of epigenetic states, an ongoing development in modern biology is the discovery and characterization of microRNAs (miRNAs). Pre-miRNAs are processed through the protein DICER to mature into functional miRNAs. miRNAs are small non-coding RNAs which average 22 nucleotides in length and which can interact with the 3'-UTR region of target mRNAs to repress their expression (O'Brien *et al*, 2018). They have been linked to numerous biological processes including the quiescence of MuSCs. DICER ablation in quiescent MuSCs promoted quiescence exit and the miRNA *mir-489* was shown to be maintain MuSCs quiescence (Cheung *et al*, 2012). Consistently, *mir-198* and *mir-497* were later proven also important to regulate MuSCs quiescence (Sato *et al*, 2014) and this list was recently completed by the mirtron – a miRNA inside an intron - *mir708* which equally stimulates MuSCs quiescence through the repression of the adhesion protein TENSIN3 and its migratory function (Baghdadi *et al*, 2018b).

More classically, the signaling status of MuSCs also influences their functions: Spry1, a receptor tyrosine-kinase inhibitor is promoting MuSCs quiescence (Shea *et al*, 2010) similarly to the tumorsuppressor and inhibitor of PI3K/AKT *Pten* (Yue *et al*, 2017). Also, MuSCs require the translation

initiation factor EIF2A to be phosphorylated to obtain sufficient translational inhibition to maintain a proper quiescent state (Zismanov *et al*, 2016).

MuSCs metabolic status is also involved in quiescence regulation. It has been demonstrated that quiescence and activation are characterized by the activity of distinct metabolic pathways, fatty-acid β -oxidation for quiescence and glycolysis for activation via the histone-deacetylase SIRT1 which sense levels of the free metabolite NAD⁺ (Ryall *et al*, 2015).

Extrinsic factors for quiescence maintenance

A set of extrinsic factors, often overlooked in the context of everyday laboratory practice, that regulate MuSCs quiescence is the physical properties of the direct micro-environment. It has been demonstrated in a seminal study that substrate rigidity – its elastic modulus - modulates the self-renewal (*e.g.* the reestablishment of quiescence) in cultured MuSCs, with physiological levels of stiffness having a positive impact on self-renewal in contrast to the plastic's high rigidity (Gilbert *et al*, 2010). Such integration of extrinsic mechanical cues by a cell is called mechanotransduction. Another important study was published the following year, describing YAP/TAZ, the signaling pathway at the nexus of mammalian mechanotransduction (Dupont *et al*, 2011). Not surprisingly, YAP/TAZ signaling has been implicated in MuSCs activation and cell fate decisions (Judson *et al*, 2012; Sun *et al*, 2017). Besides its elasticity, the substrates that occupy MuSCs can also influence their behavior through specific adhesions mediated by integrins. β 1-integrin is responsible for such cell-matrix adhesions in adult MuSCs and its deletion break MuSCs quiescence and prime the cells to differentiate prematurely (Rozo *et al*, 2016). β 1-integrin mediates the polarized attachment of MuSCs to the basal lamina of the myofiber and the reverse side of the cell is therefore the location for cell-cell adhesion between individual MuSCs and the myofiber. Such adhesions are usually mediated through cadherins and the MuSC-fiber junction is mediated through N-CADHERIN and M-CADHERIN. The simultaneous deletion of both of these cadherins in MuSCs leads to a partial break of quiescence due to ectopic B-CATENIN activation (Goel *et al*, 2017).

Along with cadherins, another axis has been found critical in quiescence regulation through MuSCs-fiber interaction: Notch signaling. Notch signaling is a heterotypic signaling pathway known to be active in MuSCs. Under the basal lamina, the sole possible source of Notch signaling (through DLL1 and/or DLL4 ligand) is the myofiber. Indeed, MuSCs conditionally deleted of its effector - *Rbpj* - spontaneously differentiate (Mourikis *et al*, 2012; Bjornson *et al*, 2012). Interestingly, Notch signaling has also been shown critical to establish and maintain MuSCs quiescent niche through their microenvironment (Bröhl *et al*, 2012). Moreover, RBPJ has been shown to bind regulatory elements of genes encoding for the

chains of the fibrillar collagen V (COLV) in MuSCs, an ECM component primarily produced by fibroblasts (Castel *et al*, 2013). It has been demonstrated that NOTCH signaling induces COLV expression from the MuSCs, which in turn interacts with CALCR, - a G-protein coupled receptor highly specific in the muscle of quiescent MuSCs– to promote and maintain quiescence. MuSCs conditionally deleted for Col5a1 (COLV main chain) or *Calcr* spontaneously differentiate, after entering the cell-cycle, indicating the importance of the COLV-CALCR axis to regulate quiescence (Yamaguchi *et al*, 2015; Baghdadi *et al*, 2018a). Interestingly, the member of the forkhead family of transcription factors FOXO3 has also been demonstrated to be important for MuSCs quiescence through the promotion of NOTCH signaling (Gopinath *et al*, 2014), adding another level of regulation to the NOTCH-COLV-CALCR axis.

The Syndecan family is a group of transmembrane proteoglycans responsible for cell-cell and cell-niche adhesions, receptors co-activation and signal transduction (Couchman *et al*, 2015). Quiescent and activated MuSCs express SYNDECAN-3 and SYNDECAN-4 and SYNDECAN-3 has been proven critical for MuSCs quiescence maintenance through the regulation of the MuSCs-myofiber adhesion and NOTCH signaling (Cornelison *et al*, 2001, 2004, Pisconti *et al*, 2010, 2016). Inversely, SYNDECAN-4 is required for MuSCs activation and proliferation (Cornelison *et al*, 2004).

Another classical extrinsic cue is the presence of secreted signaling molecules. For example it has been shown that ANGIOPOIETIN-1 through the TIE-2 receptor can signal MuSCs to maintain quiescence (Abou-Khalil *et al*, 2009). Along those lines, it has been demonstrated that the interleukin-6 family member ONCOSTATIN M is also inducing MuSCs quiescence (Sampath *et al*, 2018).

Inducing and maintaining quiescent MuSCs *ex vivo* is a goal for many laboratories in order to understand and modulate the behavior of isolated MuSCs for research or cell-therapy purposes. To this end, there have been attempts to modulate MuSCs behavior toward quiescence through anchorage-dependence in a 3D gel-like structure (Milasincic *et al*, 1996; Sellathurai *et al*, 2013; Arora *et al*, 2017) or by combining diverse quiescence-promoting factors in a quiescence medium (Quarta *et al*, 2016). However, none of these methods fully recapitulates the complexity of the quiescence niche of MuSCs and the feasibility of mimicking quiescence up to the molecular features of the MuSCs remains questionable. Nevertheless, the emergence of rare self-renewing quiescent-like myocytes under specific culture conditions – also called *reserve cells* – provides evidence that such goal is attainable

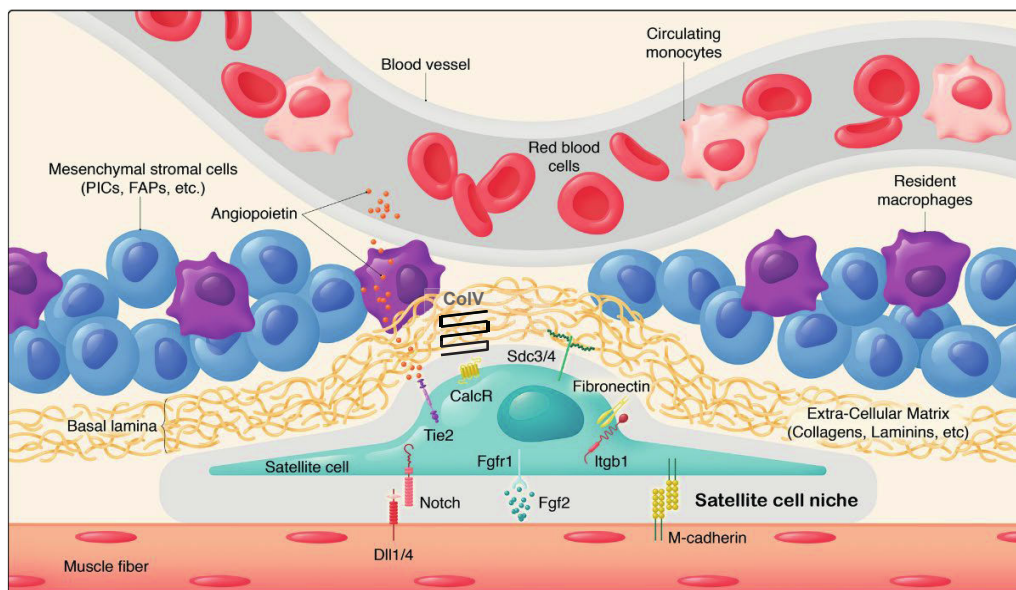


Figure 11: Representation of MuSCs quiescent niche and extrinsic quiescence regulators (Evano & Tajbakhsh, 2018).

Activation of MuSCs

The activation of MuSCs is a nebulous term which can define the early hours of quiescence exit as well as the first days of the myogenic program – the proliferative phase – until the onset of differentiation. The earliest researchers have looked to define MuSCs activation are studies of the P38 α / β MAPK pathway. P38 α / β MAPK is active (phosphorylated) in satellite cells less than 20 min after the isolation of individual myofibers and precedes the induction of MYOD1 protein (Jones *et al*, 2005). Of interest, *Myod1* gene is transcribed but post-transcriptionally repressed in MuSCs. This mechanism is thought to allow for accelerated transcription and translation when the inhibitory signals are lifted upon activation (Hausburg *et al*, 2015; de Morrée *et al*, 2017).

In this report, MuSCs chemically inhibited for P38 α / β MAPK failed to enter the cell cycle upon isolation. This proliferative impairment is comparable with the phenotype observed by the inhibition of another MAPK pathway, ERK1/2 on a myogenic cell line (Jones *et al*, 2001). What signal then can trigger the activation of these MAPK pathways? A seminal study described the presence of a MuSCs mitogenic factor in crushed muscle extracts (Bischoff, 1986b). Since then, several growth factors and signaling molecules have been shown to promote MuSCs activation, among which TNF-alpha (Li, 2003) or IL-6 (Muñoz-Cánoves *et al*, 2013). MuSCs express several receptors for FGF signaling and are activated by FGF (Sheehan & Allen, 1999), notably FGF2 (Chakkalakal *et al*, 2012). Interestingly,

MuSCs also express the HGF receptor C-MET (Allen *et al*, 1995; Cornelison & Wold, 1997). HGF promotes MuSCs activation and proliferation (Allen *et al*, 1995; Tatsumi *et al*, 1998) and is released after mechanical stimulation of the muscle tissue (Tatsumi *et al*, 2002). HGF has recently been involved in priming of MuSCs to a pre-activated state called G_{Alert} through MTORC1 signaling (Rodgers *et al*, 2014). Consistently, MTORC1 signaling is activated by PI3K/AKT and the P110 α subunit of PI3K has therefore been demonstrated crucial to transduce MuSCs activation signals through this axis (Wang *et al*, 2018b).

TGF- β signaling pathway is involved in MuSCs activation and proliferation as MuSCs impaired for SMAD3 expression exhibit deficient expansion and a regenerative impairment (Ge *et al*, 2011, 2012). One possible mechanism was shown by the role of KLF7 in MuSCs quiescence maintenance and its active downregulation upon TGF- β signaling (Wang *et al*, 2016). Notch signaling, in addition to quiescence, sustains MuSCs proliferation through the pro-survival effect of p53 (Liu *et al*, 2018). Proliferation can also be epigenetically enforced, for example through the epigenetic silencing of the cell-cycle inhibitor *p21* by the methyltransferase PRMT5 (Zhang *et al*, 2015).

When activated, MuSCs also deploy safeguards against over-proliferation. For example, MuSCs expansion is tamed by JAK2-STAT3 signaling (Price *et al*, 2014; Tierney *et al*, 2014) or decreased Wnt/ β -Catenin signaling (Murphy *et al*, 2014). Similarly, the methyltransferase SETD7 has been shown to limit MuSCs expansion, possibly through modulating Wnt/ β -Catenin signaling (Judson *et al*, 2018). Also, adequate proteolysis is necessary for correct MuSCs proliferation. Autophagy and the ubiquitin-proteasome system have been shown important for proper MuSCs amplification and regeneration capacity (Fiacco *et al*, 2016; Kitajima *et al*, 2018).

The myogenic program

One of the greatest features of MuSCs is their clocklike activation sequence, called the *myogenic program*. In response to an activatory stimuli, the MuSCs will orchestrate a sequence of transcription factors inductions and repressions whose interplay results in MuSCs proliferation, differentiation or self-renewal and fusion to reconstruct muscle tissue. Besides PAX7, a family of basic helix-loop-helix (bHLH) factors are responsible for the myogenic program: the myogenic regulatory factor family (MRF). The first of these factors to be identified was *Myod1* as a factor sufficient to induce the transformation of fibroblasts into myoblasts (Davis *et al*, 1987). Subsequently, *Myog*, *Myf5* and *Mrf4* were discovered (Wright *et al*, 1989; Braun *et al*, 1989; Rhodes & Konieczny, 1989). During development, these factors

determines the skeletal muscle lineage (reviewed in Weintraub *et al*, 1991; Comai & Tajbakhsh, 2014; Zammit, 2017).

During homeostasis, MYF5 is expressed in almost all quiescent MuSCs (Gayraud-Morel *et al*, 2012). Upon muscle injury, its expression levels rise in less than 3 hours (Cooper *et al*, 1999), notably with the mobilization of *Myf5* mRNA previously stored in stress granules (Crist *et al*, 2012). *Myod1* and *Myog* proteins are also induced upon injury at specific time-intervals, setting boundaries for the proliferation and differentiation of activated MuSCs. *Myod1* and *Myog* are induced shortly after muscle injury (Grounds *et al*, 1992; Füchtbauer & Westphal, 1992; Cooper *et al*, 1999) however *Myog* is really induced in MuSCs concomitantly with their cell-cycle exit between 3 and 5 days post-injury (Zhao *et al*, 2002), initiating the process of terminal differentiation. One of the most fascinating features of MuSCs is their ability to fuse to produce long myotubes which mature into functional muscle fibers. This process of fusion is initiated by the action of many genes among which *Myomaker* (Millay *et al*, 2013) and microprotein *Minion* (Zhang *et al*, 2017) for the initiation of cell-cell hemifusion (Leikina *et al*, 2018) and *Myomerger* (Quinn *et al*, 2017) for the creation of fusion pores (Leikina *et al*, 2018) have recently been described. Finally, the myogenic program culminates with the expression of developmental myosin-heavy chain isoforms (Schiaffino *et al*, 2015).

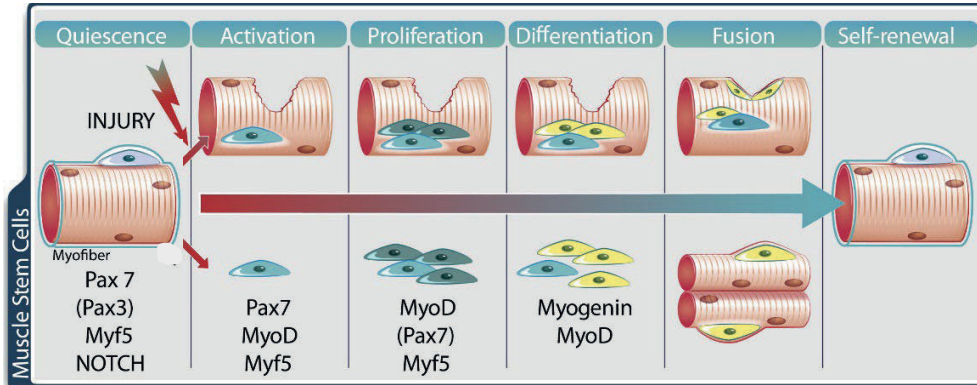


Figure 12: Graphical representation of the myogenic program during MuSCs activation (Baghdadi & Tajbakhsh, 2018)

Muscle injury: different models and cell types that drive tissue regeneration

The skeletal muscle tissue is fascinating by its capacity to fully regenerate after a disruption of its tissue integrity. Such injuries can take many forms: physiological minor injuries caused by mechanical stress during physical activity as well or major injuries leading to the partial or total

destruction of the muscle tissue. Such major injuries are displayed in **Figure 12** and consist of four main categories: 1) denervation, 2) chemical injury, 3) myotoxins and 4) freeze injury. Alternatively, crush injuries or volumetric muscle loss injuries can be performed but are less widely accepted as an experimental model. There is a striking heterogeneity in injury models, from the protocols used to the type of damage impinged on the fibers (Lefaucheur & Sébille, 1995; Hardy *et al*, 2016).

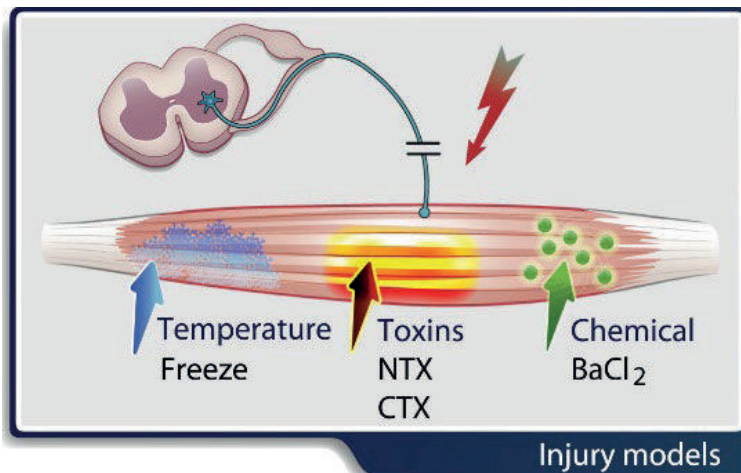


Figure 13: Different models of skeletal muscle injury (Baghdadi & Tajbakhsh, 2018).

This lack of standardization is a challenge for the field of muscle regeneration. Nevertheless, all these procedures share a common denominator which is the necrosis of the myofiber. During normal muscle regeneration, the necrotic degeneration of the myofiber – which may be focal or total and triggered and/or amplified by aberrant calcium signaling (Chargé & Rudnicki, 2004) leaves intact a scaffold of basal lamina composed of ECM components called the *ghost fiber* (Vracko & Benditt, 1972; Alameddine *et al*, 1991; Webster *et al*, 2016). The MuSCs then divide and migrate along the longitudinal axis of the ghost fibers which direct MuSCs alignment and fusion into a functional muscle fiber (Webster *et al*, 2016).

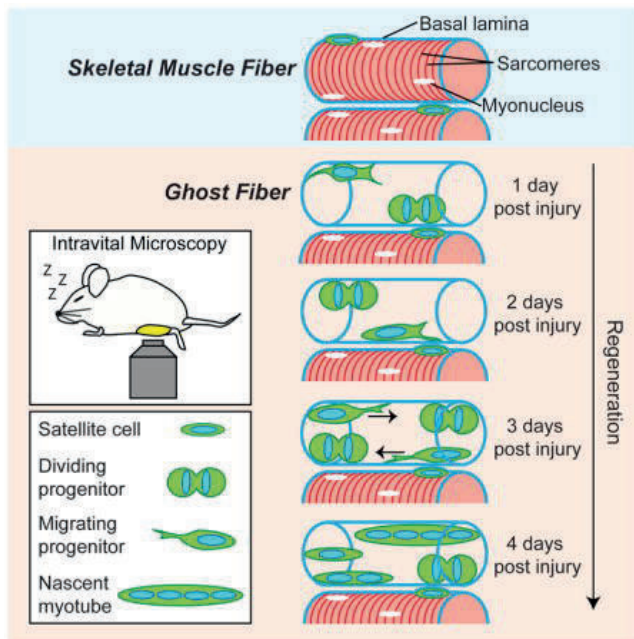


Figure 14: MuSCs longitudinal colonization of the ghost fiber after muscle injury (Webster *et al*, 2016).

MuSCs are not the sole contributor to muscle regeneration multiple resident and circulating cells are participating in the restoration of the tissue after an injury.

Neutrophils are the first responder to a muscle injury and are recruited - notably by resident macrophages (Brigitte et al, 2010) - only hours after the damage. The neutrophils are increasing in numbers through the first day post-injury (Chazaud et al, 2003; Tidball & Villalta, 2010) and are necessary to clear necrotic area for proper regeneration (Teixeira et al, 2003).

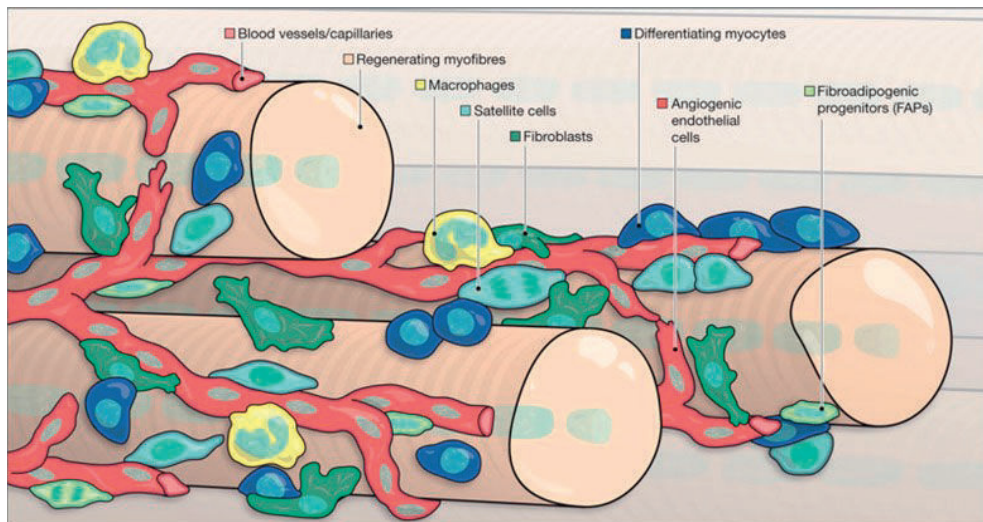


Figure 15: Different cellular types in the skeletal muscle taking part to the regeneration process (Bentzinger *et al*, 2013a)

During day 2 and 3 post-injury, pro-inflammatory M1 macrophages are recruited in numbers at the expense of neutrophils (Bencze *et al*, 2012) before switching to an anti-inflammatory M2 phenotype for the rest of the regeneration course (Arnold *et al*, 2007). Besides their phagocytic role, the infiltrating macrophages have been found closely associated to MuSCs (Ceafalan *et al*, 2018). The inflammatory macrophages notably activate MuSCs through the secretion of the metalloprotease ADAMTS1 which diminishes NOTCH1 activity (Du *et al*, 2017) while the anti-inflammatory macrophages secretes GDF-3 to promotes MuSCs fusion (Varga *et al*, 2016).

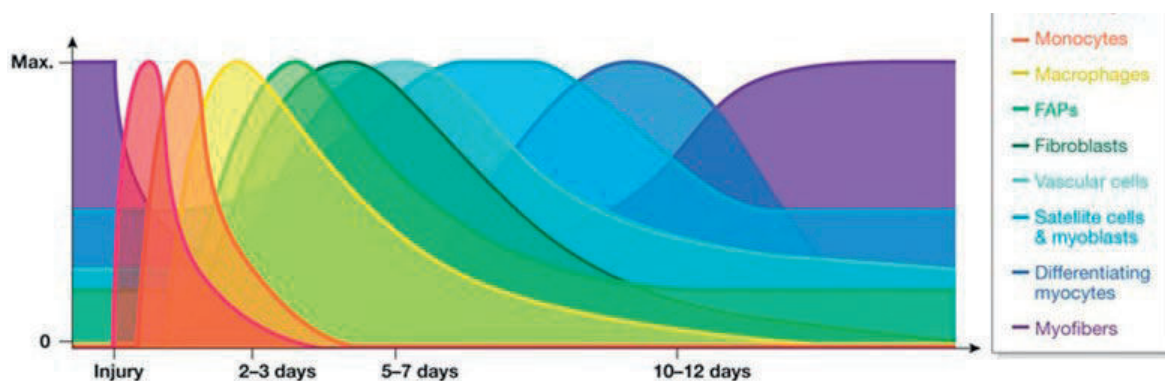


Figure 16: Kinetics of different cellular types recruitment to site of injury during skeletal muscle regeneration (Bentzinger *et al*, 2013a)

The vasculature that support the recruitment of these circulating cells also plays a role during normal muscle regeneration. Endothelial cells and MuSCs are physically associated (Christov *et al*, 2007; Verma *et al*, 2018) and angiogenesis is therefore tightly coupled to myogenesis (Rhoads *et al*, 2009; Latroche *et al*, 2017). The blood vessels are lined with support cells called pericytes (Armulik *et al*, 2011) which also participates in the regulation of myogenesis through the timely promotion of MuSCs quiescence (Abou-Khalil *et al*, 2009; Kostallari *et al*, 2015). Such cells have also been proven myogenic under certain conditions and could participate in normal muscle regeneration (Dellavalle *et al*, 2007, 2011).

The connective tissue which bundles myofibers is critical for normal muscle function. This connective tissue is mainly made of ECM and fibroblasts responsible for the production and maintenance of it. Fibroblasts have been shown to proliferate in response to muscle injury and the muscle tissue cannot properly be repaired without this population (Mathew *et al*, 2011; Murphy *et al*, 2011; Mackey *et al*, 2017).

Finally, the last decade delineated the contribution of fibro/adipogenic progenitors (FAPs) to muscle regeneration (Joe *et al*, 2010; Uezumi *et al*). These cells proliferate in response to injury and are necessary for a proper muscle regeneration (Heredia *et al*, 2013; Fiore *et al*, 2016; Lukjanenko *et al*, 2019; Wosczyzna *et al*, 2019). These cells can give rise to different lineages under different conditions and therefore exhibit a heterogeneous transcriptome composed of different dynamical sub-states at the single-cell level (Malecova *et al*, 2018).

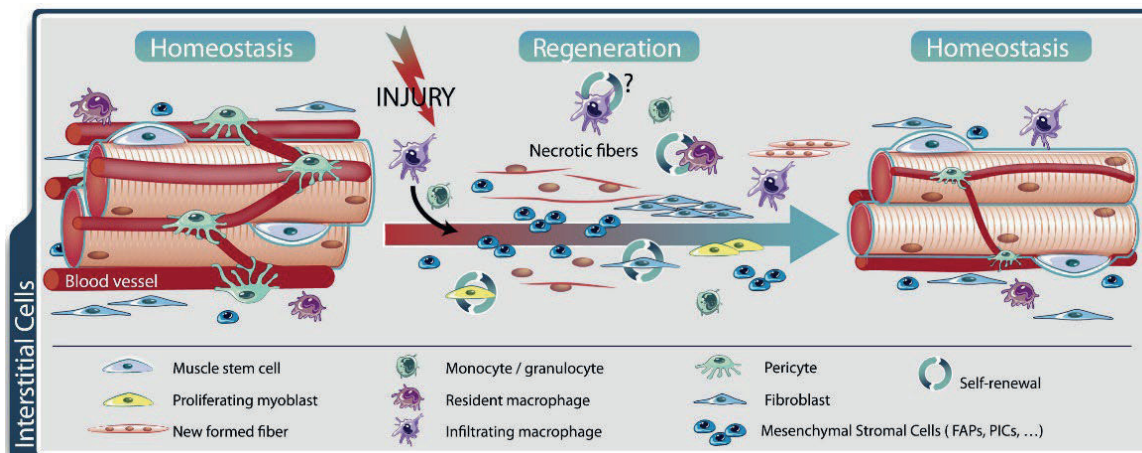


Figure 17: Graphical representation of the multi-cellular regeneration process taking place during skeletal muscle injury (Baghdadi & Tajbakhsh, 2018)

Heterogeneity

Despite contradicting reports (Brack *et al*, 2007; Yin *et al*, 2013), one of the main features of MuSCs is their unipotency. It allowed the characterization of the myogenic program and its use as a simple model of stem cell activation and differentiation. It is tempting to extrapolate from MuSCs unipotency that such cells must be homogeneous.

One evident source of MuSCs heterogeneity comes from the muscle they originate from. It is unclear whether the embryonic origin or the muscle function and/or composition are responsible for this heterogeneity. For example, it has been shown that muscles from different body-parts originate from different embryonic signaling cascades and exhibit distinct transcriptional profiles for trunk, pharyngeal arches, extraocular and head muscles (Harel *et al*, 2009; Sambasivan *et al*, 2009). Consistently, it was subsequently shown that head (masseter) and limb (*extensor digitorum longus*) muscles differed in their transcriptional profile and clonal output upon transplantation (Ono *et al*, 2010).

Moreover, the transcription factor PAX3, which is critical for the specification of the muscle lineage (Relaix *et al*, 2005), is partially expressed by MuSCs in the adult, with varying number of MuSCs expressing it according to their muscle of origin (Relaix *et al*, 2006; Der Vartanian *et al*, 2019). Interestingly, PAX3 expression confers resistance to environmental stress or irradiation and seems to represent a sub-population of reserve MuSCs resistant to stressors (Der Vartanian *et al*, 2019; Scaramozza *et al*, 2019). The myogenic factor MYF5 has also been linked with heterogeneous distribution and enhanced stem cell capacity (Beauchamp *et al*, 2000; Kuang *et al*, 2007; Gayraud-Morel *et al*, 2012).

Another clue that MuSCs are heterogeneous are reports of a slow-cycling population – also called *label retaining cells* – that enter the cell cycle less often (Schultz, 1996; Chakkalakal *et al*, 2012) and with slower kinetics (Schultz, 1996; Ono *et al*, 2010, 2012). Some MuSCs also perform better in functional assays such as transplantation, which is highly heterogeneous at the single-cell (Sacco *et al*, 2008) or population level (Collins *et al*, 2005; Montarras *et al*, 2005).

The obvious question raised by these studies is whether such experimental heterogeneity is stochastic, resulting from random fluctuations in biological states inherent to the nature of molecular regulatory processes. Indeed, several studies highlighted the oscillatory and stochastic nature of cell fate choices (Chang *et al*, 2008; Imayoshi *et al*, 2013) and the mechanism by which such random fluctuations could determine a tissue clonality due to a statistical process called *neutral drift* (Snippert *et al*, 2010; Klein *et al*, 2010; Doupé *et al*, 2010). It was observed that only a fraction of MuSCs take part to muscle regeneration after a tissue injury (Collins *et al*, 2007). Recent work using multicolor

lineage tracing highlighted that the clonal heterogeneity of MuSCs was preserved in homeostasis and aging but lost upon repeated bouts of tissue injuries due to a random neutral drift process (Tierney *et al*, 2018), which support the hypothesis that MuSCs functional heterogeneity originates from stochastic processes.

The only non-linear fate choice that MuSCs undertake is the decision to self-renew or differentiate (Zammit *et al*, 2004). This decision could lead to a symmetric or an asymmetric division and it remains unclear if MuSCs heterogeneity governs this division choice. It was reported using isolated single myofibers that isolated MuSCs divisions could be planar – parallel to the myofiber – or apical-basal – perpendicular to the myofiber – and that asymmetric division mostly took place during apical-basal divisions (Kuang *et al*, 2007; Siegel *et al*, 2011). Subsequently, it was shown on isolated myofibers that WNT7A signaling was required to promote symmetric and planar divisions through the planar cell polarity complex proteins (Le Grand *et al*, 2009) and through fibronectin-syndecan-4 co-activation (Bentzinger *et al*, 2013b). Moreover, the Par-complex (Troy *et al*, 2012), the polarity regulators SCRIB (Ono *et al*, 2015), and DYSTROPHIN (Dumont *et al*, 2015) has been demonstrated crucial to regulate divisions symmetry and MuSCs fate. However, these findings were challenged by the aforementioned *in vivo* observation that MuSCs divisions following injury were mostly planar along the ghost fiber scaffold (Webster *et al*, 2016).

An enticing idea in the stem cell field is the immortal strand hypothesis: the possibility that cycling cells non-randomly segregate the DNA strand that undergo replication during a division to preserve the parent cell from replication-induced mutations (Cairns, 1975). This hypothesis raised controversy and was not always supported by data (Tomasetti & Bozic, 2015). However several studies reported that MuSCs non-randomly segregate their template DNA strand and that the replicative-strand recipient cell was associated with increased stemness (Shinin *et al*, 2006; Conboy *et al*, 2007). It was shown that replicative-strand conservation is enriched in cells expressing the highest levels of PAX7 within the MuSCs population (Rocheteau *et al*, 2012) or that replicative-strand conservation can be triggered *ex vivo* by geometric micro-patterning of the culture substrate (Yennek *et al*, 2014).

Finally, many different forms of MuSCs heterogeneity have been identified based on non-random DNA segregation, regenerative potential differences, marker genes levels or division polarity and with differing functional impact on MuSCs fate. From the data it is not clear how much those different heterogeneity levels overlap with each other and whether stochastic processes could express part or all of it. Therefore, the high-throughput methods described in **Chapter 1** are needed to decipher MuSCs identity and potential sub-states.

Molecular profiling of skeletal muscle stem cells

Once MuSCs existence and role had been elucidated, and the experimental tools for their isolation had been developed, it became feasible to study their molecular state. A seminal study did so using single-cell RT-qPCR to study MuSCs heterogeneity (Cornelison & Wold, 1997) but was limited technically to only a handful of markers. As described in **Chapter 1**, the advent of microarrays permitted a more complex cartography of MuSCs transcriptome. Early skeletal muscle microarrays studies were performed on regenerating whole-muscle (Porter *et al*, 2003; Zhao & Hoffman, 2004; van Lunteren & Leahy, 2007) or cultured myogenic cells (Seale *et al*, 2004; McKinnell *et al*, 2008; Kumar *et al*, 2009). Such approaches, however, cannot capture the reality of quiescent MuSCs *in vivo*. Many laboratories therefore attempted to characterize the molecular state of quiescent and activated MuSCs by comparing freshly-isolated to *in vivo* injury-activated or *ex vivo* culture-activated MuSCs. One report using antibodies-based flow-cytometry comparing freshly-isolated to injury-activated MuSCs found an enrichment for collagens, adhesion molecules and the aforementioned quiescence regulator CALCR in quiescent MuSCs (Fukada *et al*, 2007). Another report performed the same comparison from PAX3-GFP+ MuSCs but also analyzed MuSCs from freshly isolated dystrophic muscles to also obtain a signature of *in vivo* activation. They found that *in vivo* and *ex vivo* activation are markedly different and that quiescent MuSCs were enriched for genes of resistance to xenobiotic and oxidative stress while activated MuSCs were enriched in metalloproteinases and adhesion and matrix remodeling factors (Pallafacchina *et al*, 2010). A third microarray study was more recently performed on freshly-isolated MuSCs, this time compared to *in vivo* activated MuSCs after BaCl₂ injury and discovered that quiescent MuSCs were enriched in genes related to regulation of transcription and cell adhesion while activated MuSCs were enriched in genes related to cell cycle, wound healing and chemotaxis (Liu *et al*, 2013). Moreover, this last study also performed histone modifications ChIP-sequencing and found that MuSCs activation was associated with increased deposition of the silencing mark H3K27me₃ on genes promoter (Liu *et al*, 2013).

Mirroring the evolution of transcriptomic technologies, MuSCs high-throughput analyses switched from microarrays analysis to RNA-sequencing. This prompted the discovery of the metabolic switch from fatty-acid oxidation to glycolysis mentioned earlier by comparing freshly-isolated MuSCs to cultured-activated MuSCs (Ryall *et al*, 2015).

The last development in the transcriptomic analysis of MuSCs was the transition from bulk to single-cell analysis in order to assess population heterogeneity. The first of such studies found a surprising amount of heterogeneity in the MuSCs population, notably for the myogenic regulators PAX7 and MYOD1 (Cho & Doles, 2017). However, the low number of cells analyzed prevented any robust analysis. The Mouse Cell Atlas (Han *et al*, 2018) and the Tabula Muris cell atlas (Schaum *et al*,

2018) solved this conundrum by providing high-profile, high-quality cellular atlases encompassing MuSCs. Finally, two skeletal muscle specific publications completed this list with similar datasets (Dell'Orso *et al*, 2019; Giordani *et al*, 2019).

While these reports provided invaluable results to our field, some discrepancies in the data could not be ignored. Most of the aforementioned high-throughput studies compare freshly-isolated to injury-activated or culture-activated MuSCs. Despite comparing quiescent to activated MuSCs, many stress-response genes, oncogenes, cycling related genes or heat-shock proteins are found enriched in quiescent MuSCs, with a signature highly overlapping with the IEGs evoked in **chapter 2**. Such a signature is extremely surprising for cells supposedly in a dormant state and far from the low-profile molecular state expected from quiescent cells (Cheung & Rando, 2013). One hypothesis is that quiescent MuSCs accumulate inactive activatory transcripts in order to unleash rapidly their activatory response when required. While this “poised state” hypothesis might turn true for some transcripts, especially in light of some recent reports (Crist *et al*, 2012; de Morrée *et al*, 2017), it is not entirely satisfactory when applied genome-wide. One critical piece of evidence is that many of these discrepant transcripts are mitogens-response genes and/or growth-factors response genes such as the members of the AP-1 family C-JUN and C-FOS (Herschman, 1991). Given that these genes are induced at high levels in less than 30 minutes when cells are stimulated with mitogenic signals (Amit *et al*, 2007) and that most MuSCs isolation protocols take more than 2-3 hours to perform, it is tempting to hypothesize that the presence of these transcripts in freshly-isolated quiescent MuSCs transcriptome could represent an artefact of the isolation procedure. If true, freshly-isolated MuSCs therefore deviates from their *in vivo* nature and might not represent a great model to study quiescence. Confirming this hypothesis, three reports identified these IEGs as dissociation-induced in freshly-isolated MuSCs (van den Brink *et al*, 2017; Machado *et al*, 2017; van Velthoven *et al*, 2017). Two of these reports harnessed methods presented in **Chapter 2** - *in situ fixation* and nascent mRNA profiling - to describe the first accurate quiescent MuSCs transcriptome. It was found that indeed, freshly-isolated MuSCs highly induce IEGs expression as well as markers of myogenic program initiators such as *Myod1*. Also, it highlighted the pathways induced in quiescent MuSCs but repressed upon dissociation such as fatty-acid oxidation, cilium related processes or Notch signaling (Machado *et al*, 2017).

Results

Part I: In Situ Fixation Redefines Quiescence and Early Activation of Skeletal Muscle Stem Cells

Machado et al. 2017

Cell Reports, Volume 21, Issue 7, 1982 - 1993

Part II: Dissociation Distorts the Profile of Isolated Cells and Drives Quiescent Muscle Stem Cells to an Activated State

Machado et al. 2019

Manuscript in preparation

Part I: *In Situ* Fixation Redefines Quiescence and Early Activation of Skeletal Muscle Stem Cells

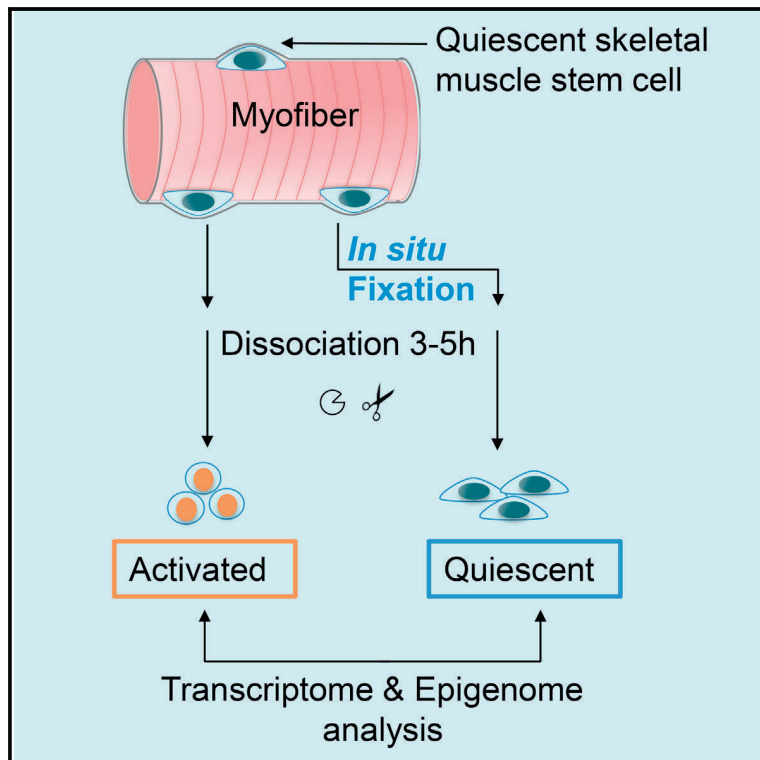
Machado et al. 2017

Cell Reports, Volume 21, Issue 7, 1982 - 1993

Cell Reports

***In Situ* Fixation Redefines Quiescence and Early Activation of Skeletal Muscle Stem Cells**

Graphical Abstract



Authors

Léo Machado, Joana Esteves de Lima, Odile Fabre, ..., Romain Barrès, Frédéric Relaix, Philippos Mourikis

Correspondence

frederic.relaix@inserm.fr

In Brief

Machado et al. demonstrate that muscle stem cells undergo changes in transcripts and histone modifications during isolation. The authors develop an *in situ* fixation-based methodology, which allows capture of cells in their native state. In light of these findings, some high-throughput analyses of tissue extracted cells may need to be revisited.

Highlights

- Quiescent muscle stem cells undergo major transcriptomic alterations during isolation
- Isolation induces histone H3 modifications but leaves intact DNA methylation
- *In situ* fixation allows isolation of quiescent cells in their native, *in vivo* state
- *In situ* fixation detects quiescence and early activation factors

Data and Software Availability

GSE103162
GSE103163
GSE104543
GSE103164



Machado et al., 2017, Cell Reports 21, 1982–1993
November 14, 2017 © 2017 The Author(s).
<https://doi.org/10.1016/j.celrep.2017.10.080>

CellPress

In Situ Fixation Redefines Quiescence and Early Activation of Skeletal Muscle Stem Cells

Léo Machado,¹ Joana Esteves de Lima,^{1,5} Odile Fabre,^{2,5} Caroline Proux,³ Rachel Legendre,^{3,4} Anikó Szegedi,¹ Hugo Varet,^{3,4} Lars Roed Ingerslev,² Romain Barrès,² Frédéric Relaix,^{1,6,*} and Philippos Mourikis¹

¹Biology of the Neuromuscular System, INSERM IMRB U955-E10, UPEC, ENVA, EFS, Creteil 94000, France

²Novo Nordisk Foundation Center for Basic Metabolic Research, Faculty of Health and Medical Sciences, University of Copenhagen, Copenhagen, Denmark

³Institut Pasteur, Plate-forme Transcriptome & Epigénome, Biomix, Centre d'Innovation et Recherche Technologique (Citech), Paris, France

⁴Institut Pasteur, Hub Bioinformatique et Biostatistique, Centre de Bioinformatique, Biostatistique et Biologie Intégrative (C3BI, USR 3756 IP CNRS), Paris, France

⁵These authors contributed equally

⁶Lead Contact

*Correspondence: frederic.relaix@inserm.fr
<https://doi.org/10.1016/j.celrep.2017.10.080>

SUMMARY

State of the art techniques have been developed to isolate and analyze cells from various tissues, aiming to capture their *in vivo* state. However, the majority of cell isolation protocols involve lengthy mechanical and enzymatic dissociation steps followed by flow cytometry, exposing cells to stress and disrupting their physiological niche. Focusing on adult skeletal muscle stem cells, we have developed a protocol that circumvents the impact of isolation procedures and captures cells in their native quiescent state. We show that current isolation protocols induce major transcriptional changes accompanied by specific histone modifications while having negligible effects on DNA methylation. In addition to proposing a protocol to avoid isolation-induced artifacts, our study reveals previously undetected quiescence and early activation genes of potential biological interest.

INTRODUCTION

The microenvironment of a cell can have a major impact on its properties. Both during physiological and pathological conditions, cell-to-cell contacts, paracrine signaling, oxygen and nutrient availability, extracellular matrix, and mechanical stress impact cells and influence their behavior (Rojas-Ríos and González-Reyes, 2014). This is especially true for stem cells, which, due to their plasticity, can radically alter their proliferation and differentiation state in response to changes in their niche. Based on this premise, a large number of studies have used cells directly isolated from the tissue of interest instead of using cultured or otherwise manipulated cells. However, the extent and nature of the actual modifications that arise in cells during the isolation procedure are unknown, calling into question

whether analyses reported to date fully reflect the physiological status.

Adult stem cells can assume different cellular states, either quiescent or proliferating (Liu and Clevers, 2010). Quiescent stem cells are arrested in a reversible, non-cycling phase, and the cellular and molecular mechanisms that maintain this state remain largely undetermined. To understand these mechanisms, it is important to obtain a precise view of the transcriptomic and epigenetic landscapes of these cells present in their native *in vivo* state. With this goal, we have developed a protocol that relies on paraformaldehyde (PFA) fixation of the tissue prior to cell isolation, enabling capture of the molecular state of the cells as found in their niche. We have applied this *in situ* fixation technique to skeletal muscle stem cells (MuSCs), which are an indispensable stem cell population for regenerating injured or diseased muscle as well as maintaining tissue homeostasis (Zammit et al., 2004). Adult MuSCs are G0 arrested, and their quiescent niche is largely defined by a confined anatomical location, as these cells are positioned between the membrane of the myofiber and the overlying basement membrane. Disturbance of the niche, which occurs during muscle injury or experimental extraction, triggers activation of the MuSCs. Activation is manifested by an exit from G0 into a prolonged G1-phase (25–35 hr) (Mourikis et al., 2012; Rocheteau et al., 2012), phosphorylation of p38 α / β mitogen-activated protein kinase, expression of the muscle regulatory factor MYOD (Jones et al., 2005; Zhang et al., 2010), and an increase in cellular volume (Rodgers et al., 2014). Therefore, MuSCs provide a suitable model for investigating the putative consequences of isolation procedures on the molecular signature of a cell.

In this study, we show that massive changes in transcript composition occur during MuSC purification. These changes do not involve alterations in DNA methylation but are associated with histone H3 modifications. By eliminating isolation-induced artifacts, we provide a precise quiescence signature of MuSCs and also identify putative regulators of early activation. Finally, this study describes an efficient and affordable method to isolate molecularly preserved cells amenable to

whole-genome analyses that could be applicable to a broad range of cell types.

RESULTS

Analysis of G0-Fixed MuSCs Isolated with the *In Situ* Fixation Protocol

For the isolation of MuSCs using standard protocols, muscles are dissected, mechanically minced into 1- to 2-mm pieces, and subsequently incubated with proteolytic enzymes at 37°C for up to 2 hr to allow detachment of the myofiber bundles and dissociation of the MuSCs (Figure 1A). Following several steps of washes and filtrations, MuSCs are isolated by fluorescence-activated cell sorting (FACS), based on specific plasma membrane receptors or genetically expressed fluorescent markers (Liu et al., 2015).

In order to isolate quiescent MuSCs, muscles were fixed *in situ* by ice-cold 0.5% PFA before cell dissociation (Figure 1A; Supplemental *In Situ* Fixation Protocol; Supplemental Experimental Procedures). We refer to these fixed cells as time-zero stem cells (T0-SCs) and the cells isolated by the standard 3-hr-long protocol as T3-SCs. We applied both the standard and the *in situ* fixation protocols for the isolation of MuSCs from transgenic *Tg:Pax7-nGFP* mice, in which nuclear GFP is expressed in MuSCs (Sambasivan et al., 2009) (Figure 1B). The purity of the isolated fixed cells was assessed by PAX7 staining and was similar to that of the cells isolated using the standard protocol ($94\% \pm 3.1\%$ and $92\% \pm 1.4\%$ of PAX7⁺ cells for T3- and T0-SCs, respectively; Figure S1A). Notably, equivalent numbers of GFP⁺ cells were isolated from fixed and fresh muscles, indicating that *in situ* fixation did not lead to loss of cells (Figures 1B and S1B).

To ensure that the T0-SCs had been properly fixed and were biologically inert, we assessed their proliferation capacity by measuring incorporation of 5-ethynyl-2'-deoxyuridine (EdU), *de novo* RNA synthesis by the presence of the modified nucleotide ethynyl uridine (EU), and uptake of DAPI, a compound actively excluded from live cells. As expected for fixed cells, the T0-SCs did not incorporate EdU (Figure 1C), were transcriptionally inactive (Figure 1D), and were positive for DAPI (Figures S1C and S1D). Of note, the light scattering of T0-SCs was drastically different compared to the non-fixed T3-SCs, suggesting differences in the morphological complexity of the isolated cells. Indeed, MuSCs have a small cytoplasmic/nuclear ratio and *in vivo* are spindle shaped, with multiple branches emanating from their poles. Upon detachment from the myofibers, the stretched plasma membrane retracts to form small, round, uniform cells (Figure 1B, bottom left). Instead, when fixed, the dissociated MuSCs exhibit a complex morphology (Figure 1B, bottom right), possibly reflecting that found *in vivo*, as has been shown for fixed cardiomyocytes (Mollova et al., 2013). To confirm the differences in cell shape inferred from light scattering, we used the lectin marker WGA (wheat germ agglutinin) to stain cell membranes of T0- and T3-SCs (Figure 1E). Using an image-processing software (see Experimental Procedures), we calculated the mean eccentricity of T0- and T3-SCs, a circle having an eccentricity of 0 and a straight line of 1. Interestingly, we found that *in situ* fixed T0-SCs have a mean eccentricity

significantly greater than that of T3-SCs (0.80 ± 0.009 versus 0.40 ± 0.013), corroborating that *in situ* fixation retains the physiological spindle shape of MuSCs that is lost during the conventional dissociation protocol (Figure 1E).

In summary, we have developed a protocol that allows efficient isolation of MuSCs from fixed tissue, with comparable purity and yield to those of non-fixed muscles. Moreover, we show that the cells isolated from PFA-treated samples are efficiently fixed and, hence, safeguarded from the strong stimuli to which they are exposed during the dissociation procedure.

PFA Fixation Does Not Alter mRNA Yield, Quality, and Composition

Having developed a method to isolate a highly pure population of *in situ* fixed MuSCs, we then sought to analyze its transcriptional profile. First, however, a series of experiments was performed to measure the putative effects of PFA fixation on mRNA quality and composition. As shown in Figure 2A, fresh muscles from *Tg:Pax7-nGFP* mice were digested, and GFP⁺ MuSCs were isolated by FACS. Subsequently, half of the sorted MuSCs were immediately lysed, and the other half were fixed in 0.5% PFA before being lysed for RNA extraction. Of note, RNA extraction from fixed cells was optimized (Experimental Procedures), as standard protocols were not suitable (data not shown). We found that the RNA quality was not compromised by fixation, as the RNA integrity numbers (RINs) were similar between the fixed and non-fixed T3-SCs (Figure 2B). Moreover, RNA yields were comparable between fixed and non-fixed T3-SCs (Figure 2C). In order to extend our comparison, the extracted RNA was subjected to next-generation RNA sequencing (RNA-seq). Analysis of the distribution of the sequencing reads to all genes showed no 5' or 3' bias for the fixed or the non-fixed T3-SCs, further indicating that the fixation protocol did not interfere with RNA integrity (Figure 2D). Also, the mRNA composition of fixed and live T3-SCs transcriptomes were highly similar, as only 3 differentially expressed genes were identified (Figure 2E). Finally, the simple error ratio estimate (SERE) statistic (Schulze et al., 2012) and principal-component analysis demonstrated high similarity between live and fixed T3-SCs (Figures 2F, S2A, and S2B). In conclusion, the quality and composition of the total RNA extracted from 0.5% PFA-fixed MuSCs is comparable to those from non-fixed cells and suitable for transcriptomic analysis.

Significant Transcriptional Alterations Are Induced during the MuSC Isolation Protocol

We compared the transcripts of T0-SCs (*in situ* fixed), T3-SCs (standard isolation protocol), and time-five (T5)-SCs (Figures 3A and 3B). T5-SC samples were prepared from minced muscles incubated for an additional 2 hr (total preparation, 5 hr) at 37°C, aiming to capture secondary-response genes (Herschman, 1991) (Figure S3A). Of note, both T3- and T5-SCs were fixed following FACS isolation in order to ensure comparability with T0-SC RNA preparations.

Comparison of the T0-, T3-, and T5-SC transcriptomes demonstrated that the standard MuSC isolation procedure induced significant transcriptional changes. Strikingly, a large number of genes showed strong transcript inductions during

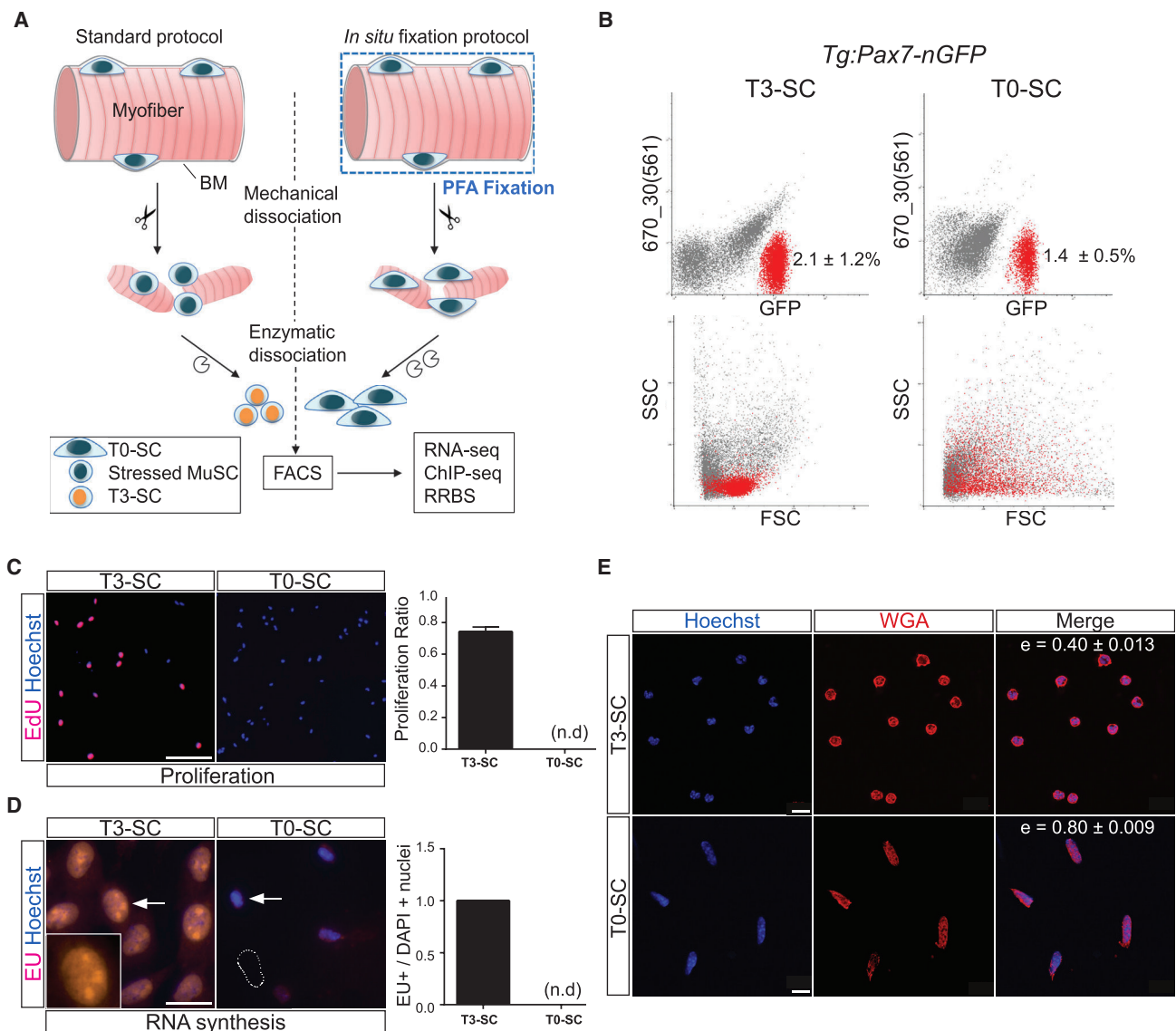


Figure 1. Isolation of MuSCs in a Fixed, G0-Arrested State

(A) Graphical scheme of the *in situ* fixation protocol for MuSCs isolation and comparison to the standard protocol. A detailed description of the protocols is available in the [Supplemental Information](#). BM, basement membrane; T0-SC, time-zero/quiescent MuSC; T3-SC, time 3 hr/activated MuSC.

(B) FACS profiles of non-fixed (T3-SC) and fixed (T0-SC) GFP⁺ MuSCs from *Tg:Pax7-nGFP* muscle preparations. Sorted GFP⁺ cells are marked as red dots in all plots. SSC, side scatter; FSC, forward scatter. Values on the plots indicate mean percentage of sorted GFP⁺ cells of the total number of events, excluding small SSC/FSC and doublets; n = 5.

(C) Proliferation of FACS-isolated T3-SCs and T0-SCs cultured for 48 hr and stained with EdU (24-hr chase); n = 3. EdU⁺ cells: 0% for T0-SCs and 74% ± 0.03% for T3-SCs.

(D) Nascent RNA synthesis in FACS-isolated T3-SCs and T0-SCs cultured for 48 hr and incubated with labeled ethynyl uridine (EU) ribonucleoside for 2 hr; n = 3. Average of 80 nuclei counted per sample, 100% EU⁺ and EU⁻ for T3-SC and T0-SC, respectively. Dotted line delineates cell's nucleus.

(E) Morphology of T3 and T0 MuSCs immediately after the FACS. Cells were spun on Matrigel-coated slides, and membranes were stained with the lectin marker WGA (wheat germ agglutinin). Mean eccentricity of the cells was computationally calculated ([Experimental Procedures](#)).

Data are reported as mean ± SD; n.d., not detected. Scale bars, 90 μm in (C), 20 μm in (D), 8 μm in (D, insets), and 10 μm in (E). See also [Supplemental Information](#).

the isolation (2,822 T3/T0 upregulated genes with a fold change [FC] > 2 and a false discovery rate [FDR] < 0.05), whereas the changes were moderate between the T3 and T5 time points (222 T5/T3 upregulated genes; FC > 2, and FDR < 0.05) ([Figures 3A, 3B, and S3B; Table S1](#)). Of interest, a large number of

transcripts was downregulated during the isolation process (4,840 T3/T0 downregulated genes; FC > 2, and FDR < 0.05), suggesting that RNA degradation mechanisms, in addition to attenuation of transcription, may operate at the early phases of MuSC activation.

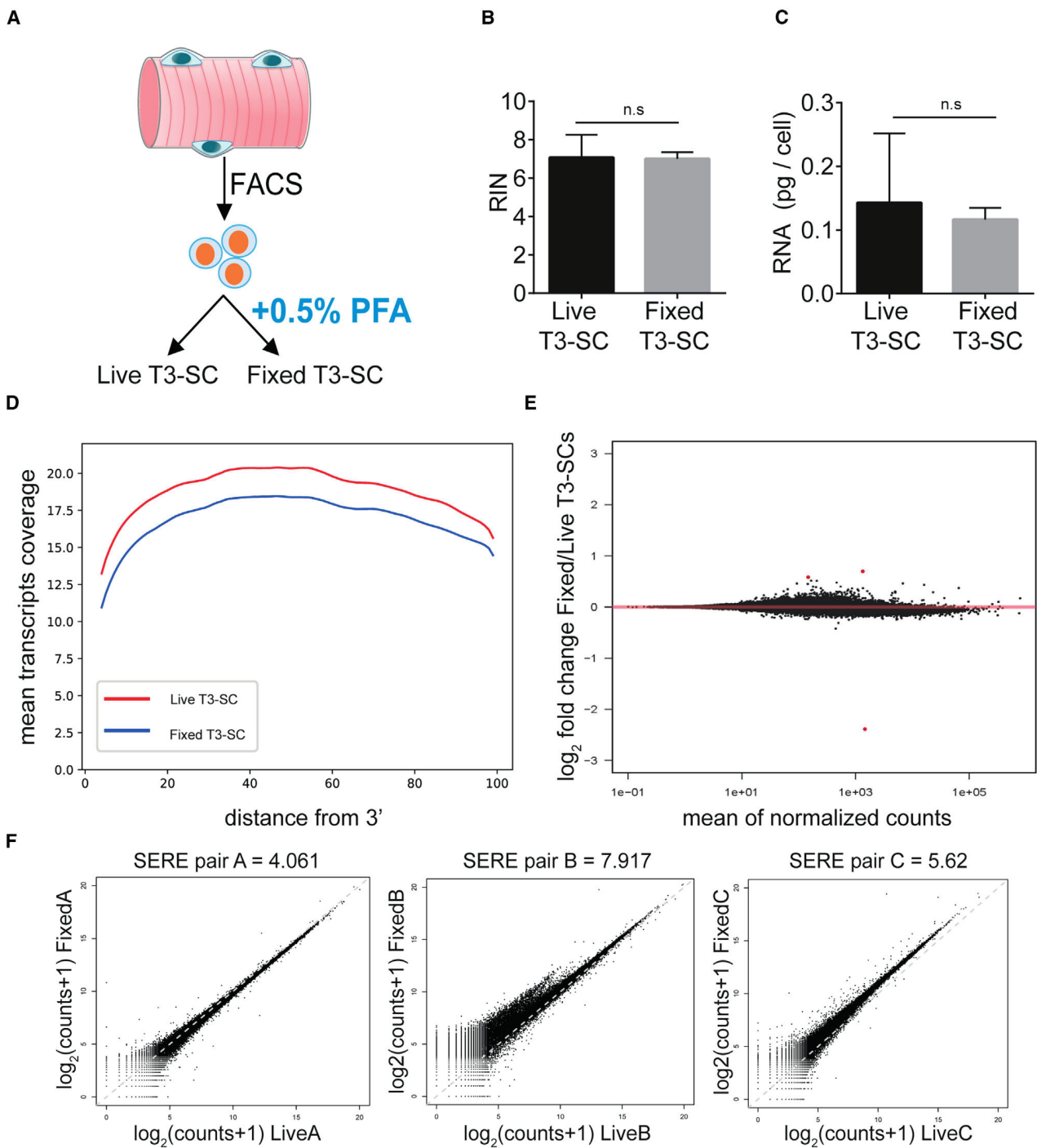


Figure 2. Assessment of the Effects of PFA Fixation on RNA Quality and Composition

(A) Graphical scheme of the procedure for the isolation of non-fixed (Live T3-SC) and fixed MuSCs (Fixed T3-SC). Following the standard protocol, half of the FACS-isolated MuSCs were fixed in 0.5% PFA for 30 min, and total RNA was extracted and compared to that of live T3-SCs.

(B) Mean RNA integrity numbers of live and fixed T3-SCs.

(C) Mean of total RNA recovered per cell in live and fixed T3-SCs preparations, calculated with the Bioanalyzer 2100.

(D) Normalized distribution of the sequencing reads to the predicted transcripts length (5' to 3').

(legend continued on next page)

Gene ontology analysis for biological processes of the T3/T0 upregulated genes (early response and dissociation-induced genes) showed a transcriptional signature consistent with a transition from quiescence to activation and proliferation, with enriched rRNA maturation and cell-cycle re-entry terms (Figure 3C; Table S1). Instead, the signature of the T3/T0 downregulated transcripts (quiescence-enriched genes) included genes related to fatty-acid metabolism, in agreement with the metabolic switch from fatty-acid oxidation to glycolysis taking place during MuSC activation (Ryall et al., 2015) (Figures 3C and 3D). The GO analysis also highlighted genes related to cilia as quiescence enriched, a structure described to be present in quiescent MuSCs but disassembled in the activated cells (Jaafar Marican et al., 2016) (Figure 3C).

The comparison between the T0 and T3 transcriptomes identified MuSC activation-induced genes already described, validating our approach but also revealing that these changes occur earlier than previously estimated. Within just 3 hr, the downstream targets of Notch signaling *Hes1* and *HeyL* were decreased by 5- and 8-fold, respectively, consistent with what has been reported for *in-vivo*-activated MuSCs at 20 hr post-injury (Mourikis et al., 2012). Similarly, the hallmark MuSC gene *Pax7*, whose encoded protein marks both stem and progenitor muscle cells, was found 10-fold downregulated in T3-SCs, supporting a quiescence-specific function of this paired-type homeodomain transcription factor. Instead, expression of the muscle regulatory factor *Myod* was rapidly upregulated 10-fold in T3-SCs. As shown in Figure 3D, the dissociation procedure also induced the expression of early response genes, which are known to be transiently activated in response to a variety of stimuli (Herschman, 1991). Among these, we found members of the *Immediate early response* *ler-2*, *-3*, *-5*, and *-5l* and *Early growth response* genes *Egr-1*, *-2*, and *-3*. Also, in the T3-SCs, which correspond to the MuSCs isolated to date by the standard protocols, we found an over-representation of a number of oncogenes, like *c-myc* and *Maff* and also members of the AP-1 transcription factor family, like *c-Fos*, *c-Jun*, and others (Figure 3D). To investigate the functional role of AP-1 in the early activation of quiescent MuSCs, we incubated freshly isolated cells in the presence of the pathway inhibitor SR-11302 (Fanjul et al., 1994; Huang et al., 1997). We found that SR-11302 resulted in a 3-fold decrease of proliferating cells after 48 hr in culture, indicating that AP-1 is involved in the exit of MuSCs from quiescence (Figures S3C and S3D).

The *in-situ*-fixed MuSC transcriptome enabled us to identify potentially important quiescence factors that were previously missed, due to their sharp downregulation during the isolation process. Of interest, we uncovered a substantial number of zinc finger protein-encoding genes (223 in total [FC > 2, and FDR < 0.05], of which 143 had at least one transcriptional repression Krüppel Associated Box (KRAB) domain and 182 had at least one DNA-binding zinc finger C2H2 type [ZNF-C2H2] motif). Also, we identified a large group of *Hox-a*, *-b*, and *-c* genes and,

further, confirmed them as quiescence specific. We validated by immunofluorescence the differential expression of HOXA9, which we found present in quiescent but absent in activated MuSCs following muscle injury (Figure 3E). Our observation suggests a role of HOXA9 in quiescence, extending a recent study that found HOXA9 absent in freshly isolated and activated MuSCs (Schwörer et al., 2016).

Paradoxically, several proto-oncogenes, including the AP-1 members, have been proposed as quiescence enriched, based on comparisons between freshly isolated and tissue-cultured or *in-vivo*-activated and even proliferating MuSCs (Fukada et al., 2007; Liu et al., 2013; Pallafacchina et al., 2010). In fact, on average, 21% of the microarray-based quiescent signatures reported in the literature (transcripts enriched in freshly isolated MuSCs, FC > 5) correspond to genes that we found as specific for the T3-SC transcripts (Figure 3F) and, hence, are not quiescence-related genes but, instead, consist of early-activation- and isolation-induced artifacts. Of note, the fact that these genes were found at higher levels in the freshly isolated cells than in the activated and/or proliferating cells indicates that they could constitute transiently and highly induced transcripts, a characteristic feature of early-response genes (Amit et al., 2007).

Overall, only 34%, on average, of the T0/T3 downregulated transcripts were present in the microarray-based published quiescent signatures reported earlier (Figure 3F) and 16% in a more recent RNA-seq-based study (Ryall et al., 2015) (Figure 3G). Taken together, despite any bias introduced by technical and biological differences among samples, these comparisons underscore the fact that the majority of the quiescence-enriched transcripts that we identified by the *in situ* fixation technique were missed by the standard protocols. Overall, our data highlight that the presumably quiescent MuSCs isolated and analyzed to date are, in fact, already activated, with a transcriptional profile that diverges significantly from that of the MuSCs in their niche *in vivo*.

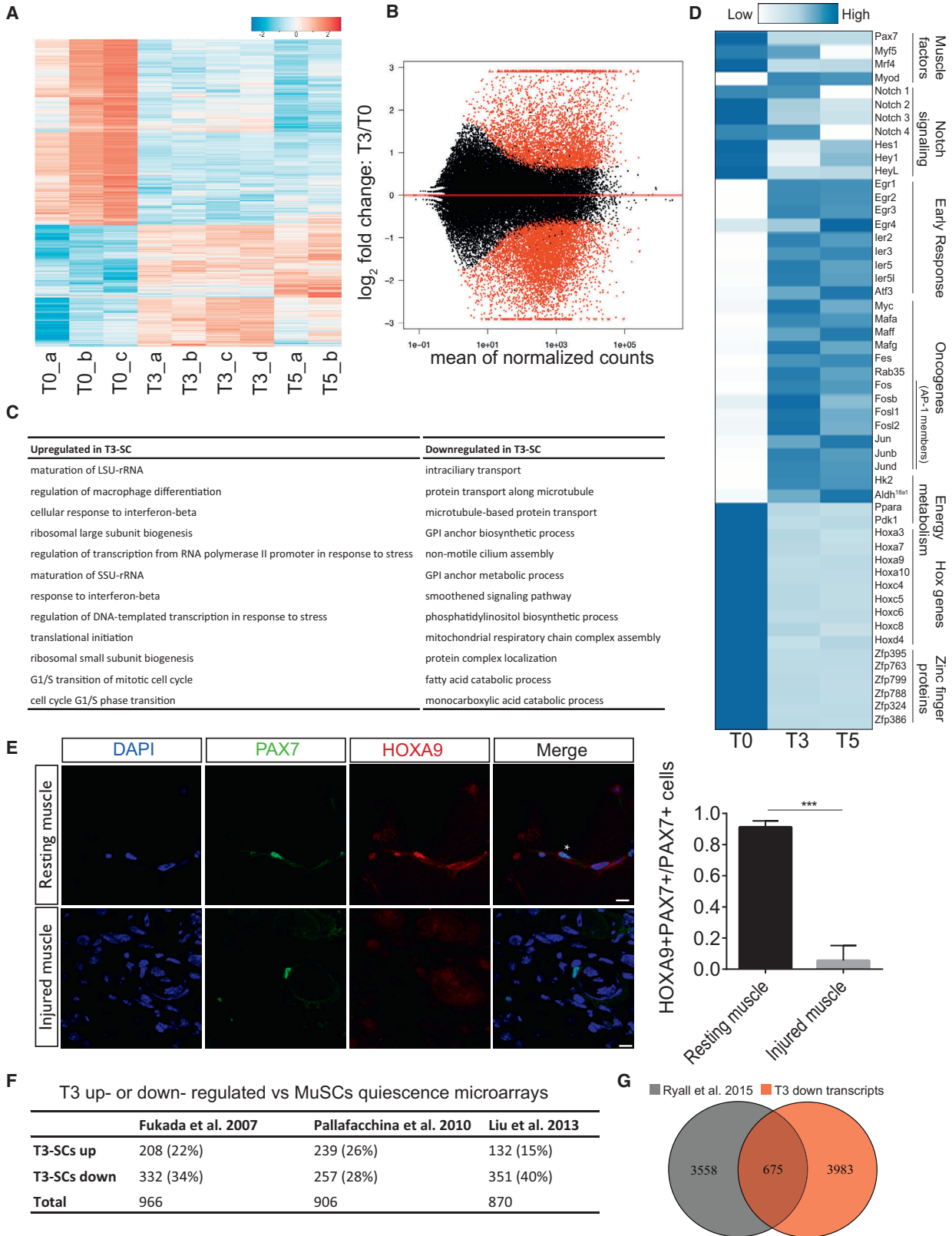
The *In Situ* Fixation Protocol Is Compatible with MuSC-Antibody-Based Cell Sorting

To validate the adequacy of our *in situ* fixation protocol for the isolation of cells devoid of transgenic fluorescent markers, we applied antibody-based cell sorting of T0- and T3-SCs, using a published protocol (Pannérec et al., 2013; Figure 4A). Both T0- and T3-SC populations sorted with this strategy presented a similarly high purity of MuSCs, as assessed by PAX7 immunostaining (94% ± 0.6% and 94% ± 1.9 for T0- and T3-SCs, respectively) (Figures 4B and 4C). To ensure that the transcriptional changes observed by the T0/T3 comparisons from *Tg:Pax7-nGFP* muscles were reproducible on antibody-sorted MuSCs, we performed qRT-PCR analysis on a set of 24 differentially expressed genes (12 up- and 12 downregulated genes). Notably, all tested transcripts displayed a highly similar pattern and level of expression in the antibody-sorted T0- and T3-SCs, compared to their GFP⁺-sorted counterparts (Figure 4D). Using

(E) MA plot of live versus fixed T3-SCs RNA-seq data. Only three significantly deregulated transcripts (FDR < 0.05) were identified and are highlighted in red; n = 3.

(F) Simple error ratio estimate (SERE) coefficient for the three sets of paired live and fixed T3-SC RNA-seq samples (pairs A, B, and C). For comparison, a matrix table with the SERE coefficients between all the samples used in this study is shown in Figure S2A.

n.s., not significant. Data are reported as mean ± SD. See also Figure S2.



(legend on next page)

two completely independent approaches (RNA-seq on GFP⁺ cells from *Tg:Pax7-nGFP* mice and qRT-PCR on antibody-sorted cells), we obtained the same gene responses, thus cross-validating the RNA-seq results and the antibody-based isolation on fixed MuSCs. In conclusion, the *in situ* fixation protocol is compatible with antibody-based cell sorting for the aforementioned antigens and, depending on the antigens, should be applicable to other sorting strategies.

MuSC Isolation Protocols Induce Specific Histone Modification Changes but No DNA Methylation Changes

A comprehensive characterization of the epigenetic landscape of a cell allows the functional annotation of the genome and delineates the determinants of cell identity (Barrero et al., 2010). Histone modifications and DNA methylation are among the most studied epigenetic alterations. To gain insights on the epigenetic features of quiescent MuSCs, the quiescence-to-activation transition, but also to investigate the compatibility of the *in situ* fixation protocol to diverse high-throughput techniques, we performed chromatin immunoprecipitation (ChIP) sequencing (ChIP-seq) for histone H3 modifications and DNA methylation analysis by reduced representation bisulfite sequencing (RRBS) on T0-SCs and T3-SCs.

H3 lysine 4 trimethylation (H3K4me3) is a marker of active transcription on promoters (Barski et al., 2007), while acetylation on lysine 27 (H3K27ac) has been associated with active enhancers (Creyghton et al., 2010). Other H3 modifications have been linked to transcriptional repression, such as H3K27me3, which is associated with promoters of silenced genes (Barski et al., 2007). Of interest, we observed that the isolation procedure was sufficient to induce a global increase of H3K4me3 on promoters (Figure 5A; Table S2), concomitantly with a decrease of H3K27ac levels on distal enhancers (Figure 5B; Table S2). In T3-SCs, we identified 14,518 promoters with H3K4me3 peaks, compared to 11,597 promoters in the quiescent T0-SCs. Of note, during the isolation procedure, essentially all (99.9%) H3K4me3-labeled promoters kept their methylation mark, and many (2,936) newly labeled promoters were identified (Figure 5A). Representative examples of gain of H3K4me3 at promoters are shown in Figure 5C for *Fosl* and *Egr3*, two primary response genes identified as isolation induced (Figure 3D). Moreover, using H3K27ac ChIP-seq, we found 5,909 genes in T0-SCs and 4,031 in T3-SCs with at least one associated active distal enhancer (Figure 5B).

Similarly, examples of net decrease of H3K27ac are shown in Figure 5D, around the Notch signaling downstream target *Hes1* and the MuSCs hallmark gene *Pax7*.

The observation that almost every H3K4me3⁺ promoter in T0-SCs is also labeled in T3-SCs indicated that transcriptional silencing induced during isolation is not mediated by the loss of H3K4me3. Gain of repressive marks, such as H3K27me3, could provide an alternative mechanism of transcriptional repression, although its presence in MuSCs is controversial (Boonsanay et al., 2016; Liu et al., 2013). Our ChIP-seq results indicate that MuSCs have almost undetectable levels of H3K27me3, consistent with previous immunofluorescence and ChIP-seq data (Liu et al., 2013), (Figure 5E).

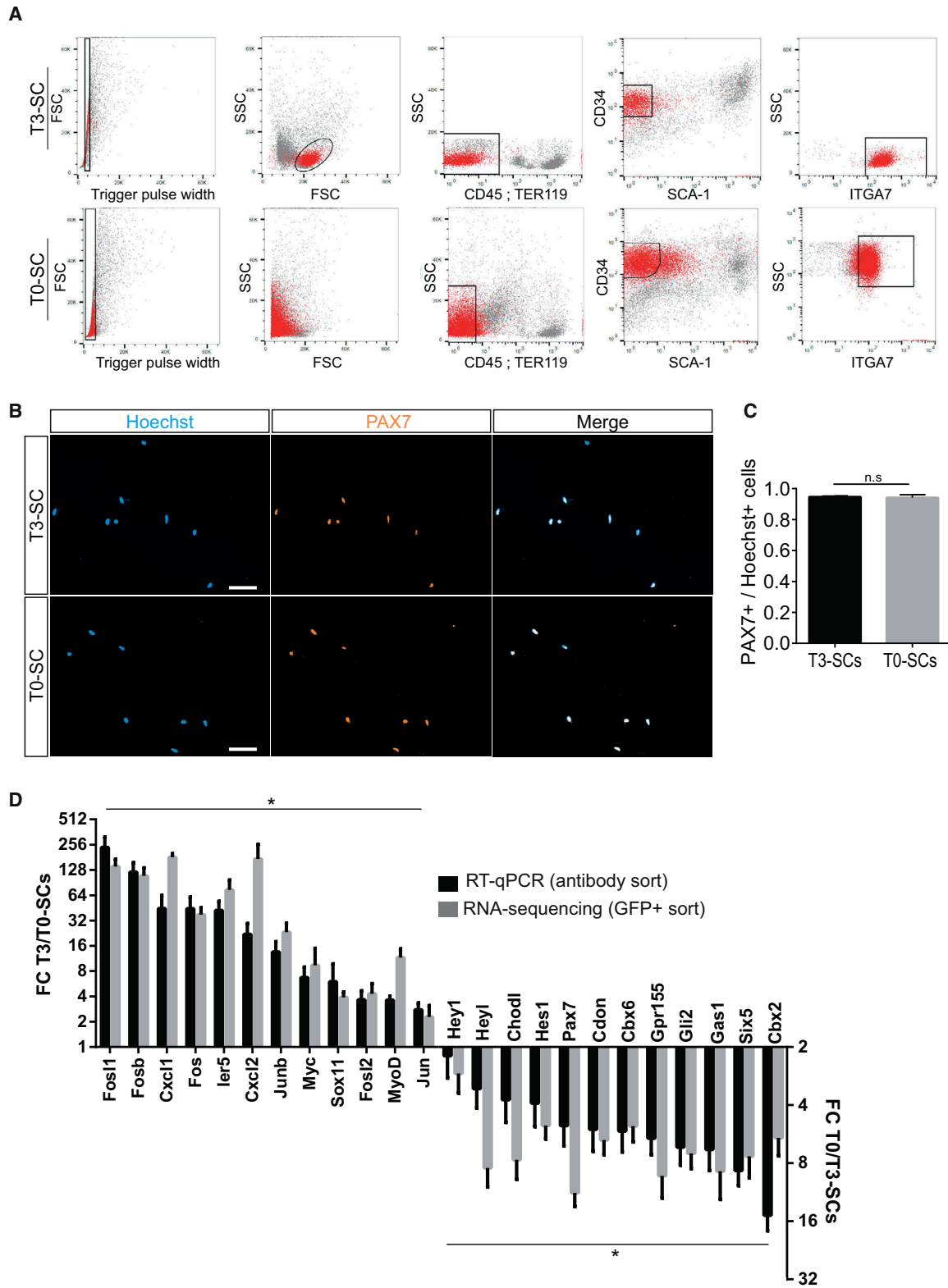
DNA methylation is generally associated with gene silencing (Miranda and Jones, 2007), although the exact effect of methyl groups on enhancers or promoters and transcriptional activity is complex (King et al., 2016). We assessed whether the DNA methylation status in MuSCs was different between T0-SCs and T3-SCs. RRBS, however, detected just 21 out of the 27,878 CpG clusters interrogated as differentially methylated (Figure 5F; Table S2), suggesting that DNA methylation is not a driving force of the transcriptional variations that we observed.

DISCUSSION

The stem cell niche is a critical determinant of a cell's properties. However, all the parameters that constitute the microenvironment are drastically altered when a cell is isolated. Therefore, we hypothesized that the molecular profile of a freshly isolated cell is significantly different from that encountered in its tissue of origin. Indeed, an elegant study, published recently, showed with single-cell analysis on MuSCs that a number of changes do occur during isolation at the levels of transcription and mitochondrial metabolism (van den Brink et al., 2017). In an era when biologists rely increasingly on next-generation sequencing and molecular profiling of cells to study biological phenomena, the isolation-induced alterations could constitute a major technical pitfall for many studies. For transcriptomic analysis, several methods have been developed to overcome this problem. Most of these studies rely on microscopy to infer the composition and topological distribution of transcripts (Chen et al., 2017; Lee et al., 2015; Peng et al., 2016). However, these methods remain technically challenging, costly, and with limited gene coverage. To address this problem, we have developed an

Figure 3. Drastic Transcriptional Changes Occurring during the Dissociation and Early Activation of MuSCs

(A) Heatmap of 12,582 differentially expressed transcripts between T0-SC, T3-SC, and T5-SC based on RNA-seq.
 (B) MA plot of T3-SC over T0-SC RNA-seq data. Significantly deregulated transcripts (FDR < 0.05) are highlighted in red; n = 3 for T0, and n = 4 for T3.
 (C) Gene ontology for biological processes of the up- and downregulated genes. Top 12 enriched terms are presented. All p values < 0.05; individual p values are given in Table S1.
 (D) Heatmap showing average number of normalized reads of T0-SC, T3-SC, and T5-SC RNA-seq data for a selection of genes. n = 3 for T0, n = 4 for T3, and n = 2 for T5.
 (E) Immunostaining of PAX7, HOXA9 and DAPI in resting TA muscles or after cardiotoxin injection (4 days post injury). The arrows indicate PAX7⁺ MuSCs. Scale bars, 10 μm. Quantification is shown on the right. n = 3; ***p < 0.001; data are reported as mean ± SD.
 (F) Comparison between the T3 and T0 differentially expressed transcripts (both directions) and three published MuSC quiescent signatures based on microarrays (Fukada et al., 2007; Liu et al., 2013; Pallafacchina et al., 2010). Percentages depict the overlap of the published quiescent signatures with the T3 and T0 up- or downregulated transcripts (by gene symbols). See Experimental Procedures for details.
 (G) Overlap between the gene symbols of the T3 and T0 downregulated transcripts (quiescence enriched) and a published RNA-seq-based quiescence signature (Ryall et al., 2015).
 See also Table S1.



(legend on next page)

in situ fixation, a protocol for the isolation and downstream analysis of quiescent MuSCs. *In situ* fixation preserves the molecular characteristics of isolated MuSCs and is compatible with RNA-seq, ChIP-seq, and RRBS.

The significant transcriptional and epigenetic modifications that we observed demonstrate that the MuSCs isolated by the standard protocols to date have exited quiescence and are already activated. Hence, our results confirmed what the field had suspected for a long time: the extent of alterations that we observed during the dissociation procedure, however, was much greater than previously assumed. Moreover, our findings further underscore the complications of studying quiescence on isolated cells. The development of tissue culture systems that would revert and maintain cells in a true quiescent state would be valuable for dissecting the molecular mechanisms that orchestrate entry, maintenance, and exit from quiescence. Indeed, several groups have made significant progress toward the development of such systems (Arora et al., 2017; Martynoga et al., 2013; Quarta et al., 2016). Quiescence protocols could also be beneficial for cell-based therapies, as the regenerative potential of cultured, activated cells is inferior to freshly isolated MuSCs (Montarras et al., 2005; Sakai et al., 2017).

Applying *in situ* fixation to MuSCs cells permitted us to detect undescribed quiescence and early activation regulators. Using complementary approaches, a study being published concurrently in this issue of *Cell Reports* found similarly that there are transcriptional changes associated with the process of isolation and purification of MuSCs by FACS (van Velthoven et al., 2017). Building reliable quiescent and activation transcriptional and epigenetic signatures, like the ones presented in this report, could provide a valuable source for understanding and manipulating the quiescent state. Quiescent stem cells, like MuSCs, are probably more prone to dissociation-induced signals, as these cells are specialized to get activated for regeneration, in response to disruption of their niche during damage or in pathological conditions. Nevertheless, it is likely that every cell type, especially from cohesive tissues, will be transcriptionally and epigenetically modified during the isolation procedure. As high-throughput characterization is becoming the predominant method of studying and classifying cell types, *in situ* fixation offers an inexpensive and accessible way to improve the accuracy of cellular and molecular analysis.

EXPERIMENTAL PROCEDURES

Isolation of MuSCs from Fixed and Live Tissue

A detailed protocol is described in the [Supplemental Information](#). For the antibody-based cell sorting, the filtered muscle preparations were addi-

tionally incubated 45 min on ice with conjugated anti-TER119-PECy7 (1.4 μ g/mL; BD Biosciences, #557853), anti-CD45-PECy7 (1.4 μ g/mL; BD Biosciences, #552848), anti-CD34-BV421 (5.6 μ g/mL; BD Biosciences, #562608), anti-SCA-1-PE (3.5 μ g/mL; BD Biosciences, #553108), and anti-ITGA7-Alexa Fluor 700 (0.56 μ g/mL; R&D Systems, #FAB3518N) in DMEM (GIBCO)/0.2% BSA. For T0-SCs, the TER119⁻; CD45⁻; CD34⁺; SCA-1⁻; ITGA7⁺ cells were sorted. For T3-SCs, the same strategy was used, with the addition of an empirical selection on size and granularity (SSC/FSC).

Mice

Eight- to 12-week-old heterozygous female *Tg:Pax7-nGFP* mice were used to isolate MuSCs (Sambasivan et al., 2009). Animals were handled per French and European Community guidelines.

Muscle Injury

For muscle injury, WT mice were anesthetized with 0.5% Imalgene/2% Rompun, and the tibialis anterior (TA) muscles were injected with 50 μ L cardiotoxin (10 mM; Latoxan).

Cell Culture

FACS-isolated T0-SCs and T3-SCs were plated on Matrigel (Corning, #354248)-coated 8-chamber slides (Sarstedt, #94.6140.802) in growth medium (GM) composed of DMEM (GIBCO) with 20% fetal bovine serum (FBS), 1% penicillin/streptomycin (PS; GIBCO), and supplemented with 5 ng/ μ L basic FGF (bFGF; Peprotech, #450-33) at 37°C. To measure proliferation, after 24 hr in culture, cells were pulsed with 10 μ M 5-ethynyl-2'-deoxyuridine (EdU) for 24 hr (EdU Click-iT PLUS Kit C10640, Life Technologies). To assess nascent RNA production, after 46 hr in culture, cells were pulsed with 2 mM 5-ethynyl uridine (EU) for 2 hr (Click-iT nascent RNA imaging kit; Life Technologies, #C10330). EdU and EU labeling was performed according to manufacturer's guidelines. To assess the role of AP-1 pathway activation, the chemical inhibitor SR-11302 (Tocris) was administered at a concentration of 2×10^{-5} M to FACS-isolated MuSCs 24 hr after plating for a duration of 24 hr, including a 4-hr EdU chase.

Immunofluorescence

For cell culture, following fixation (2% PFA, 20 min), MuSCs were washed three times in PBS, permeabilized, and blocked using a blocking solution (BS) containing 2% BSA (Jackson Laboratories), 10% goat serum (GIBCO), and 0.25% Triton X-100 (Sigma) for 30 min at room temperature. The purity of the FACS-isolated cells was assessed with anti-PAX7 antibody (mouse monoclonal; Santa Cruz Biotechnology, #sc-81648) diluted 1:100 in BS and incubated for 16 hr at 37°C. For the membrane staining, WGA was used following manufacturer's guidelines (Thermo Fisher Scientific, #W32464) on T0- or T3-SCs after a 15-min centrifugation (300 \times g, 4°C) on Matrigel (Corning, #354248)-coated 8-chamber slides (Sarstedt, #94.6140.802).

Cryosections of 10 μ m were performed on TA muscles frozen in liquid-nitrogen-cooled isopentane (resting conditions and 4 days post cardiotoxin injury). The sections were fixed in 4% PFA for 15 min at room temperature, permeabilized in cold methanol for 6 min, and boiled in citrate buffer (Dako) for epitope retrieval. To reduce background, the slides were incubated 30 min at room temperature with anti-mouse immunoglobulin G (IgG) Fab fragment (Jackson

Figure 4. Isolation of *In Situ* Fixed MuSCs Using a Combination of Antibodies

- (A) FACS profiles of T0 (fixed) and T3 (non-fixed) MuSCs of *Tg:Pax7-nGFP* mice, isolated based on the TER119⁻; CD45⁻; CD34⁺; SCA-1⁻; Integrin- α 7⁺ selection. Note the scatter pattern of the T0-SCs in the SSC/FSC plot (similar to that in [Figure 1B](#)). The GFP⁺ cells are highlighted in red.
- (B) Freshly FACS-isolated T0- and T3-SCs using an antibody cocktail and stained for PAX7. Scale bars, 60 μ m.
- (C) Quantification of PAX7⁺ cells in isolated MuSCs: 94% \pm 0.6% and 94% \pm 1.9% for T0- and T3-SCs, respectively. Data are presented as means \pm SD. n.s., not significant.
- (D) qRT-PCR analysis on T0 and T3 antibody-based isolated MuSCs for 12 upregulated and 12 downregulated genes (black bars). The targeted transcripts were selected out of the differentially expressed genes from the T0- and T3-SCs RNA-seq analysis (gray bars). For qRT-PCR, data are presented as normalized T3/T0 transcript ratios ($2^{-\Delta\Delta C_t}$) using the mean of *Tbp1* and *Hprt* housekeeping genes. FC, fold change. Data are presented as means \pm SD. * p < 0.05, with a correction for a FDR of 5%.

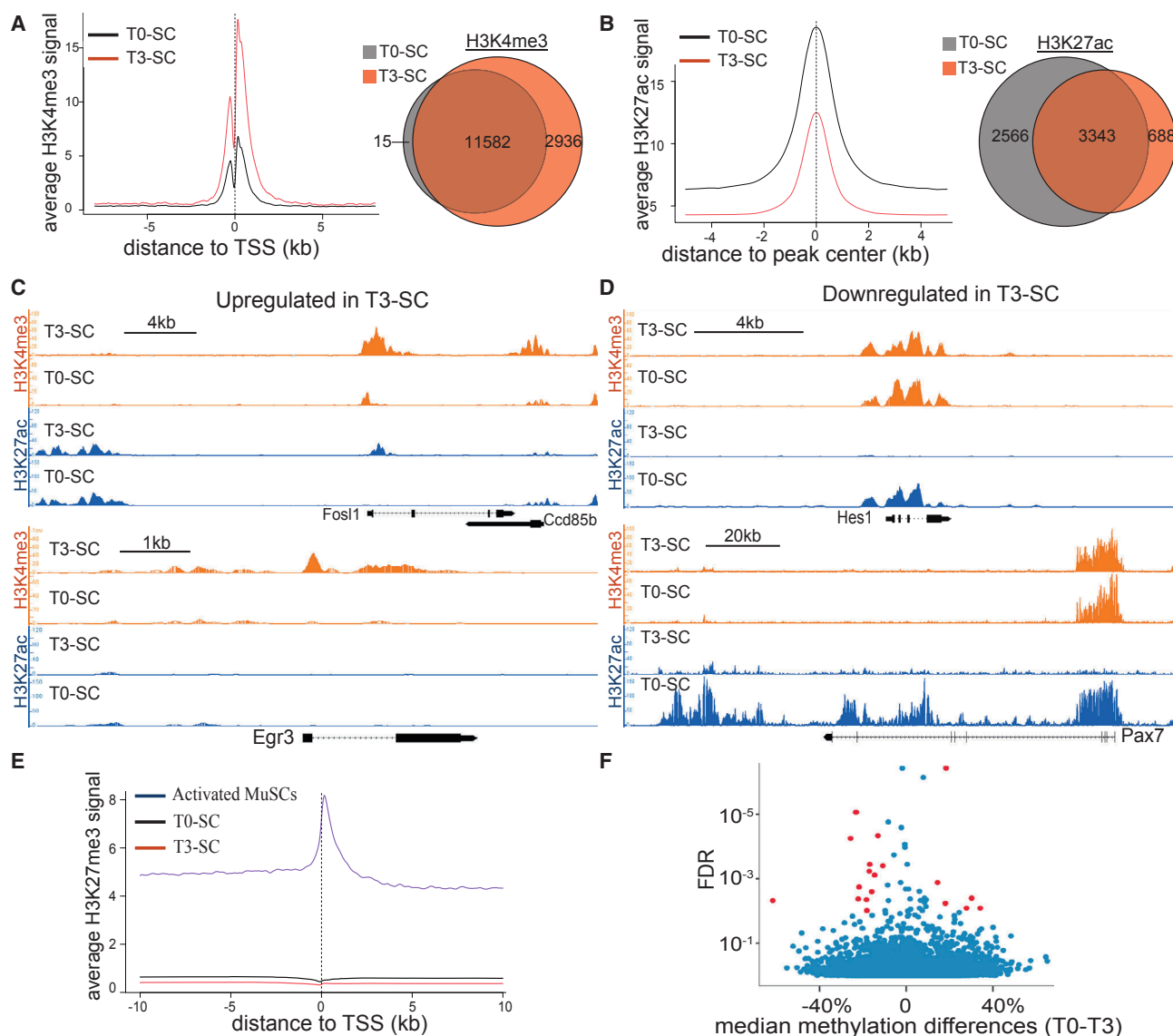


Figure 5. Histone H3 Modifications and DNA Methylation during Early MuSCs Activation

(A) Left: H3K4me3 ChIP-seq averaged signal at promoters. Right: overlap between T0-SC and T3-SC genes with H3K4me3 peaks at promoters. TSS, transcription start site.

(B) Left: H3K27ac ChIP-seq averaged signal at active distal enhancers (H3K27ac peaks outside gene body) from T0-SC and T3-SC samples. Right: overlap of genes that present at least one distal enhancer between T0-SCs and T3-SCs.

(C) Examples of H3K4me3 and H3K27ac ChIP-seq tracks from T3 and T0 upregulated genes *Fos1* and *Egr3*.

(D) Examples of H3K4me3 and H3K27ac ChIP-seq tracks from T3 and T0 downregulated genes *Hes1* and *Pax7*.

(E) H3K27me3 ChIP-seq averaged signal at promoters between T0-SCs, T3-SCs, and activated MuSCs from a published dataset (Liu et al., 2013).

(F) Volcano plot representing genomic DNA methylation changes between T0-SCs and T3-SCs. Each dot represents one of 27,878 CpG clusters interrogated. Among all clusters (blue), those with a methylation change $\geq 10\%$ and an FDR < 0.01 were considered significantly different (red). FDR, false discovery rate (logarithmic scale).

Laboratories) at a 1:50 dilution. The blocking was performed for 1 hr at room temperature in 5% BSA. The following primary antibodies were used: anti-HOXA9 (Millipore 07-178) and anti-PAX7 (Santa Cruz, #sc-81648), all at a dilution of 1:100. Incubation with primary antibodies was performed overnight at 4°C. Secondary antibody incubation was performed for 1 hr at room temperature (Thermo Fisher Scientific, Alexa Fluor secondary antibodies diluted at 1:500), and DAPI staining was performed for 10 min at room temperature at 0.5 $\mu\text{g}/\text{mL}$.

Image Analysis

Images were acquired using AxioImager D1, a Zeiss microscope, or a Leica LSM 800 confocal microscope. The eccentricity of the cells, defined as the ratio of the distance between the foci of the ellipse and its major length axis, was calculated using CellProfiler (<http://cellprofiler.org/>) after automatically drawing all WGA-positive areas per field and filtering out the ones without Hoechst-positive areas inside using an in-house pipeline. A minimum of 100 cells have been analyzed per replicate.

DAPI Incorporation by MuSCs in Total Muscle Preparations

Following enzymatic dissociation and filtering, muscle preparations were incubated on ice for 50 min with 1 μ g/mL DAPI. A minimum of 1×10^3 cells per replicate was analyzed using the BD Influx Software.

RNA Extraction

A minimum of 2.5×10^5 cells per replicate were isolated by FACS. Cells were washed three times with cold PBS, and RNA was extracted using the RecoverAll Kit for FFPE (Ambion, #AM1975) following the manufacturer's guidelines, with slight modifications: the incubation step at 50°C was performed for 1 hr instead of 15 min to improve RNA yield, and the incubation step at 80°C was omitted, as it deteriorated the quality of the recovered RNA, a conclusion also reached by an independent study (Hrvatin et al., 2014). Note that the T3- and T5-SCs were fixed post-FACS isolation for 30 min on ice with 0.5% PFA in PBS to ensure comparability with the fixed T0-SCs. For the experiments in Figure 2, the live T3-SCs were not fixed prior to RNA isolation, and for these samples, the 50°C incubation step was performed for 15 min instead of 1 hr.

qRT-PCR

Reverse transcription was performed using the SuperScript III Reverse Transcriptase kit (Thermo Fisher Scientific, #18080093) with random primers, following the manufacturer's guidelines. qPCR was performed using the Power SYBR Green PCR Master Mix (Applied Biosystems, #4367659). All reactions were run in triplicates and normalized to the mean expression of two housekeeping genes: *Tbp* and *Hprt1*. Primers' sequences are available in Table S3.

High-Throughput Analysis

All procedures related to high-throughput analyses (RNA-seq, ChIP-seq, and RRBS) as well as their corresponding bioinformatics analyses can be found in the Supplemental Experimental Procedures.

Statistical Analysis

For comparison between two groups, unpaired Student's *t* test was performed to calculate *p* values and to determine statistically significant differences (**p* < 0.05; ***p* < 0.01; ****p* < 0.001). All statistical analyses were performed with GraphPad Prism 6 software. The letter "n" represents biological replicates. A minimum of three independent mice were analyzed for all experiments (except for ChIP-sequencing; see Supplemental Experimental Procedures for details). Data are presented as means \pm SD.

DATA AND SOFTWARE AVAILABILITY

The accession numbers for RNA-seq, ChIP-seq, and RRBS raw and processed files are GEO: GSE103162, GSE103163, and GSE104543, respectively, and can be downloaded from the Gene Expression Omnibus website (<https://www.ncbi.nlm.nih.gov/geo/>) under the accession number GEO: GSE103164.

SUPPLEMENTAL INFORMATION

Supplemental Information includes Supplemental Experimental Procedures, Supplemental *In Situ* Fixation Protocol, three figures, and three tables and can be found with this article online at <https://doi.org/10.1016/j.celrep.2017.10.080>.

AUTHOR CONTRIBUTIONS

L.M., O.F., J.E.d.L., R.B., F.R., and P.M. designed the experiments. L.M., O.F., J.E.d.L., C.P., A.S., and P.M. performed the experiments. L.M., O.F., J.E.d.L., C.P., R.L., H.V., L.R.I., R.B., F.R., and P.M. analyzed the data. L.M., F.R., and P.M. wrote and edited the manuscript.

ACKNOWLEDGMENTS

We would like to thank A. Guguin and A. Henry of the flow cytometry platform of IMRB, Inserm U955, Creteil. We are grateful to D. Mademtzoglu,

M. Gervais-Taurel, A. Prola, D. Hardy, and M. Borok for critical reading of the manuscript and A. Fu for technical assistance. This work was supported by funding to F.R. from the Association Française contre les Myopathies (AFM) via TRANSLAMUSCLE (PROJECT 19507), Labex REVIVE (ANR-10-LABX-73), Fondation pour la Recherche Médicale (FRM; grants FDT20130928236 and DEQ20130326526), Agence Nationale pour la Recherche (ANR) grant Epimuscle (ANR 11 BSV2 017 02), Bone-muscle-repair (ANR-13-BSV1-0011-02), BMP-myomass (ANR-12-BSV1-0038-04), Satnet (ANR-15-CE13-0011-01), Crestnetmetabo (ANR-15-CE13-0012-02), and RHU CARMMA (ANR-15-RHUS-0003). O.F. was a recipient of a research grant from the Danish Diabetes Academy (1077471001) supported by the Novo Nordisk Foundation.

Received: May 11, 2017

Revised: September 13, 2017

Accepted: October 21, 2017

Published: November 14, 2017

REFERENCES

- Amit, I., Citri, A., Shay, T., Lu, Y., Katz, M., Zhang, F., Tarcic, G., Siwak, D., Lahad, J., Jacob-Hirsch, J., et al. (2007). A module of negative feedback regulators defines growth factor signaling. *Nat. Genet.* 39, 503–512.
- Arora, R., Rumman, M., Venugopal, N., Gala, H., and Dhawan, J. (2017). Mimicking muscle stem cell quiescence in culture: methods for synchronization in reversible arrest. In *Muscle Stem Cells: Methods and Protocols*, E. Perdiguerro and D.D.W. Cornelison, eds. (Springer New York), pp. 283–302.
- Barrero, M.J., Boué, S., and Izpisua Belmonte, J.C. (2010). Epigenetic mechanisms that regulate cell identity. *Cell Stem Cell* 7, 565–570.
- Barski, A., Cuddapah, S., Cui, K., Roh, T.Y., Schones, D.E., Wang, Z., Wei, G., Chepelev, I., and Zhao, K. (2007). High-resolution profiling of histone methylations in the human genome. *Cell* 129, 823–837.
- Boonsanay, V., Zhang, T., Georgieva, A., Kostin, S., Qi, H., Yuan, X., Zhou, Y., and Braun, T. (2016). Regulation of skeletal muscle stem cell quiescence by Suv4-20h1-dependent facultative heterochromatin formation. *Cell Stem Cell* 18, 229–242.
- Chen, J., Suo, S., Tam, P.P.L., Han, J.J., Peng, G., and Jing, N. (2017). Spatial transcriptomic analysis of cryosectioned tissue samples with Geo-seq. *Nat. Protoc.* 12, 566–580.
- Creyghton, M.P., Cheng, A.W., Welstead, G.G., Kooistra, T., Carey, B.W., Steine, E.J., Hanna, J., Lodato, M.A., Frampton, G.M., Sharp, P.A., et al. (2010). Histone H3K27ac separates active from poised enhancers and predicts developmental state. *Proc. Natl. Acad. Sci. USA* 107, 21931–21936.
- Fanjul, A., Dawson, M.I., Hobbs, P.D., Jong, L., Cameron, J.F., Harlev, E., Graupner, G., Lu, X.P., and Pfahl, M. (1994). A new class of retinoids with selective inhibition of AP-1 inhibits proliferation. *Nature* 372, 107–111.
- Fukada, S., Uezumi, A., Ikemoto, M., Masuda, S., Segawa, M., Tanimura, N., Yamamoto, H., Miyagoe-Suzuki, Y., and Takeda, S. (2007). Molecular signature of quiescent satellite cells in adult skeletal muscle. *Stem Cells* 25, 2448–2459.
- Herschman, H.R. (1991). Primary response genes induced by growth factors and tumor promoters. *Annu. Rev. Biochem.* 60, 281–319.
- Hrvatin, S., Deng, F., O'Donnell, C.W., Gifford, D.K., and Melton, D.A. (2014). MARIS: method for analyzing RNA following intracellular sorting. *PLoS ONE* 9, e89459.
- Huang, C., Ma, W.Y., Dawson, M.I., Rincon, M., Flavell, R.A., and Dong, Z. (1997). Blocking activator protein-1 activity, but not activating retinoic acid response element, is required for the antitumor promotion effect of retinoic acid. *Proc. Natl. Acad. Sci. USA* 94, 5826–5830.
- Jaafar Marican, N.H., Cruz-Migoni, S.B., and Borycki, A.-G. (2016). Asymmetric distribution of primary cilia allocates satellite cells for self-renewal. *Stem Cell Reports* 6, 798–805.

- Jones, N.C., Tyner, K.J., Nibarger, L., Stanley, H.M., Cornelison, D.D.W., Fedorov, Y.V., and Olwin, B.B. (2005). The p38 α / β MAPK functions as a molecular switch to activate the quiescent satellite cell. *J. Cell Biol.* **169**, 105–116.
- King, A.D., Huang, K., Rubbi, L., Liu, S., Wang, C.Y., Wang, Y., Pellegrini, M., and Fan, G. (2016). Reversible regulation of promoter and enhancer histone landscape by DNA methylation in mouse embryonic stem cells. *Cell Rep.* **17**, 289–302.
- Lee, J.H., Daugharthy, E.R., Scheiman, J., Kalhor, R., Ferrante, C., Terry, R., Turczyk, B.M., Yang, J.L., Lee, H.S., Aach, J., et al. (2015). Fluorescent in situ sequencing (FISSEQ) of RNA for gene expression profiling in intact cells and tissues. *Nat. Protoc.* **10**, 442–458.
- Liu, L., and Clevers, H. (2010). Coexistence of quiescent and active adult stem cells in mammals. *Science* **327**, 542–545.
- Liu, L., Cheung, T.H., Charville, G.W., and Rando, T.A. (2015). Isolation of skeletal muscle stem cells by fluorescence-activated cell sorting. *Nat. Protoc.* **10**, 1612–1624.
- Liu, L., Cheung, T.H., Charville, G.W., Hurgo, B.M., Leavitt, T., Shih, J., Brunet, A., and Rando, T.A. (2013). Chromatin modifications as determinants of muscle stem cell quiescence and chronological aging. *Cell Rep.* **4**, 189–204.
- Martynoga, B., Mateo, J.L., Zhou, B., Andersen, J., Achimastou, A., Urbán, N., van den Berg, D., Georgopoulou, D., Hadjir, S., Wittbrodt, J., et al. (2013). Epigenomic enhancer annotation reveals a key role for NFIX in neural stem cell quiescence. *Genes Dev.* **27**, 1769–1786.
- Miranda, T.B., and Jones, P.A. (2007). DNA methylation: the nuts and bolts of repression. *J. Cell. Physiol.* **213**, 384–390.
- Mollova, M., Bersell, K., Walsh, S., Savla, J., Das, L.T., Park, S.-Y., Silberstein, L.E., Dos Remedios, C.G., Graham, D., Colan, S., and Kühn, B. (2013). Cardiomyocyte proliferation contributes to heart growth in young humans. *Proc. Natl. Acad. Sci. USA* **110**, 1446–1451.
- Montarras, D., Morgan, J., and Collins, C. (2005). Direct isolation of satellite cells for skeletal muscle regeneration. *Science* **309**, 2064–2068.
- Mourikis, P., Sambasivan, R., Castel, D., Rocheteau, P., Bizzarro, V., and Tajbakhsh, S. (2012). A critical requirement for notch signaling in maintenance of the quiescent skeletal muscle stem cell state. *Stem Cells* **30**, 243–252.
- Pallafacchina, G., François, S., Regnault, B., Czarny, B., Dive, V., Cumano, A., Montarras, D., and Buckingham, M. (2010). An adult tissue-specific stem cell in its niche: a gene profiling analysis of in vivo quiescent and activated muscle satellite cells. *Stem Cell Res.* **4**, 77–91.
- Pannérec, A., Formicola, L., Besson, V., Marazzi, G., and Sassoon, D.A. (2013). Defining skeletal muscle resident progenitors and their cell fate potentials. *Development* **140**, 2879–2891.
- Peng, G., Suo, S., Chen, J., Chen, W., Liu, C., Yu, F., Wang, R., Chen, S., Sun, N., Cui, G., et al. (2016). Spatial transcriptome for the molecular annotation of lineage fates and cell identity in mid-gastrula mouse embryo. *Dev. Cell* **36**, 681–697.
- Quarta, M., Brett, J.O., DiMarco, R., De Morree, A., Boutet, C., Chacon, R., Gibbons, M.C., Garcia, V.A., Su, J., Shrager, J.B., et al. (2016). An artificial niche preserves the quiescence of muscle stem cells and enhances their therapeutic efficacy. *Nat. Biotechnol.* **34**, 752–759.
- Rocheteau, P., Gayraud-Morel, B., Siegl-Cachedenier, I., Blasco, M.A., and Tajbakhsh, S. (2012). A subpopulation of adult skeletal muscle stem cells retains all template DNA strands after cell division. *Cell* **148**, 112–125.
- Rodgers, J.T., King, K.Y., Brett, J.O., Cromie, M.J., Charville, G.W., Maguire, K.K., Brunson, C., Mastey, N., Liu, L., Tsai, C.R., et al. (2014). mTORC1 controls the adaptive transition of quiescent stem cells from G0 to G(Alert). *Nature* **510**, 393–396.
- Rojas-Ríos, P., and González-Reyes, A. (2014). Concise review: The plasticity of stem cell niches: a general property behind tissue homeostasis and repair. *Stem Cells* **32**, 852–859.
- Ryall, J.G., Dell’Orso, S., Derfoul, A., Juan, A., Zare, H., Feng, X., Clermont, D., Koulis, M., Gutierrez-Cruz, G., Fulco, M., and Sartorelli, V. (2015). The NAD(+)-dependent SIRT1 deacetylase translates a metabolic switch into regulatory epigenetics in skeletal muscle stem cells. *Cell Stem Cell* **16**, 171–183.
- Sakai, H., Fukuda, S., Nakamura, M., Uezumi, A., Noguchi, Y.T., Tajbakhsh, S., and Fukada, S.I. (2017). Notch ligands regulate the muscle stem-like state ex vivo but are not sufficient for retaining regenerative capacity. *PLoS One* **12**, e0177516.
- Sambasivan, R., Gayraud-Morel, B., Dumas, G., Cimper, C., Paisant, S., Kelly, R.G., and Tajbakhsh, S. (2009). Distinct regulatory cascades govern extraocular and pharyngeal arch muscle progenitor cell fates. *Dev. Cell* **16**, 810–821.
- Schulze, S.K., Kanwar, R., Gölzenleuchter, M., Therneau, T.M., and Beutler, A.S. (2012). SERE: Single-parameter quality control and sample comparison for RNA-seq. *BMC Genomics* **13**, 524.
- Schwörer, S., Becker, F., Feller, C., Baig, A.H., Köber, U., Henze, H., Kraus, J.M., Xin, B., Lechel, A., Lipka, D.B., et al. (2016). Epigenetic stress responses induce muscle stem-cell ageing by Hoxa9 developmental signals. *Nature* **540**, 428–432.
- van den Brink, S.C., Sage, F., Vértessy, Á., Spanjaard, B., Peterson-Maduro, J., Baron, C.S., Robin, C., and van Oudenaarden, A. (2017). Single-cell sequencing reveals dissociation-induced gene expression in tissue subpopulations. *Nat. Methods* **14**, 935–936.
- van Velthoven, C.T.J., de Morree, A., Egner, I.M., Brett, J.O., and Rando, T.A. (2017). Transcriptional profiling of quiescent muscle stem cells in vivo. *Cell Rep* **21**, this issue, 1994–2004.
- Zammit, P.S., Golding, J.P., Nagata, Y., Hudon, V., Partridge, T.A., and Beauchamp, J.R. (2004). Muscle satellite cells adopt divergent fates: a mechanism for self-renewal? *J. Cell Biol.* **166**, 347–357.
- Zhang, K., Sha, J., and Harter, M.L. (2010). Activation of Cdc6 by MyoD is associated with the expansion of quiescent myogenic satellite cells. *J. Cell Biol.* **188**, 39–48.

Supplemental Information

***In Situ* Fixation Redefines Quiescence and Early**

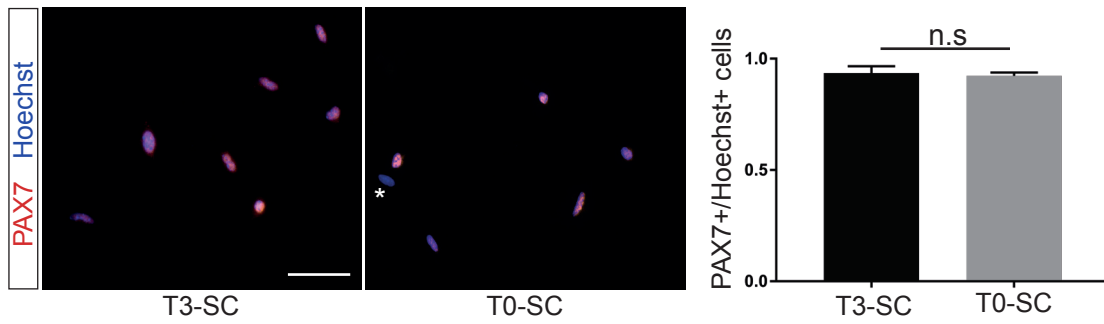
Activation of Skeletal Muscle Stem Cells

Léo Machado, Joana Esteves de Lima, Odile Fabre, Caroline Proux, Rachel Legendre, Anikó Szegedi, Hugo Varet, Lars Roed Ingerslev, Romain Barrès, Frédéric Relaix, and Philippos Mourikis

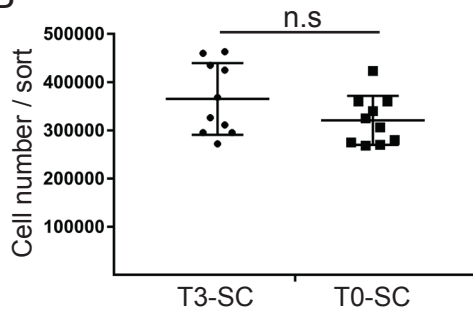
Supplementary Files Inventory :

- Supplementary Figures S1 to S3
- *In situ* Fixation Protocol
- Supplementary Experimental Procedures
- Supplementary Table 1 : RNA-sequencing
- Supplementary Table 2 : ChIP-sequencing
- Supplementary Table 3 : Primers used for RT-qPCR

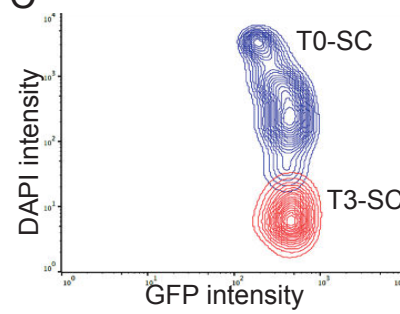
A



B



C



D

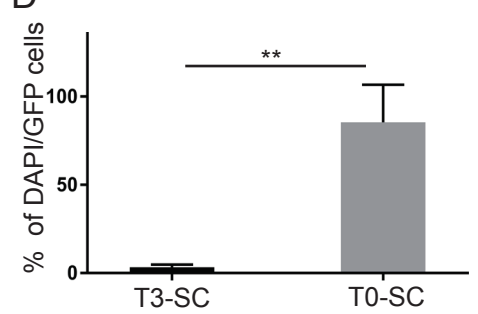


Figure S1. Quality controls of FACS-isolated MuSCs from *in situ* fixed and non-fixed muscles, related to Figure 1.

A. Purity of FACS-isolated T3-SCs and T0-SCs. Cells were left for 16h to adhere and then stained for PAX7. Asterisk indicates a rare PAX7⁻ cell. Quantification shown on the right: 94% ±3.1 and 92% ±1.4 for T3- and T0-SCs, respectively; n=3.

B. Yields of FACS-isolated T3 and T0 MuSCs from hindlimb and forelimb muscle preparations; n=10.

C. Nuclear marker DAPI uptake by dissociated T3-SCs and T0-SCs.

D. Quantification of DAPI-positive cells; n=4.

n.s = not significant, ** p<0.01; data are reported as mean ± SD.

Machado_Figure S2

A

SERE statistics from Figure 2 RNA-sequencing

Sample	liveA	liveB	liveC	fixA	fixB	fixC
liveA	0	7.03	3.807	4.061	7.494	9.242
liveB	7.03	0	5.365	6.199	7.917	8.445
liveC	3.807	5.365	0	3.918	4.995	5.62
fixA	4.061	6.199	3.918	0	5.773	7.272
fixB	7.494	7.917	4.995	5.773	0	6.339
fixC	9.242	8.445	5.62	7.272	6.339	0

SERE statistics from Figure 3 RNA-sequencing

Sample	T0a	T0b	T0c	T3a	T3b	T3c	T3d	T5a	T5b
T0a	0	10.55	15.189	19.396	21.472	20.239	18.988	23.068	22.066
T0b	10.55	0	9.279	18.457	19.856	18.263	19.799	20.758	19.707
T0c	15.189	9.279	0	19.568	21.356	18.666	21.874	21.034	19.586
T3a	19.396	18.457	19.568	0	6.13	6.513	5.178	9.496	8.505
T3b	21.472	19.856	21.356	6.13	0	6.193	7.083	10.838	9.791
T3c	20.239	18.263	18.666	6.513	6.193	0	8.7	10.213	8.502
T3d	18.988	19.799	21.874	5.178	7.083	8.7	0	11.432	11.13
T5a	23.068	20.758	21.034	9.496	10.838	10.213	11.432	0	7.247
T5b	22.066	19.707	19.586	8.505	9.791	8.502	11.13	7.247	0

B

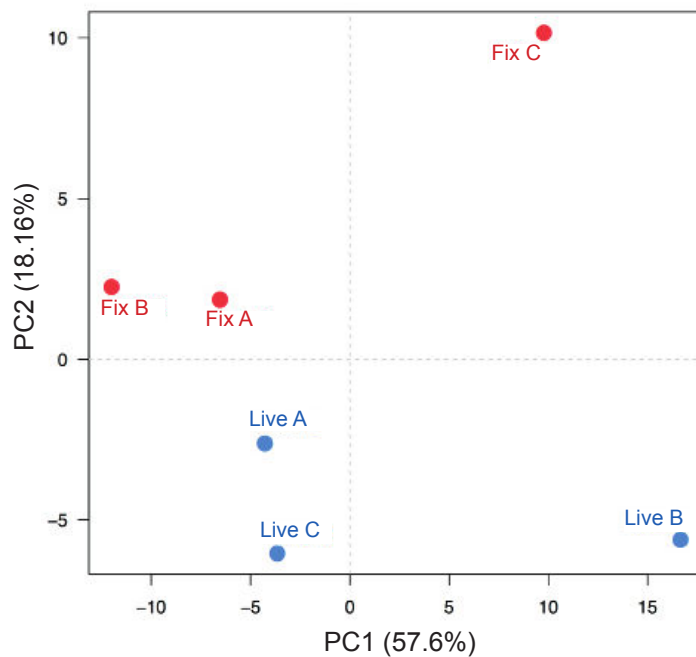


Figure S2. Statistical comparisons of RNA-seq data, related to Figure 2.

A. Comparison of all RNAseq-derived transcriptomes by SERE statistics.

B. Visualization of variability between the Live and Fixed T3-SCs RNA-sequences using principal component analysis (PCA) on the gene expression matrix. The first two components (PC1 and PC2) are presented, with percentages of variance explained.

Machado_Figure S3

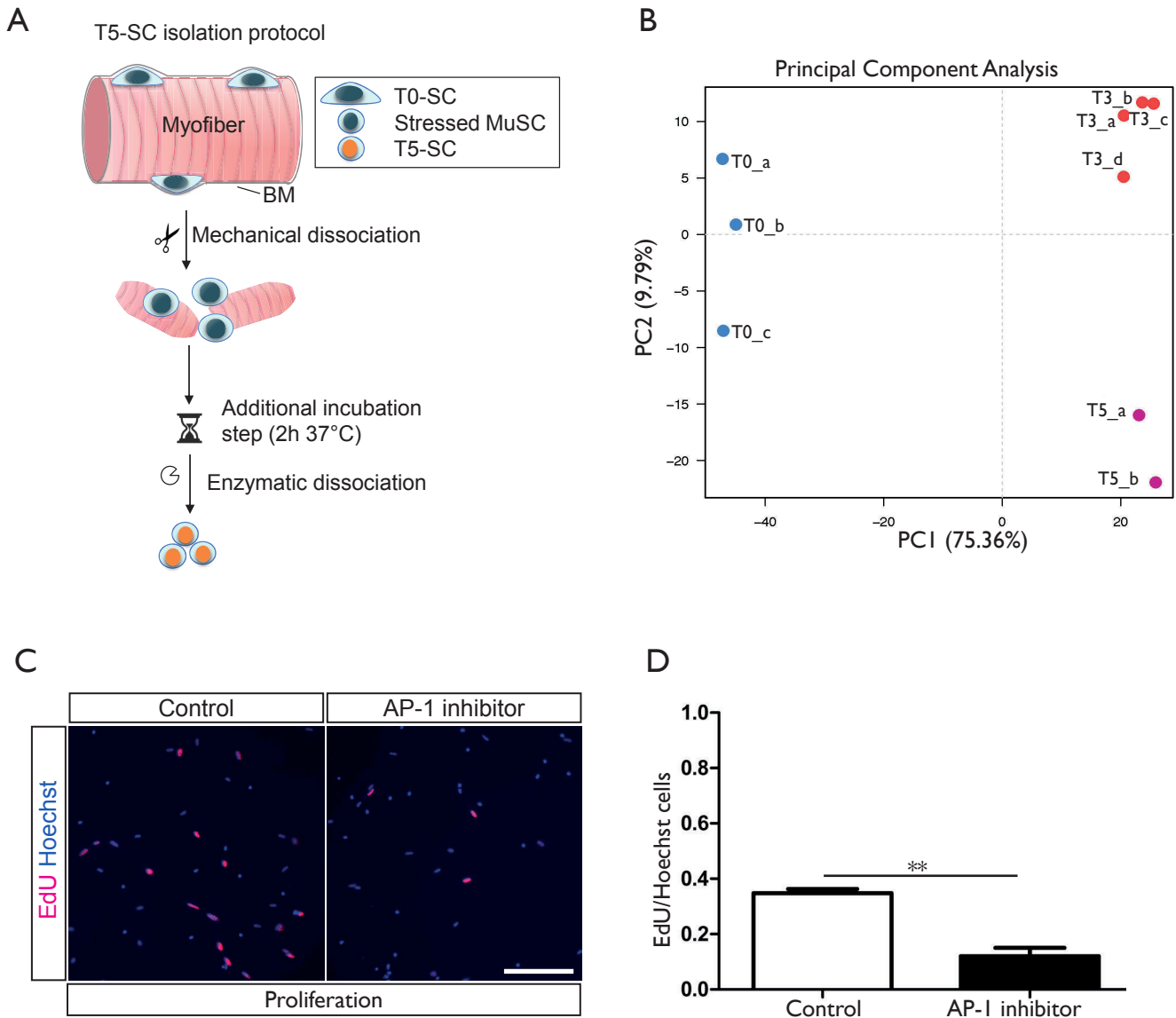


Figure S3. AP-1 activity, identified by the comparison of T0-, T3-, and T5-SCs, is promoting exit from quiescence, related to Figure 3.

A. Graphical scheme of the protocol used to prepare and isolate T5-SCs, which introduces a step of prolonged incubation of minced muscles at 37°C in DMEM. *Abbreviation:* BM, basement membrane.

B. Visualization of variability between the T0-SC, T3-SC, and the T5-SC samples using principal component analysis (PCA) on the gene expression matrix. The first two components (PC1 and PC2) are presented, with percentages of variance explained.

C. Cultured MuSCs treated for 24h with the AP-1 inhibitor SR-11302 or DMSO control 24h after FACS-isolation. EdU was added 4h before fixation to mark proliferating cells. Scale bar: 50µm.

D. Quantification of EdU⁺ cells in SR-11302 or DMSO treated MuSCs, as described in figure S3C. ** p<0.01; data are reported as mean ± SD.

Dissociation of MuSCs from fresh and fixed skeletal muscles

Standard protocol for the isolation of live MuSCs (T3-SCs). Duration approximately 3h.

- i. Kill mouse by an instant method, like cervical dislocation.
- ii. Dissect muscles from tendon to tendon when possible. Clean muscle from fat and other associated tissue.
- iii. Immerse the dissected muscle in a 50ml conical tube filled with ice-cold DMEM.
- iv. Repeat steps (ii) and (iii) until sufficient amount of muscle tissue has been collected.
- v. Use a 100µm cell strainer to discard DMEM and place all muscle on a clean 10cm Petri dish.
- vi. Chop tissue with scissors for up to 10min until a homogeneous, paste-like slurry is formed. Transfer the muscle preparation into a 50ml tube and fill with ice-cold DMEM.
- vii. Centrifuge at 4°C for 5min/600g and discard the supernatant.
- viii. Go directly to step 16.

In situ fixation of skeletal muscle stem cells, T0-SC (isolation of fixed MuSCs, time zero):

I. Skeletal muscle dissection (~1h)

1. Kill mouse by cervical dislocation
2. Dissect muscles from tendon to tendon when possible. Clean off fat and other associated tissue from muscle.
3. Place the dissected muscle piece in a clean 10cm Petri dish
4. Rapidly cut the muscle 5-10 times (according to size) to break the fascia and expose muscle to the fixative agent. The obtained muscle pieces should range between 1 and 5mm.
5. Dip muscle pieces in 30ml of ice-cold 0.5% paraformaldehyde (PFA).
6. Repeat steps 3 to 5 until sufficient amount of muscle tissue has been collected (maximum total dissection time no more than 15min).
7. Use a 100µm cell strainer to discard the PFA and place the dissected muscle on a clean 10cm Petri dish.
8. Chop tissue with scissors for up to 10min, until a homogeneous paste-like slurry is formed.

Attention: During step 8, 2-3 drops of ice-cold 0.5% PFA should be added every 1min with a Pasteur pipette to maintain a constant exposure of muscle tissue to ice-cold PFA.

II. Fixation & washes (~2h)

9. Place the minced muscle preparation into a new 50ml tube and fill it with ice-cold 0.5% PFA.
10. Gently rotate the tube for 1h at 4°C.
11. Centrifuge at 4°C for 5min/600g and discard the supernatant to wash out the fixative solution.
12. Fill the tube with ice-cold PBS and gently invert the tube 10 times to resuspend the pellet.
13. Gently rotate 4°C for 15min.
14. Repeat the PBS wash (steps 11 to 13) two more times to remove residual PFA.
15. Centrifuge at 4°C for 5min/600g and discard the supernatant.

III. Digestion (~2h)

16. Resuspend the cell pellet in 20ml of warm (37°C) digestion solution for a full-body muscle preparation or 5ml/g of dissected muscle.

Attention: The digestion solution is different for T0- and T3-SCs.

17. Seal with parafilm the 50ml tube and shake at 70rpm for 1h at 37°C (ideally in a shaking water bath).
18. Gently pipette up and down 5-10 times (according to volume) the digesting muscle with a 10ml pipette, to mechanically help the dissociation of MuSCs from the myofibres.
19. Seal the tube with parafilm and continue the incubation for 1h at 37°C / 70rpm. Total digestion time should not exceed 2h.

IV. Washes & filtration (~1h)

20. Fill the 50ml conical tube with ice-cold DMEM and mix gently 5-10 times by inverting the tube.

21. Pass the digested muscle through a 100 μ m cell strainer into a new 50ml conical tube and spin at 4°C for 5min/600g.
22. Discard the supernatant and gently resuspend the cell pellet in 1ml of ice-cold DMEM with a P1000 pipette.
23. Fill the tube with ice-cold DMEM and mix gently by inverting 5-10 times.
24. Pass the digested muscle through a 70 μ m cell strainer into a new 50ml tube and spin **at 50g** for 5min at 4°C.
Attention: Keep the supernatant and discard the pellet. This 50g step is critical to discard cell debris. MuSCs are retained in the supernatant.
25. Pass the supernatant through a 40 μ m cell strainer and spin at 4°C for 5min/600g.
26. Discard the supernatant and resuspend the cell pellet in the desired volume of ice-cold DMEM (usually 1ml).
The sample is ready for FACS.

Reagents:

- **T3 digestion solution prepared in DMEM medium**
 1. Dispase II, 3U/ml (Roche, 4942078001)
 2. Collagenase A 0.5U/ml (Roche, 10103586001)
 3. 0.2% BSA
 4. 100 U/ml of penicillin, and 100 mg/ml of streptomycin (if the cells are cultured after sorting)
- **T0 digestion solution prepared in DMEM medium**
 1. Dispase II, 6U/ml (Roche, 4942078001)
 2. Collagenase A 1U/ml (Roche, 10103586001)
 3. 0.2% BSA
 4. 100U/ml of penicillin, and 100mg/ml of streptomycin
- **Fixation solution:** 0.5% para-formaldehyde in PBS
- **Cell strainers:** 100, 70, and 40 μ m, Corning, Inc. 352360, 352350, and 352340, respectively.

Supplementary Experimental Procedures

RNA-Sequencing

RNA quality and yield were assessed by the RNA integrity number (RIN) algorithm, using the 2100 Bioanalyzer. Samples with a RIN between 6.4 and 7.5 were used for library preparation. Directional libraries were prepared using the Smarter Stranded Total RNA-Seq kit-Pico Input Mammalian kit following the manufacturer's instructions (Clontech, 635005). The quality of all libraries was verified with the DNA-1000 kit (Agilent) on a 2100 Bioanalyzer and quantification was performed with Quant-It assays on a Qubit 3.0 fluorometer (Invitrogen). Clusters were generated for the resulting libraries, with the Illumina HiSeq SR Cluster Kit v4 reagents. Sequencing was performed using the Illumina HiSeq 2500 system and HiSeq SBS kit v4 reagents. Runs were carried out over 65 cycles, including seven indexing cycles, to obtain 65-bp single-end reads. Sequencing data were then processed with the Illumina Pipeline software, Casava version 1.9.

ChIP-sequencing

8×10^5 FACS-isolated T0-SCs or T3-SCs were pooled from two or three animals and fixed on ice with 1% formaldehyde for 10min. The fixative was quenched with 1/10^e volume of glycine for 5min on ice and the samples were washed twice with cold PBS. The cell pellets were lysed using Diagenode iDeal ChIP-seq kit for Histones (C01010051) and the genomic DNA was sheared using 10 cycles of 30sec on/off ultra-sonication with a Bioruptor Pico (Diagenode B01060001). The equivalent of 2×10^5 cells was used per ChIP or Input samples, with the following ChIP-grade polyclonal antibodies from Diagenode: anti-H3K4me3 (C15410003-50), anti-H3K27me3 (C15410195) and anti-H3K27ac (C15410196) as per manufacturer's guidelines. The purification of the immunoprecipitated DNA was performed using Diagenode DiaPure columns (C03040001). All ChIP and Input experiments were prepared in duplicates from different pools of T0-SCs or T3-SCs. After quantifying the enrichment of the immunoprecipitated DNA by RT-qPCR, ChIP-sequencing libraries were constructed and sequenced by Integragen (<http://www.integragen.com>). Libraries were prepared with the NEBNext ultra 2 kit (NEB E7645L). Library pools were separated on agarose gel and DNA of a 100-280 bp size-range was selected for sequencing on an Illumina HiSEQ 4000 as paired-end 75-bp reads. Image analysis and base calling were performed using Illumina Real Time Analysis (RTA) Pipeline version 2.7.6 with default parameters.

Reduced Representation Bisulfite Sequencing (RRBS)

3-4x10⁵ sorted T0- and T3-SCs were lysed and their genomic DNA was extracted using the RecoverAll Kit for FFPE (Ambion, AM1975) following the manufacturer's guidelines (one animal per replicate, n=4). Genomic DNA samples were first concentrated with Genevac EZ-2 Evaporation System and diluted in water to reach 95ng in 26µl.

Sequencing library pool was prepared with the Premium Reduced Representation Bisulfite Sequencing (RRBS) Kit (Diagenode, C02030033) following manufacturer's instructions, quantified with the Qubit dsDNA HS Assay Kit (Thermo Fisher Scientific, Q32854) and average size of DNA fragments was estimated with a 2100 Bioanalyzer instrument using Agilent High Sensitivity DNA Kit (5067-4626). Library pool was then denaturated in NaOH and diluted at 1.9pM with 20% of PhiX Control v3 (Illumina, FC-110-3001). To improve cluster density consistency, the diluted library pool was heat-denaturated at 96°C for 2min, inverted twice to mix, and quickly moved to ice for 5min before loading to the sequencer. The library pool was sequenced with NextSeq 500 (Illumina), using the NextSeq 500/550 High Output v2 Kit, 75 cycles (Illumina, FC-404-2002). Sequencing was single-read, 76 cycles, index 1: 6 bases.

Bioinformatics

RNA-seq analysis: Reads were cleaned of adapter sequences and low-quality sequences using an in-house program (https://github.com/bajl2/clean_ngs). Only sequences at least 25nt in length were considered for further analysis. STAR version 2.5.0a (Dobin et al., 2013), with default parameters was used for alignment on the reference genome (GRCm38 from Ensembl database). Genes were counted using featureCounts version 1.4.6-p3 (Liao et al., 2014) from Subreads package (parameters: -t gene -s 0 -O). Count data were analyzed using R version 3.3.1 (R Core Team, 2016) and the Bioconductor package DESeq2 version 1.12.3 (Love et al., 2014). The normalization and the dispersion estimation were performed with DESeq2 using the default parameters, but statistical tests for differential expression were performed without applying the independent filtering algorithm. A generalized linear model was set in order to test for the differential expression between T0-, T3-, and T5-SCs or between live T3-SCs and fixed T3-SCs. For each pairwise comparison, raw p-values were adjusted for multiple testing according to the Benjamini and Hochberg (BH) procedure (Benjamini and Hochberg, 1995) and genes with an adjusted p-value lower than 0.05 were considered differentially expressed.

Mean transcript coverage was performed by RNA-seQC version 1.1.8 (Deluca et al., 2012), by merging all the mean coverages among high, medium and low transcripts. Plotting was performed by an in-house python script using pandas version 0.20.1 (<http://pandas.pydata.org/>).

Gene ontology: Gene ontology analyses have been performed on <http://www.geneontology.org/> using the biological process option.

Published microarray comparison: Three gene expression datasets were downloaded from the editors website or transmitted by the authors (Fukada et al., 2007; Liu et al., 2013; Pallafacchina et al., 2010). The quiescent signature is extracted from statistically up-regulated genes (gene symbols) in freshly isolated MuSCs, compared to activated MuSCs, with an $FC > 5$ based on statistical testing of the authors. The T0-SCs and T3-SCs transcriptomes have been compared to the microarray-based quiescent signatures (using the gene symbol of all genes differentially expressed with a $FDR < 0.05$). The overlap between the T0/T3 transcriptomes and the three published quiescent signatures were averaged to obtain mean overlap and standard error.

Published RNA-seq comparison: The RNA-sequencing dataset of Ryall et al., 2015 was downloaded from the website of the journal. The extracted quiescent signature represents the gene symbols of all the genes enriched in freshly isolated MuSCs with an $FC > 2$ compared to activated MuSCs based on the statistical testing of the authors. This quiescent signature has been compared with ours by overlapping it with the T0-SC transcriptome (gene symbols of the statistically enriched genes in T0-SC compared to T3-SC, with an $FC > 2$).

Heatmap: The gene expression heatmap in Figure 3D was created with R version 3.3.1 (R Core Team, 2016), using the *heatmap* command with length-normalized, depth-normalized reads number averaged from replicates within groups.

ChIP-seq analysis: The ChIP-seq analysis was performed using GALAXY (Afgan et al., 2016), (<https://usegalaxy.org/>): the FASTQ files were aligned to the mm10 mouse genome build using Bowtie2 v2.2.6.2 (Langmead, 2013) and the peaks were called using MACS2 v2.1.0 (with the `-broad` parameter for H3K27ac and H3K27me3) after pooling duplicates. All the tools were used with standard parameters unless specified. Subsequent analyses were performed using BEDTools v2.24.0 (Quinlan and Hall, 2010) and SitePRO v1.0.0 (Liu et al., 2011), <http://cistrome.dfci.harvard.edu/ap/>. Genes with H3K4me3-bound promoters are all of the ENSEMBL genes with at least one H3K4me3 peak within 100bp of the TSS. Distal enhancers are defined as H3K27ac peaks outside of gene bodies. Distal enhancers have been attributed to the closest ENSEMBL gene and each gene with at least one distal

enhancer was considered for the overlap. H3K27me3 and Input FASTQ files of activated MuSCs were downloaded from the Gene Expression Omnibus website GSE47177 (Liu et al., 2013) and analysed with the pipeline presented above.

DNA-methylation analysis: RRBS reads were pre-processed with Trim Galore v0.4.0 and Cutadapt v1.9.1 using standard settings and the --rrbs flag. Preprocessed reads were aligned to the mm10 genome and CpG coverage computed using bismark v0.14.4 (Krueger and Andrews, 2011) assisted by bowtie2 v2.2.6 (Langmead, 2013).

Methylation levels were estimated using BiSeq v1.14 (Hebestreit et al., 2013). Settings were as in the manual, except for the function: “clusterSites”, which was run with the parameters perc.samples = 3/4 and min.sites = 5. Rather than performing the trimming step, clusters were deemed significant if they had an FDR <0.01 and an absolute methylation change $\geq 10\%$.

Supplemental References

- Afgan, E., Baker, D., van den Beek, M., Blankenberg, D., Bouvier, D., Čech, M., Chilton, J., Clements, D., Coraor, N., Eberhard, C., et al. (2016). The Galaxy platform for accessible, reproducible and collaborative biomedical analyses: 2016 update. *Nucleic Acids Res.* *44*, gkw343.
- Benjamini, Y., and Hochberg, Y. (1995). Controlling the false discovery rate: a practical and powerful approach to multiple testing. *J. R. Stat. Soc. Ser. B* *57*, 289–300.
- Deluca, D.S., Levin, J.Z., Sivachenko, A., Fennell, T., Nazaire, M.D., Williams, C., Reich, M., Winckler, W., and Getz, G. (2012). RNA-SeQC: RNA-seq metrics for quality control and process optimization. *Bioinformatics* *28*, 1530–1532.
- Dobin, A., Davis, C.A., Schlesinger, F., Drenkow, J., Zaleski, C., Jha, S., Batut, P., Chaisson, M., and Gingeras, T.R. (2013). STAR: Ultrafast universal RNA-seq aligner. *Bioinformatics* *29*, 15–21.
- Fukada, S., Uezumi, A., Ikemoto, M., Masuda, S., Segawa, M., Tanimura, N., Yamamoto, H., Miyagoe-Suzuki, Y., and Takeda, S. (2007). Molecular signature of quiescent satellite cells in adult skeletal muscle. *Stem Cells* *25*, 2448–2459.
- Hebestreit, K., Dugas, M., and Klein, H.U. (2013). Detection of significantly differentially methylated regions in targeted bisulfite sequencing data. *Bioinformatics* *29*, 1647–1653.
- Krueger, F., and Andrews, S.R. (2011). Bismark: A flexible aligner and methylation caller for Bisulfite-Seq applications. *Bioinformatics* *27*, 1571–1572.
- Langmead (2013). Bowtie2. *Nat. Methods* *9*, 357–359.
- Liao, Y., Smyth, G.K., and Shi, W. (2014). FeatureCounts: An efficient general purpose program for assigning sequence reads to genomic features. *Bioinformatics* *30*, 923–930.
- Liu, L., Cheung, T.H., Charville, G.W., Hurgu, B.M., Leavitt, T., Shih, J., Brunet, A., and Rando, T.A. (2013). Chromatin modifications as determinants of muscle stem cell quiescence and chronological aging. *Cell Rep* *4*, 189–204.
- Liu, T., Ortiz, J.A., Taing, L., Meyer, C.A., Lee, B., Zhang, Y., Shin, H., Wong, S.S., Ma, J., Lei, Y., et al. (2011). Cistrome: an integrative platform for transcriptional regulation studies. *Genome Biol.* *12*, R83.
- Love, M.I., Huber, W., and Anders, S. (2014). Moderated estimation of fold change and dispersion for RNA-seq data with DESeq2. *Genome Biol.* *15*, 550.
- Pallafacchina, G., Francois, S., Regnault, B., Czarny, B., Dive, V., Cumano, A., Montarras, D., and Buckingham, M. (2010). An adult tissue-specific stem cell in its niche: A gene profiling analysis of in vivo quiescent and activated muscle satellite cells. *Stem Cell Res.* *4*, 77–91.
- Quinlan, A.R., and Hall, I.M. (2010). BEDTools: A flexible suite of utilities for comparing genomic features. *Bioinformatics* *26*, 841–842.
- R Core Team (2016). R: A Language and Environment for Statistical Computing.

Part II: Dissociation Distorts the Profile of Isolated Cells and Drives Quiescent Muscle Stem Cells to an Activated State

Machado et al. 2019

Manuscript in preparation

Dissociation distorts the profile of isolated cells and drives quiescent muscle stem cells to an activated state

Léo Machado^{1,2}, Matthieu Dos Santos^{3,4}, Jordi Camps⁵, Jens Van Herck⁶, Hugo Varet^{7,8}, Rachel Legendre^{7,8}, Maurilio Sampaolesi^{5,9}, Thierry Voet^{6,10}, Pascal Maire^{3,4}, Frederic Relaix^{1,2,11,12,13,14,15,*}, and Philippos Mourikis^{1,*}.

** co-lead authors*

1. Inserm, IMRB U955-E10, 94000, Créteil, France
2. Faculté de Médecine, Université Paris Est Créteil, 94000, Créteil, France
3. Inserm U106, Institut Cochin, 75014 Paris, France
4. CNRS UMR8104, Paris, France
5. Laboratory of Translational Cardiomyology, Department of Development and Regeneration, Stem Cell Research Institute, KU Leuven, Leuven, Belgium
6. Laboratory of Reproductive Genomics, Department of Human Genetics, KU Leuven, Leuven, Belgium
7. Hub de Bioinformatique et Biostatistique – Département Biologie Computationnelle, Institut Pasteur, USR 3756 CNRS, Paris, France
8. Plate-forme Biomics - Centre de Ressources et Recherches Technologiques (C2RT), Institut Pasteur, Paris, France
9. Human Anatomy Unit, Department of Public Health, Experimental and Forensic Medicine, University of Pavia, Pavia, Italy.
10. Wellcome Sanger Institute, Wellcome Genome Campus, Cambridge CB10 1SA, UK.
11. Ecole Nationale Vétérinaire d'Alfort, 94700, Maisons-Alfort, France
12. Etablissement Français du Sang, 94017, Créteil, France
13. APHP, Hopital Henri Mondor, DHU Pepsy & Centre de Référence des Maladies Neuromusculaires GNMH, 94000, Créteil, France
14. Lead Contact
15. Correspondence: frederic.relaix@inserm.fr

Highlights

- Cell dissociation distorts the transcriptome of most cells from dissociated muscle and liver
- Published single-cell atlases exhibit a strong dissociation-induced artefact
- Exposure time to dissociative stimuli is a major parameter of transcriptional modifications
- Construction of minute-scale transcriptional activation network of dissociated MuSCs
- Dynamically co-regulated genetic modules uncover a precise sequence of ontologies during MuSCs early activation.
- *Ex vivo* MuSCs activation mimics the early response to muscle injury
- MuSCs follow a unique activation trajectory but with different kinetics
- In activated cells, proliferation signals are uncoupled from pathways regulating myogenic differentiation

Every cell in a multicellular organism is dynamically interacting with its microenvironment, which acts as a major regulator of its properties and gene-expression profile. Recent work on quiescent muscle stem cells (MuSCs) demonstrated that during dissociation they undergo unexpectedly broad transcriptional changes. To date, however, it remains unclear if this represented a general cellular response, and whether these changes are a transient stress reaction or part of a programmed activation process. Here we generated single cell transcriptional organ atlases and found strong alternations across cell types and tissues. The majority of the modifications were cell type specific, yet we defined a core dissociation signature that revealed a high degree of distortion in published datasets, in a dissociation-time dependent manner. To assess the functional significance of these changes, we focused on MuSCs and compared their dissociation response to muscle injury-induced activation. Time-course analysis revealed that the same kinetically co-regulated genetic modules that elicit the dissociation response operate to drive early activation of MuSCs in vivo. By capturing the primary responses to dissociation, we uncovered the cartography of MuSCs quiescence exit, whereby initial ERK signalling-driven proliferation signals act independently of later cellular differentiation, partially regulated by Notch signalling. Overall, our study proposes that during isolation cells execute specialized genetic programs, which lead to cellular state alterations. Therefore, by using cells isolated with conventional methods the initiating events of cell transitions, like quiescence exit, are overlooked, and reference cell maps, like cell atlases, are fundamentally distorted.

Introduction

Many recent initiatives have employed the power of single-cell transcriptome profiling to systematically characterize different cell types at the whole-organism level of diverse models, from planarians to adult mouse and human tissues¹⁻⁶. Cells respond to changes in the microenvironment, including stress and growth factors, in a matter of minutes⁷. Yet, this response period is an order of magnitude shorter than standard cell dissociation protocols, which for most tissues last from one to several hours^{4,8}. In fact, the cells used for building tissue reference maps are extracted from their *in vivo* microenvironment; and recent work on skeletal muscle stem cells has demonstrated that during dissociation their transcriptome is significantly modified, exhibiting a strong stress response signature⁹⁻¹¹. If this is a general cellular response to dissociation or MuSC-specific remains unclear, and resolving this question could have important implications on the fidelity of transcriptomic approaches, such as cellular atlases. The development of techniques that circumvent the modifications induced by dissociation are also essential for dissecting the primary responses of a cell to external stimuli *in vivo*, like injury or exposure to toxins, which could be otherwise buffered during the course of cell isolation.

In this report, we have analysed two highly regenerative tissues, the murine skeletal muscle and the liver, and demonstrated that during dissociation diverse cell types undergo transcriptional alternations comparable in ontology and magnitude to what has been reported for MuSCs. Moreover, computational analysis uncovered a strong correlation between the length of tissue enzymatic digestion and the degree of modifications, introducing dissociation kinetics as a critical parameter of the transcriptomic differences observed between samples. To further investigate the kinetics of dissociation-induced alterations, we focused on MuSCs which are mitotically quiescent yet upon niche disruption get readily activated⁹⁻¹¹.

Quiescence exit of MuSCs is accompanied by posttranslational modifications, like the phosphorylation of the mitogen-activated protein kinase p38 α / β , induction of muscle-specific genes, like the muscle regulatory factor *MyoD1*, and the downregulation of quiescence regulators, like the paired homeodomain transcription factor *Pax7* and Notch signalling^{9,12,13}. However, the mechanisms that control the transition from quiescence to early activation *in vivo* are poorly understood, primarily because the freshly isolated stem cells have altered their quiescence

signature. Here, we harnessed the power of *in Situ Fixation (iSiFi)* - a method developed to irreversibly fix the transcriptome of cells while still in their physiological environment⁹ - to capture the primary molecular events that drive MuSCs out of quiescence, in a temporally resolved manner. Based on a comprehensive time-course analysis of the dissociation process, we confirmed that the transcriptional response to dissociation is indeed time-dependant. Moreover, we have assembled a dynamic gene network of primary MuSCs exiting quiescence. Comparison with *in vivo* activated MuSCs, demonstrated that enzymatic dissociation closely recapitulated the response of these cells to *in vivo* muscle injury. Our analysis also uncovered that under homeostatic conditions, quiescent MuSCs constitute a transcriptionally uniform population with a homogeneous response to injury-induced activation. Moreover, we found that early mitogenic signals drive cells out of quiescence and into the cell cycle, yet act independently from differentiation that requires abrogation of Notch signalling.

Results

Transcriptional atlases of single nuclei from muscle and liver are impacted by tissue dissociation

We have previously shown that during dissociation, almost half of the transcriptome of quiescent MuSCs is modified⁹. In order to test the impact of cell dissociation across cell types and tissues we performed RNA-sequencing (RNA-seq) using a droplet-based platform (10X Genomics) on single nuclei isolated from intact or dissociated murine skeletal muscle and liver (Fig. 1a). It has been shown that single nuclei RNA-seq prevents the cell isolation-induced artefacts as it does not involve cellular dissociation¹⁴⁻¹⁶. Single nuclei sequencing was selected over *iSiFi* as a mean to avoid the modification of the isolation procedure, since aldehyde-fixed cells are not compatible with droplet-based platform (personal observation). Intact-tissue nuclei were obtained directly from dissected liver and limb muscles while dissociated-tissue nuclei were collected after a supplementary treatment for 2 h with the proteolytic enzymes collagenase and dispase at 37 °C with agitation. After quality-filtering (Fig. S1), we resolved 26,074 single-nucleus expression measurements with a median of 2,664 mapped counts and 1,352 detected genes per nucleus (Fig. 1b, S1) using exonic and intronic sequences as previously described¹⁷. Clustering analysis of the

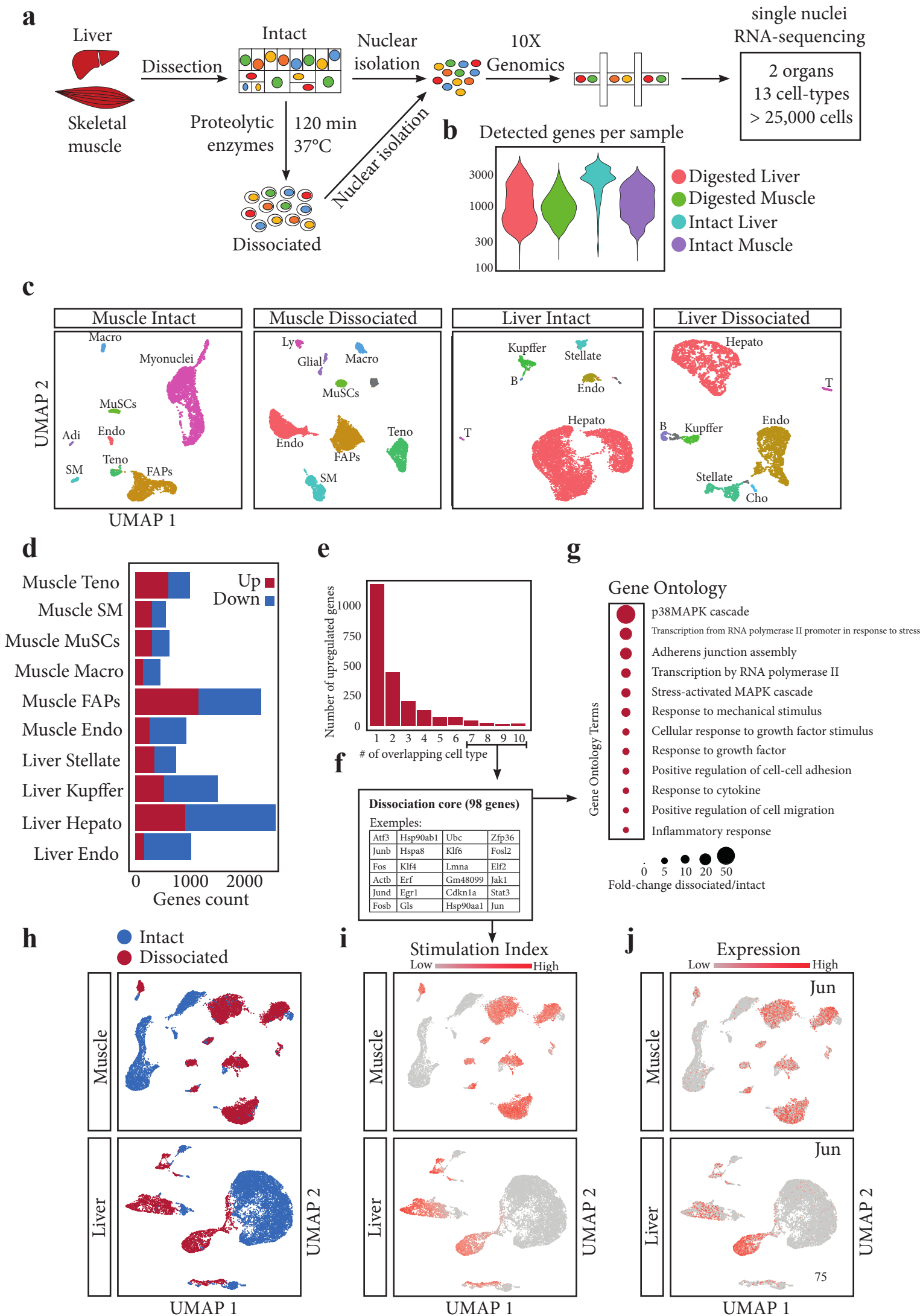


Figure 1 | Dissociation drastically alters the nuclear transcriptome of liver and muscle single-cells

- a) Graphical scheme of the experiment. Single nuclei from muscle (hindlimbs) and liver were isolated from intact tissues or after 2h of dissociation at 37°C with proteolytic enzymes. The nuclei were captured and lysed using the Chromium technology from 10X Genomics. Samples are a pool of three adult female mice.
- b) Violin plots representing the number of genes detected per sample using intronic and exonic sequences before quality-control filtering. Median number can be found in **Fig S1A**.
- c) Uniform Manifold Approximation and Projection (UMAP) plots displaying the different populations **inferred** from intact or dissociated muscle and liver single-nuclei transcriptomes. Endo: endothelial cells; Hepato: Hepatocytes; T: T cells; B: B cells; FAPs: Fibro-adipogenic progenitors; Teno: Tenocytes; SM: Smooth-Muscle cells; Macro: Macrophages; MuSCs: Skeletal muscle stem cells; Ly: Lymphatic cells; Adi: Adipocytes; Cho: Cholangiocytes.
- d) Differential-expression testing of the cellular populations defined in **Fig 1C** using Seurat (see methods). Each population is tested in the direction Dissociated / Intact. The up-regulated genes (induced during dissociation) are shown in red while the down-regulated genes are shown in blue.
- e) Histogram representing the distribution of genes induced by dissociation in the 10 populations displayed in **Fig 1D**. As displayed, approximately half of the up-regulated genes are cell-specific while the other half are up-regulated in at least two populations.
- f) Genes up-regulated by at least 7 population - as shown in **Fig 1E** - compose the dissociation core. Selected examples are displayed in the table.
- g) Gene ontology analysis of the dissociation core genes defined in **Fig 1F** using the biological process category. Selected terms with corrected p-value < 0.05 were displayed and ranked by their fold-change.
- i) UMAP plots of muscle (top) and liver (bottom) tissues showing little intermingling of intact (blue) and dissociated (red) cells, due to a different transcriptome.
- j) UMAP plots of muscle (top) and liver (bottom) intact and dissociated cells showing the correlation between the dissociation status (**Fig 1I**) and the Stimulation Index calculated using the average expression of the dissociation core genes defined in **Fig 1G**.
- k) UMAP plots of muscle (top) and liver (bottom) intact and dissociated cells showing the correlation between the dissociation status (**Fig 1I**) and the expression of a typical dissociation-response gene *Jun*.

transcriptomes was consistent with previously published liver and muscle atlases^{4,8,18,19} (Fig. 1c, S2). We detected 4 major populations in the liver: hepatocytes, endothelial/sinusoidal cells, kupffer cells and stellate cells and 7 main populations in the muscle: myonuclei, MuSCs, fibro-adipogenic progenitors, tenocytes, macrophages and endothelial cells. However, significant differences in relative abundance and even presence of cell-types between intact and dissociated samples were identified. We observed a strong relative enrichment of endothelial cells in both muscle and liver tissues after dissociation and the total loss of myonuclei in the muscle following dissociation (Fig. 1c). Moreover, immune cells – at the exception of macrophages – were surprisingly scarce in our datasets. These discrepancies likely originate from technical and biological factors such as cellular morphology, resistance to the dissociation process and single nuclei capture efficiency. Importantly, however, when we performed differential gene expression analysis on the same cell populations, isolated with or without the dissociation step, we scored variable yet very strong modifications (Fig. 1d). We detected an average of 1,226 differentially expressed genes (DEGs) with a corrected p-value < 0.05 among the 10 cell-types studied (excluding myonuclei). Of note, the number of DEGs was directly correlated with the number of cells within each population suggesting that we have probably underestimated the magnitude of changes in smaller populations. For example, MuSCs – which is a relatively infrequent cell-type within our muscle atlas with 519 nuclei – exhibited 631 DEGs while published reports using bulk RNA-seq found the impact of dissociation to be several folds greater. Of note, 71% of these are overlapping with the published MuSCs dissociation-induced DEGs, validating our single nuclei approach (Fig S3a). We then scored the extent to which the dissociation-induced differences are cell type. As shown in Figure 1e, approximately half of the up-regulated genes are cell-type specific while the other half are up-regulated in at least two populations. A similar pattern can be found for down-regulated genes (Fig. S3b). 98 genes, instead, were induced by dissociation in 7 or more cell types and were designated as the *Dissociation Core* (Fig. 1e, f, S3c). Gene ontology analysis of the dissociation core genes enriched for terms linked to MAPK signalling, response to growth factors and cytokines, and initiation of transcription amongst others (Fig. 1g) which are highly similar to what was previously described for stimulated MuSCs⁹. Consistently, we found a significant induction of MAPK activity in as little as 15 min of whole-muscle digestion by Western blot against phospho-ERK1/2 (Supplemental Fig. S3d). Of interest, when all the transcriptomes of a tissue were projected in one plot, we noticed that although the same cell types tended to cluster close to each other, there was a

clear separation between the intact and dissociated cells, with essentially no intermingling, indicating clear transcriptome-wide differences (Fig. 1h). Moreover, when we calculated a *Stimulation Index* for every cell (average expression of the dissociation core genes) to measure the degree of dissociation perturbation we uncovered that virtually all dissociated cells, both from muscle and liver, scored a high value, while cells from intact tissues were spared (Fig. 1i). The same pattern was obtained when projecting *Jun* expression – a prototypical stress-response gene – on dissociated and intact cells from muscle and liver (Fig. 1j). In conclusion, we demonstrated that the dissociation-induced artefact is not limited to MuSCs: indeed, dissociated liver and muscle cells exhibited a similar stress signature of great magnitude when separated from their microenvironment. These data highlight that the majority of freshly isolated cells acquire a distinct molecular state from their *in vivo* counterparts, which can potentially mislead downstream analyses.

Published single-cell atlases are contaminated with a time-dependent dissociation-induced artefact

To assess the degree of contamination of published atlases by dissociation-induced distortions we systematically monitored the expression of the dissociation core genes within the Tabula Muris dataset⁸, a state-of-the-art multi-organ murine cellular atlas (Fig. 2a). The Tabula Muris dataset encompass more than 120,000 single-cells from 20 organs and tissues, sequenced by two different platforms (droplet-based or Smart-Seq2). First, we calculated the *Stimulation Index* of isolated limb muscle and liver cells from the Smart-Seq2 dataset. Consistent to our single nuclei RNA-seq results (Fig. 1), the limb muscle tissue exhibited a high degree of dissociation core genes expression. Intriguingly, however, the liver did not (Fig. 2b). One possible explanation for this discrepancy was dissociation time. Indeed, the muscle tissue was dissociated for 90 min at 37 °C while the liver tissue was processed in less than 20 min. Instead, in our single nuclei experiment, where we detected high stimulation in the liver cells (Fig. 1i), both muscle and liver tissues were digested for 120 min at 37 °C. To corroborate the potential correlation between dissociation kinetics and dissociation-induced distortions we estimated the digestion time at 37 °C for all cells from the Tabula Muris dataset (see methods). Of interest, we observed a clear correlation between dissociation time and stimulation index for both Smart-Seq2 (Fig. 2c, 2d) and droplet-based (Fig.

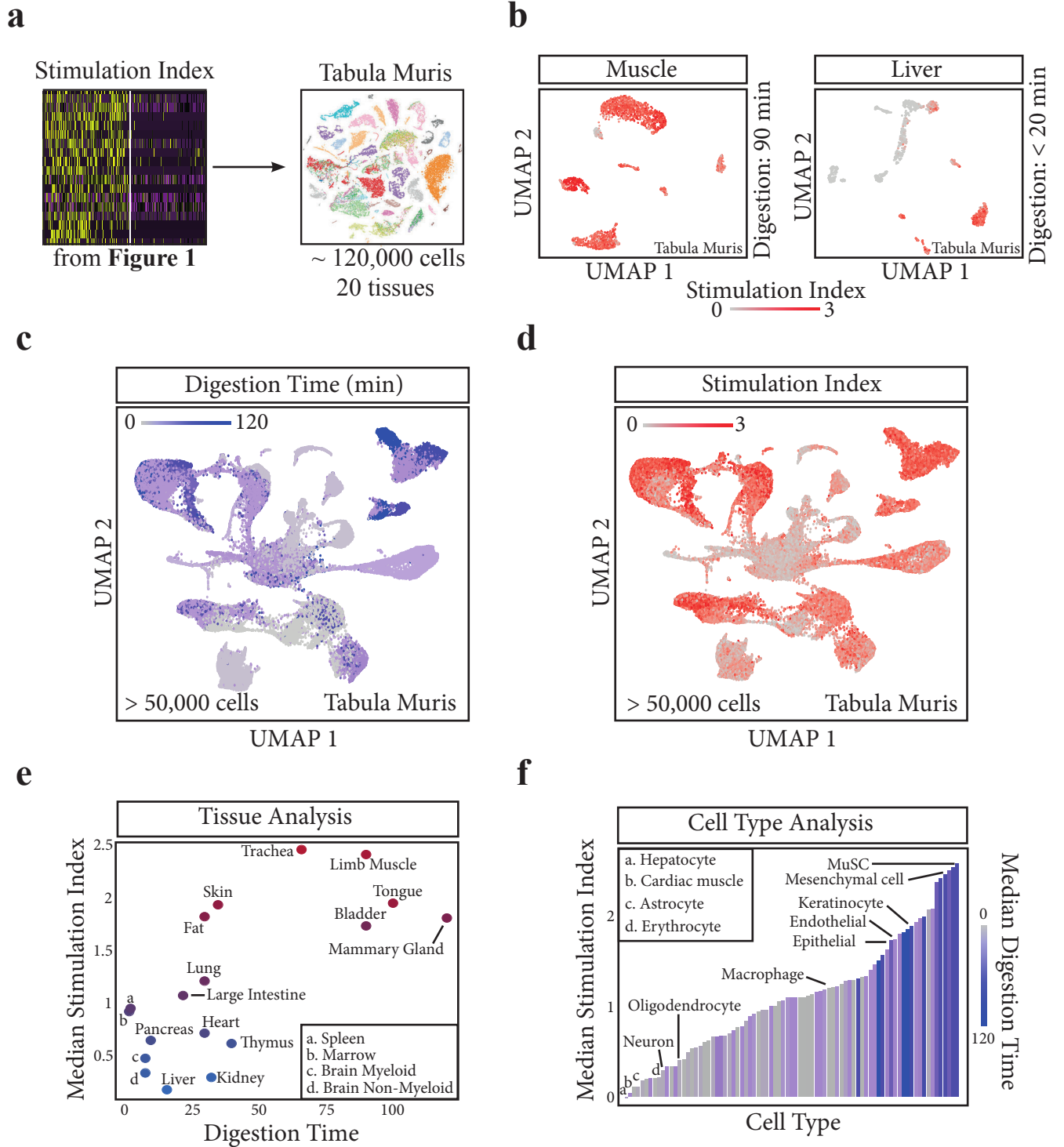


Figure 2 | Published single-cell atlases are contaminated with a time-dependent dissociation-induced artefact

- a) Graphical representation of the experiment. Dissociation core genes from **Fig 1F** were used to calculate the Stimulation Index - as in **Fig 1J** - into the Tabula Muris datasets using more than 120,000 cells from the droplet (> 50,000 cells) and the Smart-Seq2 (> 70,000) datasets across 20 tissues.
- b) UMAP plots representing the Stimulation Index across 2102 muscle single-cells (left) and 981 liver single-cells (right) from the published Tabula Muris Smart-Seq2 dataset. Adjacent to the panels are the digestion time at 37°C for each tissue: 90 minutes for the muscle and 15 minutes for the liver.
- c) UMAP plot representing the digestion time at 37°C of every cell from the published Tabula Muris Smart-Seq2 dataset (53760 cells), inferred from the supplemental methods.
- d) UMAP plot representing the Stimulation Index of every cell from the published Tabula Muris Smart-Seq2 dataset (53760 cells). Note the correlation between high digestion time in **Fig 2C** and high Stimulation Index.
- e) Correlation between tissue digestion time at 37°C and median tissue Stimulation Index calculated from the Tabula Muris Smart-Seq2 dataset (53760 cells).
- f) Correlation between cell-type and median cell-type Stimulation Index calculated from the Tabula Muris Smart-Seq2 dataset (53760 cells). Median cell-type digestion time at 37°C is coded in grey-blue gradient.

S4a, S4b) datasets, with a Pearson correlation coefficient of 0.49. This correlation holds when looking at the median stimulation index per tissue (Fig. 2e, S4c). Indeed, all the tissues dissociated for more than 60 min - such as the bladder, the tongue, the trachea, the limb muscle or the mammary gland - presented a high median stimulation index while all the tissues dissociated in less than 20 min – such as the liver, the marrow, the spleen, the pancreas or the brain presented a low stimulation index. To avoid bias due to cell type composition we also looked at the median stimulation index per cell type across all tissues and consistently observed a correlation with median dissociation time (Fig. 2f, S4d). Cells digested frequently for more than 60 min - such as MuSCs, mesenchymal cells or keratinocytes - exhibited a high stimulation index while cells digested often in less than 20 min – such as neurons, hepatocytes or cardiac muscle cells – presented a low stimulation index.

In conclusion, we observed a similar distortion of transcriptomes in our single nuclei RNA-seq experiment from Figure 1 and in published datasets that affects essentially all cell types, irrespectively of the tissue of origin, and depends on the length of dissociation. Although this seemed to be universally true, what remained unclear was the actual kinetics of the time-dependant dissociation-induced distortions and, importantly, the functional significance of it on the state of a cell.

Minute-scale time-course transcriptomic analysis of MuSCs dissociation response

To dissect the kinetics of the time-dependant modifications observed in Figures 1 and 2, and understand their impact on cell identity we focused on adult, G_0 -arrested MuSCs, a well-established system for stem cell quiescence and rapid activation following stimulation²⁰. Here, we have applied the fixation *iSiFi* methodology⁹ to isolate and analyse MuSCs at different time intervals of the standard cell isolation procedure and thus capture their activation kinetics. MuSCs were isolated every 30 min (T30, T60, T90, and T120) of the standard dissociation procedure (120 min), and compared to quiescent T0-MuSCs. An earlier time-point (T15) was also added to detect the most precocious transcriptional events. MuSCs were collected using flow-cytometry from *Tg:Pax7-nGFP* mice in which nuclear GFP (nGFP) is expressed under the control of the regulatory sequences of *Pax7*, a marker of MuSCs²¹. Subsequently, bulk RNA-seq was performed for each time-point (Fig. 3a). Principal component analysis (PCA) cohesively clustered the samples by time-points and formed a clear activation trajectory along the three main principal components. Of

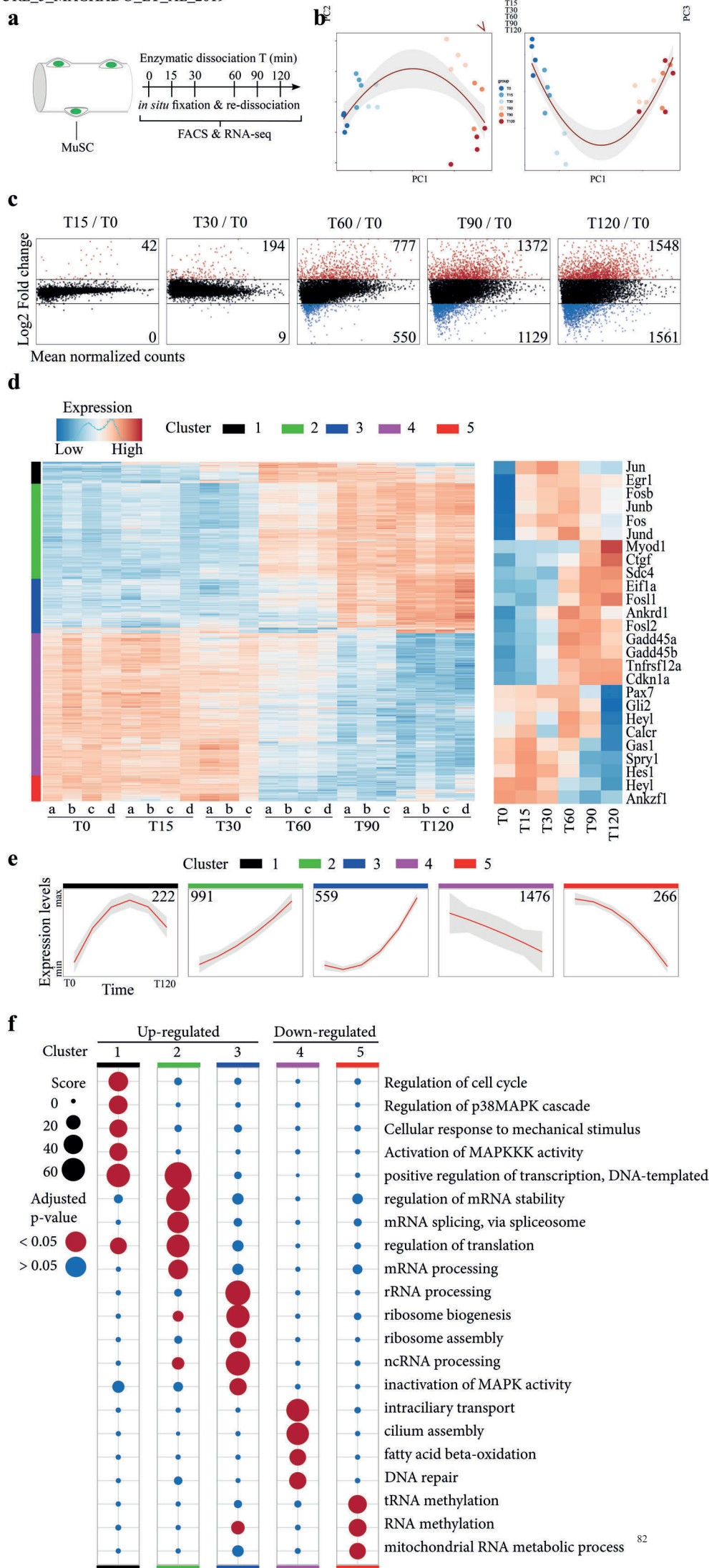


Figure 3 | Time-course analysis of *ex vivo* MuSCs dissociation via bulk RNA-sequencing reveals modules of co-regulated genes.

a) Graphical scheme of the time-course experiment: MuSCs from forelimbs and hindlimbs of *Tg:Pax7-nGFP* mice were fixed with ice-cold 0.5% paraformaldehyde at different time-points during the enzymatic digestion (15, 30, 60, 90, and 120 min) and sorted for GFP for RNA extraction and sequencing.

b) Principal component (PC) analysis during MuSCs *ex vivo* dissociation delineating the transcriptional trajectories during early activation. Trend line and IC-75 have been added for visualization. PC1, PC2 and PC3 represent 27, 10 and 8% of the variance explained, respectively.

c) MA-plots during MuSCs *ex vivo* dissociation. Colored dots represent statistically differentially expressed genes with $p < 0.05$ and absolute FC > 2 (red dots) or < 0.5 (blue dots), using DEseq2 against T0 for each time-point. The number of up- and down-regulated genes is indicated in each panel.

d) Hierarchical clustering of gene expression during MuSC *ex vivo* dissociation reveals transcriptional modules of co-expressed genes. The clusters were extracted from the row dendrogram using $k = 5$ and indicated with a color code (left). The mean expression of specific genes per time-point is shown magnified at the right panel.

e) Clusters of upregulated (clusters 1, 2, and 3) and downregulated (clusters 4 and 5) genes as defined by the hierarchical analysis (Figure 1d). Linear regression with second-order polynomial was performed on the mean gene expression per time-point for each cluster. Samples are ordered from T0 to T120. Standard error is displayed in grey.

f) Gene ontology analysis using EnrichR (GO_Biological_Processes_2018) for all of the genes within each of the five clusters defined in Figure 1d. Color code indicates p-value and circle size the combined enrichment score (0 to 60).

interest, the main biological variation, described by the first principal component (PC1), was detected between 30 and 60 min of dissociation (Fig. 3b). This distribution was confirmed by the number of DEGs with time: the first transcriptional inductions occurred at 15 and 30 min of dissociation and concerned less than 200 transcripts ($FC > 2$) yet most differential expression events took place at 60 min of the isolation procedure, reaching a maximum at 120 min when they reached a scale reminiscent of the previously reported T0-T120 transition number REF (> 3000 DEGs, $FC > 2$; Fig. 3c) with comparable gene expression (Supplemental Fig. S5a).

During the enzymatic incubation, MuSCs are progressively detaching from the chopped myofibers (2-3 mm pieces) and released in the enzyme-containing medium. Complete MuSCs dissociation is achieved in 90-120 min. Since we analysed bulk Pax7-GFP populations, one concern was that the cells responded differently according to their degree of dissociation. We assessed the relative impact of physical cell dissociation versus digestion time by comparing the expression of dissociation-sensitive transcripts at mid-digestion (60 min) between MuSCs within muscle pieces (pelleted with gravity) and already dissociated cells (solubilized). Consistent to the observation that digestion time (here, exposure to growth factors and micro-disturbance of the MuSC niche even when found adjacent to the myofibers), no significant differences in transcript levels between the two groups were detected by RT-qPCR (Supplemental Fig. S5b).

In conclusion, we found that MuSCs dissociation-induced response follow a coherent transcriptional trajectory depending on digestion time, with inductions happening in as little as 15 min of digestion, and the majority of the transcriptional changes occurring between 30 and 60 min.

Temporally resolved transcriptional network of MuSCs activation

In order to systematise the time-course dataset, genes with similar transcriptional kinetics were grouped using hierarchical clustering (Fig. 3d). We identified 5 transcriptional clusters with distinct expression patterns: clusters 1/2/3 (up-regulated genes compared to T0) and clusters 4/5 (down-regulated genes compared to T0) (Fig. 3d-e). Of interest, Cluster 1 comprised 36 out of the 42 genes upregulated after just 15 min of dissociation (T15/T0, $FC > 2$, $p < 0.05$), including transcription factor encoding immediate and early response genes *Ier2*, *Ier3*, *Egr1*, and *Egr2*. Also,

members of the AP-1 family of oncogenes, classically induced by ERK1/2 mediated MAPK signalling, were drastically up-regulated at T15: *Jun*, *Junb*, *Jund*, *Fos* and *Fosb* were respectively induced 21.3, 37.6, 8.1, 165.1 and 210.3-fold, relative to quiescent T0 MuSCs. Cluster 1 pattern of expression was characterized by an early T60 peak that rapidly reverted back or close to T0-levels after 2h of digestion. Consistently we scored an up-regulation of the stress sensor genes *Gadd45a*, *Gadd45b*, *Gadd45g* with fold-changes of 9.1, 33.6 and 11.7, respectively, in T60 compared to T0 with decreasing levels in later time-points²². This bell-shape expression pattern, partially explained by protein-mediated negative auto-regulatory loops⁷, is stereotypical of growth-factor or stress driven responses^{23,24}. This finding indicates that the MuSCs isolated by standard methods have undergone complete cycles of biological processes which have been disregarded until now.

Transcriptional events directly linked to the myogenic program were found well into the second hour of digestion (90-120 min after its initiation), such as the induction of *Myod1* (cluster 3, fold-change of 11.9 in T120 compared to T0) or the downregulation of the MuSCs quiescence markers *Pax7*²⁵, *Spry1*²⁶ and *Calcr*^{27,28} (cluster 4, fold-changes of 3.5, 3.2 and 1.7 respectively in T0 compared to T120). Similarly, we scored attenuation of Notch signalling at the latest time-points, with pathway canonical target genes *Hey1*, *Hes1* and *HeyL* being downregulated at T60, T90 and T120, respectively compared to T0. Counterintuitively, but consistent with its role as an adaptor protein of kinase complexes²⁹ and a member of the *Dissociation Core* (Fig. 1g), the cell cycle inhibitor encoding gene *Cdkn1a* (*p21*) was up-regulated by the dissociation procedure (cluster 2, fold-change of 29.9 in T120 compared to T0). Finally we observed that *Sdc4*, an established marker of freshly-isolated MuSCs³⁰, was also up-regulated by the dissociation-procedure (cluster 2, fold-change of 6.1 in T120 compared to T0) which was also observed at the single nuclei level (Fig. S2a, S2b).

To obtain an unbiased view of the processes implicated during the MuSCs dissociation-response, we performed ontology analysis on the gene clusters we defined using hierarchical clustering. We found that these clusters did not differ merely on the gene expression patterns, but also exhibited distinct functional identities (Fig. 3f). In fact, the ontology terms that emerged during MuSCs dissociation resembled the global cell responses (Fig. 1d), yet now were time-resolved and represented a sequence of coherent biological processes: the triggering events of quiescence exit

was stimulation of the mitogenic MAPK cascade and initiation of transcription, consistent with the observation that activated cells express more transcripts than the quiescent cells^{28,31}, (cluster 1). This was followed by mRNA processing, including splicing and initiation of translation (cluster 2), and in a later phase by ontologies related to ribosome assembly and biosynthesis (cluster 3). Of note, late cluster 3 (maximum induction at T120) also contains ontologies related to inactivation of MAPK signalling, which coincides with the attenuation of the related genes of early cluster 1 (drop of induction at T120). The quiescence-to-activation transition is nevertheless characterized by a downregulation of a significant number of genes⁹. Indeed, we validated previous findings on T0-MuSCs enriched ontologies, including a switch from fatty-acid beta-oxidation to glycolysis, and processes related to cilium disassembly^{9,32,33} (cluster 4). Of interest, cluster 5 was enriched in ontologies related to RNA methylation and mitochondrial RNA metabolic genes, yet the significance of these processes in quiescence-exit remains to be uncovered. In conclusion we have established the first transcriptional map of the activation kinetics for primary, *in vivo* quiescent stem cells. This map outlines a series of sequential biological processes, distinct yet correlated, that mediates this transition.

Dissociation-induced activation correlates with early MuSCs response to injury

To decipher the transcriptional network characterizing *in vivo* MuSCs quiescence exit as well as to gain insights into pre- and post-activation MuSCs heterogeneity, we performed single-cell RNA-seq (scRNA-seq), time-course analysis of fixed MuSCs following skeletal muscle injury. Hind limb *Tibialis Anterior* (TA) muscles of *Tg:Pax7-nGFP* mice were injected with the myotoxin BaCl₂ to induce injury (Fig. 4a, b) and MuSCs were collected using *iSiFi* prior to injury (scT0, Fig. 4a) or 2 and 4 h after injury (scT2, scT4, Fig. 2a). These time intervals were selected based on a preliminary RT-qPCR screening for *Pax7*, *Myod1*, and *Jun* transcripts (Fig. S7a). We adapted the SMARTseq2 scRNA-seq protocol (see Materials & Methods) to obtain individual cell transcriptomes from *iSiFi*-treated samples (note that 10X Genomics methodology is not yet compatible with aldehyde-fixed cells). After quality controls we obtained 280 cells with a median of 1 581 detected genes per cell (Fig. S5). PCA analysis delineated a clear trajectory from scT0 to scT4 through scT2 cells, which grouped the cells according to their experimental condition and showed transcriptional consistency within clusters, yet marked differences between time-points (Fig. 4c).

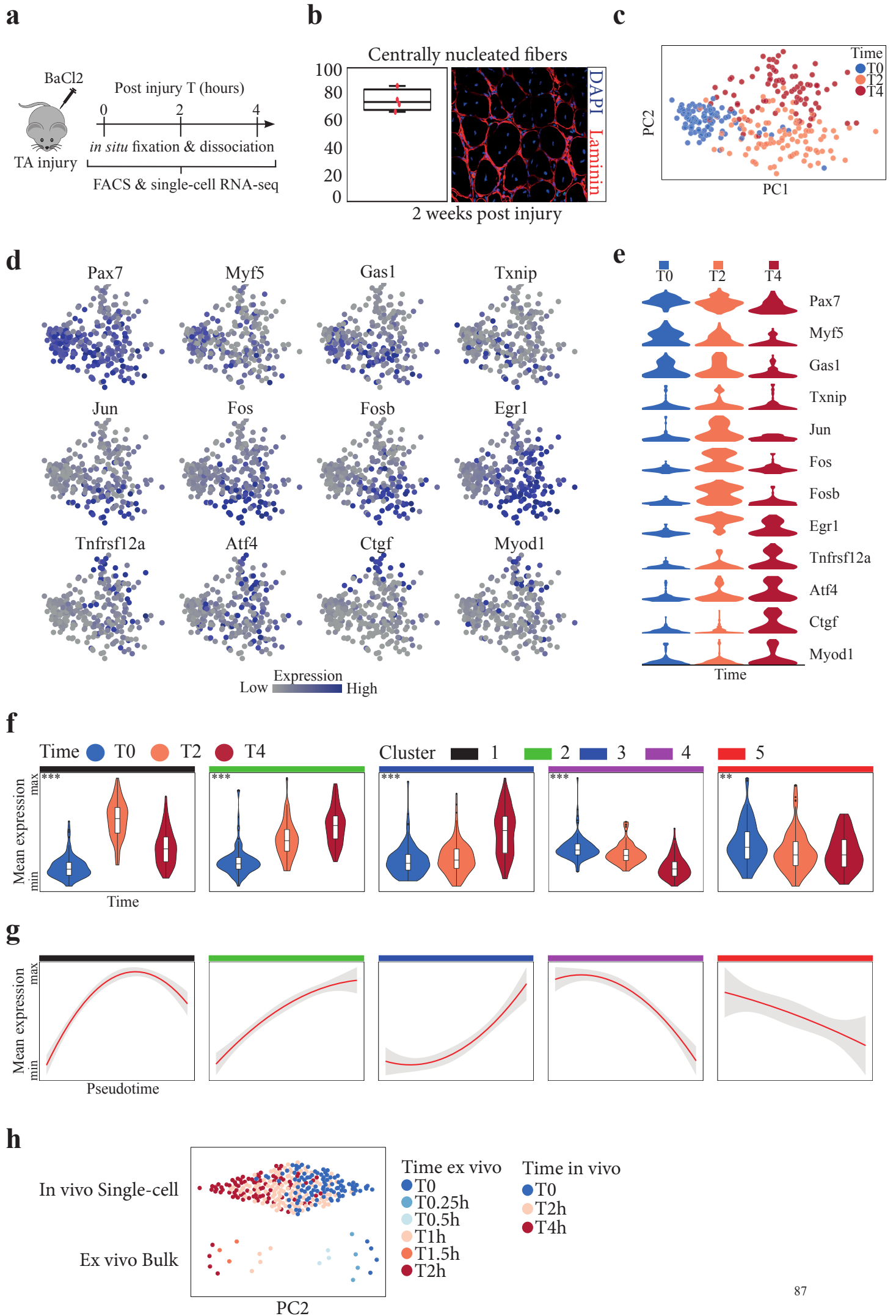


Figure 4 | *In vivo* single-MuSC transcriptional response to muscle injury

- a) Graphical scheme of the experiment: TA muscles of *Tg:Pax7-nGFP* mice were injected with BaCl₂ and single MuSCs were isolated by *iSiFi* at 0, 2 and 4 h post-injury.
- b) Validation of the BaCl₂ injury efficiency by staining for DAPI and laminin two weeks post-injury. Graph shows the percentage of centrally located nuclei in regenerated myofibers; n=4.
- c) Principal component analysis (PCA) of resting (T0) and *in vivo* activated MuSCs (T2 and T4). PC1 and PC2 represent 4 and 3% of variance explained, respectively.
- d) Dynamic expression of selected genes displayed on the PCA plot of Figure 3c, showing enrichment in T0 (top row), T2 (middle row) or T4 cells (bottom row).
- e) Violin plot of the expression of the genes displayed in Figure 3d per time-point.
- f) Mean expression of the genes from the 5 clusters during *in vivo* activation across the three time-points (T0 and post-injury T2 h and T4 h). Statistical test for Cluster 1 was T2 against T0, for the rest T4 against T0.
- g) Linear regression with second-order polynomial (red line) on the mean gene expression per cell along pseudotime. Gene sets are based on the 5 clusters identified in the *ex vivo* experiment (Figure 1d) and samples are ordered from minimum to maximum pseudotime value. Standard error is displayed in grey.
- h) PCA analysis of bulk *ex vivo* dissociation samples combined with *in vivo* activation single-cells (ranked list). PC2 separated the samples based on experimental time and represent 2% of variance explained.

Unpaired Student t-test was performed; * p < 0.05 ** p < 0.01 *** p < 0.001

In contrast to previous single-MuSCs datasets^{8,18,34,35}, using *iSiFi* we found strong *Pax7* expression in nearly all scT0-MuSCs (94% of scT0 cells with more than 10 counts) and a marked, progressive down-regulation upon injury (75% and 39% of scT2 and scT4 cells respectively with more than 10 counts, Fig. 4d, e), consistent to our *ex vivo* dissociation bulk RNA-seq data (Fig. 3d). Moreover, many transcripts exhibited similar kinetics during *in vivo* activation and *ex vivo* dissociation. For example, *Myod1* and *Ctgf* transcripts were merely expressed until 4 h post-injury in scT4-MuSCs (Fig. 4d, e), whereas transcripts with peak-expression motifs during *ex vivo* dissociation (cluster 1, Fig. 3) behaved analogously in *in vivo* activation (Fig. 4d, e). Once again, cluster 1 oncogenes, like *Junb*, have been falsely assigned to quiescent MuSC in published atlases⁸, (95% *Junb* positive versus 10% in scT0-MuSCs, Fig. 4d, e). To extend this correlation, we plotted the behaviour of the differentially expressed genes of the 5 clusters (*ex vivo* dissociation, Fig. 3) in the *in vivo* scRNA-seq dataset. As shown in Figure 4f and 4g, these genes displayed very similar behaviours *in vivo*: cluster 1 DEGs exhibited a bell curve, cluster 2 DEGs a linear up-regulation, cluster 3 DEGs a late logistic curve, cluster 4 DEGs a sigmoidal-like down-regulation and cluster 5 DEGs a more linear one (compare to Fig. 3e). Finally, more than 70% of the DEGs across time *in vivo* were also found as differentially expressed during *ex vivo* activation (Supplemental Fig. S7b, c). Ontology and pathway analysis during *in vivo* activation reproduced the phenomenon observed during *ex vivo* dissociation, with an initial MAPK signalling activity and initiation of transcription followed by ribosomes biogenesis and translation related enriched terms (Supplemental Fig. S7d).

To unbiasedly compare the *ex vivo* dissociation and *in vivo* activation, we also performed PCA analysis on the shared transcripts amongst the two conditions. As expected, the first principal component (PC1) described the technical variation between bulk RNA-seq and scRNA-seq data (Supplemental Fig. S7e). However, PC2 separated the cells of the two experimental paradigms along time with corresponding chronological order, so that, for example, *in vivo* T0 correlated to *ex vivo* T0, and *in vivo* T2h to *ex vivo* T1h (Fig. 4h).

Taken together, our results displayed a surprisingly high degree of overlap between *ex vivo* dissociation and *in vivo* activation (albeit with twice slower kinetics for *in vivo* activation). In

addition, our data demonstrate that freshly isolated MuSCs display the transcriptional status of at least 4 h *in vivo* activated MuSCs.

MuSCs engage in a unique transcriptional program following muscle injury

The existence of heterogeneity within the adult MuSC pool has been extensively studied yet the relationship across the different subpopulation remains unclear^{34,36–39}. As shown on the PCA graph, quiescent MuSCs from resting TA muscle (scT0) formed a unique, compact cluster (Fig. 4c and 5a, median Euclidian distance 2.8). The activated scT2 and scT4 cells were more scattered, yet remained distinct despite some intermingling at the interfaces between the three clusters (Fig. 4c and 5a, median Euclidian distance 4.8 and 4.9, respectively).

To precisely order cells along the activation trajectory we performed trajectory analysis using the pseudotiming tool Monocle2⁴⁰. The MuSCs formed three discrete cellular states along this trajectory corresponding to the 3 time points, without further branching events, indicating homogeneity in the activation response (Fig. 5b). Limited intermingling was scored between the time-points along this trajectory despite the presence of cells along the entire length of the main branches, suggesting that all cells transition evenly from scT0 to scT2 to scT4 state yet with variable kinetics. Supporting this conclusion, when we compared real time to pseudo-time we found that the density curves of the latter obeyed the actual chronological order (Fig. 5c).

To further refine the separation already obtained by PCA, we performed k-median clustering on the first two principal components and resolved 5 discrete populations (Population 1 to 5), defining cellular sub-states along the activation trajectory (Fig. 5d, e). Pseudotime analysis placed density curves in chronological order (Fig. 5f), suggesting that each sub-population is a transition state between two time points and not a group of cells with differential response. The same conclusion was reached when the expression of the DEGs from the *ex vivo* time-course was scored in the 5 Populations. As shown in Figure 5g, the sub-populations further refined the correspondence between *in vivo* activation and *ex vivo* dissociation time-points.

In conclusion, our *in vivo* analysis indicates no strong transcriptional heterogeneity in the quiescent MuSCs population of the TA muscle nor differential responses to activation stimuli. Despite

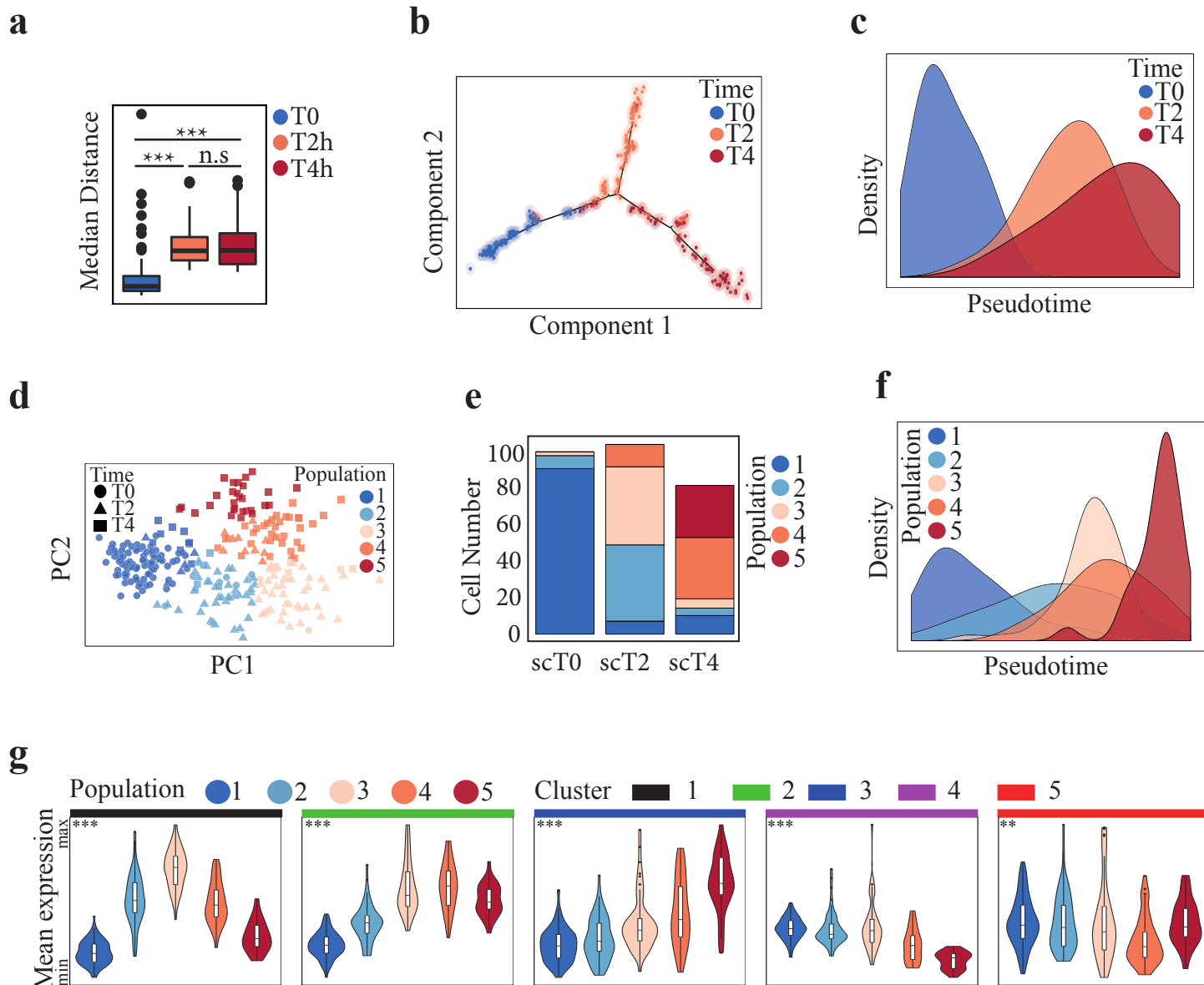


Figure 5 | MuSCs do not exhibit strong heterogeneity pre- and post-injury.

- a) Median Euclidian distance of each cell from the other cells within its group (time-point) to show transcriptional heterogeneity. The first two principal components from Figure 3c were used as coordinates.
- b) Pseudotime-analysis using Monocle2 shows the differentiation trajectories of MuSCs during *in vivo* activation.
- c) Density analysis displaying the distribution of cells from each group (time-point) along pseudotime.
- d) Clustering of the cells in homogeneous sub-groups (populations) via *k-median* using the first two principal components from Figure 3c as coordinates and $k = 5$.
- e) Bar-plot showing the distribution of the cells from each population per time-point.
- f) Density analysis displaying the distribution of cells from each population along pseudotime.
- g) Mean expression of genes from each cluster (Figure 3d) during *in vivo* activation across the *k-median* defined populations. Cluster 1 statistical test was P1 against P3, for the rest P1 against P5.

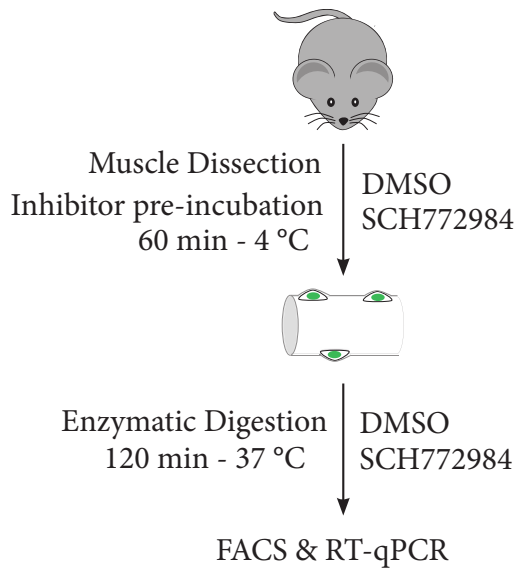
different kinetics, we suggest that all MuSCs exit the T0 state upon injury and follow the same trajectory. We propose that the different kinetics are the outcome of stochasticity in transcriptional kinetics or in the exposure to activatory signals, but do not represent real transcriptional heterogeneity as previously suggested^{34,39}.

ERK 1/2 signalling is required for the activation of MuSCs

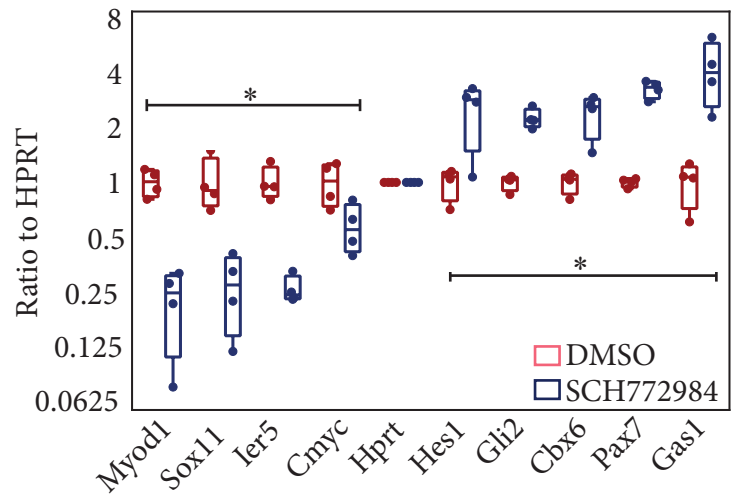
Extracellular signal-regulated kinase (ERK) signalling is a known regulator of cell proliferation in many cell types⁴¹. Studies in culture myoblasts have shown that growth factor-stimulated ERK1/2 signalling is required during the G1 phase of the cell cycle¹². Nuclear, active ERK has also been shown to promote myoblasts proliferation during chick embryogenesis, where signalling abrogation, mediated by cytoplasmic shuttling of ERK, is required for terminal muscle differentiation⁴². Here, we investigated the role of this pathway in quiescence exit. As described above, the first transcripts upregulated in MuSCs exiting G0 are transcription factor genes induced by MAPK ERK 1/2 signalling. We, therefore, hypothesized that this pathway could be the initiator of the later transcriptional modifications imposed on the cells during activation. To test this hypothesis, we performed standard MuSCs dissociation from hind limb muscles in the presence of the small molecule inhibitor SCH772984, which abrogates ERK 1/2 activity via the inhibition of p90 RSK and ERK 1/2 phosphorylation (Fig. 6a). At the end of the enzymatic digestion, MuSCs were FACS-isolated and RT-qPCR was performed for a handful of transcripts significantly induced or repressed during MuSCs dissociation⁹. We found a significant tempering of the activation response even in secondary response genes that are modified at later time-points (Fig. 6b).

To test whether ERK 1/2 would also play a role on the G0-to-S transition, we isolated MuSCs via standard procedures and seeded them in the presence of the inhibitor. The first S-phase was assessed by the incorporation of the nucleotide analogue 5-ethynyl-2'-deoxyuridine (EdU). Indeed, we found that MuSCs treated with SCH772984 were entirely impaired in their capacity to enter the cell cycle as virtually all treated cells were negative for EdU (2% EdU positive), even 72 h after seeding (Fig. 6c, d) whereas 83% of the control cells went through at least one S-phase. Of interest, MYOD1 protein induction, which is detected 4-8 h following MuSCs dissociation and is considered a hallmark of activated MuSCs¹², was not impacted by SCH772984 after 40 h of treatment (Fig. 6e). To conclude, we found that ERK signalling inhibition only partially mitigated

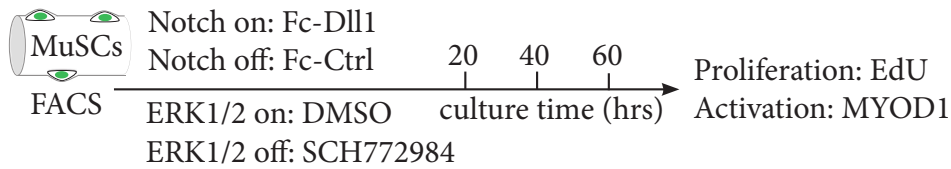
a



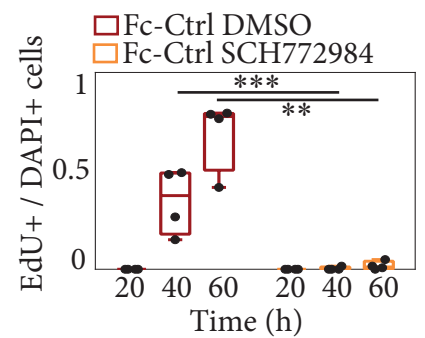
b



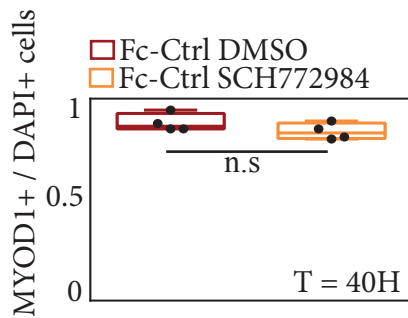
c



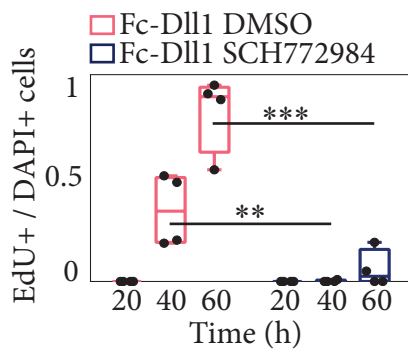
d



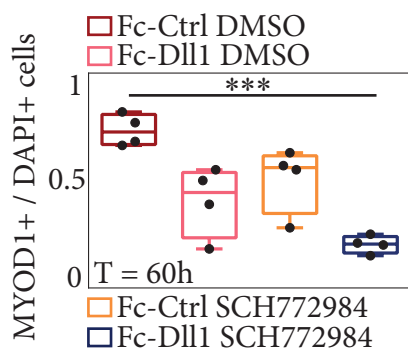
e



f



g



h

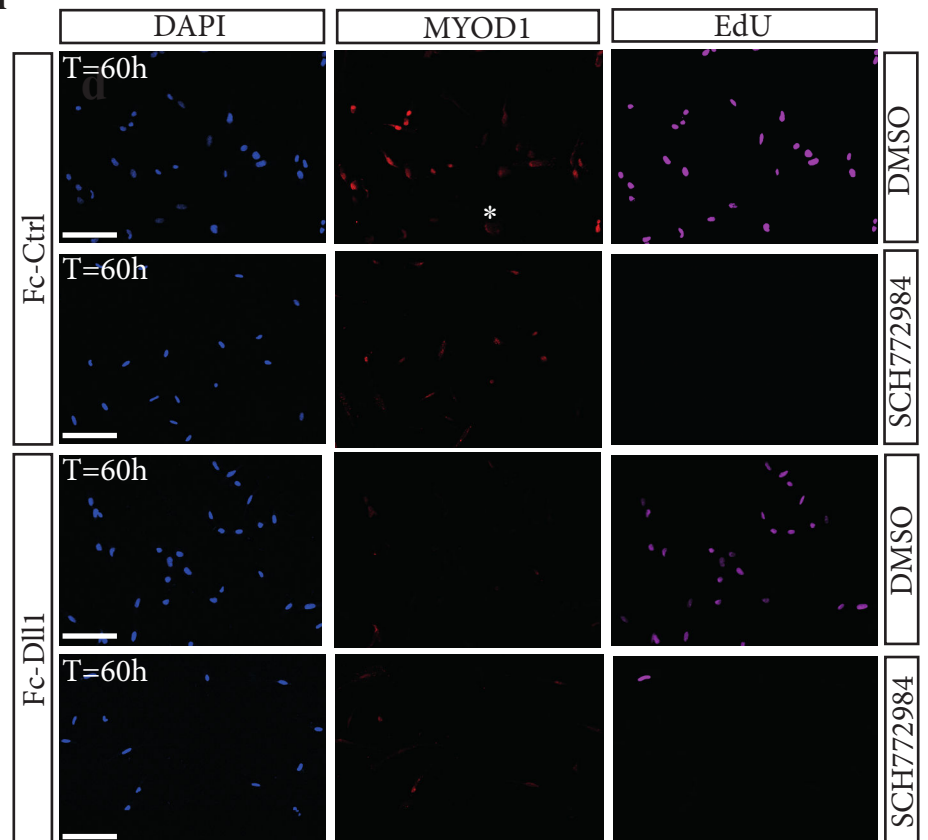


Figure 6 | Combinatorial signaling drives MuSCs quiescence exit

- a) Graphical scheme of the experiment: chopped 1-2mm muscle pieces were incubated with the Erk 1/2 inhibitor SCH772984 or DMSO carrier for 60 min at 4°C before being digested for 120 min at 37°C in the presence of the inhibitor or its control. MuSCs were sorted for GFP (Tg:Pax7-nGFP mice) directly in lysis buffer for RNA extraction; n=4.
- b) RT-qPCR analysis of dissociation-sensitive transcripts after MuSCs isolation in the presence of SCH772984 or DMSO. The test was corrected for multiple hypothesis testing with an FDR of 5%.
- c) Graphical scheme of the experiment: Isolated MuSCs were cultured for 20, 40 or 60 h in the presence of SCH772984 or DMSO, on Fc-Dll1 or Fc-Ctrl coated plates.
- d) EdU incorporation 20, 40 or 60 h after plating with SCH772984 or DMSO on Fc-Ctrl coated plates. EdU was added at t= 0 h.
- e) Quantification of MYOD1 positive cell by immunostaining 40 h after plating with SCH772984 or DMSO on Fc-Ctrl coated plates.
- f) EdU incorporation 20, 40 or 60 h after plating with SCH772984 or DMSO on Dll1-Ctrl coated plates. EdU was added at t= 0 h.
- g) Quantification of MYOD1 positive cell by immunostaining 40 h after plating with SCH772984 or DMSO on Fc-Dll1 coated plates.
- h) MYOD1 immunostaining 60 h after plating with SCH772984 or DMSO on Fc-Ctrl or Fc-Dll1 coated plates. The asterisk indicates cytoplasmic background staining that in MYOD1 negative cells.

Independent student t-test were performed. * $p < 0.05$ ** $p < 0.01$ *** $p < 0.001$

exit from quiescence, as MuSCs fail to enter S-phase yet are not retained in an undifferentiated G0 phase, indicated by the presence of the early activation marker MYOD.

Combinatorial signals are necessary for MuSCs to exit quiescence

ERK signalling inhibitors blocked G0-to-S transition, however, did not prevent MuSCs early differentiation, suggesting that these two processes are uncoupled. Interestingly, our time-course analysis indicated that induction of *Myod1* expression is concomitant with the downregulation of Notch signalling (*Hes1*, *Hey1* and *HeyL* targets), an established antagonist of myogenesis⁴³⁻⁴⁵, (Fig. 3d). With the aim to maintain culture MuSCs in a quiescent state, cells were seeded on plates coated with the Notch ligand Delta-like 1 combined with SCH772984 and were evaluated for proliferation and expression of MYOD1 during 60 h of culture. Notch signalling activation alone had no effect on cell cycle re-entry of freshly isolated MuSCs (Fig. 6c, f). However, the combination maintained MuSCs at a non-cycling (EdU negative) and undifferentiated state (Fig. 6g, h). Taken together, we identified two independent pathways controlling proliferation and differentiation during early activation phase of MuSCs, hence providing a powerful approach to maintain MuSCs in a quiescent-like state.

Discussion

It appears explicit that extracting a cell from its microenvironment would impact its transcriptome. The first systematic demonstration of the extent of changes imposed by the dissociation procedure, however, was only recently reported by three independent studies on MuSCs⁹⁻¹¹. Nevertheless, this perturbation has been overlooked by the vast majority of studies, considered as a particular behaviour of this specialised stem cell type.

In the present report, we comprehensively assessed the effect of dissociation using single nuclei RNA-seq on two regenerative tissues, the skeletal muscle and the liver, across more than a dozen of different cellular ontologies. We uncovered that dissociation is extensively impacting most cell types, refuting the notion that dissociation sensitivity is an idiosyncratic response of MuSCs. By systematically analysing a comprehensive organismal cellular atlas we confirmed the ubiquitous presence of dissociation-induced signatures, in a dissociation-time dependant manner.

Dissociation induces cell state transitions greater than simple stress signatures that cannot be overlooked or retrospectively removed. It induces genome-wide alterations, frequently in cell-specific processes unrelated to stress.

For example, a puzzling finding in the field has been the high number of cells with no or low *Pax7* expression in scRNA-seq analyses of freshly isolated MuSCs^{8,18,34,35}; Schaum et al., 2018 described 70% of the MuSCs as *Pax7* negative. In fact, *Pax7* gene is unambiguously the most well-established marker of MuSCs in adult muscle and is used as the gold-standard of MuSC identity²⁵. This conundrum was often interpreted as a technical limitation related to the sensitivity of scRNA-seq. We observe a drastic decrease of *Pax7* transcripts in all three of our experimental models, underscoring how dissociation can impact critical components of cellular identity. Another example of overlap between cellular processes of interest and stress response can be found in the nerve cells. Many members of the dissociation core genes, such as the AP-1 family members *Jun* and *Fos*, are involved in processes such as learning and represent a critical readout for neuronal activity⁴⁶. The induction of these genes by cellular dissociation can therefore distort data interpretation from freshly-isolated neurons, as previously suggested^{14,47}. Moreover, it has been reported that dissociation could lead to spurious clustering of populations in the brain⁴⁷, kidney¹⁶ and skeletal muscle³⁹. Of note, the latter study reported that just a minor sub-population of MuSCs (about 20%) responded to a 60 min dissociation. Our data do not support the existence of such heterogeneous response. Instead, we find that all MuSCs are readily activated by the 120 min mark following the same trajectory, yet with different kinetics. We propose that the reason of this apparent contradiction lies in the logistic nature of the MuSCs response to dissociation: most of the transcriptomic alterations are manifested between 30 min and 60 min of dissociation. Therefore, minutes differences in the isolation protocols and stochastic heterogeneity in the transcription of cells at the inflection point can lead to drastic transcriptional changes and misguided data analysis. Such sensitivity in experimental conditions can also partially explain the troubling importance of batch effect variability in transcriptional studies, which greatly complicates downstream analysis⁴⁸.

The surprising high percentage of cell-type specific responses to dissociation indicates that different cells activate distinct genetic programs in response to niche disturbance. Our literature analysis indicates that dissociation time is dominant important over tissue of origin in determining

the magnitude of the dissociation-induced alterations. Nevertheless, our single-nuclei atlas study focused on highly regenerative organs – skeletal muscle and liver - which could present an exacerbated response to dissociation. Models of extreme tissue remodelling such as axolotl⁴⁹ or planarian regeneration⁵⁰ will be invaluable tools to understand the connection between dissociation-response, tissue injury and regenerative processes.

By performing high-throughput analysis on MuSCs we demonstrated that the quiescence-to-activation transition is hardwired and not readily influenced by the microenvironment. Indeed, we showed that *in vivo* activation and *ex vivo* dissociation initiated the same genetic program. Our data further support that MuSCs dissociation protocol is a strong experimental paradigm to study quiescence exit and early activation. Of note, despite the qualitative similarities, we noticed a delay by a factor of almost 2 in the *in vivo* responses, probably due to the nature of the experimental models (distribution of BaCl₂ versus mechanical and proteolytic muscle digestion). On the other hand, given the complexity of cellular niches, it seems less feasible to develop an *ex vivo* system to revert or even sustain a cell in a status equivalent to an *in vivo* state. Our analysis proposes that the primordial quiescence-breaking event is the induction of MAPK signalling response genes, in close resemblance to growth factor signalling. Antagonizing ERK1/2 activity with pharmacological inhibitors completely blocked cells from entering S-phase, but did not prevent MuSCs from differentiating. Instead, Notch signalling has an established anti-myogenic activity, with no direct effect on the cell cycle⁴⁵. Therefore, by adding sustained Notch activity to the equation, we were able to retain the isolated MuSCs in a quiescent-like state (non-cycling, MYOD1 negative cells). Overall, dissection of the epistatic relationships of the different pathways that act during the activation phase, provides a powerful tool for MuSCs manipulation.

In conclusion, we demonstrated that dissociation dynamically distorts the profile of isolated cells in a dissociation-time dependant manner, polluting published datasets and eliciting cell state transitions such as quiescence exit. The present work is aimed to be a wake-up call for the field of transcriptomic studies. Careful dissociation-time management or techniques that allow to preserve the *in vivo* molecular profile of a cell, like *iSiFi*^{9,11}, single nuclei RNA-seq^{15,16}, cold dissociation⁵¹ or spatial transcriptomics⁵²⁻⁵⁴ should be considered for the production of more accurate, second-generation single-cell atlases.

Acknowledgements

We would like to thank Hanne Grosemans for performing the muscle injuries for the single-cell RNA-sequencing. We would like to thank Caroline Proux for generating next-generation sequencing libraries for the *ex vivo* dissociation time-course experiment. We would like to thank Brigitte Izac and Benjamin Saintpierre from the genomic facility of the Institut Cochin (Université de Paris, Institut Cochin, CNRS, INSERM, F-75014 Paris, France) for the generation of single nuclei sequencing libraries and data processing. FR laboratory receives funding from Association Française contre les Myopathies (AFM) via TRANSLAMUSCLE (PROJECT 19507), Labex REVIVE (ANR-10-LABX-73), Agence Nationale pour la Recherche (ANR) grant Bone-muscle-repair (ANR-13-BSV1-0011-02), Satnet (ANR-15-CE13-0011-01), BMP-MyoStem (ANR-16-CE14-0002-03), MyoStemVasc (ANR-17-CE14-0018-01) and RHU CARMMA (ANR-15-RHUS-0003). Caroline Proux from the Biomics Platform of the Institut Pasteur are supported by France Génomique (ANR-10-INBS-09-09) and IBISA.

AUTHOR CONTRIBUTIONS

Designed experiments, L.M., Ph.M. and F.R.; Performed experiments, L.M., M.D.S, J.C., J.V.H. and Ph.M.; Interpreted data, L.M., Ph.M. and F.R.; Bioinformatic analysis L.M., J.C., H.V. and R.L. Wrote the manuscript, L.M., Ph.M. and F.R.; Funding Acquisition, M.S., T.V., P.M., Ph.M. and F.R.; Supervision, Ph.M. and F.R.

DECLARATION OF INTERESTS

The authors declare no competing interests.

Materials and methods

Mouse RT-qPCR primers

Gene	Forward primer	Reverse primer
Cbx6	GTATGGGCCCAAGAAGAGGG	CGCTCGGCTTGACAGAGAAA
Cmyc	GATTCCACGGCCTTCTCTCC	GCCTCTTCTCCACAGACACC
Gas1	TCTGCAGAATTCGGGACACC	CTTGAAAGACCCCCACCGTT

Gli2	CCTGCATGCTAGAGGCAAACCTT	AGTCTCCATCTCAGAGGCTCAT
Hes1	ACACCGGACAAACCAAGAC	AATGCCGGGAGCTATCTTTC
Irf5	CTACCCCTCTCAAGAAGCCG	CCGAGAAGCTAGACCCGAAG
MyoD	GGCTACGACACCGCTACTA	GAGATGCGCTCCACTATGCT
Pax7	AGGCCTTCGAGAGGACCCAC	CTGAACCAGACCTGGACGCG
Sox11	GCGAGAAGATCCCGTTCATCA	GGGTCCGTCTTGGGCTTTTTG
Hprt1	AGGGCATATCCAACAACAACTT	GTTAAGCAGTACAGCCCCAAA

Animals

Eight- to 12-week-old heterozygous *Tg:Pax7-nGFP* [C57/Bl6]⁵⁵ were used to isolate MuSCs. Animals were handled as per French and European Community guidelines and protocols were approved by the ethics committee at the French Ministry (Project No: 15-018).

Muscle Injury

For muscle injury, mice were anesthetized with an intraperitoneal injection of 1.6:1 ketamine and xylazine (2%, VMD), 60 μ l per 20g of bodyweight. Both *Tibialis Anterior* muscles were injected with 50 μ l BaCl₂ (1.2%, Sigma 202738 lot # MKBZ2444V). The mice were sacrificed 2, 4 or 6 h post-injury. For BaCl₂ efficiency control the mice were sacrificed 14 days post-injury.

ERK1/2 inhibition during muscle dissociation

1-2 mm dissected muscle pieces were incubated for 60 min at 4 °C in the presence of the ERK inhibitor SCH772984 (Selleckchem, S7101) at 10 μ g/ml or DMSO control to allow penetration of the inhibitors in the tissue prior to dissociation. Samples were spun down (600 g, 5 min) and incubated in 1X digestion solution (Dispase II, 3 U/ml [Roche, 4942078001], Collagenase A 0.5 U/ml [Roche, 10103586001] and 0.2% BSA) for 120 min at 37°C in the presence of SCH772984 at 10 μ g/ml or DMSO control. The samples were then spun (600 g, 5 min) and filtered successively through 100 μ m and 70 μ m cell strainers (MACS, 130-110-917 and 130-110-916, respectively), spun (600 g, 5 min), resuspended in ice-cold DMEM and filtered through a 40 μ m cell strainer (Corning, 352340). Recovered pellet was centrifuged (600 g, 5 min) and resuspended in 0.2% BSA:DMEM for cell sorting in the presence of SCH772984 at 10 μ g/ml or DMSO control.

Cell culture of primary muscle cells

FACS-isolated T3-MuSCs were plated on Matrigel (Corning, 354248)-coated 8-chamber slides (Sarstedt, 94.6140.802) in growth medium (GM) composed of DMEM (GIBCO) with 20% fetal bovine serum (FBS), 1% penicillin/streptomycin (GIBCO), and supplemented with 5 ng/ml basic FGF (Peprotech, 450-33) at 37°C. For ligand-dependent activation of Notch signalling, cells were grown in the presence of the extracellular domain of human Delta-like 1 fused to the Fc fragment of human IgG (Hicks et al. 2002), (cells kindly provided by N. Gupta upon permission from G. Weinmaster). As a control, cells were grown in the presence of the Fc fragment only (cells kindly provided by T. Kadesch). Culture substrates were first coated with 10 µg/ml anti-Fc antibody (Jackson ImmunoResearch, 109-005-098) for 1 h at room temperature (RT). Dishes were then incubated with conditioned medium from stably transfected 293T cells expressing the fusion proteins, for 1 h at room-temperature (RT). Cells were plated for 20, 40 or 60 h on Fc-Dll1 or Fc-Ctrl 8-well slides in the presence of the ERK inhibitor SCH772984 (Selleckchem, S7101) at 1 µg/ml or DMSO control with 10 mM 5-ethynyl-20 -deoxyuridine (EdU Click-iT PLUS Kit C10640, Life Technologies).

Single nuclei isolation

Single nuclei preparations were obtained following Dos Santos et al. 2019 (in preparation) guidelines. Briefly, 6 *tibialis anterior*, *gastrocnemius*, *soleus*, *plantaris*, and *extensor digitorum longus* muscles from 3 8-week old female mice were dissected and pulled in cold PBS with 0,2 U/µl RNase inhibitor (Roche, 03335399001). PBS was removed and muscles were minced in cold lysis buffer (10mM Tris-HCl, 10mM NaCl, 3mM MgCl₂, and 0.1% NonidetTM P40 in Nuclease-Free Water) with scissors. After 2 min, cold lysis buffer was added and muscles were lysed for 3 min at 4 °C. Cold wash buffer (PBS, BSA 2% and 0,2 U/µl RNase inhibitor) was subsequently added and the lysate was dounced with 10 strokes of loose pestle using a douncer homogenizer. The homogenate was filtered with 70 µm and 40 µm cells strainers. Nuclei were pelleted by centrifugation for 5min (500 g, 4 °C). Nuclei were washed in 1 ml of cold wash buffer, transferred in a 1,5 ml tube and centrifuged 5 min (500 g, 4 °C). The pellet was resuspended in 250 µl of wash buffer and stained during 15 min in the dark at 4 °C with DAPI at 10 µg/ml. The nuclei were therefore washed and span down 5 min (500 g, 4 °C), resuspended in 300 µl of wash buffer and filtered with 30 µm cell strainers. Nuclei were then FACS sorted to exclude debris with a BD FACSAria III and the BD FACSDIVA software.

Immunostaining

For cell culture, following fixation (2% paraformaldehyde (PFA), 20 min), MuSCs were washed three times in PBS, permeabilized, and blocked using a blocking solution (BS) containing 5% BSA (Jackson Laboratories) and 0.25% Triton X-100 (Sigma) for 60 min at room temperature. The samples were then incubated with chicken anti-GFP (abcam 13970, 1:1000) and rat anti-MYOD1 antibodies (Active motif, 39991, clone 5F11; 1:200) overnight at 4 °C in BS. After three PBS washes, the samples were incubated with anti-chicken (Thermofisher A11039, 1:1000) and anti-rat (Thermofisher A21434, 1:1000) secondary antibodies for 1 h at room-temperature. The samples were subsequently washed three times with PBS and stained for EdU and Hoechst (EdU Click-iT PLUS Kit C10640, Life Technologies) following the manufacturer guidelines before a final wash and mounting. For tissue sections, dissected and injured TA muscles were immediately frozen in liquid-nitrogen-cooled isopentane and sectioned transversely at 8 µm. The sections were fixed for 10 min with 4% PFA, washed three times, permeabilized and blocked with BS for 1 h at RT before being incubated with anti-laminin primary antibody (Sigma, L9393, 1:500) overnight. After three washes, the sections were incubated with the corresponding secondary antibodies and Hoechst (1:1000) for 1 h at RT.

Western Blot

T0 and T15 muscles were dissected and digested for 0 or 15 min at 37 °C in 1X digestion solution. Next, tissues were fixed in 0.5% PFA for 1 h at 4 °C before being washed 3 times in PBS (600 g, 5 min). The samples were then re-digested for 2 h in 2X digestion solution minus the initial digestion time before being filtered successively through 100 µm and 70 µm cell strainers (MACS, 130-110-917 and 130-110-916 respectively) then spun down (600 g, 5 min), resuspended in ice-cold DMEM and filtered through 40 µm cell strainer (Corning, 352340) before a last centrifugation (600 g, 5 min). The cells were lysed using RIPA buffer: 50 µM Tris HCl pH 8, 150 µM NaCl, 1% NP40, 0.5% Sodium Deoxycholate, 0.1% SDS, 1 µM EDTA pH 8, protease inhibitor cocktail (Merck, 4693159001) and phosphoSTOP (Merck, 4906845001). After BCA protein assay measurements, 800 ng of protein per lane were loaded on a Bolt™ 4-12% Bis-Tris Plus Gels (Thermofisher, NW04120BOX) for 1 h at 150 V. The gel was washed once in H₂O and fixed for

5 min in 20% ethanol. The proteins were then transferred on a membrane (15V, 7 min) using the iBlot™ 2 Transfer Stacks, PVDF, mini kit (ThermoFisher, IB24002). The membrane was washed twice with PBST (0.1% triton:PBS, 5 min), blocked with 5% BSA in PBST for 1 h at RT with rotation. The membrane was the stained with primary antibodies overnight for ERK1/2 (EMD Millipore 06-182 rabbit polyclonal, 1:10000) and for phosphor-ERK1/2 (Abcam ab50011-100 mouse, 1:1000) in PBST. After the staining, the membrane was washed twice with PBST (5 min) and stained for secondary antibodies (conjugated anti-rabbit PI-1000 ZD0821 and anti-mouse PI-2000-1 ZC1212 from Vector Laboratories, 1:5000) for 1 h at RT. The proteins were revealed using SuperSignal™ West Femto Maximum Sensitivity Substrate (ThermoFisher, 34094) for 3 min at RT.

In Situ Fixation

For *ex vivo* dissociation, after mouse sacrifice muscles were dissected (hindlimb and forelimb) and minced in small pieces. Tissue pool from two mice were separated in 6 groups (T0, T15, T30, T60, T90, and T120). T0 samples were prepared according to the original *iSiFi* protocol⁹. Briefly, the samples were fixed for 1 h in 0.5% PFA, washed 3 times in ice-cold PBS and digested for 2 h at 37 °C with agitation in 2X digestion solution: Dispase II, 6U/ml (Roche, 4942078001), Collagenase A 1U/ml (Roche, 10103586001) and 0.2% BSA:DMEM. T15, T30, T60, T90 and T120 samples were digested for 15, 30, 60, 90 and 120 min respectively in 1X digestion solution: Dispase II, 3 U/ml (Roche, 4942078001), Collagenase A 0.5 U/ml (Roche, 10103586001) and 0.2% BSA:DMEM at 37 °C with agitation. The samples were then span down (600 g, 5 min) and resuspended in ice-cold 0.5% PFA and incubated for 1 h at 4 °C with gentle agitation to fix the cells. The samples were washed 3 time with ice-cold PBS (600 g, 5 min) and resuspended in 2X digestion solution to terminate digestion for 105, 90, 60 and 30 min for T15, T30, T60 and T90 samples respectively. T120 samples were not re-digested. At this point, all the samples were filled with DMEM (Gibco, 41966-029) and filtered successively through 100 µm and 70 µm cell strainers (MACS, 130-110-917 and 130-110-916 respectively) then span down (600 g, 5 min), resuspended in ice-cold DMEM and filtered through 40 µm cell strainer (Corning, 352340) before a last centrifugation (600 g, 5 min) and resuspension in 0.2% BSA:DMEM for cell sorting.

For the experiment comparing T60 MuSCs in the supernatant or in intact tissue pieces, T0, T60 and T120 samples were obtained from the dissection of hindlimbs and forelimbs from the same mice. For this experiment T0 and T120 samples were processed as indicated above. T60 samples were incubated for 60 min in 1X digestion solution. The samples were then separated simply with gravity by incubating the tube (50 ml conical) vertically at RT for 5 min to pellet intact tissue pieces and to carefully pass the supernatant successively through 100, 70 and 40 μ m filters (references above) to obtain dissociated cells. Both samples were filled with ice-cold DMEM, span down (600 g, 5 min) and resuspended in ice-cold 0.5% PFA for 1 h at 4 °C with agitation. The T60-pellet samples were then re-digested for 60 min in 2X digestion solution. All samples were then filtered as indicated above.

For *in vivo* activation, after mouse sacrifice injured TA muscles were dissected and minced in small pieces. The samples were prepared according to the original *iSiFi* protocol⁹, (see above for brief summary) with the following modification: 0.5M glycine:PBS was used in the first post-PFA wash.

RNA extraction

For *ex vivo* dissociation time-course, *in vivo* activation control and *ex vivo* ERK1/2 inhibition during dissociation RT-qPCR, the cells were sorted directly in lysis buffer from the Quick RNA FFPE kit (Zymo, R1008) and the RNA extracted following the manufacturer guidelines (without the tissue digestion step). For T60 supernatant/pellet RT-qPCR, the cells were sorted directly in lysis buffer from the RecoverAll FFPE kit (Thermo, AM1975) and the RNA extracted following the manufacturer guidelines (without the tissue digestion step, without the incubation step at 80 °C and with the incubation step at 50 °C for 1 h instead of 15 min). For *in vivo* activation time-course, Pax7-nGFP cells were sorted single-cell by FACS in 96 well plates (4titude, 4ti-0960). Each well contained 2.5 μ l PKD buffer (Qiagen, 1034963) supplemented with 1:16 proteinase K (Qiagen, 19131). Prior to RNA separation, plates were decrosslinked for 1 h at 56 °C. RNA separation was performed on a Hamilton STAR according to the G&T-seq protocol^{56,57}. Briefly, oligo-dt30VN-labeled beads and wash buffer were prepared. 10 μ l of beads were added to every well with the liquid-handling robot and incubated for 20 min at RT while mixing (2,000 rpm). Thereafter, the beads were washed twice with wash buffer and 5 μ l of Reverse Transcriptase master mix was added to every well of the bead-containing 96-well plate.

RT-qPCR

Reverse transcription was performed using the SuperScript IV VILO Master Mix (ThermoFisher, 11756050) following the manufacturer's guidelines. RT-qPCR was performed using the Power SYBR Green PCR Master Mix (Applied Biosystems, 4367659).

Library preparation

For single-nuclei RNA-seq:

Single-cell Gel Bead-In-EMulsions (GEMs) were generated using a Chromium Controller instrument (10x Genomics). Sequencing libraries were prepared using Chromium Single Cell 3' Reagent Kits (10x Genomics, 1000074), according to the manufacturer's instructions. Briefly, GEM-RT was performed in a thermal cycler: 53 °C for 45 min, 85 °C for 5 min. Post GEM-RT Cleanup using DynaBeads MyOne Silane Beads was followed by cDNA amplification (98 °C for 3 min, cycled 12 x 98 °C for 15 s, 67 °C for 20 s, 72 °C for 1 min, and 72 °C 1 min). After a cleanup with SPRIselect Reagent Kit and fragment size estimation with High Sensitivity™ HS DNA kit run on 2100 Bioanalyzer (Agilent), the libraries were constructed by performing the following steps: fragmentation, end-repair, A-tailing, SPRIselect cleanup, adaptor ligation, SPRIselect cleanup, sample index PCR, and SPRIselect size selection.

The fragment size estimation of the resulting libraries were assessed with High Sensitivity™ HS DNA kit run on 2100 Bioanalyzer (Agilent) and quantified using the Qubit™ dsDNA High Sensitivity HS assay (ThermoFisher Scientific). Libraries were then sequenced by pair with a HighOutput flowcell using an Illumina Nextseq 500 with the following mode: 26 base-pairs (bp) (10X Index + UMI), 8 bp (i7 Index) and 57 bp (Read 2).

For Bulk RNA-seq:

Directional libraries were prepared using the Smarter Stranded Total RNA-Seq kit- Pico Input Mammalian following the manufacturer's instructions (Clontech, 635005). The quality of all libraries was checked with the DNA-1000 kit (Agilent) on a 2100 Bioanalyzer and quantification was performed with Quant-It assays on a Qubit 3.0 fluorometer (Invitrogen). Clusters were generated for the resulting libraries, with Illumina HiSeq SR Cluster Kit v4 reagents. Sequencing was performed with the Illumina HiSeq 2500 system and HiSeq SBS kit v4 reagents. Runs were

carried out over 65 cycles, including seven indexing cycles, to obtain 65 bp single-end reads. Sequencing data were processed with Illumina Pipeline software (Casava version 1.9).

For single-cell RNA-seq:

cDNA libraries were generated based on the Smart-seq2 protocol⁵⁸. Briefly, mRNA was reverse transcribed and cDNA was amplified via PCR for 27 cycles. Amplification was done with KAPA HIFI Hot Start ReadyMix (Roche, 07958919001) and purification by magnetic beads (CleanNA CPCR). Quantity and quality of cDNA was assessed with the quantifluor RNA system (Promega E3310) and Agilent 2100 BioAnalyzer with a high-sensitivity chip. Library preparation was done with the Nextera XT library prep and index kit (Illumina FC-131-1096 and FC-131-2001). 100 pg of cDNA was tagged by transposase Tn5 and amplified with dual-index primers (i7 and i5, Illumina, 12 cycles). Reagents were mixed together by the Echo 555 (Labcyte) and pooled-nextera XT libraries were purified. 384 single-cell libraries were pooled together and sequenced single-end 50 bp on a single lane of a HiSeq4000 (Illumina). All results related to scRNA-seq are based on 2 pooled biological replicates per group, experiments were performed on the same day.

Bioinformatics

For single nuclei RNA-seq:

The sequencing data was processed into transcript count tables with the Cell Ranger Single Cell Software Suite 3.0.2 by 10X Genomics. Raw base call files from the Nextseq 500 were demultiplexed with the cellranger mkfastq pipeline into library-specific FASTQ files. The FASTQ files for each library were then processed independently with the cellranger count pipeline. This pipeline used STAR21 to align cDNA reads to the *Mus musculus* transcriptome (Sequence: GRCm38, Mouse reference provided by 10X.). Once aligned, barcodes associated with these reads – cell identifiers and Unique Molecular Identifiers (UMIs), underwent filtering and correction. Reads associated with retained barcodes were quantified and used to build a transcript count table. We re-ran this same pipeline with the pre-mRNA reference, build with cellranger mkgtf and cellranger mkref. The subsequent visualizations, clustering and differential expression tests were performed in R (v 3.4.3) using Seurat⁵⁹ (v3.0.2). The Tabula Muris droplet and Smart-Seq2 datasets were loaded from the TabulaMuris R package (v1.0) and visualized and analyzed using Seurat. The Stimulation Index was calculated using the Seurat function “AddModuleScore” using the

dissociation core from Figure 1F as a feature set. The Tabula Muris tissue digestion time were inferred from the original paper supplemental methods. An arbitrary conversion factor of 0.5 and 0.2 were applied to correct kinetics of digestion steps at RT or on ice respectively.

For bulk RNA-seq:

Bioinformatics analysis was performed using the RNA-seq pipeline from Sequana⁶⁰. Reads were cleaned of adapter sequences and low-quality sequences using cutadapt version 1.11⁶¹. Only sequences at least 25 nt in length were considered for further analysis. STAR version 2.5.0a⁶², with default parameters, was used for alignment on the reference genome (Mus musculus GRCm38 assembly from Ensembl release 87). Genes were counted using featureCounts version 1.4.6-p3⁶³ from Subreads package (parameters: -t exon -g gene_id -s 1) under gencode mm10 annotation version M11.

Count data were analysed using R version 3.4.3 and the Bioconductor package DESeq2 version 1.18.1⁶⁴. Due to putative genomic DNA contamination, only genes with an average number of reads greater than 150 were used as input of the differential analysis (N=8059 genes). The normalization was performed using the "shorth" parameter and dispersion estimation was performed using the default parameters. A generalized linear model was set in order to test for the differential expression between the different time points. For each pairwise comparison, the independent filtering algorithm was applied and raw p-values were adjusted for multiple testing according to the Benjamini and Hochberg (BH) procedure⁶⁵. Genes with an adjusted p-value lower than 0.05 and an absolute fold-change higher than 2 were then considered differentially expressed.

For single-cell RNA-seq:

Fastq files contained 50-bp-long single-end sequenced tags (reads) from 384 cells each were trimmed with cutadapt 1.5⁶¹ with the parameters '-q 20,20 --minimum-length 35' and the nextera adapter sequence. The retained tags were aligned to the Ensembl 84⁶⁶ gene annotation of the NCBI38/mm10 mouse genome using STAR 2.4.0⁶² with the parameters '--outSAMunmapped Within --runThreadN⁶⁷ --genomeDir {reference_genome} --readFilesCommand zcat --outSAMtype BAM SortedByCoordinate'. The number of tags per gene was calculated using htseq-count 0.6.0⁶⁸ with the parameters '-format=bam --order=pos --mode=intersection-strict --stranded=no --type=exon --idattr=gene_id {input.bam} {reference_gtf} > {output.count}'. Quality

control on alignment and counting was done with ngsplot⁶⁷ with parameters ‘-G mm10 -R genebody -C {input.bam} -O {results_dir}/genecoverage/{wildcards.sample}.gene -F rnaseq’ and multiqc⁶⁹. Quality control on aligned and counted reads was performed with Scater 1.8.4⁷⁰, cells with < 200,000 reads, < 900 detected genes, > 6 percent mitochondrial DNA and > 0.75 percent of spike-in ERCCs. Read normalization was done with Scrn 1.8.4, reads were normalized separately from ERCCs. For each gene, expression estimates per gene were expressed as log-transformed counts by taking the \log^2 (counts + 1). We used the top 500 highest variable genes to obtain a 2D representation of the cells, while maintaining the similarity relationships between them using PCA as implemented in the package Scater 1.8.4⁷⁰. All data analysis was conducted in Python v3.6 (Python software foundation) or R v3.5.1 (CRAN). Differential expression was performed using MAST⁷¹ and Monocle2⁴⁰ across all time-points. Differentiation trajectory analysis was performed using Monocle2.

Statistical analysis

For comparison between two groups, unpaired Student’s t test was performed to calculate p values and to determine statistically significant differences (*p < 0.05; **p < 0.01; ***p < 0.001).

References

1. Briggs, J. A. *et al.* The dynamics of gene expression in vertebrate embryogenesis at single-cell resolution. *Science* (80-.). (2018).
2. Farrell, J. A. *et al.* Single-cell reconstruction of developmental trajectories during zebrafish embryogenesis. *Science* (80-.). (2018).
3. Wagner, D. E. *et al.* Single-cell mapping of gene expression landscapes and lineage in the zebrafish embryo. *Science* (80-.). (2018).
4. Han, X. *et al.* Mapping the Mouse Cell Atlas by Microwell-Seq. *Cell* **172**, 1091–1107.e17 (2018).
5. Plass, M. *et al.* Cell type atlas and lineage tree of a whole complex animal by single-cell transcriptomics. *Science* (80-.). **1723**, eaaq1723 (2018).
6. Fincher, C. T., Wurtzel, O., de Hoog, T., Kravarik, K. M. & Reddien, P. W. Cell type transcriptome atlas for the planarian *Schmidtea mediterranea*. *Science* (80-.). **874**, eaaq1736 (2018).

7. Amit, I. *et al.* A module of negative feedback regulators defines growth factor signaling. doi:10.1038/ng1987
8. Schaum, N. *et al.* Single-cell transcriptomics of 20 mouse organs creates a Tabula Muris. *Nature* **562**, 367–372 (2018).
9. Machado, L. *et al.* In Situ Fixation Redefines Quiescence and Early Activation of Skeletal Muscle Stem Cells. *Cell Rep.* **21**, (2017).
10. Brink, S. C. van den *et al.* Single-cell sequencing reveals dissociation-induced gene expression in tissue subpopulations. **14**, (2017).
11. van Velthoven, C. T. J., de Morree, A., Egner, I. M., Brett, J. O. & Rando, T. A. Transcriptional Profiling of Quiescent Muscle Stem Cells In Vivo. *Cell Rep.* **21**, 1994–2004 (2017).
12. Jones, N. C. *et al.* The p38^{MAPK} functions as a molecular switch to activate the quiescent satellite cell. *J. Cell Biol.* **169**, 105–116 (2005).
13. Zhang, K., Sha, J. & Harter, M. L. Activation of Cdc6 by MyoD is associated with the expansion of quiescent myogenic satellite cells. *J. Cell Biol.* **188**, 39–48 (2010).
14. Lacar, B. *et al.* Nuclear RNA-seq of single neurons reveals molecular signatures of activation. *Nat. Commun.* **7**, 11022 (2016).
15. Bakken, T. E. *et al.* Single-nucleus and single-cell transcriptomes compared in matched cortical cell types. *PLoS One* **13**, e0209648–e0209648 (2018).
16. Wu, H., Kirita, Y., Donnelly, E. L. & Humphreys, B. D. Advantages of Single-Nucleus over Single-Cell RNA Sequencing of Adult Kidney: Rare Cell Types and Novel Cell States Revealed in Fibrosis. *J. Am. Soc. Nephrol.* **30**, 23 LP-32 (2019).
17. Gaidatzis, D., Burger, L., Florescu, M. & Stadler, M. B. Analysis of intronic and exonic reads in RNA-seq data characterizes transcriptional and post-transcriptional regulation. *Nat. Biotechnol.* **33**, 722 (2015).
18. Giordani, L. *et al.* High-Dimensional Single-Cell Cartography Reveals Novel Skeletal Muscle-Resident Cell Populations. *Mol. Cell* (2019). doi:10.1016/j.molcel.2019.02.026
19. Aizarani, N. *et al.* A human liver cell atlas reveals heterogeneity and epithelial progenitors. *Nature* **572**, 199–204 (2019).
20. Baghdadi, M. B. & Tajbakhsh, S. Regulation and phylogeny of skeletal muscle regeneration. *Dev. Biol.* **433**, 200–209 (2018).

21. Sambasivan, R. *et al.* Distinct regulatory cascades govern extraocular and pharyngeal arch muscle progenitor cell fates. *Dev Cell* **16**, 810–821 (2009).
22. Liebermann, D. A. & Hoffman, B. Gadd45 in stress signaling. *J. Mol. Signal.* **3**, 15 (2008).
23. Barton, K. *et al.* Defective thymocyte proliferation and IL-2 production in transgenic mice expressing a dominant-negative form of CREB. *Nature* **379**, 81–85 (1996).
24. Fu, S., Bottoli, I., Goller, M. & Vogt, P. K. Heparin-binding epidermal growth factor-like growth factor, a v-Jun target gene, induces oncogenic transformation. *Proc. Natl. Acad. Sci.* **96**, 5716 LP-5721 (1999).
25. Seale, P. *et al.* Pax7 is required for the specification of myogenic satellite cells. *Cell* **102**, 777–786 (2000).
26. Chakkalakal, J. V, Jones, K. M., Basson, M. A. & Brack, A. S. The aged niche disrupts muscle stem cell quiescence. *Nature* **490**, 355–360 (2012).
27. Yamaguchi, M. *et al.* Calcitonin Receptor Signaling Inhibits Muscle Stem Cells from Escaping the Quiescent State and the Niche. *Cell Rep* **13**, 302–314 (2015).
28. Fukada, S. *et al.* Molecular signature of quiescent satellite cells in adult skeletal muscle. *Stem Cells* **25**, 2448–2459 (2007).
29. Labaer, J. *et al.* New functional activities for the p21 family of CDK inhibitors. *Genes Dev.* (1997). doi:10.1101/gad.11.7.847
30. Cornelison, D. D. W., Filla, M. S., Stanley, H. M., Rapraeger, A. C. & Olwin, B. B. Syndecan-3 and Syndecan-4 Specifically Mark Skeletal Muscle Satellite Cells and Are Implicated in Satellite Cell Maintenance and Muscle Regeneration. *Dev. Biol.* **239**, 79–94 (2001).
31. Gothot, A., Pyatt, R., McMahel, J., Rice, S. & Srour, E. F. Functional heterogeneity of human CD34(+) cells isolated in subcompartments of the G0 /G1 phase of the cell cycle. *Blood* (1997).
32. Jaafar Marican, N. H., Cruz-Migoni, S. B. & Borycki, A.-G. Asymmetric Distribution of Primary Cilia Allocates Satellite Cells for Self-Renewal. *Stem cell reports* **6**, 798–805 (2016).
33. Ryall, J. G. *et al.* The NAD⁺-dependent sirt1 deacetylase translates a metabolic switch into regulatory epigenetics in skeletal muscle stem cells. *Cell Stem Cell* **16**, 171–183 (2015).
34. Dell’Orso, S. *et al.* Single-cell analysis of adult skeletal muscle stem cells in

- homeostatic and regenerative conditions. *Development* dev.174177 (2019).
doi:10.1242/dev.174177
35. Hernando-Herraez, I. *et al.* Ageing affects DNA methylation drift and transcriptional cell-to-cell variability in muscle stem cells. *bioRxiv* 500900 (2018). doi:10.1101/500900
 36. Kuang, S., Gillespie, M. A. & Rudnicki, M. A. Niche regulation of muscle satellite cell self-renewal and differentiation. *Cell Stem Cell* **2**, 22–31 (2008).
 37. Tajbakhsh, S., Rocheteau, P. & Le Roux, I. Asymmetric cell divisions and asymmetric cell fates. *Annu Rev Cell Dev Biol* **25**, 671–699 (2009).
 38. Der Vartanian, A. *et al.* PAX3 Confers Functional Heterogeneity in Skeletal Muscle Stem Cell Responses to Environmental Stress. *Cell Stem Cell* (2019).
doi:10.1016/j.stem.2019.03.019
 39. van den Brink, S. C. *et al.* Single-cell sequencing reveals dissociation-induced gene expression in tissue subpopulations. **14**, (2017).
 40. Qiu, X. *et al.* Reversed graph embedding resolves complex single-cell trajectories. *Nat. Methods* (2017). doi:10.1038/nmeth.4402
 41. Sun, Y. *et al.* Signaling pathway of MAPK/ERK in cell proliferation, differentiation, migration, senescence and apoptosis. *J. Recept. Signal Transduct.* **35**, 600–604 (2015).
 42. Michailovici, I. *et al.* Nuclear to cytoplasmic shuttling of ERK promotes differentiation of muscle stem/progenitor cells. *Development* **141**, 2611 LP-2620 (2014).
 43. Bjornson, C. R. *et al.* Notch signaling is necessary to maintain quiescence in adult muscle stem cells. *Stem Cells* **30**, 232–242 (2012).
 44. Jarriault, S. *et al.* Signalling downstream of activated mammalian Notch. *Nature* **377**, 355–358 (1995).
 45. Mourikis, P. *et al.* A Critical Requirement for Notch Signaling in Maintenance of the Quiescent Skeletal Muscle Stem Cell State. *Stem Cells* **30**, 243–252 (2012).
 46. Yap, E. L. & Greenberg, M. E. Activity-Regulated Transcription: Bridging the Gap between Neural Activity and Behavior. *Neuron* **100**, 330–348 (2018).
 47. Wu, Y. E., Pan, L., Zuo, Y., Li, X. & Hong, W. Detecting Activated Cell Populations Using Single-Cell RNA-Seq. *Neuron* **96**, 313–329.e6 (2017).
 48. Leek, J. T. *et al.* Tackling the widespread and critical impact of batch effects in high-throughput data. *Nat. Rev. Genet.* **11**, 733–739 (2010).

49. Haas, B. J. & Whited, J. L. Advances in Decoding Axolotl Limb Regeneration. *Trends Genet.* **33**, 553–565 (2017).
50. Reddien, P. W. The Cellular and Molecular Basis for Planarian Regeneration. *Cell* **175**, 327–345 (2018).
51. Adam, M., Potter, A. S. & Potter, S. S. Psychrophilic proteases dramatically reduce single cell RNA-seq artifacts : A molecular atlas of kidney development. (2017).
doi:10.1242/dev.151142
52. Wang, G., Moffitt, J. R. & Zhuang, X. Multiplexed imaging of high-density libraries of RNAs with MERFISH and expansion microscopy. *Sci. Rep.* **8**, 4847 (2018).
53. Eng, C.-H. L. *et al.* Transcriptome-scale super-resolved imaging in tissues by RNA seqFISH+. *Nature* **568**, 235–239 (2019).
54. Rodriques, S. G. *et al.* Slide-seq: A scalable technology for measuring genome-wide expression at high spatial resolution. *Science (80-.)*. **363**, 1463 LP-1467 (2019).
55. Sambasivan, R. *et al.* Distinct Regulatory Cascades Govern Extraocular and Pharyngeal Arch Muscle Progenitor Cell Fates. *Dev. Cell* (2009). doi:10.1016/j.devcel.2009.05.008
56. Macaulay, I. C., Ponting, C. P. & Voet, T. Single-Cell Multiomics : Multiple Measurements from Single Cells. *Trends Genet.* **33**, 155–168 (2017).
57. Macaulay, I. C. *et al.* G&T-seq: Parallel sequencing of single-cell genomes and transcriptomes. *Nat. Methods* (2015). doi:10.1038/nmeth.3370
58. Picelli, S. *et al.* Full-length RNA-seq from single cells using. **9**, 171–181 (2014).
59. Satija, R., Farrell, J. A., Gennert, D., Schier, A. F. & Regev, A. Spatial reconstruction of single-cell gene expression data. *Nat. Biotechnol.* **33**, 495–502 (2015).
60. Cokelaer, T., Desvillechabrol, D., Legendre, R. & Cardon, M. ‘ Sequana ’: a Set of Snakemake NGS pipelines. **2**, 1–2 (2017).
61. Martin, M. Cutadapt removes adapter sequences from high-throughput sequencing reads. *EMBnet.journal; Vol 17, No 1 Next Gener. Seq. Data Anal.* (2011).
doi:10.14806/ej.17.1.200
62. Dobin, A. *et al.* STAR: ultrafast universal RNA-seq aligner. *Bioinformatics* **29**, 15–21 (2013).
63. Liao, Y., Smyth, G. K. & Shi, W. featureCounts: an efficient general purpose program for assigning sequence reads to genomic features. *Bioinformatics* **30**, 923–930 (2013).

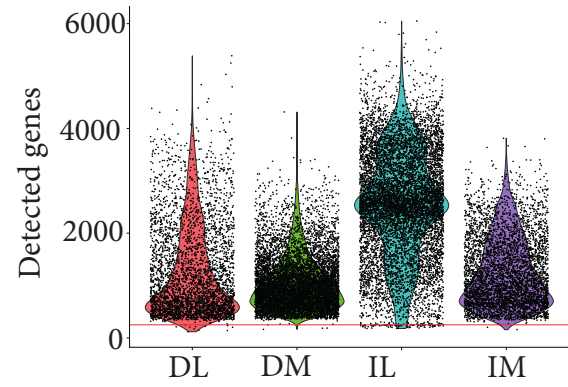
64. Love, M. I., Huber, W. & Anders, S. Moderated estimation of fold change and dispersion for RNA-seq data with DESeq2. *Genome Biol.* **15**, 550 (2014).
65. Benjamini, Y. & Hochberg, Y. Controlling the false discovery rate: a practical and powerful approach to multiple testing. *Journal of the Royal Statistical Society B* **57**, 289–300 (1995).
66. Yates, A. *et al.* Ensembl 2016. *Nucleic Acids Res.* (2016). doi:10.1093/nar/gkv1157
67. Shen, L., Shao, N., Liu, X. & Nestler, E. Ngs.plot: Quick mining and visualization of next-generation sequencing data by integrating genomic databases. *BMC Genomics* (2014). doi:10.1186/1471-2164-15-284
68. Anders, S., Pyl, P. T. & Huber, W. HTSeq-A Python framework to work with high-throughput sequencing data. *Bioinformatics* (2015). doi:10.1093/bioinformatics/btu638
69. Ewels, P., Magnusson, M., Lundin, S. & Källner, M. MultiQC: Summarize analysis results for multiple tools and samples in a single report. *Bioinformatics* (2016). doi:10.1093/bioinformatics/btw354
70. McCarthy, D. J., Campbell, K. R., Lun, A. T. L. & Wills, Q. F. Scater: Pre-processing, quality control, normalization and visualization of single-cell RNA-seq data in R. *Bioinformatics* (2017). doi:10.1093/bioinformatics/btw777
71. Finak, G. *et al.* MAST: A flexible statistical framework for assessing transcriptional changes and characterizing heterogeneity in single-cell RNA sequencing data. *Genome Biol.* (2015). doi:10.1186/s13059-015-0844-5

FIGURE_S1_MACHADO_ET_AL_2019

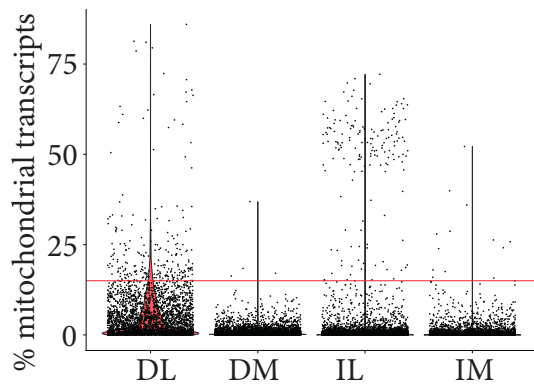
a

Genes (median)	mRNA (exons)	pre-mRNA (exons + introns)
IL	1099	2579
IM	372	1114
DL	525	993
DM	490	933

b



c



d

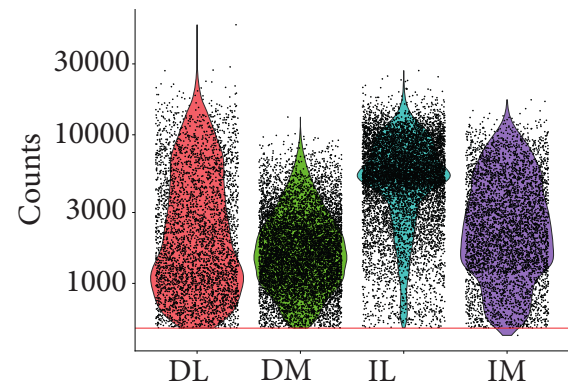


Figure S1 | Quality controls of the single nuclei RNA-sequencing experiment from Figure 1

- a) Median number of detected genes using mRNA (exonic sequences only) or pre-mRNA (exonic and intronic sequences).
- b) Number of detected genes per sample using pre-mRNA sequences. The red line represents the quality cutoff set at 250.
- c) Percentage of mitochondrial genes detected per sample. The red line represents the quality cutoff set at 15%.
- d) Number of reads per sample using pre-mRNA sequences. The red line represents the quality cutoff set at 500.

For each panel: IL: Intact Liver; IM: Intact Muscle; DL: Digested Liver; DM: Digested Muscle.

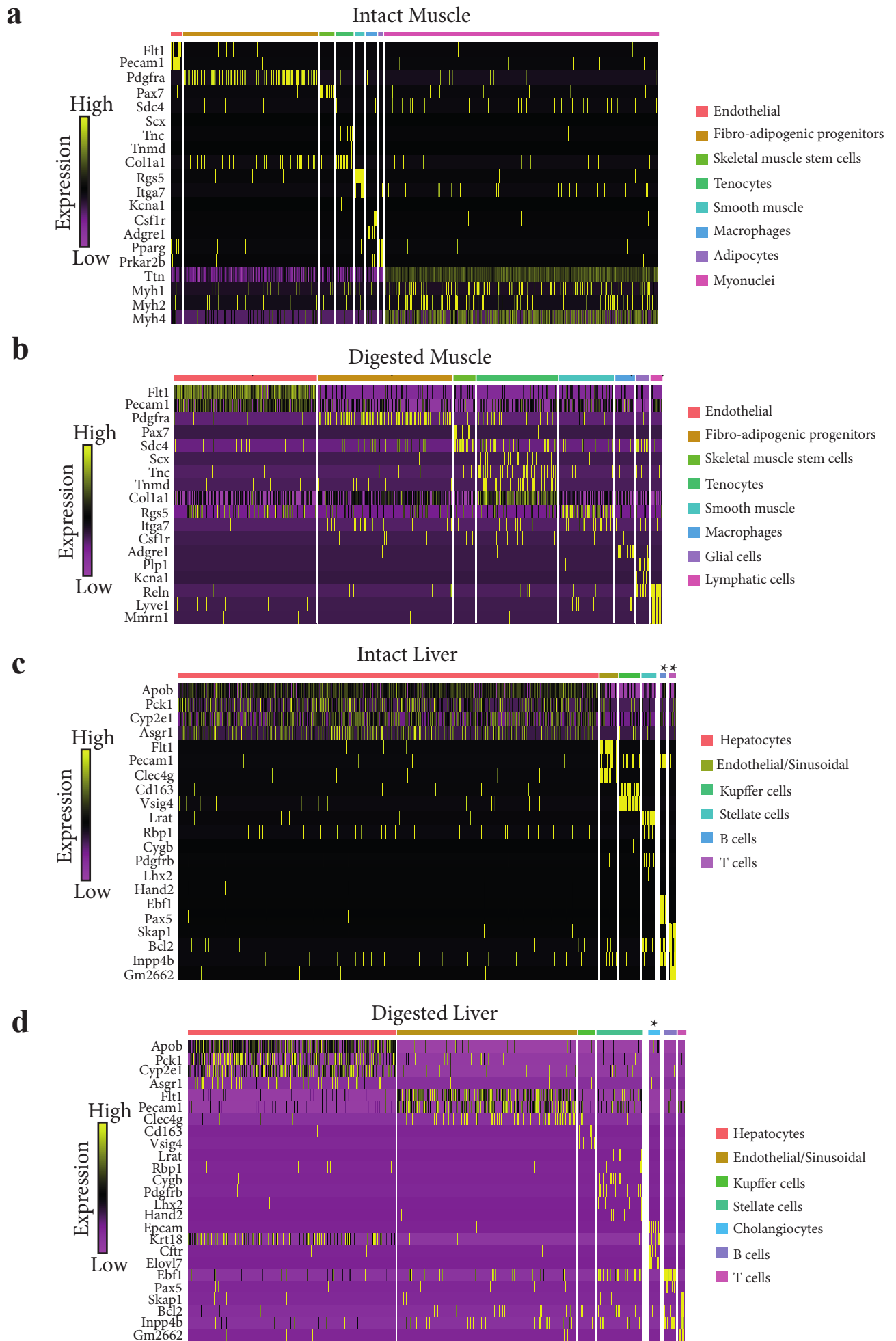
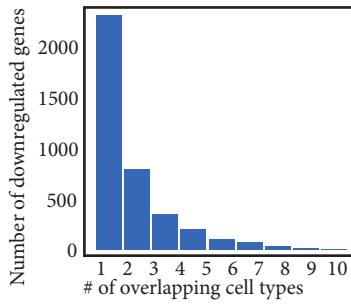


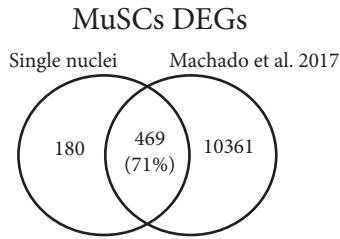
Figure S2 | Identity of the cellular populations defined in Figure 1

a) ,b),c),d) Heatmap displaying the expression of common cellular populations markers used to annotate the nuclei from (a) intact muscle, (b) digested muscle, (c) intact liver, (d) digested liver.

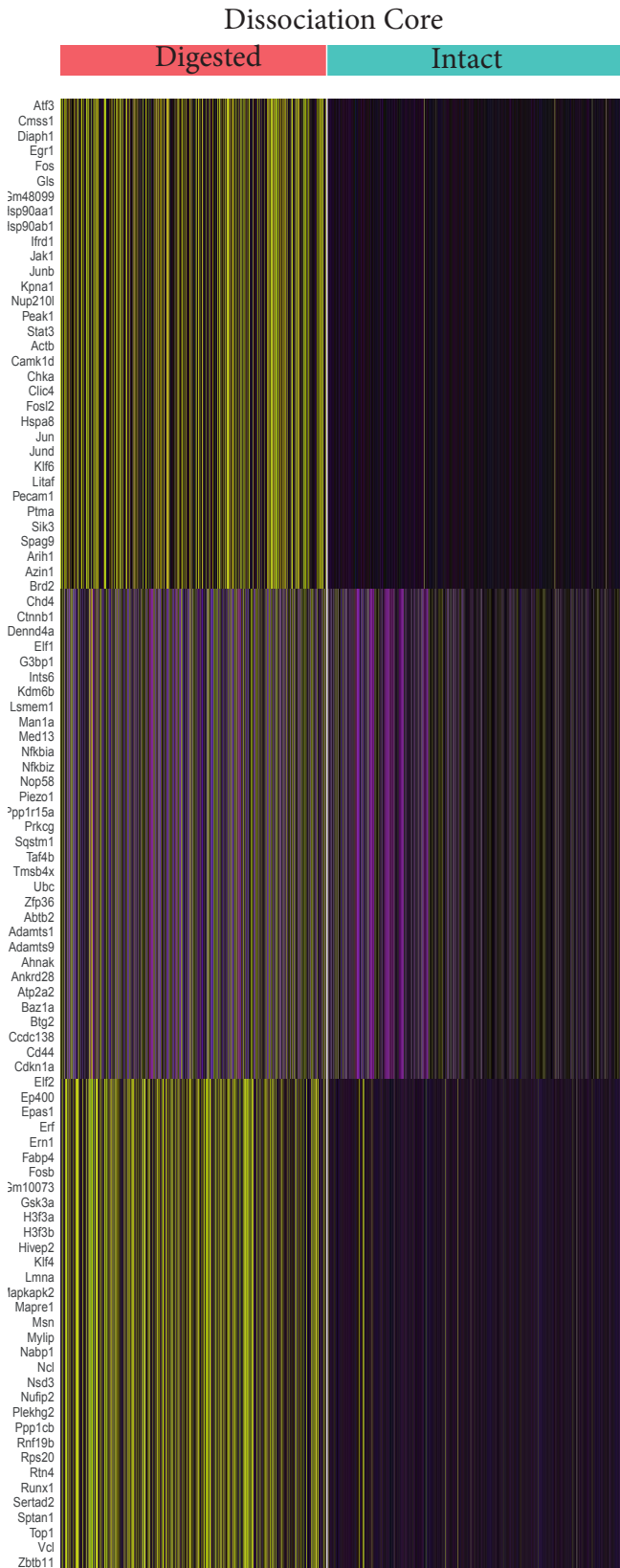
a



b



c



d

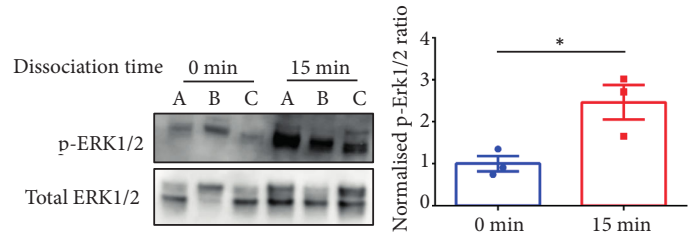


Figure S3 | Representation of dissociation-repressed genes among populations defined in Figure 1 and expression of the dissociation core genes

- a) Histogram representing the distribution of genes repressed by dissociation in the 10 populations displayed in **Fig 1D**.
- b) Venn Diagram showing the overlap between single nuclei and bulk RNA-seq MuSCs dissociation-induced DEGs (both up- and down-regulated, adjusted p-value < 0.05). The bulk RNA-seq DEGs are extracted from Machado et al. 2017.
- c) Heatmap displaying the expression of the dissociation core genes from **Figure 1F** in all cells from muscle and tissue single nuclei RNA-sequencing, grouped by dissociation status (dissociated in blue and intact in red).
- d) Western-Blot analysis of ERK1/2 phosphorylation on T0 and T15 min digested whole muscle protein extracts showing early, global MAPK activation during dissociation.

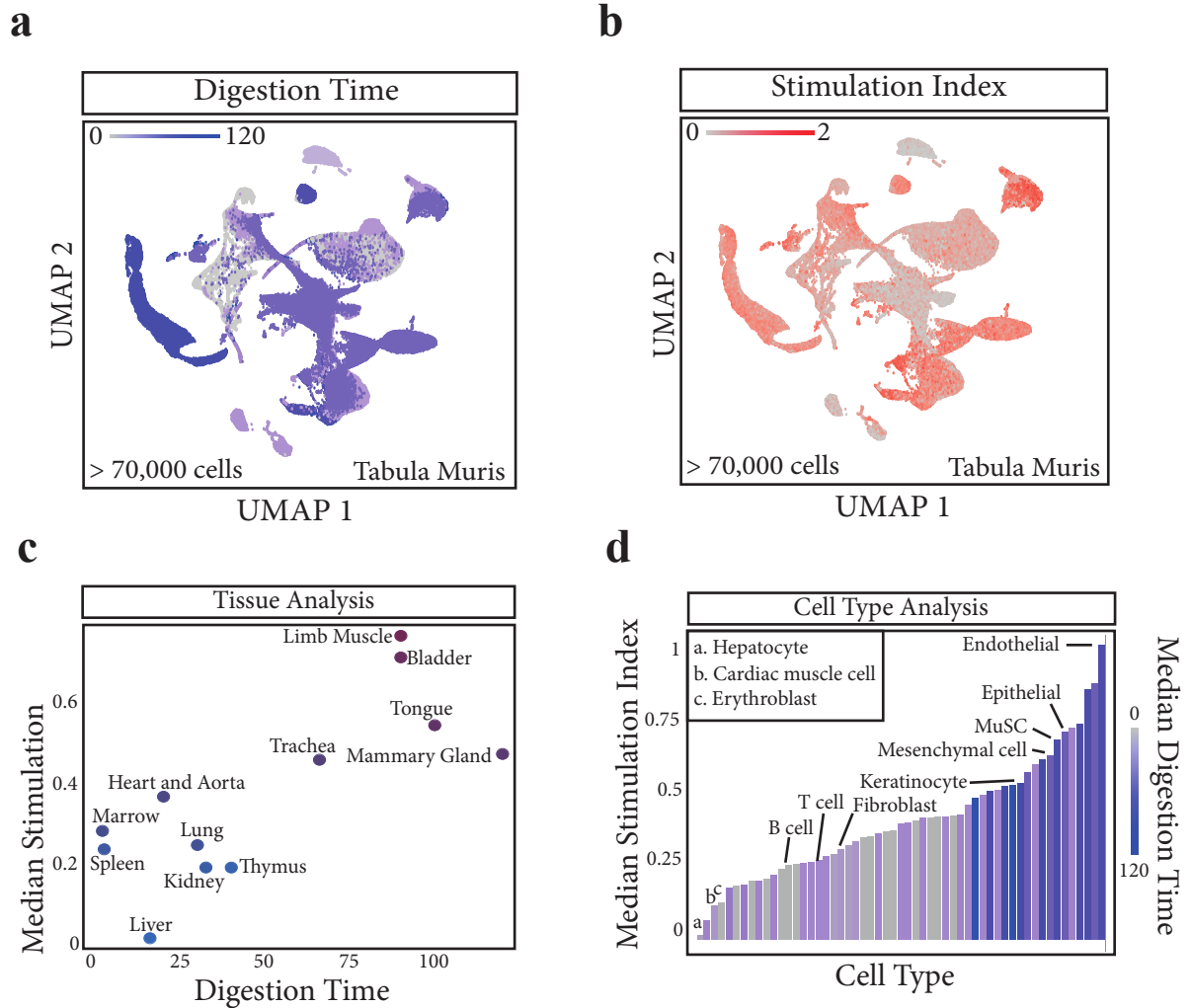
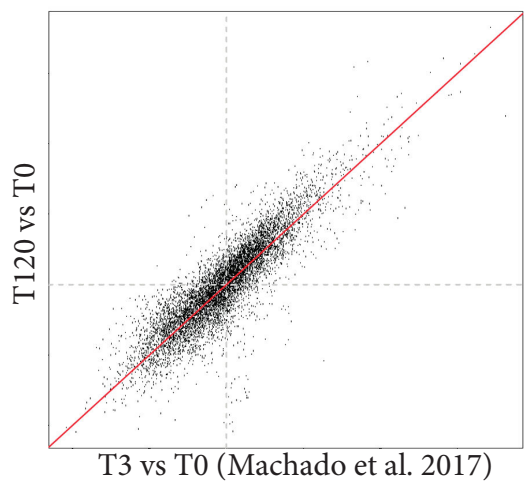


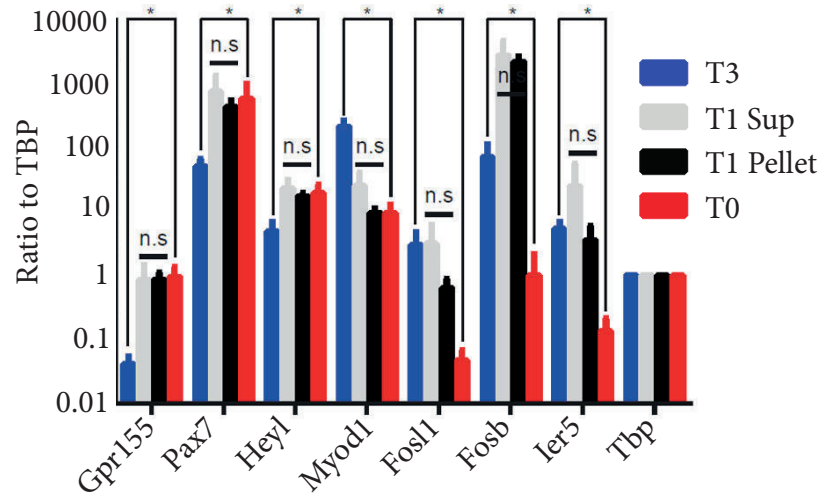
Figure S4 | Systematic study of the time-dependent dissociation-induced artefact in the Tabula Muris droplet dataset

- a) UMAP plot representing the digestion time at 37°C of every cell from the published Tabula Muris droplet dataset (70118 cells), inferred from the supplemental methods.
- b) UMAP plot representing the Stimulation Index of every cell from the published Tabula Muris droplet dataset (70118 cells). Note the correlation between high digestion time in **Fig 2C** and high Stimulation Index.
- c) Correlation between tissue digestion time at 37°C and median tissue Stimulation Index calculated from the Tabula Muris droplet dataset (70118 cells).
- d) Correlation between cell-type and median cell-type Stimulation Index calculated from the Tabula Muris droplet dataset (70118 cells). Median cell-type digestion time at 37°C is coded in grey-blue gradient.

a



b



c

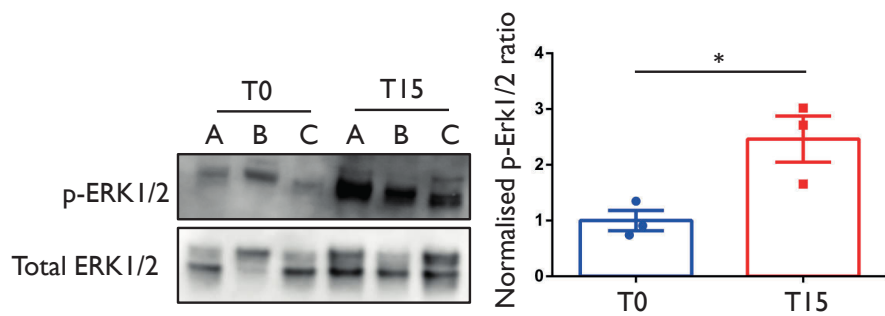


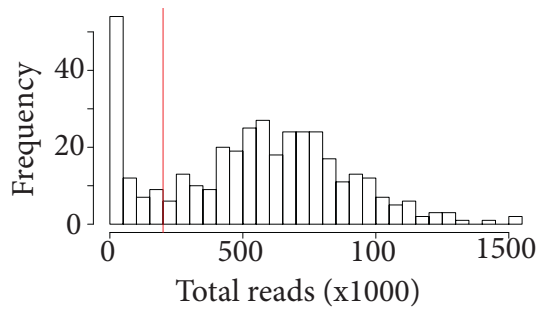
Figure S5 | Transcriptional and post-translational modification during different steps of the *ex vivo* MuSCs dissociation

a) Comparison of the T0/T120 fold changes (Figure 1a) and the T0/T3 (Machado et al., 2017) fold changes for shared genes, showing strong reproducibility between the two RNA-seq experiments.

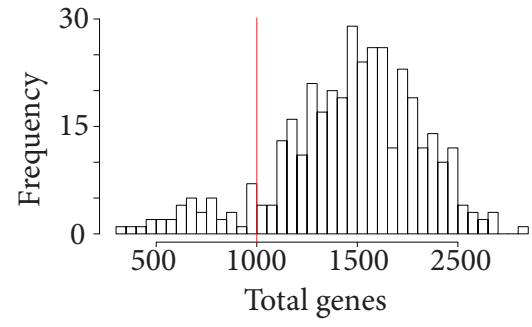
b) RT-qPCR analysis of dissociation-sensitive transcripts during muscle digestion between T0, T120 and T60 cells (pelleted by gravity or released in the medium) to study the impact of mechanical dissociation versus the effect of dissociation time.

Independent student t-test were performed. * $p < 0.05$ ** $p < 0.01$ *** $p < 0.001$

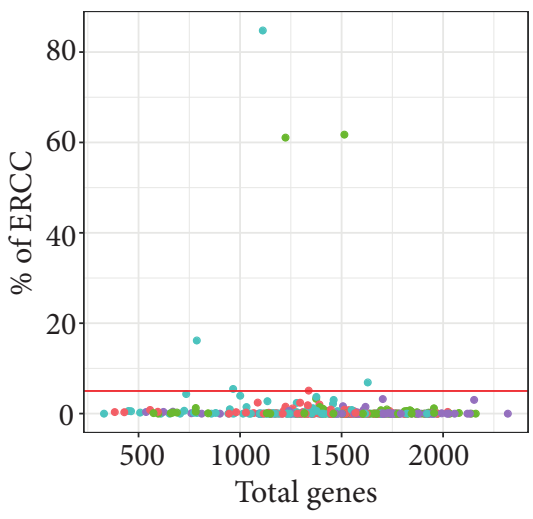
a



b



c



d

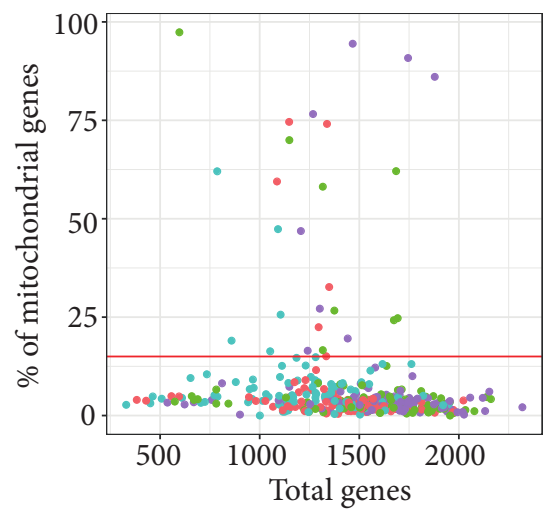
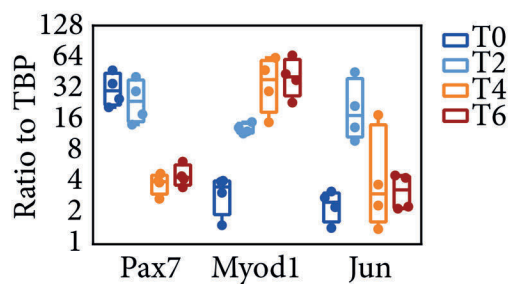


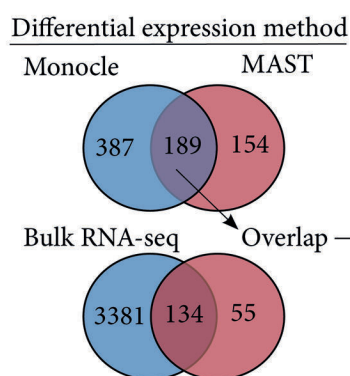
Figure S6 | Quality controls of the single cell RNA-sequencing experiment from Figure 4

- a) Histogram displaying the distribution of reads per cell and the quality control cutoff (red line) set at 200,000.
- b) Histogram displaying the distribution of detected genes per cell and the quality control cutoff (red line) set at 1000.
- c) Dot plot representing the percentage of ERCC spikes-in contamination across all cells and the quality control cutoff (red line) set at 5%.
- d) Dot plot representing the percentage of mitochondrial genes contamination across all cells and the quality control cutoff (red line) set at 15%.

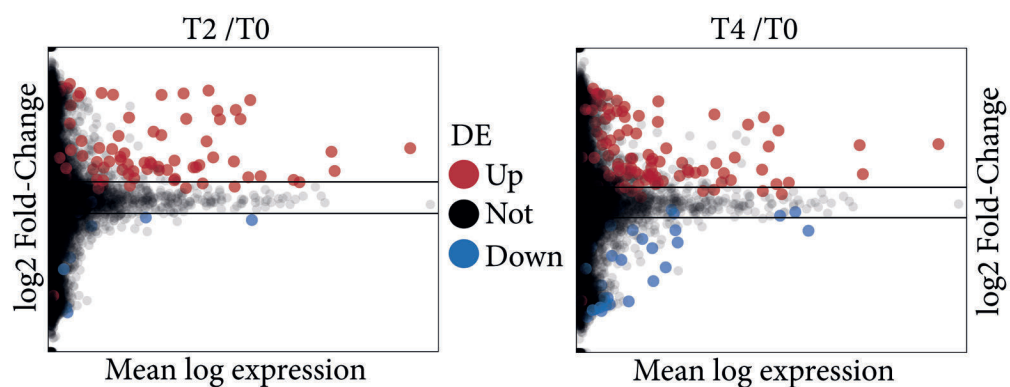
a



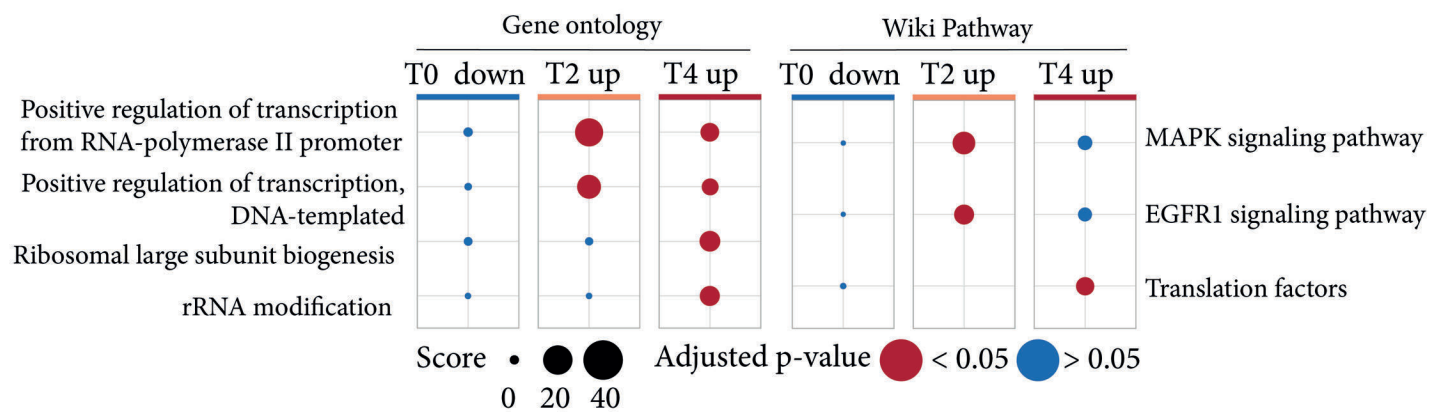
b



c



d



e

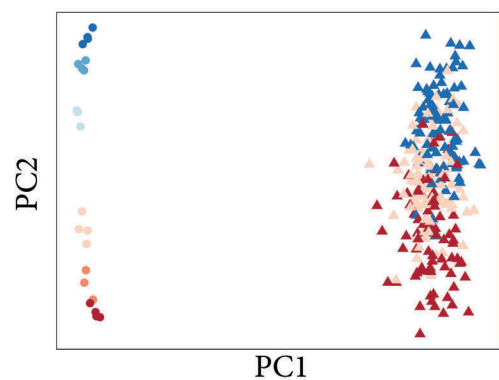


Figure S7 | RT-qPCR control, Population analysis, differential-expression and gene ontology analysis related to Figure 3

- a) Initial assessment of early MuSCs response to muscle injury (1.2% BaCl₂) by RT-qPCR 0, 2, 4 and 6 h post-injury. Transcripts were measured in FACS-isolated, *iSiFi*-treated MuSCs.
- b) Comparison of two differential expression tools Monocle2 (qval < 10%) and MAST (FDR < 10%) during *in vivo* muscle injury. The overlap between the two datasets was compared to the differentially-expressed genes of Figure 3c (DESeq2).
- c) MA plot of the overlapping genes across all time-points.
- d) Gene ontology and pathways analysis using EnrichR (GO_Biological_Processes_2018, WikiPathways_2016) for all of the DEGs between T0, T2 and T4 (T0 versus T2 and T0 versus T4 comparisons).
- e) PCA analysis of bulk *ex vivo* dissociation samples combined with *in vivo* activation single-cells (ranked list). PC1 separated samples based on experimental method (single-cell versus bulk RNA-sequencing) and represents 7% of variance explained.

Discussion

I – Summary

The present work can be summarized with a grim allegory. If an external and seemingly totipotent entity were to violently and totally remove humans from their social and material microenvironment, a sensible amount of physiological stress – such as an elevation of blood pressure or systemic cortisol levels – would undoubtedly be detected. We believe that freshly-isolated cells exhibit a similar behavior when isolated and placed under our scrutiny.

It is difficult to conceive a non-lethal intervention more jarring to a cell than dissociation. We know that the extracellular micro-environment determines the internal state of cell. We know that cell-cell and cell-matrix interactions are critical. We also know the importance of tissue architecture and biophysical properties. We know the importance of nutrients and oxygen availability. We know that the protocols we use to isolate cells often last several hours. We know that cells respond to stimuli in a matter of minutes and that thousands of genes can be altered in less than an hour. In light of what we know, it is therefore self-evident that freshly isolated cells will deviate significantly from their *in vivo* molecular state. Nevertheless, it took more than a decade of transcriptomic studies before scientists started to investigate the effect of dissociation on different cell types. Unsurprisingly, we –in the present thesis - and others demonstrated that dissociation critically impact many cells' transcriptome (Lacar *et al*, 2016; Brink *et al*, 2017; Adam *et al*, 2017; Wu *et al*, 2017; van Velthoven *et al*, 2017; Bakken *et al*, 2018; Wu *et al*, 2019).

Focusing first on MuSCs and then on multi-cellular atlases we exploited multiple strategies to study the impact of dissociation on freshly-isolated cells transcriptome. After successively scouting the published literature for signs of dissociation-induced signatures, we utilized MuSCs to prove that such alterations were sufficient to promote critical cell-fate transitions, such as MuSCs quiescence exit and activation. We dissected the kinetics of the dissociation-induced modifications and uncovered that MuSCs activation was independent of cell-cycle entry, which was mediated through ERK1/2 signaling.

A discussion on the main results of my thesis is included in the Results section, as part of the corresponding manuscripts. In this last section, however, I would like to expand on the overall importance of the present work and discuss some unresolved questions.

II – The impact of dissociation

One could argue that if the impact of dissociation was so significant, it would have been detected much earlier as the field would have had difficulties to publish meaningful and reproducible results. Altogether, several factors can answer this reasoning. First, true valuable results are still present in great quantity in published datasets, from which researchers have generated original discoveries. Such discoveries validated the methodologies and lowered researchers' potential suspicion towards them. Moreover, biology is renowned for its great publication bias, where negative reports are filtered out leading to an overestimation of the accuracy of such methods. Finally, we believe that the field was unconsciously aware of such dissociation-induced effects under the alias of *batch effect*. This term designates the irreproducibility between high-throughput experiments, sometimes even within the same laboratories using the exact same protocol by the same investigator but on different days (Leek *et al*, 2010). While batch effect encompasses the technical variability relative to all the techniques used in a high-throughput experimental pipeline, our time-course analysis on MuSCs activation clearly demonstrated that literally minute-scale differences in the preparation protocols can significantly alter the downstream datasets. Therefore we propose that batch effect, which is at the root of irreproducibility in high-throughput analyses, is partly due to cellular dissociation time.

Maybe others and our own reliance on the word *stress* to depict the effect of dissociation on cells was detrimental. Indeed, cellular stress is often considered to be a transient challenge to internal homeostasis. Many could say that freshly-isolated cells are merely transiently stressed and that these dissociation-induced genes should be disregarded. In the present thesis, we do not speculate about the transience of the dissociation-induced modifications, unless the cells are placed back in their microenvironment. However, for the analysis of quiescent cells researchers don't incubate further the freshly-isolated cells, but process them as soon as they are isolated. Therefore, even if the modifications were transient in nature this conundrum would remain, as most freshly-isolated cells are under considerable stress at the moment of the analysis, transient or not. As for the second part of the argument – whether these induced genes must just be overlooked – we deplore that early reports implied that those dissociation-induced modifications were somewhat of a small magnitude or impacted few cells (Brink *et al*, 2017). Indeed, such data enforced the idea that the effect of

dissociation was manageable within existing datasets and that this limited signature could just be bioinformatically removed or ignored. Our work represents the first attempt to systematically characterize the impact of dissociation across tissues and cell-types. We uncovered that cells' internal states – approximated by their transcriptome – were considerably altered by dissociation. Dissociated cell populations clustered separately from their intact counterpart after undergoing dimensionality reduction algorithms, indicating that the transcriptomic changes underlying these differences were broad and of a great magnitude. Moreover, thousands of genes were identified as differentially-expressed in many cellular populations, after only two hours of dissociation. It is not because expected cellular populations can still be neatly clustered on high-throughput datasets or that these cells consistently express their most specific marker genes that the underlying transcriptional maps are not distorted. To use an analogy, it is as having a chronological map of a country with the name of all of its main cities throughout history, but having these cities represented systematically and unpredictably at the wrong locations and often in the wrong time-window.

One piece of evidence against the notion that dissociation merely induce stress is our study of MuSCs dissociation-induced cell fate transition. Over multiple experimental models, we uncovered that dissociated MuSCs primarily initiate the generic dissociation core genetic program before secondarily exhibiting a cell specific fate transition through the repression of its quiescence pathways and the initiation of the myogenic program. This is not a stress response. The myogenic program is the core of MuSCs function and identity, the central component of skeletal muscle regeneration. Hence, freshly isolated MuSCs underwent a cell fate transition. We hypothesize that similar transitions will be observed in different cell-types - such as angiogenesis induction for freshly-isolated endothelial cells - as the genetic dissociation-response program appears conserved.

One subtlety of the dissociation-induced artefact is its dynamic nature. The precise sequence of transcriptional alterations described in our time-course strategy adds a layer of artefactuality into an already complex process. Indeed, not only one should consider the dissociation status of a cell but also the time under dissociative stimuli. Far from a qualitative difference, dissociation-induced alterations are therefore progressive and induce a continuum of stimulated sub-states. The higher risk of misinterpretation is for investigator looking at dynamic cellular behaviors. We mentioned earlier quiescence exit and cell-cycle re-entry but many more processes take place in much smaller time-frames such as signal transduction, transcription factor binding or membrane depolarization. One great example of such confusion comes from neuroscience studies on activity-induced genes. These genes are simultaneously reporters of neuronal activity (e.g. membrane depolarization), actors of engram formation through synaptic plasticity and dissociation-induced response genes. How can one study each one of these processes in isolation given their respective kinetics – from minutes to hours – and often the necessity to isolate cells? This arduous question was only recently tackled by

some methods presented in the current thesis (Lacar *et al*, 2016; Wu *et al*, 2017; Bakken *et al*, 2018).

A comprehensive epigenetic characterization is one unfortunate missing feature of the present thesis as it focuses almost solely on the transcriptional response to dissociation. In that sense, this thesis reflects the recent literature on cells molecular state characterization from which (single-cell) transcriptomic studies became dominant. Our epigenetic characterization of the dissociation-induced response was limited to the study of DNA methylation and a handful of histone modifications on MuSCs fixed *in situ* or freshly-isolated. The kinetics of DNA methylation modifications are traditionally considered slow, over many cellular generations (Otto & Walbot, 1990). However, histone modifications and transcription factor binding are thought to exhibit faster kinetics of alteration upon stimuli (Katan-Khaykovich & Struhl, 2002; Hipp *et al*, 2019). Consistently, we identified virtually no differences in the methylation status of MuSCs after dissociation while histone modifications was markedly modified in active regulatory regions. However, we did not exploit these results sufficiently and due to the technical difficulties to study these modifications we did not fully characterized the epigenetic landscape of freshly-isolated MuSCs nor extended this study to other freshly-isolated cell types. Such studies will be necessary to fully understand the ubiquitous cell-state transitions. Similarly, proteomics studies should be applied to this experimental paradigm to complete our knowledge on the effect of dissociation across all biological layers.

The evident follow-up of the current thesis will be to understand how a common genetic program – the dissociation core – can triggers cell specific secondary transcriptional responses and cellular behaviors. Interestingly, most of the IEGs induced by dissociation in the primary transcriptional response to it are members of the AP-1 family such as *Jun*, *Fos*, *Fosb*, *Atf3* or *Atf4*. One piece of this puzzle is the cooperative binding of AP-1 family members with cell-specific transcription factors to cell-specifically target enhancers and induce gene expression (Vierbuchen *et al*, 2017). The combinatorial possibilities that result from having different family members associated – and at different times – permit the generation of a great diversity of enhancer binding and transcriptional activities from only a handful of transcription factors (Madrigal & Alasoo, 2018). For example, the cooperative binding of certain AP-1 members with PU.1 and/or C/EBP family members is necessary to establish B cells and macrophages identity (Heinz *et al*, 2010). Moreover, AP-1 family activity reduction is necessary to erase somatic identity and induce pluripotency (Knaupp *et al*, 2017; Li *et al*, 2017; Cao *et al*, 2018). Single-cell ATAC-seq and/or ChIP-sequencing studies during dissociation will be required to prove the link between IEGs, enhancers' selection and cell-specific transcriptional activities.

III – Literature Contamination

The amount of high-throughput transcriptional maps published is expanding at a restless pace. To verify whether the strong dissociation-response that we scored was a peculiarity of MuSCs, we set to systematically interrogate the impact of dissociation in published studies. Aiming for quality over quantity, we set our attention to a state-of-the-art cellular murine atlas. To our surprise, the core dissociation response was shared among cell types and tissues regardless of their identity or composition and only proportional to dissociation-time. We cannot exclude that hard-to-dissociate tissues are most often enriched in specific cell-types such as epithelial cells that would exhibit a specialized dissociation-response. However, by dissociating the liver - a classical easy-to-dissociate tissue- for 2 hours, we demonstrated that given enough dissociation time any cell would undergo drastic molecular alterations. Admittedly, MuSCs were at the apex of dissociation-sensitivity. It is interesting to speculate if this is a feature of regenerative organs/species, stem cells and/or progenitors and if this could be explained by the frequency of physiological micro-injuries during skeletal muscle use (Clarkson & Hubal, 2002).

Facing the financial and human cost of the published or undergoing transcriptomic studies, it is highly unfortunate that the present thesis questions their accuracy. A pressing question is whether these dissociation-induced effects can be attenuated or totally cleaned from the existing datasets. There are efforts in the field to correct for batch effect between different projects and experimental platforms. Most recent studies have relied on complex machine learning algorithms (unsupervised or supervised mutual nearest neighbors detection) to untangle and correct biological variation from technical noise (Haghverdi *et al*, 2018; Yang *et al*, 2019). These tools perform under the assumption that biological variability (e.g. the difference between cell types) is much greater than batch effect-induced variability. However, given the extend of differences that we detected between dissociated and intact cells, batch effect regression could not be efficiently performed. Moreover, most batch effect corrections assume orthogonality in the biological sub-space (i.e. that all cells within the same experiment undergo the same batch effect). Our data proves that each cell type triggers an idiosyncratic and highly-dynamic genetic program in response to injury, further complicating batch-effect corrections. Nevertheless, batch-effect correction could attenuate some of the dissociation-induced effects. However, we do not recommend its implementation, since the dissociation-induced effects, as aforementioned, represent more of a cell state transition than a simple stress signature. Therefore, any transcriptional map digitally corrected for dissociation-induced effects would be at high-risk of impinging even more distortions to the *in vivo* transcriptional reality.

IV - Methods to preserve the transcriptome

More than exposing the effect of dissociation on isolated cells, the present work aims to provide a road-map for stress management in high-throughput transcriptional studies. However, far from perfect, every experimental intervention brings its own set of trade-offs, artefacts and complications. One must carefully analyze the benefits and risks of each method in order to choose for each specific project the procedure that will yields the most accurate transcriptional maps. Generally, to become widespread, an experimental procedure has to present a satisfactory ratio of performance, accessibility and cost-effectiveness. Several methods to preserve the transcriptome of isolated cells will be discussed below.

Dissociation-free methods are a self-evident avenue to avoid the dissociation-induced effects. Among these methods, we and other demonstrated the utility of single nuclei RNA-seq and its almost instantaneous tissue lysis in isolating and stabilizing intact nuclei for droplet-based sequencing without dissociation-induced alterations (Lacar *et al*, 2016; Bakken *et al*, 2018; Wu *et al*, 2019). However, single nuclei RNA-seq has its own problems. First, the similarity between nuclear and cytoplasmic transcriptome might not always hold true. Secondly, this method instantly homogenize an entire tissue and is not efficient when focusing on rare populations. Even if FACS-isolation of the nuclei is possible, standard tools such as (cell) membrane markers selection or non-nuclear genetic labelling cannot be used. Also, the sensitivity is decreased in single nuclei RNA-seq compared to whole cell – from which sensitivity is already a sensitive issue – and technical factors such as ambient RNA contamination can decrease the accuracy and quality of the downstream datasets. Nevertheless, we believe that single nuclei RNA-seq is the new state-of-the-art method to generate complex organismal or tissue transcriptional maps as its benefits far surpass its drawbacks.

One set of dissociation-free methods that are bound to become standard in the next decade are *in situ* sequencing based methods (Lee *et al*, 2015; Thomsen *et al*, 2016; Wang *et al*, 2018a; Rodrigues *et al*, 2019; Eng *et al*, 2019). Importantly, these methods study cells within their tissues and therefore conserve precious topological information about tissue architecture, cell interactions and transcripts localization within cellular compartments. These methods rely on nucleic acid hybridization and cryptographic algorithms to reconstitute transcriptomes from fluorescent microscopic acquisitions. Initially, the sensitivity of these methods – the number of genes detected simultaneously – was not sufficient to realistically generate high-throughput transcriptional maps. While not on par with – probably unattainable - bulk RNA-seq sensitivity, these methods are now comparable to most single-cell RNA-seq methods. So far however, the scalability of these methods prevent their widespread adoption. Indeed, the technical skills required to perform and analyze such data are not prevalent

enough, the transcriptional maps generated are far less complex – in term of cell number – than what droplet-based methods can achieve today and the cost per cell of these transcriptional maps is not competitive yet. Finally, *in situ* sequencing cannot presently rival the colossal menagerie of computational expertise, common knowledge, bioinformatics pipelines and open access analysis tools that Illumina-based sequencing methods leverages. When *in situ* sequencing will gain prominence, the breadth of knowledge stemming from its topological information will be unfathomable.

For different reasons, researchers might need to isolate intact cells by FACS. Different methods have been developed to preserve their transcriptome from the influence of dissociation. We and others developed *in situ* fixation to prevent any biochemical alterations of the RNA during dissociation (Machado *et al*, 2017; van Velthoven *et al*, 2017). This method is affordable, and accessible as it only requires the adjunction of a fixative agent – such as paraformaldehyde – to a tissue. It is easily adaptable into many dissociation protocols, requires no specialized skills, and only marginally lengthens the dissociation procedures. One drawback of this methods is a possible – however inconsistent - decrease in RNA quality and alignment statistics. Moreover, this methods does not have a straight-forward RNA extraction method for low-inputs samples. Indeed, fixed samples require specific lysis buffers that are initially developed for much larger Formalin-Fixed Paraffin-Embedded FFPE samples. Therefore, specific single-cell library preparation procedures such as SMART-Seq2 must be adapted with complicated magnetic clean-up of the lysis buffer. Other single-cell library preparation methodologies such as 10X/Gemcode are totally incompatible with aldehyde fixed samples. Therefore we believe *in situ* fixation to be a tool of choice for the characterization with bulk RNA-seq of pure or rare populations after FACS. New fixative or single-cell libraries preparation protocols would likely ensure that fixation remains the ideal approach to preserve isolated cells transcriptomes.

Methods such as dissociation in the presence of transcriptional inhibitors do not appear satisfactory to prevent the effects of dissociation due to the presence of other molecular alteration than *de novo* transcription and the impossibility to ensure total diffusion and efficacy of the chemical inhibitors in tissues (van Velthoven *et al*, 2017; Wu *et al*, 2017). Similarly, the genetic labelling of nascent transcripts, due to its decreased yields – and therefore incompatibility with single-cell studies - and reliance on genetic models seems to be confined to specific biological situations (van Velthoven *et al*, 2017).

Others methods have been proposed to solve the effect of dissociation. It has been shown that cold-digesting enzymes - on ice - such as psychrophilic proteases could be used to mitigate transcriptomic alterations during cellular isolation with promising results (Adam *et al*, 2017). Every

tissue harbors a specific combination of extra-cellular matrix proteins and a cellular composition that may require the use of different and specific enzymes –or combination of enzymes – to digest it. It remains to be proven if psychrophilic enzymes can be efficient for all tissues, and at the same temperature. Also, in the study describing it, psychrophilic enzymes digest tissues must faster than their control enzyme group. After having established the importance of dissociation time in the present thesis, researchers will need to rule out that the observed effect of psychrophilic enzymes are not partly due to dissociation-time differences. Finally, it remains unknown the extend at which cold blocks the molecular processes leading to transcriptional alterations. To be noted, despite its potentially deleterious effect on cells, cold-digestion is the only technic described here that keep cells alive. This can be a critical asset for studies other than direct transcriptomic characterization after isolation.

Finally, a much simpler guideline stemming from our present work is to dissociate fast. Indeed, our time-course during MuSCs activation and our systematic analysis of the published literature indicated that digestion times of 30 min or less induce only marginal transcriptional alterations. The majority of the tissues from the Tabula Muris cell atlas (Schaum *et al*, 2018) escape the dissociation-induced artefact through this simple route, demonstrating how well-managed methodological practices can yields great results.

V – Considerations for MuSCs quiescence

The original aim of the present thesis was to understand MuSCs quiescence exit. While we uncovered a much broader generic response to activatory signals, critical insight were nevertheless collected on MuSCs quiescence regulation.

First, by implementation of the in situ fixation protocol, we generated MuSCs transcriptional maps much closer to the *in vivo* reality. Our datasets confirm existing reports about the importance of the primary cilia for MuSCs quiescence (Jaafar Marican *et al*, 2016) and the role of fatty-acid oxidation for the metabolism of quiescent cells (Ryall *et al*, 2015). Moreover, we detected high levels of *Pax7* expression in T0 MuSCs across all experimental models, and provided an explanation about the low numbers of *Pax7*-expressing cells in previously reported single-cell RNA-seq experiments. This fact in itself would justify the use of dissociation-mitigating procedures. Furthermore, we also produced the first MuSCs transcriptional map devoid of IEGs, stress-related genes and dissociation-induced alterations. These maps are also rich in uncharted quiescence-enriched pathways, which will nurture our field with original experimental hypothesis and research endeavors. For example, we identified hundreds of *zinc finger proteins* with KRAB domains, scattered on the genome over more than a dozen clusters and globally repressed with dissociation. Such proteins are expected to exhibit a transcriptionally repressive activity (Kauzlaric *et al*, 2017) and their potential role in the regulation of the quiescence transcriptome must be investigated.

Secondly, we confirmed that freshly-isolated MuSCs already initiated a *bona fide* quiescence-breaking process, confirming our initial suspicion that freshly-isolated cells were already activated. The primary transcriptional events of MuSCs stimulation involves IEGs that could merely represent a simple stress signature mediated by MAPK signaling, but rapidly a secondary wave of transcriptional alterations – of a greater magnitude – mark a clear cellular state transition with classical quiescence regulators such as *Calcr*, *Spry1*, or Notch signaling being repressed and the myogenic program induced with the overexpression of *Myod1*. These findings fit surprisingly with a report from more than a decade ago studying MuSCs attached to isolated single myofibers and which scored an induction of first p38 α/β -MAPK phosphorylation and then MYOD1 expression only hours after myofibers isolation (Jones *et al*, 2005). It is certain, however, that activation is a stepped process as the first cellular division would not normally take place until around 30 hours after the isolation (Mourikis *et al*, 2012; Liu *et al*, 2018). It remains unknown what mechanisms take place in this window between isolation and division but we hypothesize that much steadier and linear growth processes will be observed.

Thirdly, our work indicates that MuSCs activation and proliferation are two separated and independent processes. There is no consensus about what is MuSCs activation. This debate is part semantic and part biological. Some consider MuSCs to be activated at the onset of their first cellular division or of some late cellular events such as the phosphorylation of the retinoblastoma protein. We believe that MuSCs get activated when initiating the myogenic program with the induction of *Myod1*. In that sense, we do not separate activation from differentiation and could interchangeably call activated MuSCs *early-differentiated*. One piece of evidence supporting our interpretation is the differentiation of MuSCs without cell-cycle re-entry when removing Notch signaling (Mourikis *et al*, 2012). Another supporting evidence is presented in the current thesis by the fact that blocking ERK1/2 activity on isolated MuSCs totally prevented their cell-cycle re-entry while activation (as per MYOD1 immunostaining) was unchanged for at least 40 hours. A similar albeit reduced phenotype was obtained when inhibiting the AP-1 family factors downstream of ERK1/2. Conversely, inducing Notch signaling with immobilized DLL1 reduced isolated MuSCs activation but their cycling was unmodified. Only when both pathways were modulated did MuSCs oriented toward a proto-quiescent state: non-proliferative and undifferentiated. To be noted, these experiments are preliminary and further efforts must be oriented toward delineating the relationship between activation and proliferation of isolated MuSCs. Many question marks remain on what is the primordial upstream signaling pathways induced by dissociation. We propose that growth-factor signaling receptors and/or mechanotransductive pathways should induce some of the observed phenomenon.

Finally, we uncovered the resemblance between *in vivo* activation and *ex vivo* dissociation. Albeit with slightly different kinetics, the same molecular alterations appear to take place during these two processes. This resemblance can be interpreted from two angles: one that installs *ex vivo* dissociation as a *bona fide* model for the early hours of muscle injury or one that downgrades our classical models of muscle injury as an artificial *in vivo* dissociation procedure. Regardless, we expect this similarity not to hold more than a few hours after stimulation, especially as most of muscle regeneration is a multi-cellular process relying on the intervention of infiltrating cells from the systemic circulation. The accepted models of muscle injury such as BaCl₂ injection provoke myofibre necrosis but not a total dissociation – as with proteolytic enzymes - of the muscle cells which might indicates that MuSCs employ a conserved response to multiple harmful stimuli. More work will be required on non-dissociative/necrotic MuSCs activation models (such as Notch signaling genetic disruption) to uncover the conserved and context specific modes of MuSCs activation as well as studies on multiple cell-types to uncover the link between dissociation, tissue injury and generic responses to loss of homeostasis.

VI – Concluding remarks

It is easy and tempting to blame past studies for not doing what appears obvious to us. One should resist this impulse, as scientific culture, technological context and cognitive bias are similarly impairing us today to understand what will be obvious tomorrow; as it was for those of yesterday to apprehend what is evident today. Standing on the shoulders of the giants is more productive than mocking them. However, when the evidence is sufficient, the scientific community should behave like a rational agent and embrace a more accurate paradigm.

We aimed to redefine MuSCs quiescence and activation. Incidentally, it led to the worrisome discovery that given sufficient dissociation-time virtually all freshly-isolated cells were altered by the techniques that have been developed to study them. Regrettably, the published literature displays the symptoms of such contamination. Considering the stream of high-profile high-throughput transcriptomics studies yet to be published, we expect the present thesis to deflect such efforts toward more accurate second generation atlas.

By studying MuSCs activation, an eminently dynamic system, we uncovered that cell-state transitions occur in hours rather than days. Hopefully, our work will expand the - already high - dimensionality of transcriptomics datasets with a peculiar and often disregarded dimension: time.

Tremendous efforts will be required to fully understand how dissociated cells deploy cell-specific injury-response programs from a generic dissociation core signaling cascade. We trust our peers to explore such avenues.

I always felt a great dissonance in the assumption that high-throughput datasets must be validated with a handful – most often one – thorough mechanistic validation. How can one be satisfied of such a reductionist approach when our multi-omics era lure young minds in a holistic dream of system biology, computational rationality and intricate biological networks? I definitely succeeded at producing a monumental amount of information bits but certainly failed to produce solid mechanistic evidences from it. I understand now the importance to integrate descriptive and mechanistic work in order to produce science that *does* more than science that *shows*. I sincerely hope the present thesis will remind peers to consider cells in their social and material context: the cellular microenvironment. I also sincerely hope this work will help reshaping transcriptomic studies and most importantly, that many valuable scientific discoveries will bloom from it.

References

- Abou-Khalil R, Le Grand F, Pallafacchina G, Valable S, Authier FJ, Rudnicki MA, Gherardi RK, Germain S, Chretien F, Sotiropoulos A, Lafuste P, Montarras D & Chazaud B (2009) Autocrine and paracrine angiopoietin 1/Tie-2 signaling promotes muscle satellite cell self-renewal. *Cell Stem Cell* **5**: 298–309
- Adam M, Potter AS & Potter SS (2017) Psychrophilic proteases dramatically reduce single cell RNA-seq artifacts : A molecular atlas of kidney development.
- von Ahlfen S, Missel A, Bendrat K & Schlumpberger M (2007) Determinants of RNA Quality from FFPE Samples. *PLoS One* **2**: e1261
- Alameddine HS, Hantay D, Dehaupas M & Fardeau M (1991) Role of persisting basement membrane in the reorganization of myofibres originating from myogenic cell grafts in the rat. *Neuromuscul. Disord.* **1**: 143–152
- Allen RE, Sheehan SM, Taylor RG, Kendall TL & Rice GM (1995) Hepatocyte growth factor activates quiescent skeletal muscle satellite cells in vitro. *J. Cell. Physiol.* **165**: 307–312
- Allis CD & Jenuwein T (2016) The molecular hallmarks of epigenetic control. *Nat. Rev. Genet.* **17**: 487
- Alway SE, Myers MJ & Mohamed JS (2014) Regulation of Satellite Cell Function in Sarcopenia. *Front. Aging Neurosci.* **6**: 1–15
- Amit I, Citri A, Shay T, Lu Y, Katz M, Zhang F, Tarcic G, Siwak D, Lahad J, Jacob-Hirsch J, Amariglio N, Vaisman N, Segal E, Rechavi G, Alon U, Mills GB, Domany E & Yarden Y (2007) A module of negative feedback regulators defines growth factor signaling. *Nat. Genet.* **39**: 503–512
- Armulik A, Genové G & Betsholtz C (2011) Pericytes: Developmental, Physiological, and Pathological Perspectives, Problems, and Promises. *Dev. Cell* **21**: 193–215
- Arnold L, Henry A, Poron F, Baba-Amer Y, van Rooijen N, Plonquet A, Gherardi RK & Chazaud B (2007) Inflammatory monocytes recruited after skeletal muscle injury switch into antiinflammatory macrophages to support myogenesis. *J Exp Med* **204**: 1057–1069
- Arora R, Rumman M, Venugopal N, Gala H & Dhawan J (2017) Mimicking Muscle Stem Cell Quiescence in Culture: Methods for Synchronization in Reversible Arrest. In *Muscle Stem Cells: Methods and Protocols*, Perdiguerro E & Cornelison DDW (eds) pp 283–302. New York, NY: Springer New York
- Baghdadi MB, Castel D, Machado L, Fukada S, Birk DE, Relaix F, Tajbakhsh S & Mourikis P (2018a) Reciprocal signalling by Notch–Collagen V–CALCR retains muscle stem cells in their niche. *Nature* **557**: 714–718
- Baghdadi MB, Firmino J, Soni K, Evano B, Di Girolamo D, Mourikis P, Castel D & Tajbakhsh S (2018b) Notch-Induced miR-708 Antagonizes Satellite Cell Migration and Maintains Quiescence. *Cell Stem Cell* **23**: 859–868.e5
- Baghdadi MB & Tajbakhsh S (2018) Regulation and phylogeny of skeletal muscle regeneration. *Dev. Biol.* **433**: 200–209
- Bakken TE, Hodge RD, Miller JA, Yao Z, Nguyen TN, Aevermann B, Barkan E, Bertagnolli D, Casper T, Dee N, Garren E, Goldy J, Graybuck LT, Kroll M, Lasken RS, Lathia K, Parry S, Rimorin C, Scheuermann RH, Schork NJ, et al (2018) Single-nucleus and single-cell transcriptomes compared in matched cortical cell types. *PLoS One* **13**: e0209648–e0209648
- Baran-gale J, Chandra T & Kirschner K (2018) Experimental design for single-cell RNA sequencing. **17**: 233–239
- Barski A, Cuddapah S, Cui K, Roh T-Y, Schones DE, Wang Z, Wei G, Chepelev I & Zhao K (2007) High-Resolution Profiling of Histone Methylations in the Human Genome. *Cell* **129**: 823–837
- Beauchamp JR, Heslop L, Yu DS, Tajbakhsh S, Kelly RG, Wernig A, Buckingham ME, Partridge TA & Zammit PS (2000) Expression of CD34 and Myf5 defines the majority of quiescent adult skeletal muscle satellite cells. *J*

- Cell Biol* **151**: 1221–1234
- Bencze M, Negroni E, Vallese D, Yacoub–Youssef H, Chaouch S, Wolff A, Aamiri A, Di Santo JP, Chazaud B, Butler–Browne G, Savino W, Mouly V & Riederer I (2012) Proinflammatory Macrophages Enhance the Regenerative Capacity of Human Myoblasts by Modifying Their Kinetics of Proliferation and Differentiation. *Mol. Ther.* **20**: 2168–2179
- Bentzinger CF, Wang YX, Dumont NA & Rudnicki MA (2013a) Cellular dynamics in the muscle satellite cell niche. *EMBO Rep.* **14**: 1062–1072
- Bentzinger CF, Wang YX, von Maltzahn J, Soleimani VD, Yin H & Rudnicki MA (2013b) Fibronectin regulates Wnt7a signaling and satellite cell expansion. *Cell Stem Cell* **12**: 75–87
- Bianconi E, Piovesan A, Facchin F, Beraudi A, Casadei R, Frabetti F, Vitale L, Pelleri MC, Tassani S, Piva F, Perez–Amodio S, Strippoli P & Canaider S (2013) An estimation of the number of cells in the human body. *Ann. Hum. Biol.* **40**: 463–471
- Bintliff S & Walker BE (1960) Radioautographic study of skeletal muscle regeneration. *Am. J. Anat.* **106**: 233–245
- Bischoff R (1975) Regeneration of single skeletal muscle fibers in vitro. *Anat. Rec.* **182**: 215–235
- Bischoff R (1986a) Proliferation of muscle satellite cells on intact myofibers in culture. *Dev. Biol.* **115**: 129–139
- Bischoff R (1986b) A satellite cell mitogen from crushed adult muscle. *Dev. Biol.* **115**: 140–147
- Bjornson CR, Cheung TH, Liu L, Tripathi P V, Steeper KM & Rando TA (2012) Notch signaling is necessary to maintain quiescence in adult muscle stem cells. *Stem Cells* **30**: 232–242
- Boonsanay V, Zhang T, Georgieva A, Kostin S, Qi H, Yuan X, Zhou Y & Braun T (2016) Regulation of Skeletal Muscle Stem Cell Quiescence by Suv4-20h1-Dependent Facultative Heterochromatin Formation. *Cell Stem Cell* **18**: 229–242
- Bosnakovski D, Xu Z, Li W, Thet S, Cleaver O, Perlingeiro RCR & Kyba M (2008) Prospective isolation of skeletal muscle stem cells with a Pax7 reporter. *Stem Cells* **26**: 3194–3204
- Boyle AP, Davis S, Shulha HP, Meltzer P, Margulies EH, Weng Z, Furey TS & Crawford GE (2008) High-Resolution Mapping and Characterization of Open Chromatin across the Genome. *Cell* **132**: 311–322
- Brack AS, Conboy MJ, Roy S, Lee M, Kuo CJ, Keller C & Rando TA (2007) Increased Wnt Signaling During Aging Alters Muscle Stem Cell Fate and Increases Fibrosis. *Science (80-.)*. **317**: 807 LP-810
- Brady G, Barbara M & Iscove NN (1990) Representative in Vitro cDNA Amplification From Individual Hemopoietic Cells and Colonies. **25**: 17–25
- Braun T, Buschhausen-Denker G, Bober E, Tannich E & Arnold HH (1989) A novel human muscle factor related to but distinct from MyoD1 induces myogenic conversion in 10T1/2 fibroblasts. *EMBO J.* **8**: 701–709
- Brink SC van den, Sage F, Vértesy Á, Spanjaard B, Peterson-Maduro J, Baron CS, Robin C & Oudenaarden A van (2017) Single-cell sequencing reveals dissociation-induced gene expression in tissue subpopulations. **14**:
- van den Brink SC, Sage F, Vértesy Á, Spanjaard B, Peterson-Maduro J, Baron CS, Robin C, van Oudenaarden A, Brink SC van den, Sage F, Vértesy Á, Spanjaard B, Peterson-Maduro J, Baron CS, Robin C & Oudenaarden A van (2017) Single-cell sequencing reveals dissociation-induced gene expression in tissue subpopulations. **14**:
- Bröhl D, Vasyutina E, Czajkowski MT, Griger J, Rassek C, Rahn H-P, Purfürst B, Wende H & Birchmeier C (2012) Colonization of the Satellite Cell Niche by Skeletal Muscle Progenitor Cells Depends on Notch Signals. *Dev. Cell* **23**: 469–481
- Buchwalter G, Gross C & Wasylyk B (2004) Ets ternary complex transcription factors. *Gene* **324**: 1–14
- Buenrostro JD, Giresi PG, Zaba LC, Chang HY & Greenleaf WJ (2013) Transposition of native chromatin for fast and sensitive epigenomic profiling of open chromatin, DNA-binding proteins and nucleosome position. *Nat.*

Methods **10**: 1213

- Cairns J (1975) Mutation selection and the natural history of cancer. *Nature* **255**: 197–200
- Cao J, Spielmann M, Qiu X, Huang X, Ibrahim DM, Hill AJ, Zhang F, Mundlos S, Christiansen L, Steemers FJ, Trapnell C & Shendure J (2019) The single-cell transcriptional landscape of mammalian organogenesis. *Nature* **566**: 496–502
- Cao R, Wang L, Wang H, Xia L, Erdjument-Bromage H, Tempst P, Jones RS & Zhang Y (2002) Role of Histone H3 Lysine 27 Methylation in Polycomb-Group Silencing. *Science (80-.)*. **298**: 1039 LP-1043
- Cao S, Yu S, Li D, Ye J, Yang X, Li C, Wang X, Mai Y, Qin Y, Wu J, He J, Zhou C, Liu H, Zhao B, Shu X, Wu C, Chen R, Chan W, Pan G, Chen J, et al (2018) Chromatin Accessibility Dynamics during Chemical Induction of Pluripotency. *Cell Stem Cell* **22**: 529–542.e5
- Castel D, Mourikis P, Bartels SJ, Brinkman AB, Tajbakhsh S & Stunnenberg HG (2013) Dynamic binding of RBPJ is determined by Notch signaling status. *Genes Dev* **27**: 1059–1071
- Ceafalan LC, Fertig TE, Popescu AC, Popescu BO, Hinescu ME & Gherghiceanu M (2018) Skeletal muscle regeneration involves macrophage-myoblast bonding. *Cell Adh. Migr.* **12**: 228–235
- Chakkalakal J V, Jones KM, Basson MA & Brack AS (2012) The aged niche disrupts muscle stem cell quiescence. *Nature* **490**: 355–360
- Chang HH, Hemberg M, Barahona M, Ingber DE & Huang S (2008) Transcriptome-wide noise controls lineage choice in mammalian progenitor cells. *Nature* **453**: 544
- CHARGÉ SBP & RUDNICKI MA (2004) Cellular and Molecular Regulation of Muscle Regeneration. *Physiol. Rev.* **84**: 209–238
- Cheung TH, Quach NL, Charville GW, Liu L, Park L, Edalati A, Yoo B, Hoang P & Rando TA (2012) Maintenance of muscle stem-cell quiescence by microRNA-489. *Nature* **482**: 524–528
- Cheung TH & Rando TA (2013) Molecular regulation of stem cell quiescence. *Nat Rev Mol Cell Biol* **14**: 329–340
- Cho DS & Doles JD (2017) Single cell transcriptome analysis of muscle satellite cells reveals widespread transcriptional heterogeneity. *Gene* **636**: 54–63
- Cho IJ, Lui PPW, Obajdin J, Riccio F, Stroukov W, Willis TL, Spagnoli F & Watt FM (2019) Mechanisms, Hallmarks, and Implications of Stem Cell Quiescence. *Stem Cell Reports* **12**: 1190–1200
- Christov C, Chretien F, Abou-Khalil R, Bassez G, Vallet G, Authier FJ, Bassaglia Y, Shinin V, Tajbakhsh S, Chazaud B & Gherardi RK (2007) Muscle satellite cells and endothelial cells: close neighbors and privileged partners. *Mol Biol Cell* **18**: 1397–1409
- Clarkson P & Hubal M (2002) Exercise-induced muscle damage in humans. *Am J Phys Med Rehabi*: 52–59
- Cochran BH, Zullo J, Verma IM & Stiles CD (1984) Expression of the c-fos gene and of a fos-related gene is stimulated by platelet-derived growth factor. *Science (80-.)*. **226**: 1080 LP-1082
- Collins CA, Olsen I, Zammit PS, Heslop L, Petrie A, Partridge TA & Morgan JE (2005) Stem Cell Function, Self-Renewal, and Behavioral Heterogeneity of Cells from the Adult Muscle Satellite Cell Niche. *Cell* **122**: 289–301
- Collins CA, Zammit PS, Ruiz AP, Morgan JE & Partridge TA (2007) A Population of Myogenic Stem Cells That Survives Skeletal Muscle Aging. *Stem Cells* **25**: 885–894
- Comai G & Tajbakhsh S (2014) Chapter One - Molecular and Cellular Regulation of Skeletal Myogenesis. In *bHLH Transcription Factors in Development and Disease*, Taneja RBT-CT in DB (ed) pp 1–73. Academic Press
- Conboy MJ, Karasov AO & Rando TA (2007) High incidence of non-random template strand segregation and asymmetric fate determination in dividing stem cells and their progeny. *PLoS Biol.* **5**: e102–e102

- Cooper RN, Tajbakhsh S, Mouly V, Cossu G, Buckingham M & Butler-Browne GS (1999) In vivo satellite cell activation via Myf5 and MyoD in regenerating mouse skeletal muscle. *J Cell Sci* **112** (Pt 1): 2895–2901
- Cornelison DDW, Filla MS, Stanley HM, Rapraeger AC & Olwin BB (2001) Syndecan-3 and Syndecan-4 Specifically Mark Skeletal Muscle Satellite Cells and Are Implicated in Satellite Cell Maintenance and Muscle Regeneration. *Dev. Biol.* **239**: 79–94
- Cornelison DDW, Wilcox-Adelman SA, Goetinck PF, Rauvala H, Rapraeger AC & Olwin BB (2004) Essential and separable roles for Syndecan-3 and Syndecan-4 in skeletal muscle development and regeneration. *Genes Dev.* **18**: 2231–2236
- Cornelison DDW & Wold BJ (1997) Single-Cell Analysis of Regulatory Gene Expression in Quiescent and Activated Mouse Skeletal Muscle Satellite Cells. *Dev. Biol.* **191**: 270–283
- Couchman JR, Gopal S, Lim HC, Nørgaard S & Multhaupt HAB (2015) Fell-Muir Lecture: Syndecans: from peripheral coreceptors to mainstream regulators of cell behaviour. *Int. J. Exp. Pathol.* **96**: 1–10
- Crick F (1958) On Protein Synthesis. In *The Symposia of the Society for Experimental Biology 12* pp 138–163.
- Crick F (1970) Central Dogma of Molecular Biology. *Nature* **227**: 561–563
- Crist CG, Montarras D & Buckingham M (2012) Muscle Satellite Cells Are Primed for Myogenesis but Maintain Quiescence with Sequestration of Myf5 mRNA Targeted by microRNA-31 in mRNP Granules. *Cell Stem Cell* **11**: 118–126
- Davis RL, Weintraub H & Lassar AB (1987) Expression of a single transfected cDNA converts fibroblasts to myoblasts. *Cell* **51**: 987–1000
- Dell’Orso S, Juan AH, Ko K-D, Naz F, Gutierrez-Cruz G, Feng X & Sartorelli V (2019) Single-cell analysis of adult skeletal muscle stem cells in homeostatic and regenerative conditions. *Development*: dev.174177
- Dellavalle A, Maroli G, Covarello D, Azzoni E, Innocenzi A, Perani L, Antonini S, Sambasivan R, Brunelli S, Tajbakhsh S & Cossu G (2011) Pericytes resident in postnatal skeletal muscle differentiate into muscle fibres and generate satellite cells. *Nat Commun* **2**: 499
- Dellavalle A, Sampaolesi M, Tonlorenzi R, Tagliafico E, Sacchetti B, Perani L, Innocenzi A, Galvez BG, Messina G, Morosetti R, Li S, Belicchi M, Peretti G, Chamberlain JS, Wright WE, Torrente Y, Ferrari S, Bianco P & Cossu G (2007) Pericytes of human skeletal muscle are myogenic precursors distinct from satellite cells. *Nat. Cell Biol.* **9**: 255–267
- Doupé DP, Klein AM, Simons BD & Jones PH (2010) The Ordered Architecture of Murine Ear Epidermis Is Maintained by Progenitor Cells with Random Fate. *Dev. Cell* **18**: 317–323
- Du H, Shih C-H, Wosczyzna MN, Mueller AA, Cho J, Aggarwal A, Rando TA & Feldman BJ (2017) Macrophage-released ADAMTS1 promotes muscle stem cell activation. *Nat. Commun.* **8**: 669
- Dumont NA, Wang YX, von Maltzahn J, Pasut A, Bentzinger CF, Brun CE & Rudnicki MA (2015) Dystrophin expression in muscle stem cells regulates their polarity and asymmetric division. *Nat. Med.* **21**: 1455–1463
- Dupont S, Morsut L, Aragona M, Enzo E, Giulitti S, Cordenonsi M, Zanconato F, Le Digabel J, Forcato M, Bicciato S, Elvassore N & Piccolo S (2011) Role of YAP/TAZ in mechanotransduction. *Nature* **474**: 179
- Edfors F, Danielsson F, Hallström BM, Käll L, Lundberg E, Pontén F, Forsström B & Uhlén M (2016) Gene-specific correlation of RNA and protein levels in human cells and tissues. : 1–10
- Eng C-HL, Lawson M, Zhu Q, Dries R, Kouloua N, Takei Y, Yun J, Cronin C, Karp C, Yuan G-C & Cai L (2019) Transcriptome-scale super-resolved imaging in tissues by RNA seqFISH+. *Nature* **568**: 235–239
- Fiacco E, Castagnetti F, Bianconi V, Madaro L, De Bardi M, Nazio F, D’Amico A, Bertini E, Cecconi F, Puri PL & Latella L (2016) Autophagy regulates satellite cell ability to regenerate normal and dystrophic muscles. *Cell Death Differ.* **23**: 1839–1849

- Fincher CT, Wurtzel O, de Hoog T, Kravarik KM & Reddien PW (2018) Cell type transcriptome atlas for the planarian *Schmidtea mediterranea*. *Science* (80-.). **874**: eaaq1736
- Finnell R, Zettel M & Coleman P (1992) Analysis of gene expression in single live neurons. **89**: 3010–3014
- Fiore D, Judson RN, Low M, Lee S, Zhang E, Hopkins C, Xu P, Lenzi A, Rossi FM V & Lemos DR (2016) Pharmacological blockage of fibro/adipogenic progenitor expansion and suppression of regenerative fibrogenesis is associated with impaired skeletal muscle regeneration. *Stem Cell Res.* **17**: 161–169
- Fox CH, Johnson FB, Whiting J & Roller PP (1985) Formaldehyde fixation. *J. Histochem. Cytochem.* **33**: 845–853
- Frantz C, Stewart KM & Weaver VM (2010) The extracellular matrix at a glance. *J. Cell Sci.* **123**: 4195 LP-4200
- Frontera WR & Ochala J (2015) Skeletal Muscle: A Brief Review of Structure and Function. *Calcif. Tissue Int.* **96**: 183–195
- Füchtbauer E-M & Westphal H (1992) MyoD and myogenin are coexpressed in regenerating skeletal muscle of the mouse. *Dev. Dyn.* **193**: 34–39
- Fukada S, Uezumi A, Ikemoto M, Masuda S, Segawa M, Tanimura N, Yamamoto H, Miyagoe-Suzuki Y & Takeda S (2007) Molecular signature of quiescent satellite cells in adult skeletal muscle. *Stem Cells* **25**: 2448–2459
- Gaidatzis D, Burger L, Florescu M & Stadler MB (2015) Analysis of intronic and exonic reads in RNA-seq data characterizes transcriptional and post-transcriptional regulation. *Nat. Biotechnol.* **33**: 722
- Gayraud-Morel B, Chretien F, Jory A, Sambasivan R, Negroni E, Flamant P, Soubigou G, Coppee JY, Di Santo J, Cumanò A, Mouly V & Tajbakhsh S (2012) Myf5 haploinsufficiency reveals distinct cell fate potentials for adult skeletal muscle stem cells. *J Cell Sci*
- Ge H, Walhout AJM & Vidal M (2003) Integrating ‘ omic ’ information : a bridge between genomics and systems biology. **19**: 551–560
- Ge X, McFarlane C, Vajjala A, Lokireddy S, Ng ZH, Tan CK, Tan NS, Wahli W, Sharma M & Kambadur R (2011) Smad3 signaling is required for satellite cell function and myogenic differentiation of myoblasts. *Cell Res.* **21**: 1591–1604
- Ge X, Vajjala A, McFarlane C, Wahli W, Sharma M & Kambadur R (2012) Lack of Smad3 signaling leads to impaired skeletal muscle regeneration. *Am. J. Physiol. Metab.* **303**: E90–E102
- Gilbert PM, Havenstrite KL, Magnusson KEG, Sacco A, Leonardi NA, Kraft P, Nguyen NK, Thrun S, Lutolf MP & Blau HM (2010) Substrate elasticity regulates skeletal muscle stem cell self-renewal in culture. *Science* **329**: 1078–1081
- Giordani L, He GJ, Negroni E, Sakai H, Law JYC, Siu MM, Wan R, Corneau A, Tajbakhsh S, Cheung TH & Le Grand F (2019) High-Dimensional Single-Cell Cartography Reveals Novel Skeletal Muscle-Resident Cell Populations. *Mol. Cell*
- Giordani L, Parisi A & Le Grand F (2018) Chapter Six - Satellite Cell Self-Renewal. In *Myogenesis in Development and Disease*, Sassoon DBT-CT in DB (ed) pp 177–203. Academic Press
- Goel AJ, Rieder M-K, Arnold H-H, Radice GL & Krauss RS (2017) Niche Cadherins Control the Quiescence-to-Activation Transition in Muscle Stem Cells. *Cell Rep.* **21**: 2236–2250
- Gomez-Pastor R, Burchfiel ET & Thiele DJ (2017) Regulation of heat shock transcription factors and their roles in physiology and disease. *Nat. Rev. Mol. Cell Biol.* **19**: 4
- Gopinath SD, Webb AE, Brunet A & Rando TA (2014) FOXO3 Promotes Quiescence in Adult Muscle Stem Cells during the Process of Self-Renewal. *Stem Cell Reports* **2**: 414–426
- Le Grand F, Jones AE, Seale V, Scimè A & Rudnicki MA (2009) Wnt7a activates the planar cell polarity pathway to drive the symmetric expansion of satellite stem cells. *Cell Stem Cell* **4**: 535–547

- Greenberg ME & Ziff EB (1984) Stimulation of 3T3 cells induces transcription of the c-fos proto-oncogene. *Nature* **311**: 433–438
- Grindberg R V, Yee-Greenbaum JL, McConnell MJ, Novotny M, O’Shaughnessy AL, Lambert GM, Araúzo-Bravo MJ, Lee J, Fishman M, Robbins GE, Lin X, Venepally P, Badger JH, Galbraith DW, Gage FH & Lasken RS (2013) RNA-sequencing from single nuclei. *Proc. Natl. Acad. Sci. U. S. A.* **110**: 19802–19807
- Grounds MD, Garrett KL, Lai MC, Wright WE & Beilharz MW (1992) Identification of skeletal muscle precursor cells in vivo by use of MyoD1 and myogenin probes. *Cell Tissue Res.* **267**: 99–104
- Guzowski JF, McNaughton BL, Barnes CA & Worley PF (1999) Environment-specific expression of the immediate-early gene Arc in hippocampal neuronal ensembles. *Nat. Neurosci.* **2**: 1120–1124
- Habib N, Li Y, Heidenreich M, Swiech L, Avraham-Davidi I, Trombetta JJ, Hession C, Zhang F & Regev A (2016) Div-Seq: Single-nucleus RNA-Seq reveals dynamics of rare adult newborn neurons. *Science* **353**: 925–928
- Haghverdi L, Lun ATL, Morgan MD & Marioni JC (2018) Batch effects in single-cell RNA-sequencing data are corrected by matching mutual nearest neighbors. *Nat. Biotechnol.* **36**: 421–427
- Hall J, Thomas KL & Everitt BJ (2001) Cellular Imaging of zif268 Expression in the Hippocampus and Amygdala during Contextual and Cued Fear Memory Retrieval: Selective Activation of Hippocampal CA1 Neurons during the Recall of Contextual Memories. *J. Neurosci.* **21**: 2186 LP-2193
- Han X, Wang R, Zhou Y, Fei L, Sun H, Lai S, Saadatpour A, Zhou Z, Chen H, Ye F, Huang D, Xu Y, Huang W, Jiang M, Jiang X, Mao J, Chen Y, Lu C, Xie J, Fang Q, et al (2018) Mapping the Mouse Cell Atlas by Microwell-Seq. *Cell* **172**: 1091–1107.e17
- Hardy D, Besnard A, Latil M, Jouvion G, Briand D, Thépenier C, Pascal Q, Guguin A, Gayraud-Morel B, Cavaillon J-M, Tajbakhsh S, Rocheteau P & Chrétien F (2016) Comparative Study of Injury Models for Studying Muscle Regeneration in Mice. *PLoS One* **11**: e0147198
- Harel I, Nathan E, Tirosh-Finkel L, Zigdon H, Guimarães-Camboa N, Evans SM & Tzahor E (2009) Distinct Origins and Genetic Programs of Head Muscle Satellite Cells. *Dev. Cell* **16**: 822–832
- Hausburg MA, Doles JD, Clement SL, Cadwallader AB, Hall MN, Blackshear PJ, Lykke-Andersen J & Olwin BB (2015) Post-transcriptional regulation of satellite cell quiescence by TTP-mediated mRNA decay. *Elife* **4**: e03390–e03390
- Heinz S, Benner C, Spann N, Bertolino E, Lin YC, Laslo P, Cheng JX, Murre C, Singh H & Glass CK (2010) Simple combinations of lineage-determining transcription factors prime cis-regulatory elements required for macrophage and B cell identities. *Mol. Cell* **38**: 576–589
- Heredia JE, Mukundan L, Chen FM, Mueller AA, Deo RC, Locksley RM, Rando TA & Chawla A (2013) Type 2 innate signals stimulate fibro/adipogenic progenitors to facilitate muscle regeneration. *Cell* **153**: 376–388
- Herschman HR (1991) Primary Response Genes Induced by Growth Factors and Tumor Promoters. *Annu. Rev. Biochem.* **60**: 281–319
- Hines WC, Su Y, Kuhn I, Polyak K & Bissell MJ (2014) Sorting Out the FACS: A Devil in the Details. *Cell Rep.* **6**: 779–781
- Hipp L, Beer J, Kuchler O, Reisser M, Sinske D, Michaelis J, Gebhardt JCM & Knöll B (2019) Single-molecule imaging of the transcription factor SRF reveals prolonged chromatin-binding kinetics upon cell stimulation. *Proc. Natl. Acad. Sci.* **116**: 880 LP-889
- Hooke R (1665) Micrographia, or, Some physiological descriptions of minute bodies made by magnifying glasses with observations and inquiries thereupon / by R. Hooke
- Imayoshi I, Isomura A, Harima Y, Kawaguchi K, Kori H, Miyachi H, Fujiwara T, Ishidate F & Kageyama R (2013) Oscillatory Control of Factors Determining Multipotency and Fate in Mouse Neural Progenitors. *Science (80-)*. **342**: 1203 LP-1208

- J. Fukumoto, I. Yamamoto KI (1951) No Title. *Proc. Japan Acad.*
- Jaafar Marican NH, Cruz-Migoni SB & Borycki A-G (2016) Asymmetric Distribution of Primary Cilia Allocates Satellite Cells for Self-Renewal. *Stem cell reports* **6**: 798–805
- Janknecht R, Ernst WH, Pingoud V & Nordheim A (1993) Activation of ternary complex factor Elk-1 by MAP kinases. *EMBO J.* **12**: 5097–5104
- Joe AW, Yi L, Natarajan A, Le Grand F, So L, Wang J, Rudnicki MA & Rossi FM (2010) Muscle injury activates resident fibro/adipogenic progenitors that facilitate myogenesis. *Nat Cell Biol* **12**: 153–163
- Jones NC, Fedorov Y V, Rosenthal RS & Olwin BB (2001) ERK1/2 is required for myoblast proliferation but is dispensable for muscle gene expression and cell fusion. *J. Cell. Physiol.* **186**: 104–115
- Jones NC, Tyner KJ, Nibarger L, Stanley HM, Cornelison DDW, Fedorov Y V. & Olwin BB (2005) The p38^{MAPK} functions as a molecular switch to activate the quiescent satellite cell. *J. Cell Biol.* **169**: 105–116
- Judson RN, Quarta M, Oudhoff MJ, Soliman H, Yi L, Chang CK, Loi G, Vander Werff R, Cait A, Hamer M, Blonigan J, Paine P, Doan LTN, Groppa E, He W, Su L, Zhang RH, Xu P, Eisner C, Low M, et al (2018) Inhibition of Methyltransferase Setd7 Allows the In Vitro Expansion of Myogenic Stem Cells with Improved Therapeutic Potential. *Cell Stem Cell* **22**: 177–190.e7
- Judson RN, Tremblay AM, Knopp P, White RB, Urcia R, De Bari C, Zammit PS, Camargo FD & Wackerhage H (2012) The Hippo pathway member Yap plays a key role in influencing fate decisions in muscle satellite cells. *J. Cell Sci.* **125**: 6009 LP-6019
- Katan-Khaykovich Y & Struhl K (2002) Dynamics of global histone acetylation and deacetylation in vivo: rapid restoration of normal histone acetylation status upon removal of activators and repressors. *Genes Dev.* **16**: 743–752
- Katz B. (1961) The termination of the afferent nerve fibre in the muscle spindle of the frog. *Philos. Trans. R. Soc. Lond. B. Biol. Sci.* **243**: 221–240
- Kaufmann WE, Barnes ICA, Sanders LK, Copeland NG, Gilbert DJ, Jenkins IINA, Lanahan AA & Worley PF (1995) Arc, a growth factor and activity-regulated gene, encodes a novel cytoskeleton-associated protein that is enriched in neuronal dendrites. *Neuron* **14**: 433–445
- Kauzlaric A, Ecco G, Cassano M, Duc J, Imbeault M & Trono D (2017) The mouse genome displays highly dynamic populations of KRAB-zinc finger protein genes and related genetic units. *PLoS One* **12**: e0173746–e0173746
- Kelly K, Cochran BH, Stiles CD & Leder P (1983) Cell-specific regulation of the *c-myc* gene by lymphocyte mitogens and platelet-derived growth factor. *Cell* **35**: 603–610
- Kelsey G, Stegle O & Reik W (2017) Single-cell epigenomics: Recording the past and predicting the future. *Science (80-.).* **358**: 69 LP-75
- Kitajima Y & Ono Y (2018) Visualization of PAX7 protein dynamics in muscle satellite cells in a YFP knock-in-mouse line. *Skelet. Muscle* **8**: 26
- Kitajima Y, Suzuki N, Nunomiya A, Osana S, Yoshioka K, Tashiro Y, Takahashi R, Ono Y, Aoki M & Nagatomi R (2018) The Ubiquitin-Proteasome System Is Indispensable for the Maintenance of Muscle Stem Cells. *Stem cell reports* **11**: 1523–1538
- Klein AM, Nakagawa T, Ichikawa R, Yoshida S & Simons BD (2010) Mouse Germ Line Stem Cells Undergo Rapid and Stochastic Turnover. *Cell Stem Cell* **7**: 214–224
- Klein CA, Seidl S, Petat-dutter K, Offner S, Geigl JB, Schmidt-kittler O, Wendler N, Passlick B, Huber RM, Schlimok G, Baeuerle PA & Riethmüller G (2002) Combined transcriptome and genome analysis of single micrometastatic cells. **20**: 387–392
- Knaupp AS, Buckberry S, Pflueger J, Lim SM, Ford E, Larcombe MR, Rossello FJ, de Mendoza A, Alaei S, Firas J, Holmes ML, Nair SS, Clark SJ, Nefzger CM, Lister R & Polo JM (2017) Transient and Permanent

- Reconfiguration of Chromatin and Transcription Factor Occupancy Drive Reprogramming. *Cell Stem Cell* **21**: 834–845.e6
- Konstantinides N, Kapuralin K, Fadil C, Barboza L, Satija R & Desplan C (2018) Phenotypic Convergence: Distinct Transcription Factors Regulate Common Terminal Features. *Cell* **174**: 622–635.e13
- Kostallari E, Baba-Amer Y, Alonso-Martin S, Ngoh P, Relaix F, Lafuste P & Gherardi RK (2015) Pericytes in the myovascular niche promote post-natal myofiber growth and satellite cell quiescence. *Development* **142**: 1242 LP-1253
- Kuang S, Kuroda K, Le Grand F & Rudnicki MA (2007) Asymmetric self-renewal and commitment of satellite stem cells in muscle. *Cell* **129**: 999–1010
- Kühne W (1877) Ueber das Verhalten Verschiedener organisirter und sog. ungeformter Fermente. *Heidelb. - 1877*: 190–193.
- Kumar D, Shadrach JL, Wagers AJ & Lassar AB (2009) Id3 is a direct transcriptional target of Pax7 in quiescent satellite cells. *Mol. Biol. Cell* **20**: 3170–3177
- Kurimoto K, Yabuta Y, Ohinata Y, Ono Y, Uno KD, Yamada RG, Ueda HR & Saitou M (2006) An improved single-cell cDNA amplification method for efficient high-density oligonucleotide microarray analysis. **34**:
- Lacar B, Linker SB, Jaeger BN, Krishnaswami SR, Barron JJ, Kelder MJE, Parylak SL, Paquola ACM, Venepally P, Novotny M, O'Connor C, Fitzpatrick C, Erwin JA, Hsu JY, Husband D, McConnell MJ, Lasken R & Gage FH (2016) Nuclear RNA-seq of single neurons reveals molecular signatures of activation. *Nat. Commun.* **7**: 11022
- Lake BB, Ai R, Kaeser GE, Salathia NS, Yung YC, Liu R, Wildberg A, Gao D, Fung H-L, Chen S, Vijayaraghavan R, Wong J, Chen A, Sheng X, Kaper F, Shen R, Ronaghi M, Fan J-B, Wang W, Chun J, et al (2016) Neuronal subtypes and diversity revealed by single-nucleus RNA sequencing of the human brain. *Science* **352**: 1586–1590
- Latroche C, Weiss-Gayet M, Muller L, Gitiaux C, Leblanc P, Liot S, Ben-Larbi S, Abou-Khalil R, Verger N, Bardot P, Magnan M, Chrétien F, Mounier R, Germain S & Chazaud B (2017) Coupling between Myogenesis and Angiogenesis during Skeletal Muscle Regeneration Is Stimulated by Restorative Macrophages. *Stem cell reports* **9**: 2018–2033
- Lee JH, Daugharthy ER, Scheiman J, Kalhor R, Ferrante TC, Terry R, Turczyk BM, Yang JL, Lee HS, Aach J, Zhang K & Church GM (2015) Fluorescent in situ sequencing (FISSEQ) of RNA for gene expression profiling in intact cells and tissues. *Nat. Protoc.* **10**: 442
- Lee S-M, Vasishtha M & Prywes R (2010) Activation and repression of cellular immediate early genes by serum response factor cofactors. *J. Biol. Chem.* **285**: 22036–22049
- Leek JT, Scharpf RB, Bravo HC, Simcha D, Langmead B, Johnson WE, Geman D, Baggerly K & Irizarry RA (2010) Tackling the widespread and critical impact of batch effects in high-throughput data. *Nat. Rev. Genet.* **11**: 733–739
- Lefaucheur JP & Sébille A (1995) The cellular events of injured muscle regeneration depend on the nature of the injury. *Neuromuscul. Disord.* **5**: 501–509
- Leikina E, Gamage DG, Prasad V, Goykhberg J, Crowe M, Diao J, Kozlov MM, Chernomordik L V & Millay DP (2018) Myomaker and Myomerger Work Independently to Control Distinct Steps of Membrane Remodeling during Myoblast Fusion. *Dev. Cell* **46**: 767–780.e7
- Lepper C, Conway SJ & Fan CM (2009) Adult satellite cells and embryonic muscle progenitors have distinct genetic requirements. *Nature* **460**: 627–631
- Lepper C, Partridge TA & Fan C-M (2011) An absolute requirement for Pax7-positive satellite cells in acute injury-induced skeletal muscle regeneration. *Development* **138**: 3639 LP-3646
- Li D, Liu J, Yang X, Zhou C, Guo J, Wu C, Qin Y, Guo L, He J, Yu S, Liu H, Wang X, Wu F, Kuang J, Hutchins

- AP, Chen J & Pei D (2017) Chromatin Accessibility Dynamics during iPSC Reprogramming. *Cell Stem Cell* **21**: 819–833.e6
- Li Y-P (2003) TNF- α is a mitogen in skeletal muscle. *Am. J. Physiol. Physiol.* **285**: C370–C376
- Lieberman-Aiden E, van Berkum NL, Williams L, Imakaev M, Ragozy T, Telling A, Amit I, Lajoie BR, Sabo PJ, Dorschner MO, Sandstrom R, Bernstein B, Bender MA, Groudine M, Gnirke A, Stamatoyannopoulos J, Mirny LA, Lander ES & Dekker J (2009) Comprehensive mapping of long-range interactions reveals folding principles of the human genome. *Science* **326**: 289–293
- Liguori I, Russo G, Curcio F, Bulli G, Aran L, Della-Morte D, Gargiulo G, Testa G, Cacciatore F, Bonaduce D & Abete P (2018) Oxidative stress, aging, and diseases. *Clin. Interv. Aging* **13**: 757–772
- Link W, Konietzko U, Kauselmann G, Krug M, Schwanke B, Frey U & Kuhl D (1995) Somatodendritic expression of an immediate early gene is regulated by synaptic activity. *Proc. Natl. Acad. Sci.* **92**: 5734 LP-5738
- Liu L, Charville GW, Cheung TH, Yoo B, Santos PJ, Schroeder M & Rando TA (2018) Impaired Notch Signaling Leads to a Decrease in p53 Activity and Mitotic Catastrophe in Aged Muscle Stem Cells. *Cell Stem Cell* **23**: 544–556.e4
- Liu L, Cheung TH, Charville GW, Hurgu BMC, Leavitt T, Shih J, Brunet A & Rando TA (2013) Chromatin Modifications as Determinants of Muscle Stem Cell Quiescence and Chronological Aging. *Cell Rep.*
- Lukjanenko L, Karaz S, Stuelsatz P, Gurriaran-Rodriguez U, Michaud J, Dammone G, Sizzano F, Mashinchian O, Ancel S, Migliavacca E, Liot S, Jacot G, Metairon S, Raymond F, Descombes P, Palini A, Chazaud B, Rudnicki MA, Bentzinger CF & Feige JN (2019) Aging Disrupts Muscle Stem Cell Function by Impairing Matricellular WISP1 Secretion from Fibro-Adipogenic Progenitors. *Cell Stem Cell* **24**: 433–446.e7
- van Lunteren E & Leahy P (2007) Gene expression microarrays and respiratory muscles. *Respir. Physiol. Neurobiol.* **156**: 103–115
- Macaulay IC, Ponting CP & Voet T (2017) Single-Cell Multiomics : Multiple Measurements from Single Cells. *Trends Genet.* **33**: 155–168
- Machado L, Esteves de Lima J, Fabre O, Proux C, Legendre R, Szegedi A, Varet H, Ingerslev LR, Barrès R, Relaix F & Mourikis P (2017) In Situ Fixation Redefines Quiescence and Early Activation of Skeletal Muscle Stem Cells. *Cell Rep.* **21**:
- Mackey AL, Magnan M, Chazaud B & Kjaer M (2017) Human skeletal muscle fibroblasts stimulate in vitro myogenesis and in vivo muscle regeneration. *J. Physiol.* **595**: 5115–5127
- Madrigal P & Alasoo K (2018) AP-1 Takes Centre Stage in Enhancer Chromatin Dynamics. *Trends Cell Biol.* **28**: 509–511
- Mahat DB, Salamanca HH, Duarte FM, Danko CG & Lis JT (2016) Mammalian Heat Shock Response and Mechanisms Underlying Its Genome-wide Transcriptional Regulation. *Mol. Cell* **62**: 63–78
- Majmundar AJ, Wong WJ & Simon MC (2010) Hypoxia-Inducible Factors and the Response to Hypoxic Stress. *Mol. Cell* **40**: 294–309
- Malecova B, Gatto S, Etxaniz U, Passafaro M, Cortez A, Nicoletti C, Giordani L, Torcinaro A, De Bardi M, Biciato S, De Santa F, Madaro L & Puri PL (2018) Dynamics of cellular states of fibro-adipogenic progenitors during myogenesis and muscular dystrophy. *Nat. Commun.* **9**: 3670
- von Maltzahn J, Jones AE, Parks RJ & Rudnicki MA (2013) Pax7 is critical for the normal function of satellite cells in adult skeletal muscle. *Proc. Natl. Acad. Sci. U. S. A.* **110**: 16474–16479
- Mandl I, MacLennan JD & Howes EL (1953) Isolation and characterization of proteinase and collagenase from *Cl. histolyticum*. *J. Clin. Invest.* **32**: 1323–1329
- Margulies M, Egholm M, Altman WE, Attiya S, Bader JS, Bemben LA, Berka J, Braverman MS, Chen Y, Chen Z, Dewell B, Du L, Fierro JM, Gomes X V, Goodwin BC, He W, Helgesen S, Ho CH, Irzyk GP, Jando SC, et al

- (2005) Genome Sequencing in Open Microfabricated High Density Picoliter Reactors. **437**: 376–380
- Mathew SJ, Hansen JM, Merrell AJ, Murphy MM, Lawson JA, Hutcheson DA, Hansen MS, Angus-Hill M & Kardon G (2011) Connective tissue fibroblasts and Tcf4 regulate myogenesis. *Development* **138**: 371–384
- Mauro A (1961) Satellite Cell of Skeletal Muscle Fibers. *J. Cell Biol.* **9**: 493–495
- McCarthy JJ, Mula J, Miyazaki M, Erfani R, Garrison K, Farooqui AB, Srikuea R, Lawson BA, Grimes B, Keller C, Van Zant G, Campbell KS, Esser KA, Dupont-Versteegden EE & Peterson CA (2011) Effective fiber hypertrophy in satellite cell-depleted skeletal muscle. *Development* **138**: 3657 LP-3666
- McKinnell IW, Ishibashi J, Le Grand F, Punch VGJ, Addicks GC, Greenblatt JF, Dilworth FJ & Rudnicki MA (2008) Pax7 activates myogenic genes by recruitment of a histone methyltransferase complex. *Nat. Cell Biol.* **10**: 77–84
- Milasincic DJ, Dhawan J & Farmer SR (1996) Anchorage-Dependent Control of Muscle-Specific Gene Expression in C₂C₁₂ Mouse Myoblasts. *In Vitro Cell. Dev. Biol. Anim.* **32**: 90–99
- Millay DP, O'Rourke JR, Sutherland LB, Bezprozvannaya S, Shelton JM, Bassel-Duby R & Olson EN (2013) Myomaker is a membrane activator of myoblast fusion and muscle formation. *Nature* **499**: 301
- Minatohara K, Akiyoshi M & Okuno H (2016) Role of Immediate-Early Genes in Synaptic Plasticity and Neuronal Ensembles Underlying the Memory Trace. *Front. Mol. Neurosci.* **8**: 78
- Mintz B & Baker WW (1967) Normal mammalian muscle differentiation and gene control of isocitrate dehydrogenase synthesis. *Proc. Natl. Acad. Sci. U. S. A.* **58**: 592–598
- Montarras D, Morgan J, Collins C, Relaix F, Zaffran S, Cumano A, Partridge T & Buckingham M (2005) Direct Isolation of Satellite Cells for Skeletal Muscle Regeneration. *Science (80-.).* **309**: 2064 LP-2067
- de Morrée A, van Velthoven CTJ, Gan Q, Salvi JS, Klein JDD, Akimenko I, Quarta M, Biressi S & Rando TA (2017) Staufen1 inhibits MyoD translation to actively maintain muscle stem cell quiescence. *Proc. Natl. Acad. Sci.* **114**: E8996 LP-E9005
- Moss FP & Leblond CP (1971) Satellite cells as the source of nuclei in muscles of growing rats. *Anat. Rec.* **170**: 421–435
- Mourikis P, Sambasivan R, Castel D, Rocheteau P, Bizzarro V & Tajbakhsh S (2012) A Critical Requirement for Notch Signaling in Maintenance of the Quiescent Skeletal Muscle Stem Cell State. *Stem Cells* **30**: 243–252
- Muñoz-Cánoves P, Scheele C, Pedersen BK & Serrano AL (2013) Interleukin-6 myokine signaling in skeletal muscle: A double-edged sword? *FEBS J.* **280**: 4131–4148
- Murphy MM, Keefe AC, Lawson JA, Flygare SD, Yandell M & Kardon G (2014) Transiently active Wnt/ β -catenin signaling is not required but must be silenced for stem cell function during muscle regeneration. *Stem cell reports* **3**: 475–488
- Murphy MM, Lawson JA, Mathew SJ, Hutcheson DA & Kardon G (2011) Satellite cells, connective tissue fibroblasts and their interactions are crucial for muscle regeneration. *Development* **138**: 3625 LP-3637
- Nishijo K, Hosoyama T, Bjornson CR, Schaffer BS, Prajapati SI, Bahadur AN, Hansen MS, Blandford MC, McCleish AT, Rubin BP, Epstein JA, Rando TA, Capecchi MR & Keller C (2009) Biomarker system for studying muscle, stem cells, and cancer in vivo. *FASEB J* **23**: 2681–2690
- O'Brien J, Hayder H, Zayed Y & Peng C (2018) Overview of MicroRNA Biogenesis, Mechanisms of Actions, and Circulation. *Front. Endocrinol. (Lausanne).* **9**: 402
- Ono Y, Boldrin L, Knopp P, Morgan JE & Zammit PS (2010) Muscle satellite cells are a functionally heterogeneous population in both somite-derived and branchiomeric muscles. *Dev. Biol.* **337**: 29–41
- Ono Y, Masuda S, Nam H, Benezra R, Miyagoe-Suzuki Y & Takeda S (2012) Slow-dividing satellite cells retain long-term self-renewal ability in adult muscle. *J. Cell Sci.* **125**: 1309 LP-1317

- Ono Y, Urata Y, Goto S, Nakagawa S, Humbert PO, Li T-S & Zammit PS (2015) Muscle Stem Cell Fate Is Controlled by the Cell-Polarity Protein Scrib. *Cell Rep.* **10**: 1135–1148
- Otto SP & Walbot V (1990) DNA methylation in eukaryotes: kinetics of demethylation and de novo methylation during the life cycle. *Genetics* **124**: 429–437
- Pallafacchina G, François S, Regnault B, Czarny B, Dive V, Cumano A, Montarras D & Buckingham M (2010) An adult tissue-specific stem cell in its niche: A gene profiling analysis of in vivo quiescent and activated muscle satellite cells. *Stem Cell Res.*
- Picelli S, Faridani OR, Björklund ÅK, Winberg G, Sagasser S & Sandberg R (2014) Full-length RNA-seq from single cells using. **9**: 171–181
- Pisconti A, Banks GB, Babaeijandaghi F, Betta ND, Rossi FM V, Chamberlain JS & Olwin BB (2016) Loss of niche-satellite cell interactions in syndecan-3 null mice alters muscle progenitor cell homeostasis improving muscle regeneration. *Skelet. Muscle* **6**: 34
- Pisconti A, Cornelison DDW, Olguín HC, Antwine TL & Olwin BB (2010) Syndecan-3 and Notch cooperate in regulating adult myogenesis. *J. Cell Biol.* **190**: 427–441
- Porter JD, Merriam AP, Leahy P, Gong B, Feuerman J, Cheng G & Khanna S (2003) Temporal gene expression profiling of dystrophin-deficient (mdx) mouse diaphragm identifies conserved and muscle group-specific mechanisms in the pathogenesis of muscular dystrophy. *Hum. Mol. Genet.* **13**: 257–269
- Price FD, von Maltzahn J, Bentzinger CF, Dumont NA, Yin H, Chang NC, Wilson DH, Frenette J & Rudnicki MA (2014) Inhibition of JAK-STAT signaling stimulates adult satellite cell function. *Nat. Med.* **20**: 1174
- Quarta M, Brett JO, DiMarco R, De Morree A, Boutet SC, Chacon R, Gibbons MC, Garcia VA, Su J, Shrager JB, Heilshorn S & Rando TA (2016) An artificial niche preserves the quiescence of muscle stem cells and enhances their therapeutic efficacy. *Nat Biotechnol* **34**: 752–759
- Quinn ME, Goh Q, Kurosaka M, Gamage DG, Petrany MJ, Prasad V & Millay DP (2017) Myomerger induces fusion of non-fusogenic cells and is required for skeletal muscle development. *Nat. Commun.* **8**: 15665
- Rada-Iglesias A, Bajpai R, Swigut T, Brugmann SA, Flynn RA & Wysocka J (2010) A unique chromatin signature uncovers early developmental enhancers in humans. *Nature* **470**: 279
- Ramírez-Amaya V, Vazdarjanova A, Mikhael D, Rosi S, Worley PF & Barnes CA (2005) Spatial Exploration-Induced Arc mRNA and Protein Expression: Evidence for Selective, Network-Specific Reactivation. *J. Neurosci.* **25**: 1761 LP-1768
- Razin A & Riggs AD (1980) DNA methylation and gene function. *Science (80-.).* **210**: 604 LP-610
- Regev A, Teichmann SA, Lander ES, Amit I, Benoist C, Birney E, Bodenmiller B, Campbell P, Carninci P, Clatworthy M, Clevers H, Deplancke B, Dunham I, Eberwine J, Eils R, Enard W, Farmer A, Fugger L, Göttgens B, Hacohen N, et al (2017) The human cell atlas. *Elife* **6**: 1–30
- Relaix F, Montarras D, Zaffran S, Gayraud-Morel B, Rocancourt D, Tajbakhsh S, Mansouri A, Cumano A & Buckingham M (2006) Pax3 and Pax7 have distinct and overlapping functions in adult muscle progenitor cells. *J Cell Biol* **172**: 91–102
- Relaix F, Rocancourt D, Mansouri A & Buckingham M (2005) A Pax3/Pax7-dependent population of skeletal muscle progenitor cells. *Nature* **435**: 948–953
- Rhoads RP, Johnson RM, Rathbone CR, Liu X, Temm-Grove C, Sheehan SM, Hoying JB & Allen RE (2009) Satellite cell-mediated angiogenesis in vitro coincides with a functional hypoxia-inducible factor pathway. *Am. J. Physiol. Cell Physiol.* **296**: C1321–C1328
- Rhodes SJ & Konieczny SF (1989) Identification of MRF4: A new member of the muscle regulatory factor gene family. *Genes Dev.* **3**: 2050–2061
- Ritossa F (1962) A new puffing pattern induced by temperature shock and DNP in drosophila. *New York* **55**: 571–

- Rocheteau P, Gayraud-Morel B, Siegl-Cachedenier I, Blasco MA & Tajbakhsh S (2012) A subpopulation of adult skeletal muscle stem cells retains all template DNA strands after cell division. *Cell* **148**: 112–125
- Rodgers JT, King KY, Brett JO, Cromie MJ, Charville GW, Maguire KK, Brunson C, Mastey N, Liu L, Tsai CR, Goodell MA & Rando TA (2014) mTORC1 controls the adaptive transition of quiescent stem cells from G0 to G1. *Nature* **510**: 393–396
- Rodrigues SG, Stickels RR, Goeva A, Martin CA, Murray E, Vanderburg CR, Welch J, Chen LM, Chen F & Macosko EZ (2019) Slide-seq: A scalable technology for measuring genome-wide expression at high spatial resolution. *Science* (80-.). **363**: 1463 LP-1467
- Rosen JB, Fanselow MS, Young SL, Sitcoske M & Maren S (1998) Immediate-early gene expression in the amygdala following footshock stress and contextual fear conditioning. *Brain Res.* **796**: 132–142
- Rozo M, Li L & Fan CM (2016) Targeting beta1-integrin signaling enhances regeneration in aged and dystrophic muscle in mice. *Nat Med* **22**: 889–896
- Ryall JG, Dell’Orso S, Derfoul A, Juan A, Zare H, Feng X, Clermont D, Koulunis M, Gutierrez-Cruz G, Fulco M & Sartorelli V (2015) The NAD⁺-dependent sirt1 deacetylase translates a metabolic switch into regulatory epigenetics in skeletal muscle stem cells. *Cell Stem Cell* **16**: 171–183
- Sacco A, Doyonnas R, Kraft P, Vitorovic S & Blau HM (2008) Self-renewal and expansion of single transplanted muscle stem cells. *Nature* **456**: 502–506
- Saffen DW, Cole AJ, Worley PF, Christy BA, Ryder K & Baraban JM (1988) Convulsant-induced increase in transcription factor messenger RNAs in rat brain. *Proc. Natl. Acad. Sci.* **85**: 7795 LP-7799
- Sambasivan R, Gayraud-Morel B, Dumas G, Cimper C, Paisant S, Kelly R & Tajbakhsh S (2009) Distinct Regulatory Cascades Govern Extraocular and Pharyngeal Arch Muscle Progenitor Cell Fates. *Dev. Cell*
- Sambasivan R, Yao R, Kissenpfennig A, Van Wittenberghe L, Paldi A, Gayraud-Morel B, Guenou H, Malissen B, Tajbakhsh S & Galy A (2011) Pax7-expressing satellite cells are indispensable for adult skeletal muscle regeneration. *Development* **138**: 3647–3656
- Sampath SC, Sampath SC, Ho AT V, Corbel SY, Millstone JD, Lamb J, Walker J, Kinzel B, Schmedt C & Blau HM (2018) Induction of muscle stem cell quiescence by the secreted niche factor Oncostatin M. *Nat. Commun.* **9**: 1531
- Sarge KD, Zimarino V, Holm K, Wu C & Morimoto RI (1991) Cloning and characterization of two mouse heat shock factors with distinct inducible and constitutive DNA-binding ability. *Genes Dev.* **5**: 1902–1911
- Sato T, Yamamoto T & Sehara-Fujisawa A (2014) miR-195/497 induce postnatal quiescence of skeletal muscle stem cells. *Nat. Commun.* **5**: 4597
- Scaramozza A, Park D, Kollu S, Beerman I, Sun X, Rossi DJ, Lin CP, Scadden DT, Crist C & Brack AS (2019) Lineage Tracing Reveals a Subset of Reserve Muscle Stem Cells Capable of Clonal Expansion under Stress. *Cell Stem Cell*
- Scharner J & Zammit PS (2011) The muscle satellite cell at 50: the formative years. *Skelet. Muscle* **1**: 28
- Schaum N, Karkanas J, Neff NF, May AP, Quake SR, Wyss-Coray T, Darmanis S, Batson J, Botvinnik O, Chen MB, Chen S, Green F, Jones RC, Maynard A, Penland L, Pisco AO, Sit R V, Stanley GM, Webber JT, Zanini F, et al (2018) Single-cell transcriptomics of 20 mouse organs creates a Tabula Muris. *Nature* **562**: 367–372
- Schiaffino S & Reggiani C (2011) Fiber Types in Mammalian Skeletal Muscles. *Physiol. Rev.* **91**: 1447–1531
- Schiaffino S, Rossi AC, Smerdu V, Leinwand LA & Reggiani C (2015) Developmental myosins: expression patterns and functional significance. *Skelet. Muscle* **5**: 22
- Schultz E (1996) Satellite Cell Proliferative Compartments in Growing Skeletal Muscles. *Dev. Biol.* **175**: 84–94

- Schwann T (1839) Mikroskopische Untersuchungen über die Uebereinstimmung in der Struktur und dem Wachsthum der Thiere und Pflanzen
- Seale P, Ishibashi J, Holterman C & Rudnicki MA (2004) Muscle satellite cell-specific genes identified by genetic profiling of MyoD-deficient myogenic cell. *Dev. Biol.* **275**: 287–300
- Seale P, Sabourin LA, Girgis-Gabardo A, Mansouri A, Gruss P & Rudnicki MA (2000) Pax7 is required for the specification of myogenic satellite cells. *Cell* **102**: 777–786
- Sellathurai J, Cheedipudi S, Dhawan J & Schröder HD (2013) A novel in vitro model for studying quiescence and activation of primary isolated human myoblasts. *PLoS One* **8**: e64067–e64067
- Shah K & Tyagi S (2013) Barriers to transmission of transcriptional noise in a c-fos c-jun pathway. *Mol. Syst. Biol.* **9**: 687
- Shea KL, Xiang W, LaPorta VS, Licht JD, Keller C, Basson MA & Brack AS (2010) Sproutyl1 regulates reversible quiescence of a self-renewing adult muscle stem cell pool during regeneration. *Cell Stem Cell* **6**: 117–129
- Sheehan SM & Allen RE (1999) Skeletal muscle satellite cell proliferation in response to members of the fibroblast growth factor family and hepatocyte growth factor. *J. Cell. Physiol.* **181**: 499–506
- Shendure J, Porreca GJ, Reppas NB, Lin X, Mccutcheon JP, Rosenbaum AM, Wang MD, Zhang K, Mitra RD & Church GM (2005) Accurate Multiplex Polony Sequencing of an Evolved Bacterial Genome. **309**: 1728–1733
- Shinin V, Gayraud-Morel B, Gomes D & Tajbakhsh S (2006) Asymmetric division and cosegregation of template DNA strands in adult muscle satellite cells. *Nat Cell Biol* **8**: 677–687
- Siegel AL, Kuhlmann PK & Cornelison DD (2011) Muscle satellite cell proliferation and association: new insights from myofiber time-lapse imaging. *Skelet Muscle* **1**: 7
- Snippert HJ, van der Flier LG, Sato T, van Es JH, van den Born M, Kroon-Veenboer C, Barker N, Klein AM, van Rheenen J, Simons BD & Clevers H (2010) Intestinal Crypt Homeostasis Results from Neutral Competition between Symmetrically Dividing Lgr5 Stem Cells. *Cell* **143**: 134–144
- Spangrude GJ, Heimfeld S & Weissman IL (1988) Purification and characterization of mouse hematopoietic stem cells. *Science (80-.)*. **241**: 58
- Sun C, De Mello V, Mohamed A, Ortuste Quiroga HP, Garcia-Munoz A, Al Bloshi A, Tremblay AM, von Kriegsheim A, Collie-Duguid E, Vargesson N, Matallanas D, Wackerhage H & Zammit PS (2017) Common and Distinctive Functions of the Hippo Effectors Taz and Yap in Skeletal Muscle Stem Cell Function. *Stem Cells* **35**: 1958–1972
- Svensson V, Vento-tormo R & Teichmann SA (2018) Exponential scaling of single-cell RNA-seq in the past decade. **13**:
- Tajbakhsh S (2009) Skeletal muscle stem cells in developmental versus regenerative myogenesis. *J Intern Med* **266**: 372–389
- Tang F, Barbacioru C, Wang Y, Nordman E, Lee C, Xu N, Wang X, Bodeau J, Tuch BB, Siddiqui A, Lao K & Surani MA (2009) mRNA-Seq whole-transcriptome analysis of a single cell. **6**:
- Tatsumi R, Anderson JE, Nevoret CJ, Halevy O & Allen RE (1998) HGF/SF Is Present in Normal Adult Skeletal Muscle and Is Capable of Activating Satellite Cells. *Dev. Biol.* **194**: 114–128
- Tatsumi R, Hattori A, Ikeuchi Y, Anderson JE & Allen RE (2002) Release of hepatocyte growth factor from mechanically stretched skeletal muscle satellite cells and role of pH and nitric oxide. *Mol. Biol. Cell* **13**: 2909–2918
- Thavarajah R, Mudimbaimannar VK, Elizabeth J, Rao UK & Ranganathan K (2012) Chemical and physical basics of routine formaldehyde fixation. *J. Oral Maxillofac. Pathol.* **16**: 400–405
- Thomsen ER, Mich JK, Yao Z, Hodge RD, Doyle AM, Jang S, Shehata SI, Nelson AM, Shapovalova N V, Levi BP

- & Ramanathan S (2016) Fixed single-cell transcriptomic characterization of human radial glial diversity. *Nat. Methods* **13**: 87–93
- Tichy ED, Sidibe DK, Greer CD, Oyster NM, Rompolas P, Rosenthal NA, Blau HM & Mourkioti F (2018) A robust Pax7EGFP mouse that enables the visualization of dynamic behaviors of muscle stem cells. *Skelet. Muscle* **8**: 27
- Tierney MT, Aydogdu T, Sala D, Malecova B, Gatto S, Puri PL, Latella L & Sacco A (2014) STAT3 signaling controls satellite cell expansion and skeletal muscle repair. *Nat. Med.* **20**: 1182
- Tierney MT, Stec MJ, Rulands S, Simons BD & Sacco A (2018) Muscle Stem Cells Exhibit Distinct Clonal Dynamics in Response to Tissue Repair and Homeostatic Aging. *Cell Stem Cell* **22**: 119–127.e3
- Tietjen I, Rihel JM, Cao Y, Koentges G, Zakhary L, Dulac C & Clara S (2003) Single-Cell Transcriptional Analysis of Neuronal Progenitors 3380 Central Expressway. **38**: 161–175
- Tomasetti C & Bozic I (2015) The (not so) immortal strand hypothesis. *Stem Cell Res.* **14**: 238–241
- Troy A, Cadwallader AB, Fedorov Y, Tyner K, Tanaka KK & Olwin BB (2012) Coordination of satellite cell activation and self-renewal by Par-complex-dependent asymmetric activation of p38 α / β MAPK. *Cell Stem Cell* **11**: 541–553
- Uezumi A, Fukada S, Yamamoto N, Takeda S & Tsuchida K Mesenchymal progenitors distinct from satellite cells contribute to ectopic fat cell formation in skeletal muscle. *Nat Cell Biol* **12**: 143–152
- Valdes-Mora F, Handler K, Law AMK, Salomon R, Oakes SR, Ormandy CJ & Gallego-Ortega D (2018) Single-Cell Transcriptomics in Cancer Immunobiology: The Future of Precision Oncology. *Front. Immunol.* **9**: 2582
- Vandermarliere E, Mueller M & Martens L (2013) Getting intimate with trypsin, the leading protease in proteomics. *Mass Spectrom. Rev.* **32**: 453–465
- Vann SD, Brown MW, Erichsen JT & Aggleton JP (2000) Fos Imaging Reveals Differential Patterns of Hippocampal and Parahippocampal Subfield Activation in Rats in Response to Different Spatial Memory Tests. *J. Neurosci.* **20**: 2711 LP-2718
- Varga T, Mounier R, Patsalos A, Gogolák P, Peloquin M, Horvath A, Pap A, Daniel B, Nagy G, Pintye E, Póliska S, Cuvellier S, Larbi S Ben, Sansbury BE, Spite M, Brown CW, Chazaud B & Nagy L (2016) Macrophage PPAR γ , a Lipid Activated Transcription Factor Controls the Growth Factor GDF3 and Skeletal Muscle Regeneration. *Immunity* **45**: 1038–1051
- Der Vartanian A, Quéting M, Michineau S, Auradé F, Hayashi S, Dubois C, Rocancourt D, Drayton-Libotte B, Szegedi A, Buckingham M, Conway SJ, Gervais M & Relaix F (2019) PAX3 Confers Functional Heterogeneity in Skeletal Muscle Stem Cell Responses to Environmental Stress. *Cell Stem Cell*
- van Velthoven CTJ, de Morree A, Egner IM, Brett JO & Rando TA (2017) Transcriptional Profiling of Quiescent Muscle Stem Cells In Vivo. *Cell Rep.* **21**: 1994–2004
- Verma M, Asakura Y, Murakonda BSR, Pengo T, Latroche C, Chazaud B, McLoon LK & Asakura A (2018) Muscle Satellite Cell Cross-Talk with a Vascular Niche Maintains Quiescence via VEGF and Notch Signaling. *Cell Stem Cell* **23**: 530–543.e9
- Vierbuchen T, Ling E, Cowley CJ, Couch CH, Wang X, Harmin DA, Roberts CWM & Greenberg ME (2017) AP-1 Transcription Factors and the BAF Complex Mediate Signal-Dependent Enhancer Selection. *Mol. Cell* **68**: 1067–1082.e12
- Vracko R & Benditt EP (1972) Basal lamina: the scaffold for orderly cell replacement. Observations on regeneration of injured skeletal muscle fibers and capillaries. *J. Cell Biol.* **55**: 406–419
- Waddington CH (1942) The epigenotype. *Endeav.* **1**: 18–20
- Walter P & Ron D (2011) The Unfolded Protein Response: From Stress Pathway to Homeostatic Regulation. *Science* (80-.). **334**: 1081 LP-1086

- Zhang T, Günther S, Looso M, Künne C, Krüger M, Kim J, Zhou Y & Braun T (2015) Prmt5 is a regulator of muscle stem cell expansion in adult mice. *Nat. Commun.* **6**: 7140
- Zhao P & Hoffman EP (2004) Embryonic myogenesis pathways in muscle regeneration. *Dev. Dyn.* **229**: 380–392
- Zhao P, Iezzi S, Carver E, Dressman D, Gridley T, Sartorelli V & Hoffman EP (2002) Slug is a novel downstream target of MyoD. Temporal profiling in muscle regeneration. *J. Biol. Chem.* **277**: 30091–30101
- Zheng GXY, Terry JM, Belgrader P, Ryvkin P, Bent ZW, Wilson R, Ziraldo SB, Wheeler TD, Mcdermott GP, Zhu J, Gregory MT, Shuga J, Montesclaros L, Underwood JG, Masquelier DA, Nishimura SY, Schnall-levin M, Wyatt PW, Hindson CM, Bharadwaj R, et al (2017) Massively parallel digital transcriptional profiling of single cells. *Nat. Commun.* **8**: 1–12
- Zismanov V, Chichkov V, Colangelo V, Jamet S, Wang S, Syme A, Koromilas AE & Crist C (2016) Phosphorylation of eIF2 β ; Is a Translational Control Mechanism Regulating Muscle Stem Cell Quiescence and Self-Renewal. *Cell Stem Cell* **18**: 79–90

Appendix

Part I: Reciprocal Signalling by Notch-Collagen V-CALCR Retains Muscle Stem Cells in their Niche

Baghdadi et al. 2018

Nature. volume 557, pages714–718

Part II: Waking Up Muscle Stem Cells: PI3K Signalling is Ringing

Relaix & Machado. 2018

The EMBO Journal 37:e99297

Part I: Reciprocal Signalling by Notch-Collagen V-CALCR Retains Muscle Stem Cells in their Niche

Baghdadi et al. 2018

Nature. volume 557, pages714–718

Reciprocal signalling by Notch–Collagen V–CALCR retains muscle stem cells in their niche

Meryem B. Baghdadi^{1,2,3}, David Castel^{4,5}, Léo Machado⁶, So-ichiro Fukada⁷, David E. Birk⁸, Frederic Relaix⁶, Shahrugim Tajbakhsh^{1,2*} & Philippos Mourikis^{6*}

The cell microenvironment, which is critical for stem cell maintenance, contains both cellular and non-cellular components, including secreted growth factors and the extracellular matrix^{1–3}. Although Notch and other signalling pathways have previously been reported to regulate quiescence of stem cells^{4–9}, the composition and source of molecules that maintain the stem cell niche remain largely unknown. Here we show that adult muscle satellite (stem) cells in mice produce extracellular matrix collagens to maintain quiescence in a cell-autonomous manner. Using chromatin immunoprecipitation followed by sequencing, we identified NOTCH1/RBPJ-bound regulatory elements adjacent to specific collagen genes, the expression of which is deregulated in Notch-mutant mice. Moreover, we show that Collagen V (COLV) produced by satellite cells is a critical component of the quiescent niche, as depletion of COLV by conditional deletion of the *Col5a1* gene leads to anomalous cell cycle entry and gradual diminution of the stem cell pool. Notably, the interaction of COLV with satellite cells is mediated by the Calcitonin receptor, for which COLV acts as a surrogate local ligand. Systemic administration of a calcitonin derivative is sufficient to rescue the quiescence and self-renewal defects found in COLV-null satellite cells. This study reveals a Notch–COLV–Calcitonin receptor signalling cascade that maintains satellite cells in a quiescent state in a cell-autonomous fashion, and raises the possibility that similar reciprocal mechanisms act in diverse stem cell populations.

Notch activation antagonizes myogenesis by induction of transcriptional repressors (members of the HES/HEY family) and sequestration of the co-activator Mastermind-like 1 from the muscle differentiation factor MEF2C^{10,11}. However, Notch signalling has broader functions in muscle cells, including the maintenance of quiescence^{4,5}. To explore these functions, we carried out chromatin immunoprecipitation following by sequencing (ChIP-seq) screening¹² and observed that intracellular Notch (NICD) and its downstream effector RBPJ occupied and regulated enhancers proximal to the collagen genes *Col5a1*, *Col5a3*, *Col6a1* and *Col6a2*, which code for collagens that are amongst the most abundant of those produced by satellite cells (Fig. 1a, b and Extended Data Fig. 1a–e). By analysing mouse genetic models with altered Notch activity, we showed that the expression of these collagens tightly correlated with Notch activity in vivo (Extended Data Fig. 2a–e). Moreover, transcriptional induction of *Col5a1* and *Col5a3* by NICD translated to elevated COLV protein levels, specifically the $\alpha 1(V)\alpha 2(V)\alpha 3(V)$ isoform ($\alpha 3$ -COLV), in fetal forelimb (Fig. 1c) and adult hindlimb (tibialis anterior muscle) myogenic cells (Fig. 1d and Extended Data Fig. 2f for $\alpha 3$ -COLV antibody specificity). Furthermore, we isolated collagen-depleted myofibres after treatment with collagenase, to monitor de novo $\alpha 3$ -COLV production. As *Col5a1* and *Col5a3* transcripts are downregulated upon exit from quiescence (Extended Data Figs. 1a, 2g), no $\alpha 3$ -COLV was detected in freshly isolated or activated satellite cells.

Instead, genetic overexpression of NICD resulted in abundant, newly synthesized $\alpha 3$ -COLV (Fig. 1e, f).

To assess the functional role of COLV, isolated satellite cells were incubated with COLI, COLV or COLVI in the presence of 5-ethynyl-2'-deoxyuridine (EdU) to assess proliferation and stained for PAX7, which marks muscle stem and/or progenitor cells, and the muscle commitment (MYOD) and differentiation (Myogenin) proteins. Only the COLV-complemented medium delayed entry of quiescent cells into the cell cycle (32 h, Fig. 2a), and consequently delayed their amplification and differentiation (72 h, Fig. 2b; 10 days, Extended Data Fig. 3a–c). As previously shown^{4,13}, *Rbpj*^{-/-} cells underwent precocious differentiation and this was partially antagonized by COLV, consistent with the finding that *Col5a1* and *Col5a3* genes are targets of NICD and RBPJ (Fig. 2c, d and Extended Data Fig. 3d–g). Taken together, these results show that COLV, specifically, sustains primary muscle cells in a more stem-like PAX7⁺ state, indicating that COLV could potentially have a role in maintaining the quiescent niche.

To determine whether COLV produced by satellite cells is a functional component of the niche, we generated compound *Tg:Pax7-CreERT2;Col5a1^{flox/flox};R26^{mTmG}* (hereafter referred to as '*Col5a1* cKO') mice, in which COLV was depleted and simultaneously lineage-traced in GFP⁺ satellite cells^{4,14} (Fig. 3a and Extended Data Fig. 4a). Because the $\alpha 1$ -chain of COLV is present in all COLV isoforms (which are trimeric), *Col5a1* deletion produces cells completely lacking COLV protein¹⁴. Unexpectedly—given the general stability of collagens—targeted deletion of *Col5a1* resulted in upregulation of the differentiation marker genes *Myod* (also known as *Myod1*) and *Myog*, and a concomitant reduction of the quiescence marker *Calcr*, as well as *Pax7*, only 18 days after tamoxifen treatment (Fig. 3b). Mutant cells also showed ectopic expression of Myogenin (Fig. 3c), increased 5-bromo-2'-deoxyuridine (BrdU) incorporation (Fig. 3d) and showed a significant decline in PAX7⁺ satellite cells (Fig. 3e). The *Col5a1* cKO cells did not undergo apoptosis (data not shown), but fused to give rise to GFP-marked myofibres (Fig. 3f). Therefore, blocking de novo synthesis of COLV resulted in the spontaneous exit of satellite cells from quiescence, and differentiation, a phenotype reminiscent of Notch loss-of-function^{4,5}.

To investigate the role of *Col5a1* in regeneration, we examined the morphology of tibialis anterior muscles of *Col5a1* cKO mice, 18 days after cardiotoxin-mediated injury (Fig. 3a). Notably, mutant myogenic cells produced smaller nascent myofibres compared to control cells (Fig. 3g, h). Unexpectedly, fewer self-renewing PAX7⁺ cells were observed in the *Col5a1* cKO mice (Fig. 3i) in spite of abundant COLV in regenerating muscle (data not shown), probably produced by the resident fibroblasts, suggesting a cell-autonomous role for *Col5a1*. To investigate self-renewal in a more tractable system, we targeted COLV using short interfering RNA (siRNA) on isolated myofibres in culture in which satellite cells proliferate and self-renew on the myofibre.

¹Department of Developmental & Stem Cell Biology, Institut Pasteur, Paris, France. ²CNRS UMR 3738, Institut Pasteur, Paris, France. ³Sorbonne Universités, UPMC, University of Paris 06, Paris, France. ⁴UMR8203, CNRS, Gustave Roussy, Université Paris-Sud, Université Paris-Saclay, Villejuif, France. ⁵Département de Cancérologie de l'Enfant et de l'Adolescent, Gustave Roussy, Université Paris-Sud, Université Paris-Saclay, Villejuif, France. ⁶INSERM IMRB U955-E10, UPEC, ENVA, EFS, Créteil, France. ⁷Laboratory of Molecular and Cellular Physiology, Graduate School of Pharmaceutical Sciences, Osaka University, Osaka, Japan. ⁸Department of Molecular Pharmacology & Physiology, University of South Florida Morsani College of Medicine, Tampa, FL, USA. *e-mail: shahrugim.tajbakhsh@pasteur.fr; philippos.mourikis@inserm.fr

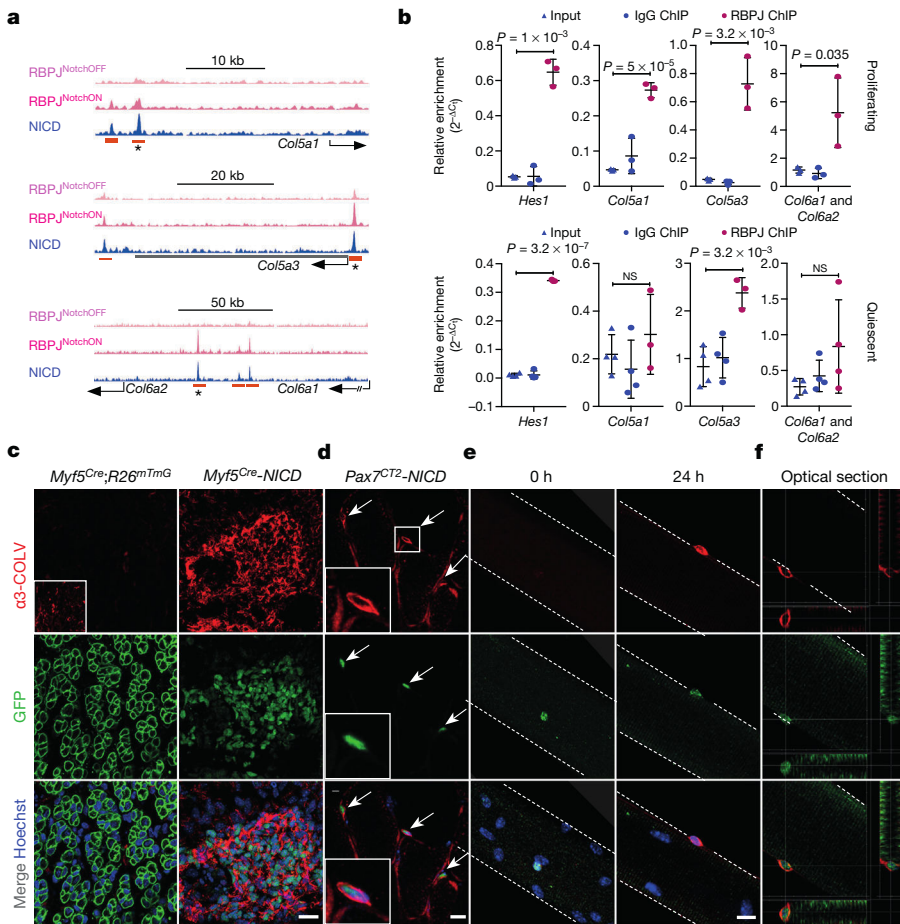


Fig. 1 | NICD and RBPJ regulate transcription of Col5 and Col6 genes by binding to distal regulatory elements. **a**, NICD and RBPJ ChIP-seq tracks from C2C12 cells indicating enhancers associated with the *Col5a1*, *Col5a3*, *Col6a1* and *Col6a2* loci. Orange rectangle, NICD and RBPJ enhancers; asterisk, enhancers used for luciferase assays (Extended Data Fig. 1c). **b**, Top, RBPJ ChIP in proliferating primary myogenic cells on Delta-like 1 ($n = 4$ ChIPs). Bottom, RBPJ ChIP in quiescent satellite cells, fixed before isolation²⁵ ($n = 3$ ChIPs). Data are mean \pm s.d.; two-sided unpaired t -test. **c**, Forelimb muscles of embryonic day (E)17.5 *Myf5*^{Cre}-NICD mouse fetuses show upregulation of COLV. Inset shows low α 3-COLV expression (higher exposure time). Note the membrane GFP-marked (mGFP) fibres in control and mononucleated NICD⁺PAX7⁺ cells in *Myf5*^{Cre}-NICD mice²⁶. **d**, Anti-GFP (satellite cells) and anti- α 3-COLV immunostaining on transverse sections of quiescent adult tibialis anterior muscles expressing NICD-IRES-GFP (*Pax7*^{CT2}-NICD). All GFP⁺ cells overexpressed COL5A3 (50 cells per mouse, $n = 3$ mice). **e**, Freshly fixed single myofibres from *Pax7*^{CT2}-NICD extensor digitorum longus muscles at 0 h (left) or after 24 h in culture (right), stained for GFP and α 3-COLV. **f**, Vertical and horizontal optical sections of myofibre presented in **e** from *Pax7*^{CT2}-NICD mice (24 h in culture) showing COLV surrounding NICD-GFP⁺ satellite cells. Scale bars, 50 μ m (**c**) and 10 μ m (**d-f**). In **c**, **d**, insets are shown at 2 \times magnification of main panels. NS, not significant.

Consistent with our in vivo observations, *Col5a1* knockdown by siRNAs resulted in a marked decrease in the number of the self-renewing PAX7⁺MYOD⁻ cells, compared to scramble control cells (Extended Data Fig. 4b, c). Of note, *Col5a3* siRNA phenocopied *Col5a1* siRNA, which demonstrates that the active triple helix contains α 3-COLV (Extended Data Fig. 4c).

Substrate rigidity and geometry have previously been demonstrated to control stem cell properties, including differentiation and self-renewal^{15,16}. However, we observed that COLV interacted with myogenic cells only when added in the medium, and not when present as a coating substrate (data not shown), which led us to speculate that it acted as a signalling molecule rather than a biomechanical modulator.

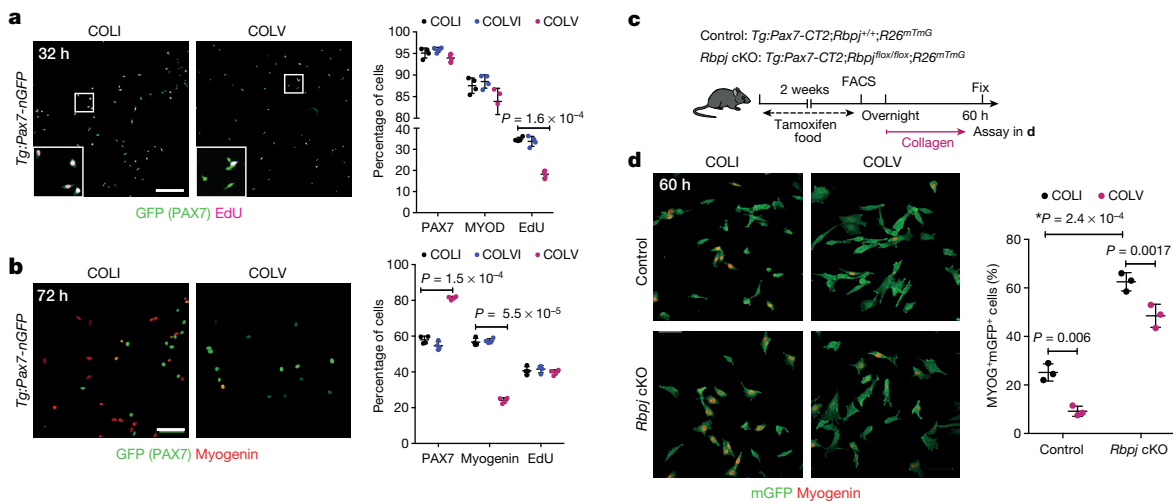


Fig. 2 | COLV delays proliferation and differentiation of satellite cells. **a**, EdU pulse (for 2 h) of freshly isolated satellite cells cultured for 32 h: COLI (35%), COLVI (34%) and COLV (18%) ($n = 4$ mice, ≥ 250 cells, 2 wells per condition). *Tg:Pax7-nGFP* mice express nuclear (n)GFP driven by *Pax7* regulatory elements. **b**, Immunostaining of freshly isolated satellite cells cultured for 72 h. PAX7: 58%, 55% and 81%; Myogenin: 56%, 57% and 24% for COLI, COLVI and COLV, respectively ($n = 4$ mice, ≥ 250

cells, 2 wells per condition). **c**, Experimental scheme for satellite cells plated overnight before collagen treatment. cKO, conditional knockout. **d**, Immunostainings of freshly isolated satellite cells incubated with collagens for 60 h ($n = 3$ mice, ≥ 200 cells, 2 wells per condition). Percentage (%) is presented over total GFP⁺ cells. Data are mean \pm s.d.; two-sided paired t -test; *, P value calculated by two-sided unpaired t -test. Scale bars, 50 μ m.

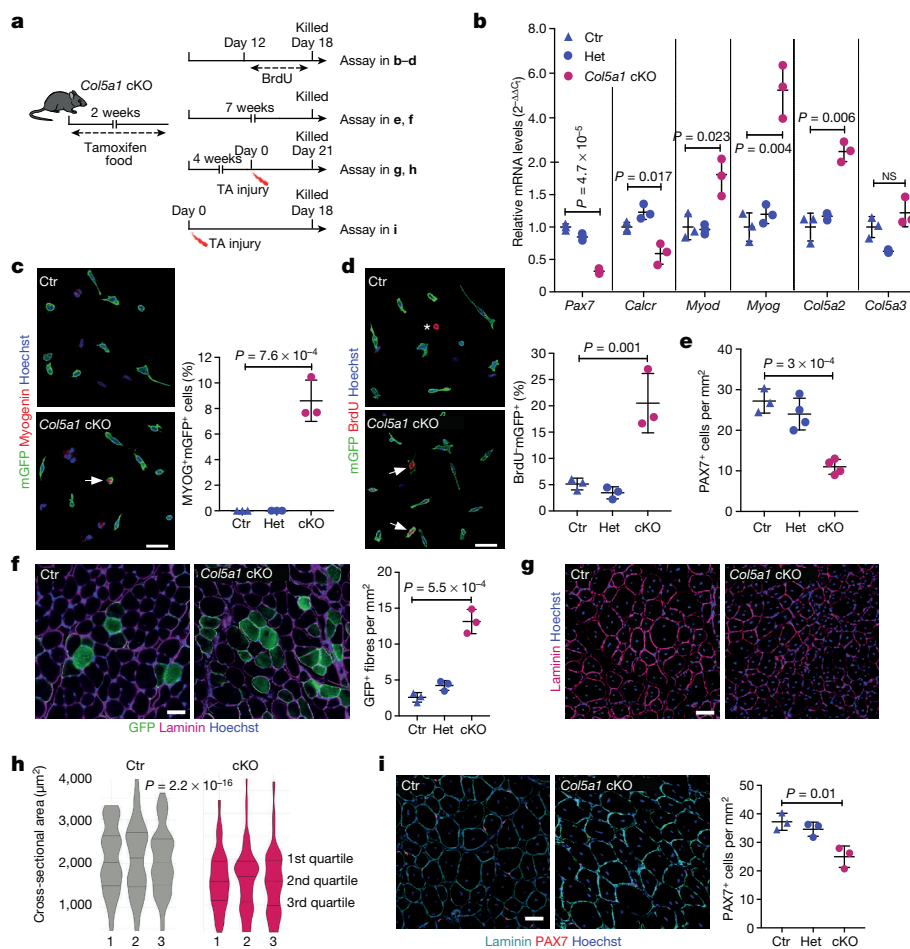


Fig. 3 | Satellite-cell-produced COLV is required in vivo for self-renewal and maintenance of quiescence.

a, Experimental schemes for control (*Tg:Pax7-CT2;Col5a1*^{+/+}; *R26*^{mTmG}), heterozygous (*Tg:Pax7-CT2;Col5a1*^{flox/+}; *R26*^{mTmG}) and conditional knockout (*Tg:Pax7-CT2;Col5a1*^{flox/flox}; *R26*^{mTmG}) mice. TA, tibialis anterior muscle. **b**, RT-qPCR of satellite cell (*Pax7*, *Calcr*) and differentiation (*Myod*, *Myog*) markers on *Col5a1*^{-/-} and control satellite cells isolated by fluorescence-activated cell sorting from resting muscle ($n = 3$ mice per genotype). Ctr, control; Het, heterozygous; cKO, conditional knockout. **c**, Representative images of membrane-bound GFP⁺ (mGFP) satellite cells from total muscle preparations from control and *Col5a1*-null mice plated for 12 h. Arrow, mGFP⁺Myogenin⁺ cell ($n = 3$ mice per genotype, ≥ 200 cells). **d**, mGFP⁺ satellite cells from total muscle preparations plated for 12 h. Asterisk, non-recombined BrdU⁺ cell; arrows, mGFP⁺BrdU⁺ cells ($n = 3$ mice per genotype, ≥ 250 cells). **e**, Satellite cell quantification in quiescent tibialis anterior muscles (seven

weeks after tamoxifen treatment) in control, heterozygous and *Col5a1* cKO mice ($n = 3$ (control) and 4 (heterozygous and cKO) tibialis anterior muscles per genotype). **f**, Immunostaining of sections from control and *Col5a1* cKO tibialis anterior muscles seven weeks after tamoxifen treatment ($n = 3$ mice per genotype). **g**, Immunostaining of sections from control and *Col5a1* cKO tibialis anterior muscles 21 days after injury ($n = 3$ mice per genotype). **h**, Muscle cross-sectional area distribution 21 days after injury (shown as violin plots) was significantly different in control versus *Col5a1* cKO tibialis anterior muscles, based on Kruskal-Wallis test ($n = 3$ mice per genotype, 1,000 fibres analysed per mouse). **i**, Immunostaining of sections 18 days after cardiotoxin injury of control and *Col5a1* cKO tibialis anterior muscles ($n = 3$ mice per genotype). Percentage (%) is presented over total GFP⁺ cells. Data are mean \pm s.d.; two-sided unpaired *t*-test. Scale bars, 50 μ m (**c**, **d**) and 100 μ m (**f**, **g**, **i**).

To identify the cell surface receptor of COLV on satellite cells, we used a myotube-formation assay (see Extended Data Fig. 3b), coupled to inhibitors against known collagen receptors, including Integrins and the RTK receptor DDR1^{17,18}, but these did not obstruct the anti-myogenic activity of COLV (Extended Data Fig. 5a). Because collagens have also previously been shown to bind G-protein coupled receptors (GPCRs)^{19,20}, we focused on Calcitonin receptor (CALCR), which is a GPCR critical for the maintenance of satellite cells²¹. Only cells that expressed CALCR showed decreased proliferation in the presence of COLV (Extended Data Fig. 5b), and *Calcr*^{-/-} satellite cells isolated from conditional knockout *Pax7*^{CreERT2}; *Calcr*^{flox/flox} mice failed to respond to COLV treatment (Fig. 4a and Extended Data Fig. 5c–e), demonstrating that CALCR constitutes an essential mediator of the COLV signal (Extended Data Fig. 4e). Accordingly, as CALCR is rapidly cleared after satellite cell activation²¹, COLV had no effect on cultured myogenic cells that had been activated in vivo (three days after injury; Extended Data Fig. 5f). However, we note that addition of COLV on freshly isolated satellite cells appeared to stabilize residual CALCR and

retain *Calcr* gene expression, thus allowing their prolonged interaction (Extended Data Fig. 5g–i). In summary, we show that CALCR is a critical mediator of the effect of COLV on maintaining quiescence and on the stemness properties of satellite cells.

To date, it has been assumed that CALCR in satellite cells is activated by circulating calcitonin peptide hormones, which are principally expressed by parafollicular thyroid cells; this points to systemic regulation of stem cell quiescence. Based on our findings, we reasoned that COLV serves as a local ligand for the CALCR receptor. Indeed, on-cell enzyme-linked immunosorbent assay experiments showed that COLV—but not COLI—selectively bound to cells expressing CALCR (Fig. 4b). Notably, this binding was functional as COLV—but not COLI—displayed rapid activation kinetics and upregulation of levels of intracellular cAMP, which is a downstream reporter of CALCR activation²² (Fig. 4c, d and Extended Data Fig. 6a). In vitro binding assays using the extracellular domain of CALCR did not result in robust interaction with COLV (data not shown). Therefore, we propose that binding of COLV to CALCR requires a specific configuration of the

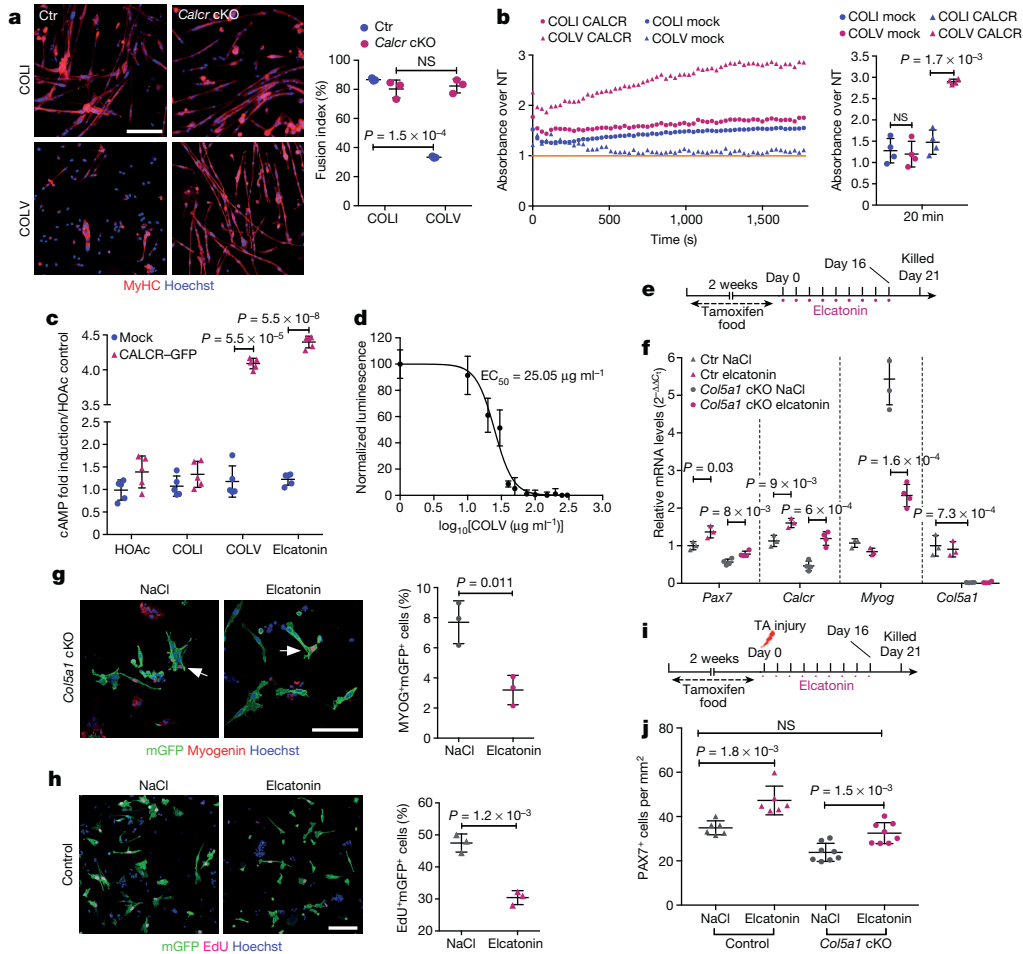


Fig. 4 | Interaction of COLV with satellite cells is mediated by CALCR.

a, Control (Ctr; *Pax7*^{CT2/+}; *Calcr*^{+/+}; *R26*^{stop-YFP}) and *Calcr*-deficient (*Calcr* cKO; *Pax7*^{CT2/+}; *Calcr*^{fllox/fllox}; *R26*^{stop-YFP}) satellite cells incubated for 10 days with COLI or COLV and immunostained for differentiation ($n = 3$ mice, ≥ 250 cells). **b**, Binding assay of COLV and CALCR by colorimetric on-cell enzyme-linked immunosorbent assay based on the measurements of horseradish peroxidase absorbance. Runs test P value < 0.0001 . Results presented as ratio of absorbance over non-treated cells (NT, orange line = 1) at 20 min of horseradish peroxidase development. **c**, cAMP measurements of *Calcr*-transduced C2C12 cells after three hours of treatment with acetic acid (HOAc), COLI, COLV or elcatonin. Graph represents fold cAMP induction over average of mock cells treated with HOAc ($n = 4$ assays). **d**, Dose–response curve of fold cAMP concentration in *Calcr*-transduced C2C12 cells treated for 3 h with increasing concentrations of COLV. Half-maximal effective concentration (EC_{50}) = $25.05 \mu\text{g ml}^{-1}$ ($n = 4$ independent assays). **e**, Experimental

scheme of tamoxifen and elcatonin administration to *Col5a1* cKO mice and their corresponding control mice. **f**, RT–qPCR of satellite cells (*Pax7*, *Calcr*) and differentiation (*Myog*) markers on *Col5a1* cKO mutant mice and control mice ($n = 3$ mice per condition) treated with elcatonin or saline. **g**, Representative images of mGFP⁺ satellite cells from total muscle preparations from *Col5a1*-null mice injected with saline or elcatonin, plated for 12 h. Arrows, mGFP⁺MYOG⁺ cells ($n = 3$ mice per condition, ≥ 200 cells). **h**, EdU (for 2 h) and mGFP staining of satellite cells from total muscle preparations from control mice treated with saline or elcatonin, plated for 36 h. Asterisk, mGFP⁺EdU⁺ cell ($n = 3$ mice per genotype, ≥ 400 cells). **i**, Experimental scheme of tamoxifen and elcatonin administration to control and *Col5a1* cKO mice. **j**, PAX7⁺ cells on tibialis anterior sections 21 days after injury in mice treated with saline or elcatonin ($n = 6$ mice for control and 8 mice for cKO, per treatment). Percentage (%) is presented over total GFP⁺ cells. Data are mean \pm s.d.; **a–c**, two-sided paired t -test; **f–j**, two-sided unpaired t -test. Scale bars, 25 μm .

receptor, possibly involving the extracellular loops or co-factors. Taken together, these data demonstrate that COLV physically and functionally interacts with CALCR.

In this study, we showed that blocking COLV production from satellite cells resulted in rupture of quiescence and impaired self-renewal in vivo. Combined with our ex vivo results, the similarity of these phenotypes to Notch and CALCR signalling abrogation points to a cell-autonomous Notch–COLV–CALCR axis that sustains muscle stem cells in their niche. Consistent with this notion, administration of the CALCR ligand elcatonin to control and *Col5a1*-null mice resulted in upregulation of the stem cell markers *Pax7* and *Calcr*, indicating that the injected ligand was readily delivered to the quiescent satellite cells (Fig. 4e, f). Notably, elcatonin mitigated the precocious *Myog* transcription and protein expression levels in *Col5a1* mutant cells (Fig. 4f, g). Elcatonin also prolonged the G0-to-S transition of control satellite cells exiting quiescence (Fig. 4h), which suggests that hyperactivation of

CALCR could drive cells into a deeper, more dormant-like quiescent state marked by higher *Pax7* expression²³. Therefore, CALCR activity appears to control quiescence quantitatively, shown by the loss of satellite cells in the absence of ligand COLV, and qualitatively, shown by the presence of dormant-like satellite cells upon hyperactivation. Elcatonin restored the number of PAX7⁺ satellite cells in regenerating *Col5a1* cKO muscles to wild-type levels (Fig. 4i, j), and in an ex vivo self-renewal reserve-cell model (Extended Data Fig. 6b, c). Therefore, we show that endogenous calcitonin levels are not sufficient to maintain *Col5a1*-null satellite cells, and that exogenous administration of a calcitonin derivative rescued the defects, probably via the activation of CALCR.

Here we describe a self-sustained signalling cascade orchestrated by the Notch pathway and propagated by the extracellular matrix of the immediate skeletal muscle stem cell niche (Extended Data Fig. 7). We propose that Notch acts as a sensor of the homeostatic environment

by reinforcing the niche with active COLV that provides cell-autonomous signals and maintains stem cell quiescence. Upon disruption of the niche and physical separation of the ligands, Notch signalling is sharply downregulated and stem cells exit quiescence^{4,24}. This halts further production of COLV and thus favours satellite cell activation, as shown in our model (Extended Data Fig. 7). It would be of interest to investigate whether the Notch–COLV–CALCR signalling cascade described here applies to stem cells in other tissues and organisms, in which an extracellular matrix protein produced by the stem cell can act as a local ligand for cell-autonomous stability of the niche through a GPCR. The regulatory mechanism that we identify provides a framework to construct a more complete view of the stem cell niche, and to manipulate stem cell behaviour in a therapeutic context.

Online content

Any Methods, including any statements of data availability and Nature Research reporting summaries, along with any additional references and Source Data files, are available in the online version of the paper at <https://doi.org/10.1038/s41586-018-0144-9>.

Received: 16 January 2017; Accepted: 6 April 2018;
Published online: 23 May 2018

- Raymond, K., Deugnier, M. A., Faraldo, M. M. & Glukhova, M. A. Adhesion within the stem cell niches. *Curr. Opin. Cell Biol.* **21**, 623–629 (2009).
- Moore, K. A. & Lemischka, I. R. Stem cells and their niches. *Science* **311**, 1880–1885 (2006).
- Watt, F. M. & Huck, W. T. Role of the extracellular matrix in regulating stem cell fate. *Nat. Rev. Mol. Cell Biol.* **14**, 467–473 (2013).
- Mourikis, P. et al. A critical requirement for notch signaling in maintenance of the quiescent skeletal muscle stem cell state. *Stem Cells* **30**, 243–252 (2012).
- Bjornson, C. R. et al. Notch signaling is necessary to maintain quiescence in adult muscle stem cells. *Stem Cells* **30**, 232–242 (2012).
- Rozo, M., Li, L. & Fan, C. M. Targeting $\beta 1$ -integrin signaling enhances regeneration in aged and dystrophic muscle in mice. *Nat. Med.* **22**, 889–896 (2016).
- Cheung, T. H. et al. Maintenance of muscle stem-cell quiescence by microRNA-489. *Nature* **482**, 524–528 (2012).
- Zismanov, V. et al. Phosphorylation of eIF2 α is a translational control mechanism regulating muscle stem cell quiescence and self-renewal. *Cell Stem Cell* **18**, 79–90 (2016).
- Chakkalakal, J. V., Jones, K. M., Basson, M. A. & Brack, A. S. The aged niche disrupts muscle stem cell quiescence. *Nature* **490**, 355–360 (2012).
- Shen, H. et al. The Notch coactivator, MAML1, functions as a novel coactivator for MEF2C-mediated transcription and is required for normal myogenesis. *Genes Dev.* **20**, 675–688 (2006).
- Buas, M. F., Kabak, S. & Kadesch, T. The Notch effector Hey1 associates with myogenic target genes to repress myogenesis. *J. Biol. Chem.* **285**, 1249–1258 (2010).
- Castel, D. et al. Dynamic binding of RBPJ is determined by Notch signaling status. *Genes Dev.* **27**, 1059–1071 (2013).
- Vasyutina, E. et al. RBP-J (Rbpsi) is essential to maintain muscle progenitor cells and to generate satellite cells. *Proc. Natl Acad. Sci. USA* **104**, 4443–4448 (2007).
- Sun, M. et al. Targeted deletion of collagen V in tendons and ligaments results in a classic Ehlers–Danlos syndrome joint phenotype. *Am. J. Pathol.* **185**, 1436–1447 (2015).
- Gilbert, P. M. et al. Substrate elasticity regulates skeletal muscle stem cell self-renewal in culture. *Science* **329**, 1078–1081 (2010).

- Yennek, S., Burute, M., Théry, M. & Tajbakhsh, S. Cell adhesion geometry regulates non-random DNA segregation and asymmetric cell fates in mouse skeletal muscle stem cells. *Cell Reports* **7**, 961–970 (2014).
- Leitinger, B. Transmembrane collagen receptors. *Annu. Rev. Cell Dev. Biol.* **27**, 265–290 (2011).
- Vogel, W., Gish, G. D., Alves, F. & Pawson, T. The discoidin domain receptor tyrosine kinases are activated by collagen. *Mol. Cell* **1**, 13–23 (1997).
- Paavola, K. J., Sidik, H., Zuchero, J. B., Eckart, M. & Talbot, W. S. Type IV collagen is an activating ligand for the adhesion G protein-coupled receptor GPR126. *Sci. Signal.* **7**, ra76 (2014).
- Luo, R. et al. G protein-coupled receptor 56 and collagen III, a receptor–ligand pair, regulates cortical development and lamination. *Proc. Natl Acad. Sci. USA* **108**, 12925–12930 (2011).
- Yamaguchi, M. et al. Calcitonin receptor signaling inhibits muscle stem cells from escaping the quiescent state and the niche. *Cell Reports* **13**, 302–314 (2015).
- Evans, B. N., Rosenblatt, M. I., Mnayer, L. O., Oliver, K. R. & Dickerson, I. M. CGRP-RCP, a novel protein required for signal transduction at calcitonin gene-related peptide and adrenomedullin receptors. *J. Biol. Chem.* **275**, 31438–31443 (2000).
- Rocheteau, P., Gayraud-Morel, B., Siegl-Cachedenier, I., Blasco, M. A. & Tajbakhsh, S. A subpopulation of adult skeletal muscle stem cells retains all template DNA strands after cell division. *Cell* **148**, 112–125 (2012).
- Mourikis, P. & Tajbakhsh, S. Distinct contextual roles for Notch signalling in skeletal muscle stem cells. *BMC Dev. Biol.* **14**, 2 (2014).
- Machado, L. et al. *In situ* fixation redefines quiescence and early activation of skeletal muscle stem cells. *Cell Reports* **21**, 1982–1993 (2017).
- Mourikis, P., Gopalakrishnan, S., Sambasivan, R. & Tajbakhsh, S. Cell-autonomous Notch activity maintains the temporal specification potential of skeletal muscle stem cells. *Development* **139**, 4536–4548 (2012).

Acknowledgements We thank H. Stunnenberg for the ChIP–seq and RNA sequencing data; D. Castro for the RBPJ ChIP protocol; D. Greenspan for the anti- $\alpha 3$ -COLV antibody and *Col5a3*-knockout muscle samples; C. Moali for the SPR assay; F. Auradé and the Protein Core Facility, Institut Curie, for the production of CalcR proteins; K. Ding for the 7rh DDR1 inhibitor; F. Ruggiero for suggesting the on-cell enzyme-linking immunosorbent assay experiment; and the Cytometry platforms of Institut Pasteur and IMRB, Inserm U955, Creteil. F.R. was funded by the Association Française contre les Myopathies via TRANSLAMUSCLE (PROJECT 19507), Agence Nationale pour la Recherche grant Satnet (ANR-15-CE13-0011-01) and RHU CARMMA (ANR-15-RHUS-0003). S.T. was funded by Institut Pasteur, Centre National pour la Recherche Scientifique and the Agence Nationale de la Recherche (Laboratoire d'Excellence Revive, Investissement d'Avenir; ANR-10-LABX-73) and the European Research Council (Advanced Research Grant 332893). M.B.B. was funded by the Doctoral School grant and Fondation pour la Recherche Médicale.

Reviewer information Nature thanks I. Conboy, G. Kardon and the other anonymous reviewer(s) for their contribution to the peer review of this work.

Author contributions M.B.B., S.T. and P.M. proposed the concept, designed experiments and wrote the manuscript, F.R. oversaw revisions, and S.T. funded most of the study. P.M. and D.C. conducted initial experiments on enhancer analysis. D.C. and L.M. performed and analysed ChIP experiments. M.B.B. performed the remaining experiments and, together with P.M., analysed the data. S.F. and D.E.B. provided mouse models.

Competing interests The authors declare no competing interests.

Additional information

Extended data is available for this paper at <https://doi.org/10.1038/s41586-018-0144-9>.

Supplementary information is available for this paper at <https://doi.org/10.1038/s41586-018-0144-9>.

Reprints and permissions information is available at <http://www.nature.com/reprints>.

Correspondence and requests for materials should be addressed to S.T. or P.M. **Publisher's note:** Springer Nature remains neutral with regard to jurisdictional claims in published maps and institutional affiliations.

METHODS

Mouse strains. Mouse lines used in this study have been described and provided by the corresponding laboratories: *Myf5^{Cre}* mice²⁷, *Pax7^{CreERT2}* mice²⁸ (used to recombine *R26^{stop-NICD}* allele), *R26^{stop-NICD-nGFP}* mice²⁹, *R26^{mTmG}* mice³⁰ (ROSA 26 gene trap with membrane-Tomato floxed/membrane-GFP), *Rbpj^{fllox/fllox}* mice³¹, *Pax7^{CT2/4}*; *Calcrl^{fllox/fllox}*; *R26^{stop-YFP/stop-YFP}* mice²¹ (triple mutant mice provided by S.F.) and *Col5a1^{fllox/fllox}* mice³². *Tg:Pax7-CreERT2* (used to recombine *Rbpj* and *Col5a1*) and *Tg:Pax7-nGFP* lines have previously been described^{4,33}. All adult mice analysed were between 8 and 12 weeks old. Animals were handled according to national and European community guidelines, and protocols were approved by the ethics committee at Institut Pasteur and the French Ministry.

Muscle injury, tamoxifen, BrdU and elcatonin administration. For muscle injury, *Tg:Pax7-CreERT2;Col5a1^{fllox/fllox};R26^{mTmG}* mice and their corresponding controls were anaesthetized with 0.5% Imalgene/2% Rompun and the tibialis anterior muscle was injected with 50 μ l of cardiotoxin (10 μ M; Latoxan). *Tg:Pax7-CreERT2;Rbpj^{fllox/fllox};R26^{mTmG}* mice and their corresponding controls were injected intraperitoneally with tamoxifen three times (250 to 300 μ l, 20mg/ml; Sigma T5648; diluted in sunflower seed oil/5% ethanol). *Pax7^{CreERT2};Calcrl^{fllox/fllox};R26^{stop-YFP}* mice and their corresponding controls were injected intraperitoneally with tamoxifen twice (1 mg per 5 g of body weight) and euthanized two weeks later. *Pax7^{CreERT2};R26^{stop-NICD-ires-nGFP}* and *Tg:Pax7-CreERT2;Col5a1^{fllox/fllox};R26^{mTmG}* mice and their corresponding controls were fed a diet containing tamoxifen for one and two weeks, respectively (Envigo, TD55125). Six days before being euthanized, *Tg:Pax7-CreERT2;Col5a1^{fllox/fllox};R26^{mTmG}* mice and their corresponding controls were given the thymidine analogue BrdU (0.5 mg/ml, #B5002; Sigma) in the drinking water supplemented with sucrose (25 mg/ml). Elcatonin (2.5 ng per g of mouse, final concentration in 0.9% NaCl; Mybiosource, MBS143228) was injected subcutaneously eight times, every other day. Comparisons were done between age-matched littermates using 8–12-week-old mice.

Muscle enzymatic dissociation and stem cell isolation. Adult and fetal limb muscles were dissected, minced and incubated with a mix of Dispase II (Roche, 04942078001) 3 U/ml, collagenase A (Roche, 11088793001) 100 μ g/ml and DNase I (Roche, 11284932001) 10 mg/ml in Hank's Balanced Salt Solution (Gibco) supplemented with 1% penicillin–streptomycin (PS; Gibco) at 37 °C at 60 r.p.m. in a shaking water bath for 2 h. The muscle suspension was successively filtered through 100- μ m and 70- μ m cell strainers (Miltenyi, 130-098-463 and 130-098-462) and then spun at 50g for 10 min at 4 °C to remove large tissue fragments. The supernatant was collected and washed twice by centrifugation at 600g for 15 min at 4 °C. Before fluorescence-activated cell sorting (FACS), the final pellet was resuspended in cold Dulbecco's modified Eagle's medium (DMEM) and 1% PS supplemented with 2% fetal bovine serum (FBS), and the cell suspension was filtered through a 40- μ m strainer. Satellite cells were sorted with Aria III (BD Biosciences) using either the GFP (*Tg:Pax7-nGFP* or *Tg:Pax-CreERT2;Rbpj^{fllox/fllox};R26^{mTmG}* or *Tg:Pax7-CreERT2;Col5a1^{fllox/fllox};R26^{mTmG}*) or the YFP (*Pax7^{CT2};Calcrl^{fllox/fllox};R26^{stop-YFP}*) cell markers. Isolated, mononuclear cells were collected in DMEM/1% PS/2% FBS. Enzymatically dissociated muscle was also plated directly without FACS on Matrigel-coated dishes (Corning, 354248; 30 min at 37 °C), and fixed 12 h later with 4% paraformaldehyde (PFA)/PBS. Cells were immunostained following the protocol described above.

Chromatin immunoprecipitation. Cultured myoblasts. Satellite cells were isolated from adult *Tg:Pax7-nGFP* mice and plated on dishes, coated with Delta-like 1, for 72 h to maintain active Notch signalling, as previously described^{4,34}. Cells were then processed for ChIP using a dual cross-linking protocol³⁵, with slight modifications. In brief, cells were fixed on the dish with 2 mM di(*N*-succinimidyl) glutarate (Sigma, 80424) in PBS for 45 min at room temperature. After two washes with PBS, cells were re-fixed with 1% formaldehyde/PBS for 10 min at room temperature, before quenching the reaction with 1/20 volume of 2.5 M glycine for 5 min at room temperature. The cells were then collected with a cell scraper in PBS supplemented with 1% BSA and protease inhibitors (Roche, 11697498001), and collected by spinning. Cell lysis and chromatin isolation were done using the Ideal ChIP-seq kit for histones (Diagenode, C01010051). Chromatin was sheared using a Bioruptor Pico (Diagenode B01060001) with 10 cycles of 30 s on/off sonication. The samples were prepared in triplicates from different plates. Primary myogenic cells (2×10^6) were used per ChIP and 2×10^4 cells were used per input. The immunoprecipitations were performed following the manufacturer's guidelines using 6 μ l of anti-RBPJ antibody (Cell Signalling, #5313) or 1.5 μ l of rabbit control IgG antibody (Diagenode, C15410206) in a final volume of 300 μ l per ChIP. The purification of the immunoprecipitated DNA was performed using DiaPure columns (Diagenode, C03040001). RT-qPCR was performed using FastStart Universal SYBR Green Master mix (Roche, 04913914001) and analysis was performed using the $2^{-\Delta\Delta C_t}$ method³⁶ normalized to the Neg16 region.

Quiescent satellite cells. Satellite cells were isolated from adult *Tg:Pax7-nGFP* mice using in situ fixation to preserve Notch signalling from dissociation-induced downregulation²⁵. Cells were fixed as above in 2 mM di(*N*-succinimidyl)

glutarate for 45 min, followed by 10 min with 1% formaldehyde at room temperature. Cell lysis and chromatin isolation were performed using Auto-TrueMicrochip kit (Diagenode, C01010140). Chromatin was sheared as above with 10 cycles of 30 s on/off sonication using a Bioruptor Pico. Two hundred thousand cells were used per ChIP and 2×10^3 per input and IPs were performed using 2 μ l of anti-RBPJ antibody (Cell Signalling, 5313) or 0.5 μ l of rabbit control IgG antibody following the manufacturer's guidelines. Immunoprecipitated chromatin preparations and input were purified using the Auto IPure kit v2 (Diagenode). RT-qPCR was performed using FastStart Universal SYBR Green Master mix (Roche, 04913914001) and analysis was performed using the $2^{-\Delta\Delta C_t}$ method³⁶ normalized to the Neg16 region. Primers used for ChIP-qPCR are listed in Supplementary Table 1.

Cell culture and collagen incubation. Satellite cells isolated by FACS were plated at 3×10^3 cells per cm^2 on ibi-treated μ -slides (Ibidi, 80826) pre-coated with 0.1% gelatin for 2 h at 37 °C. Cells were cultured in satellite cell growth medium containing DMEM (Gibco) supplemented with F12 (50:50; Gibco), 1% PS, 20% FBS (Gibco) and 2% Ultrosor (Pall; 15950-017) at 37 °C, 3% O₂, 5% CO₂ for the indicated time. Twelve hours after plating, collagens (COLI rat tail, BD Biosciences, 354236; COLV human placenta, Sigma, C3657; COLVI human placenta, AbD Serotec 2150-0230) resuspended in HOAc acid at 1 mg/ml, were added to the culture medium at a final concentration of 50 μ g/ml and cells were fixed with 4% PFA for 10 min at room temperature. To assess proliferation, cells were pulsed with the thymidine analogue EdU, 1×10^{-6} M at 2 h before fixation (ThermoFisher Click-iT Plus EdU kit, C10640). Inhibitors used: Obtustatin (Integrin α 1 β 1, Tocris, 4664, 100 nM), TC-I 15 (Integrin α 2 β 1 Tocris, 4527, 100 μ M), RGDS peptide (all Integrins, Tocris, 3498, 100 μ M), 7rh³⁷ (DDR1, a gift from K. Ding, 20 nM).

Muscle fixation and histological analysis. Embryo forelimbs were fixed in 4% PFA/0.1% Triton for 2 h, washed overnight with $1 \times$ PBS, immersed in 20% sucrose/PBS overnight, embedded in OCT, frozen in liquid nitrogen and sectioned transversely at 12–14 μ m. Isolated tibialis anterior muscles were immediately frozen in liquid-nitrogen-cooled isopentane and sectioned transversely at 8 μ m. For PAX7 staining on adult tibialis anterior muscle, sections were post-fixed with 4%PFA, 15 min at room temperature. After 3 washes with $1 \times$ PBS, antigen retrieval was performed by incubating sections in boiling 10 mM citrate buffer pH 6 for 10 min. Sections were then blocked, permeabilized and incubated with primary and secondary antibodies as described in 'Immunostaining on cells, sections and myofibres'.

Single myofibre isolation and siRNA transfection. Single myofibres were isolated from extensor digitorum longus muscles following the previously described protocol³⁸. In brief, extensor digitorum longus muscles were dissected and incubated in 0.1% w/v collagenase (Sigma, C0130)/DMEM for 1 h in a 37 °C shaking water bath at 40 r.p.m. Following enzymatic digestion, mechanical dissociation was performed to release individual myofibres that were then transferred to serum-coated Petri dishes. Single myofibres were transfected with *Col5a1* siRNA, *Col5a3* siRNA (Dharmacon SMARTpool *Col5a1* (12831) L-044167-01 and *Col5a3* (53867) L-048934-01-0005) or scramble siRNA (Dharmacon ON-TARGETplus Non-targeting siRNA #2 D-001810-02-05) at a final concentration of 200 nM, using Lipofectamine 2000 (ThermoFisher, 11668) in Opti-MEM (Gibco). Four hours after transfection, 6 volumes of fresh satellite cell growth medium were added and fibres were cultured for 72 h at 37 °C, 3% O₂. Myofibres were fixed for 15 min in 4% PFA before immunostaining for proliferation, differentiation and self-renewal markers³⁹.

Immunostaining on cells, sections and myofibres. Following fixation, cells and myofibres were washed three times with PBS, then permeabilized and blocked at the same time in buffer containing 0.25% Triton X-100 (Sigma), 10% goat serum (Gibco) for 30 min at room temperature. For BrdU immunostaining, cells were unmasked with DNaseI (1,000 U/ml, Roche, 04536282001) for 30 min at 37 °C. Cells and fibres were then incubated with primary antibodies (Supplementary Table 2) for 4 h at room temperature. Samples were washed with $1 \times$ PBS three times and incubated with Alexa-conjugated secondary antibodies (Life Technologies, 1/1,000) and Hoechst 33342 (Life Technologies, 1/5,000) for 45 min at room temperature. EdU staining was chemically revealed using the Click-iT Plus kit according to manufacturer's recommendations (Life Technologies, C10640). For collagen staining, the myofibres and the muscle sections were incubated with 0.1% Triton X-100 for 30 min at room temperature. Myofibres and sections were then washed 3×10 min and incubated with 10% goat serum in PBS for 30 min. After one wash, samples were incubated with primary antibodies and secondary antibodies as described in Supplementary Table 2. Confocal images were acquired with a Leica SPE microscope and Leica Application Suite or with Zeiss LSM 700 microscope and Zen Blue 2.0 software. Three-dimensional images were reconstructed from confocal Z-stacks using Imaris software. The Section view function was used to inspect the environment of the satellite cells by showing the cut in the x, y and z axes.

Reserve cell cultures. Enzymatically dissociated muscles were plated in gelatin-coated dishes (1/30 of total mouse muscles per cm^2) in the satellite cell growth

medium described above. When myotube formation was detected (day 7 to 10), recombination was induced by addition of 4-hydroxytamoxifen (4-OHT; Sigma, H6278) at final concentration of 1 μ M every other day. Seven days later, 4-OHT-containing medium was replaced every other day with fresh medium containing elcatonin (0.1 U/ml), for an additional 10 days. To assess proliferation, cells were pulsed with 1×10^{-6} M EdU for 6 h before fixation (10 min, 4% PFA). Reserve cells were defined by immunofluorescence as PAX7⁺EdU⁻ cells³⁹. For each medium change, only half of the conditioned medium was removed and replaced by an equal volume of fresh medium.

Construction of luciferase reporters and luciferase assays. For the generation of luciferase reporters, candidate enhancers of *Col5a1*, *Col5a3*, *Col6a1* and *Col6a2* (a shared enhancer), and *Hes1* were amplified by PCR from genomic DNA of C2C12 cells. The enhancers were then cloned into the firefly-luciferase pGL3-Basic vector (Promega, E1751) upstream of a minimal thymidine kinase promoter. The sequences of enhancers are listed in Supplementary Table 3. Transfected cells (Lipofectamine LTX, Life Technologies, 15338030) were lysed and luciferase signal was scored using the Dual-Luciferase Reporter Assay System (Promega, E1910). For normalization, *Renilla* luciferase (pCMV-Renilla) was transfected at 1:20 ratio relative to firefly-luciferase constructs.

RNA isolation and RT-qPCR. Total RNA was extracted from satellite cells isolated by FACS using QIAGEN mini RNeasy kit and reverse transcribed using SuperScript III (Invitrogen, 18080093), according to manufacturer's instructions. RT-qPCR was performed using FastStart Universal SYBR Green Master mix (Roche, 04913914001) and analysis was performed employing the $2^{-\Delta\Delta C_t}$ method and using the average of the control values as a reference³⁶. Specific forward and reverse primers used in this study are listed in Supplementary Table 1.

Stable cell line manipulations. The mouse myoblast cell line C2C12 was cultured in DMEM/ 20% FBS/ 1% PS at 37°C, 5% CO₂.

Notch activation. Notch activation was achieved by plating cells on DLL1-coated dishes or by doxycycline-inducible Notch constructs, as previously described¹².

Calcr retrovirus preparation and transduction. Calcitonin receptor C1a-type (pMXs-Calcr-C1a-IRES-GFP) and mock control (pMXs-IRES-GFP) retrovirus vectors were prepared as previously described^{21,40}. In brief, 48 h after transfection of Platinum-E cells the supernatant was recovered and used to transduce C2C12 cells. Two days later stably labelled GFP⁺ C2C12 cells were isolated by FACS. All stable cell lines used in this study are negative for mycoplasma contamination.

Quantification of cAMP. Transduced mock (IRES-GFP) and *Calcr* (Calcr-C1a-IRES-GFP) C2C12 cells were isolated by FACS based on GFP expression and seeded on 0.1% gelatin-coated, white culture 96-well plates (Falcon, 353296) at 3×10^3 cells per well. After overnight culture, the cells were incubated with the complete induction medium containing DMEM/1% PS/500 μ M isobutyl-1-methylxanthine (Sigma, 17018)/100 μ M 4-(3-butoxy-4-methoxy-benzyl)imidazolidone (Ro 20-1724 Sigma, B8279)/MgCl₂ 40 mM, collagen, solvent HOAc or elcatonin (0.1 U/ml) for 3 h. The amount of intracellular cAMP was measured using cAMP-Glo Max Assay (Promega, V1681) following the manufacturer's protocol. Luminescence was quantified with FLUOstar OPTIMA (BMG Labtech). The EC₅₀ value was determined with GraphPad Prism software using a sigmoid dose-response curve (variable slope).

Biotinylation of collagens. Commercial collagen proteins (COLI rat tail, BD Biosciences, 354236; COLV human placenta, Sigma, C3657) were biotinylated using the Pierce EZ-Link Biotinylation Kit, with slight modifications. In brief, 20 μ l of 1 M HEPES was added to 0.5 ml of 1 mg/ml collagen dissolved in 0.5 M HOAc. Then, 20 μ l of 100 mM biotin reagent were added and incubated at room temperature for 1.5 h. Biotinylated collagens were next dialysed in 25 mM HEPES, 2.5 M CaCl₂, 125 mM NaCl, 0.005% Tween (Slide-A-Lyze MINI Dialysis Device, Thermo Fisher 88401) overnight at 4°C.

On-cell enzyme-linked immunosorbent assay. Transduced mock and *Calcr* C2C12 cells were seeded on a clear-bottom 96-well plate (TPP, 92096) at a density

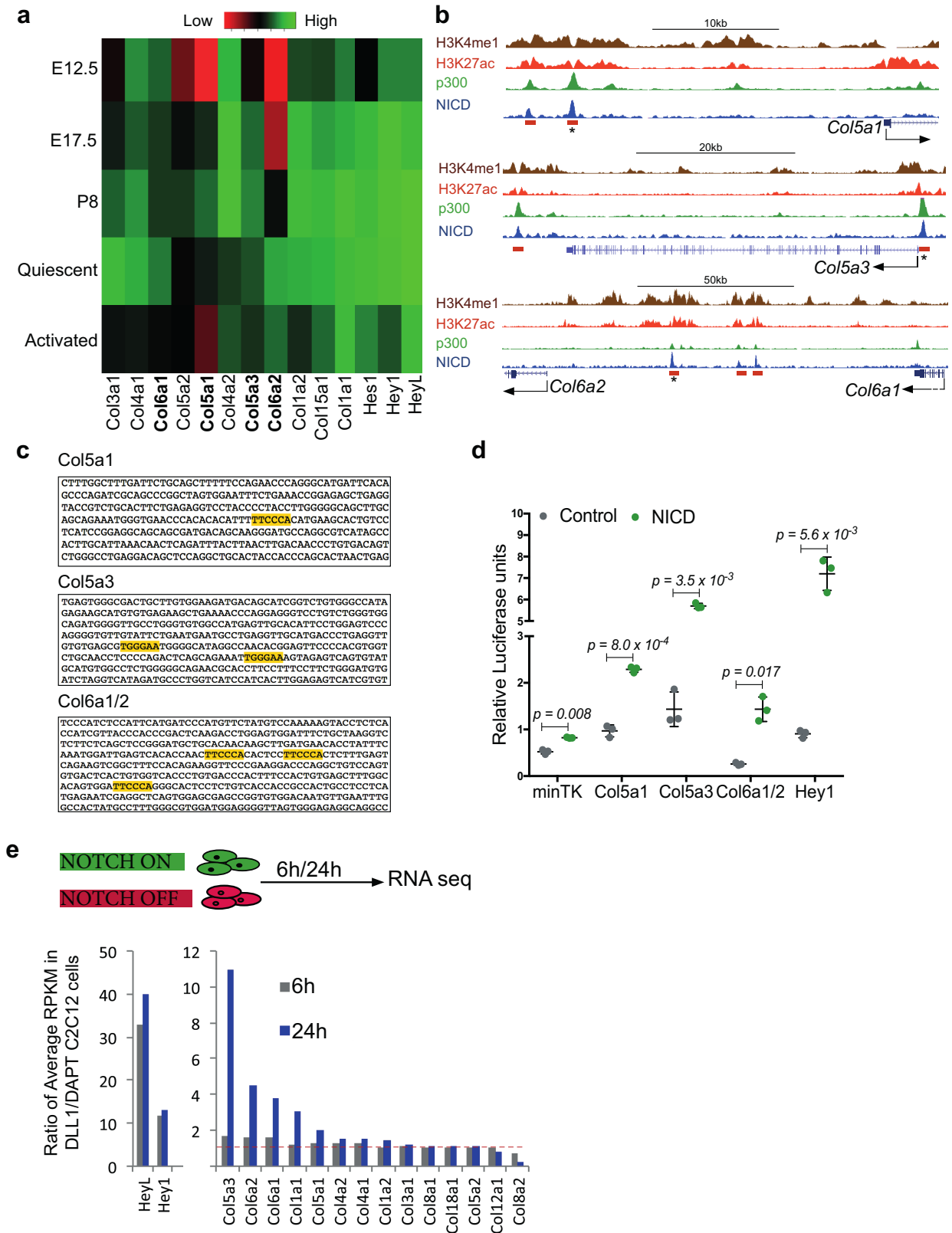
of 3×10^3 cells per well. After overnight culture, cells were treated with 50 μ g/ml of biotinylated collagens for 2 h and fixed with 4% PFA/PBS for 15 min. After $3 \times$ PBS washes, cells were blocked with a solution containing 10% goat serum, 2% BSA, PBS for 1 h at room temperature, washed and incubated for 1 h at room temperature with goat anti-mouse biotin-HRP antibody (Jackson, 1/1000e, 115-035-003). After $3 \times$ PBS washes, the HRP signal was developed by addition of 3,3',5,5'-tetramethylbenzidine (1-Step Ultra TMB-ELISA, Sigma, 34028). HRP substrate and absorbance at 650 nm was measured once every 30 s for 30 min with FLUOstar OPTIMA (BMG Labtech). The signal was normalized to the background signal (no secondary antibody) and to the number of cells assessed by Janus green staining (Abcam, ab111622).

Statistical analysis. No statistical methods were used to predetermine sample size. The investigators were not blinded to allocation during experiments and outcome assessment. No animal has been excluded from analysis and no randomization method has been applied in this study. For comparison between two groups, two-tailed paired and unpaired Student's *t*-tests were performed to calculate *P* values and to determine statistically significant differences (see legends of Figs. 1–4). Additional specific statistical tests are detailed in legends of Figs. 1–4. All experiments have been done twice with the same results. All statistical analyses were performed with Excel software or GraphPad Prism software; Kruskal–Wallis test was performed in R.

Reporting summary. Further information on experimental design is available in the Nature Research Reporting Summary linked to this paper.

Data availability. All data that support the findings of this study are available from the corresponding authors upon request.

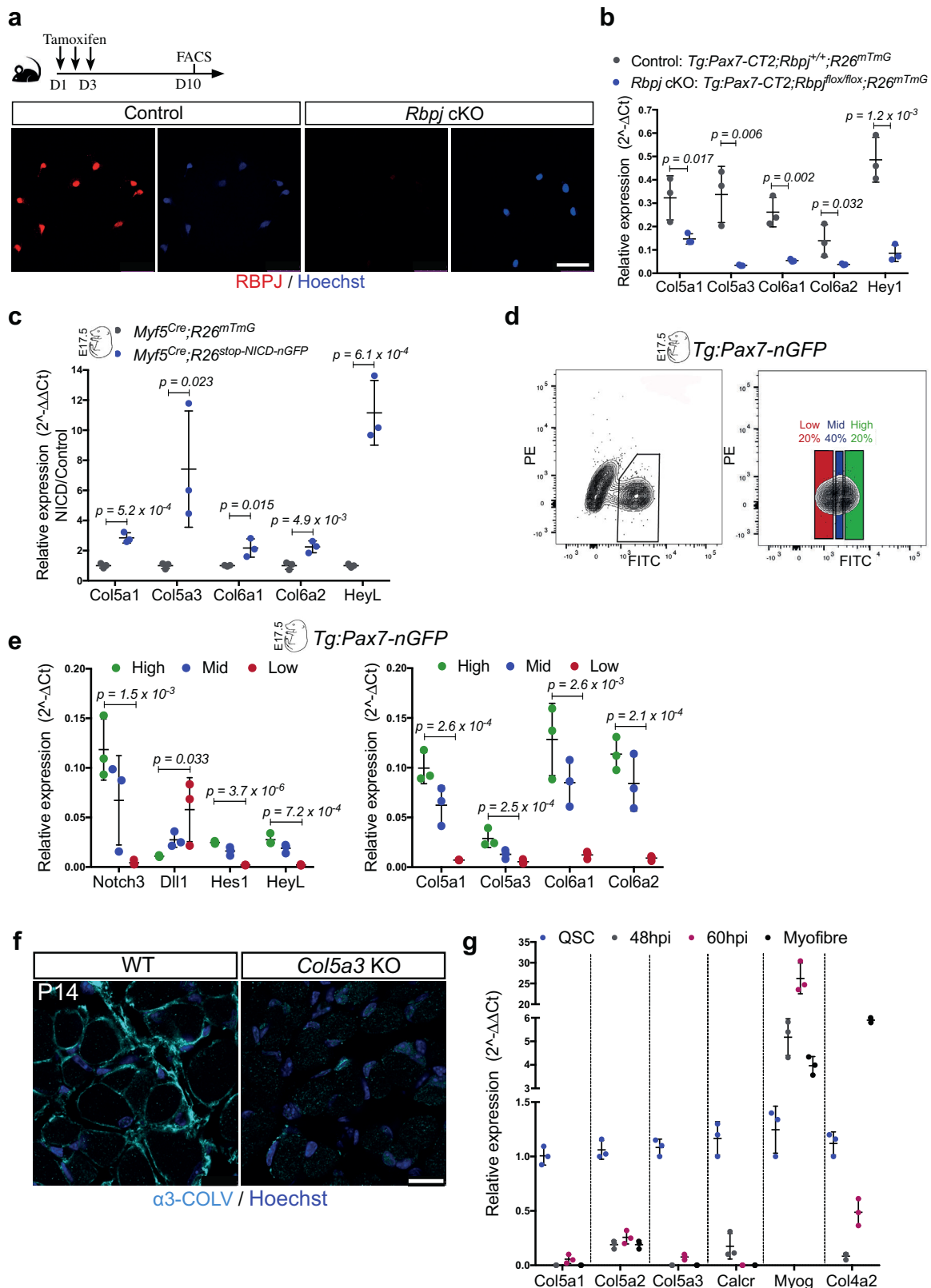
- Haldar, M., Karan, G., Tvrđik, P. & Capecchi, M. R. Two cell lineages, *myf5* and *myf5*-independent, participate in mouse skeletal myogenesis. *Dev. Cell* **14**, 437–445 (2008).
- Murphy, M. M., Lawson, J. A., Mathew, S. J., Hutcheson, D. A. & Kardon, G. Satellite cells, connective tissue fibroblasts and their interactions are crucial for muscle regeneration. *Development* **138**, 3625–3637 (2011).
- Murtaugh, L. C., Stanger, B. Z., Kwan, K. M. & Melton, D. A. Notch signaling controls multiple steps of pancreatic differentiation. *Proc. Natl Acad. Sci. USA* **100**, 14920–14925 (2003).
- Muzumdar, M. D., Tasic, B., Miyamichi, K., Li, L. & Luo, L. A global double-fluorescent Cre reporter mouse. *Genesis* **45**, 593–605 (2007).
- Han, H. et al. Inducible gene knockout of transcription factor recombination signal binding protein-J reveals its essential role in T versus B lineage decision. *Int. Immunol.* **14**, 637–645 (2002).
- Sun, M. et al. Collagen V is a dominant regulator of collagen fibrillogenesis: dysfunction regulation of structure and function in a corneal-stroma-specific *Col5a1*-null mouse model. *J. Cell Sci.* **124**, 4096–4105 (2011).
- Sambasivan, R. et al. Distinct regulatory cascades govern extraocular and pharyngeal arch muscle progenitor cell fates. *Dev. Cell* **16**, 810–821 (2009).
- Hicks, C. et al. A secreted Delta1-Fc fusion protein functions both as an activator and inhibitor of Notch1 signaling. *J. Neurosci. Res.* **68**, 655–667 (2002).
- Vasconcelos, F. F. et al. MyT1 counteracts the neural progenitor program to promote vertebrate neurogenesis. *Cell Reports* **17**, 469–483 (2016).
- Livak, K. J. & Schmittgen, T. D. Analysis of relative gene expression data using real-time quantitative PCR and the $2^{-\Delta\Delta C_t}$ method. *Methods* **25**, 402–408 (2001).
- Gao, M. et al. Discovery and optimization of 3-(2-(Pyrazolo[1,5-a]pyrimidin-6-yl)ethynyl)benzamides as novel selective and orally bioavailable discoidin domain receptor 1 (DDR1) inhibitors. *J. Med. Chem.* **56**, 3281–3295 (2013).
- Shinin, V., Gayraud-Morel, B., Gomes, D. & Tajbakhsh, S. Asymmetric division and cosegregation of template DNA strands in adult muscle satellite cells. *Nat. Cell Biol.* **8**, 677–687 (2006).
- Yoshida, N., Yoshida, S., Koishi, K., Masuda, K. & Nabeshima, Y. Cell heterogeneity upon myogenic differentiation: down-regulation of MyoD and Myf-5 generates 'reserve cells'. *J. Cell Sci.* **111**, 769–779 (1998).
- Morita, S., Kojima, T. & Kitamura, T. Plat-E: an efficient and stable system for transient packaging of retroviruses. *Gene Ther.* **7**, 1063–1066 (2000).



Extended Data Fig. 1 | See next page for caption.

Extended Data Fig. 1 | Identification of NICD/RBPJ-bound enhancers and response to activation of Notch signalling. **a**, Gene expression microarray data show that satellite cells express a specific subset of collagen types, which include the fibrillar COLI (*Col1a1* and *Col1a2*), COLIII (*Col3a1*, possibly as $(\alpha1(\text{III}))_3$ homodimer) and COLV (*Col5a1*, *Col5a2* and *Col5a3*) and the non-fibrillar COLIV (*Col4a1* and *Col4a2*), COLVI (*Col6a1* and *Col6a2*) and COLXV (*Col15a1*, possibly as $(\alpha1(\text{XV}))_3$ homodimer). Data are shown as a heat map of normalized collagen transcripts expressed at different developmental time points (E12.5, E17.5 and post-natal day (P)8; *Tg-Pax7-nGFP*, Gene Expression Omnibus (GEO) accession number GSE52192), quiescent and post-injury ($t = 60$ h after BaCl_2 injury). **b**, ChIP-seq tracks indicating NICD/RBPJ-occupied enhancers, associated with mouse *Col5a1*, *Col5a3*, *Col6a1* and *Col6a2* loci. H3K4me1, H3K27ac, p300 and NICD are shown. Orange rectangles indicate RBPJ binding positions and asterisks indicate the enhancers used for transcriptional activity assays in **c**. **c**, Core sequences of the selected NICD/RBPJ-bound enhancers (asterisked orange rectangle in

Fig. 1a and in **b**). The RBPJ consensus binding motif is highlighted in yellow. **d**, Transcriptional response of isolated enhancers to activation of Notch signalling in C2C12 cells. Firefly luciferase signal was measured in cells with doxycycline-inducible expressed human Notch1-GFP (NICD) and GFP control cells treated with (2S)-N-[(3,5-difluorophenyl)acetyl]-L-alanyl-2-phenylglycine 1,1-dimethylethyl ester (DAPT) and were normalized to internal control (pCMV-*Renilla*). Data are expressed as relative luminescence units ($n = 3$ independent experiments). Data are mean \pm s.d.; two-sided paired *t*-test. **e**, Expression measurements, based on RNA sequencing, of collagen genes in myogenic C2C12 cells, with active (treated with Delta-like 1) or inhibited (treated with DAPT) Notch signalling for 6 or 24 h (data available at GEO, accession number GSE37184). Data are shown as Delta-like 1-to-DAPT ratios of average reads per kilobase of exon model per million mapped reads (RPKMs). Genes with low expression (RPKM < 2) were eliminated. *HeyL* and *Hey1* transcripts indicate Notch pathway activation. Red line designates no change (ratio = 1).

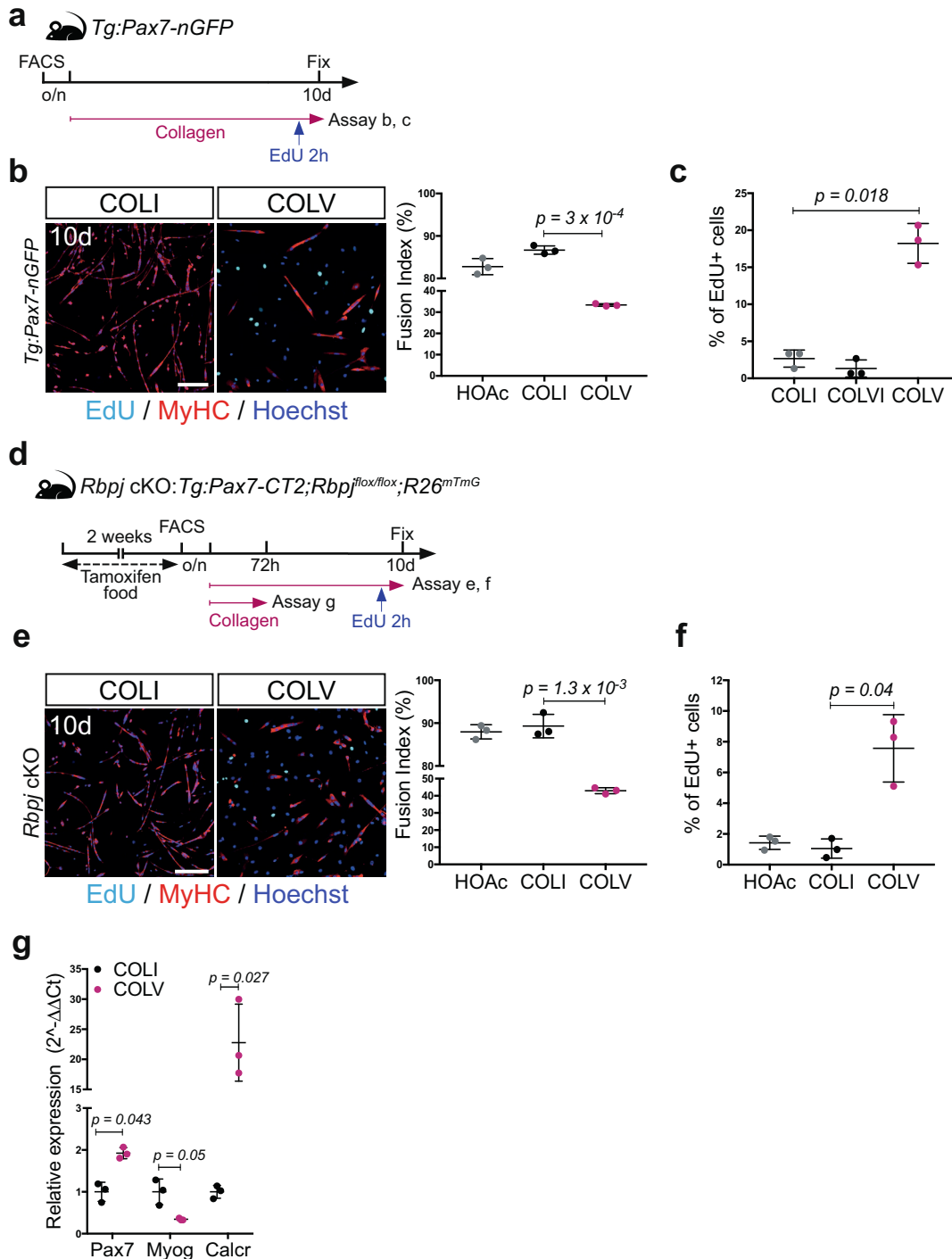


Extended Data Fig. 2 | See next page for caption.

Extended Data Fig. 2 | Notch signalling regulates *Col5* and *Col6* expression in vivo.

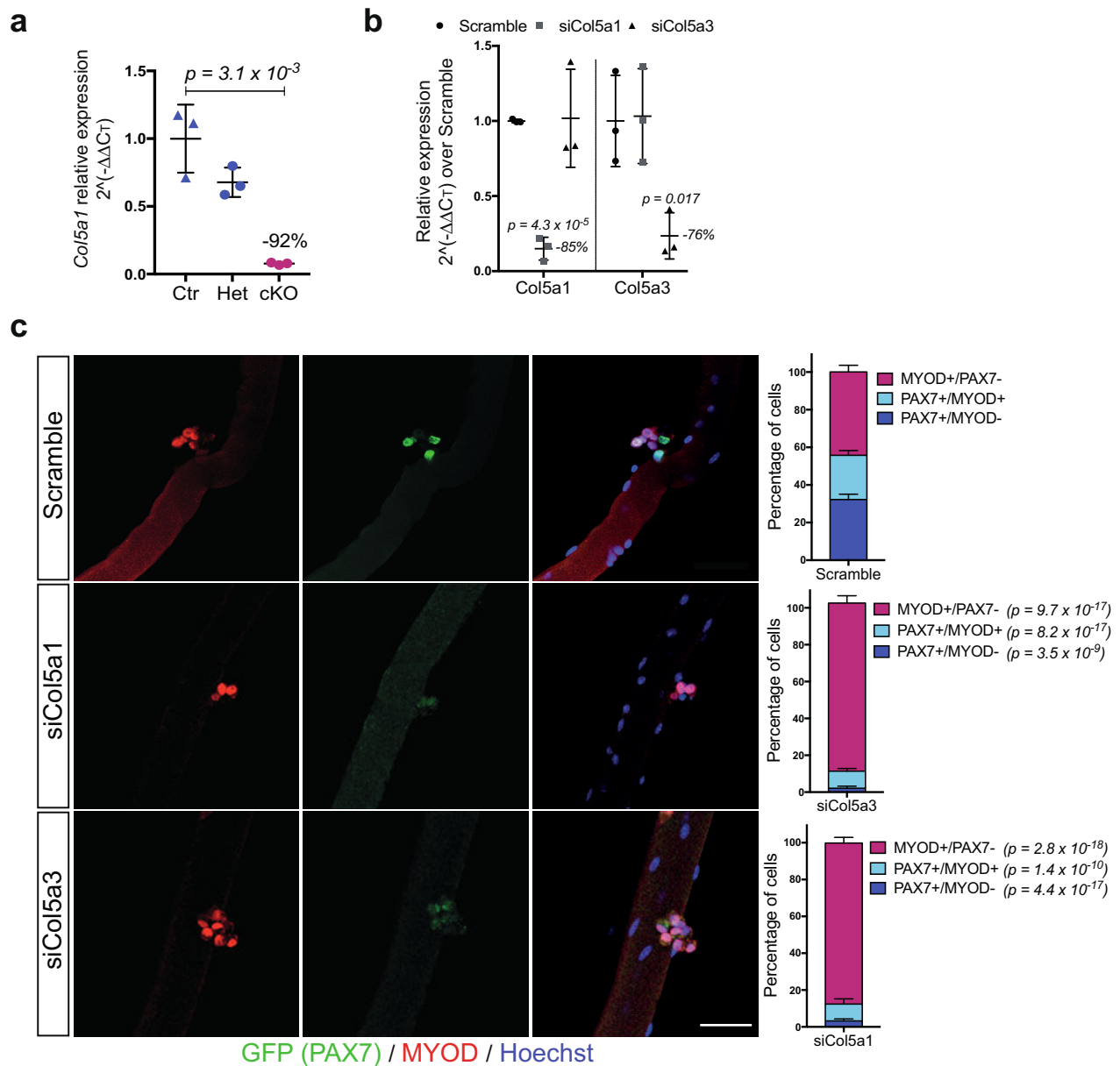
a, Satellite cells isolated by FACS at day 10 after tamoxifen injections, from resting tibialis anterior muscle from control (*Tg:Pax7-CT2;Rbpj^{+/-};R26^{mTmG/+}*) and *Rbpj*-null (*Tg:Pax7-CT2;Rbpj^{lox/-};R26^{mTmG/+}*) mice immunostained for RBPJ. **b**, RT-qPCR of collagen genes in *Rbpj* cKO and control satellite cells. *Hey1* used as control for Notch signalling ($n = 3$ mice per genotype). **c**, Induction of collagen genes in E17.5 control (*Myf5^{Cre/+};R26^{mTmG/+}*) and *Myf5^{Cre}-NICD* (*Myf5^{Cre/+};R26^{stop-NICD-nGFP/+}*) cells isolated by FACS. RT-qPCR was normalized to *Gapdh*, $n = 3$ fetuses per genotype. *HeyL* reports Notch activity. **d**, FACS plots showing fractionation of GFP⁺ cells from E17.5 *Tg:Pax7-nGFP* fetuses into Pax7^{high} (20% of population), Pax7^{mid} (40%), and Pax7^{low} (20%). The intensity of the GFP signal reflects the activity of the *Pax7* promoter. **e**, Transcript levels of GFP⁺ cells isolated by FACS show a tight

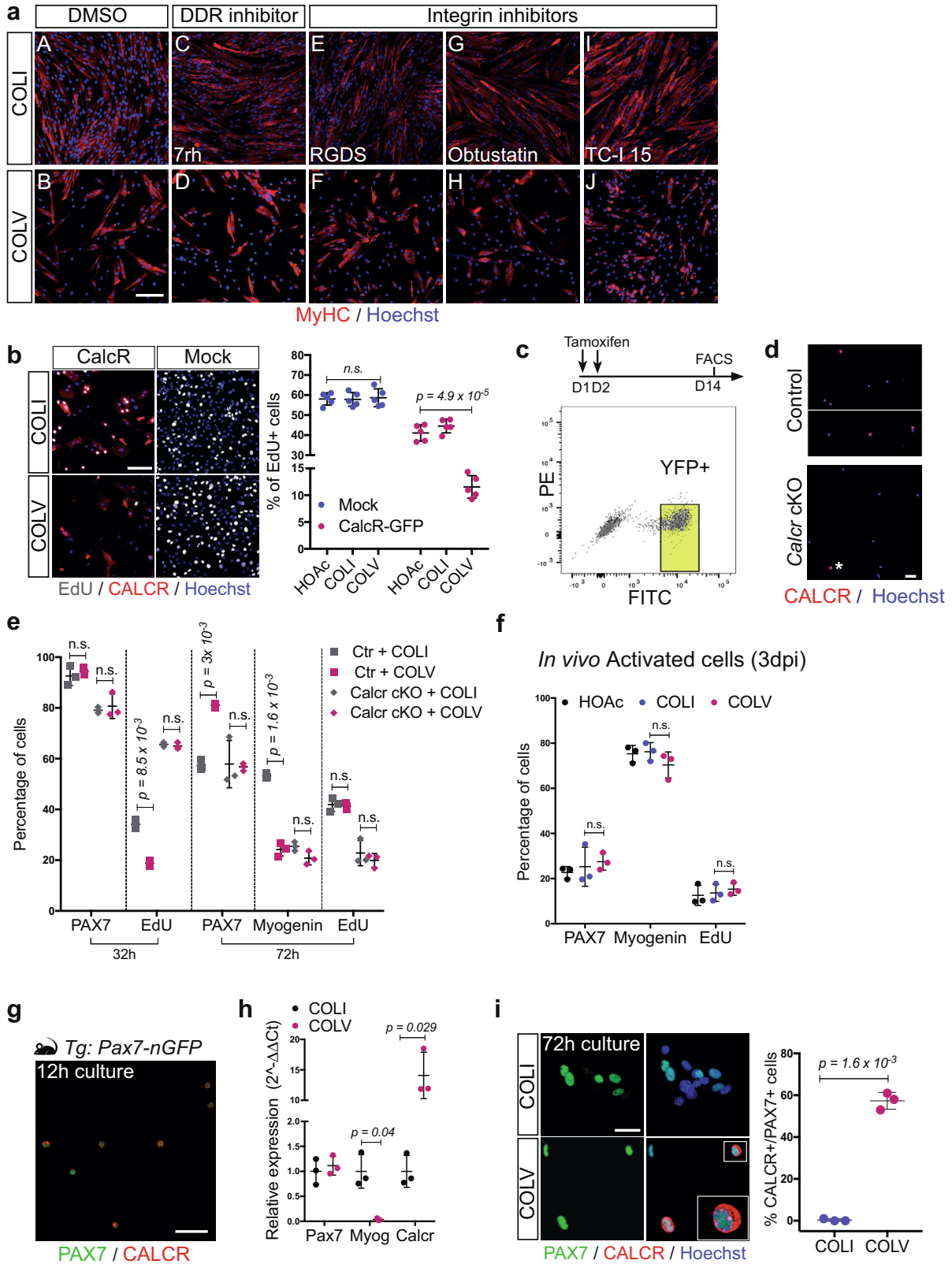
correlation between lineage progression, Notch signalling activity and collagen gene expression ($n = 3$ fetuses per genotype). **f**, Specificity of $\alpha 3$ -COLV antibody assessed by immunostaining of tibialis anterior muscle transverse section from wild-type and *Col5a3* cKO P14 postnatal pups ($n = 3$ mice per genotype). **g**, Time course of gene expression performed by RT-qPCR on freshly isolated satellite cells (Quiescent), 48 h or 60 h after cardiotoxin injury of tibialis anterior muscle (48 hours post injury (hpi), 60 hpi), and isolated single myofibres from extensor digitorum longus muscle of *Tg:Pax7-nGFP* mice. *Col5a1* and *Col5a3* were strongly downregulated in activated and differentiated cells. Quiescence (*Pax7*, *Calcr*) and differentiation (*Myog*) markers are indicated. *Col4a2*, a major component of the basement membrane, is expressed mainly by myofibres ($n = 3$ mice per condition). Data are mean \pm s.d.; one-sided unpaired *t*-test. Scale bars, 50 μ m.



Extended Data Fig. 3 | COLV delays proliferation and differentiation of satellite cells. **a**, Experimental scheme: isolated *Tg:Pax7-nGFP* satellite cells cultured overnight (o/n) before collagen treatment. **b**, Myosin heavy chain (MyHC) and EdU staining of satellite cells treated with COLI or COLV. Fusion index: 82%, 86% and 33% for HOAc solvent, COLI and COLV, respectively ($n = 3$ mice, ≥ 250 cells, 2 wells per condition). **c**, Percentage of EdU⁺ primary myogenic cells after ten days of culture with indicated collagens. EdU: 2.6%, 1.3% and 18.2% for COLI, COLVI and COLV, respectively ($n = 3$ mice, ≥ 250 cells, 2 wells per condition). **d**, Experimental scheme for control and cKO mice. Satellite cells were plated overnight before collagen treatment. **e**, GFP and MyHC

immunostaining of *Rbpj* cKO satellite cells ($n = 3$ mice per condition) incubated 60 h in presence of COLI or COLV, or with HOAc control ($n = 3$ mice, ≥ 200 cells, 2 wells per condition). **f**, Percentage of EdU⁺ cells (2 h pulse) of *Rbpj*-null primary myogenic cells, after ten days of culture with HOAc or indicated collagens. EdU: 1.0% and 7.6% for COLI and COLV, respectively ($n = 3$ mice, ≥ 150 cells, 2 wells per condition). **g**, RT-qPCR on GFP⁺ *Rbpj*-null satellite cells isolated by FACS and cultured for 72 h in the presence of COLI or COLV. Results are normalized to *Tbp*. Data are mean \pm s.d.; two-sided paired *t*-test; *P* value: two-sided unpaired *t*-test. Scale bars, 50 μ m.



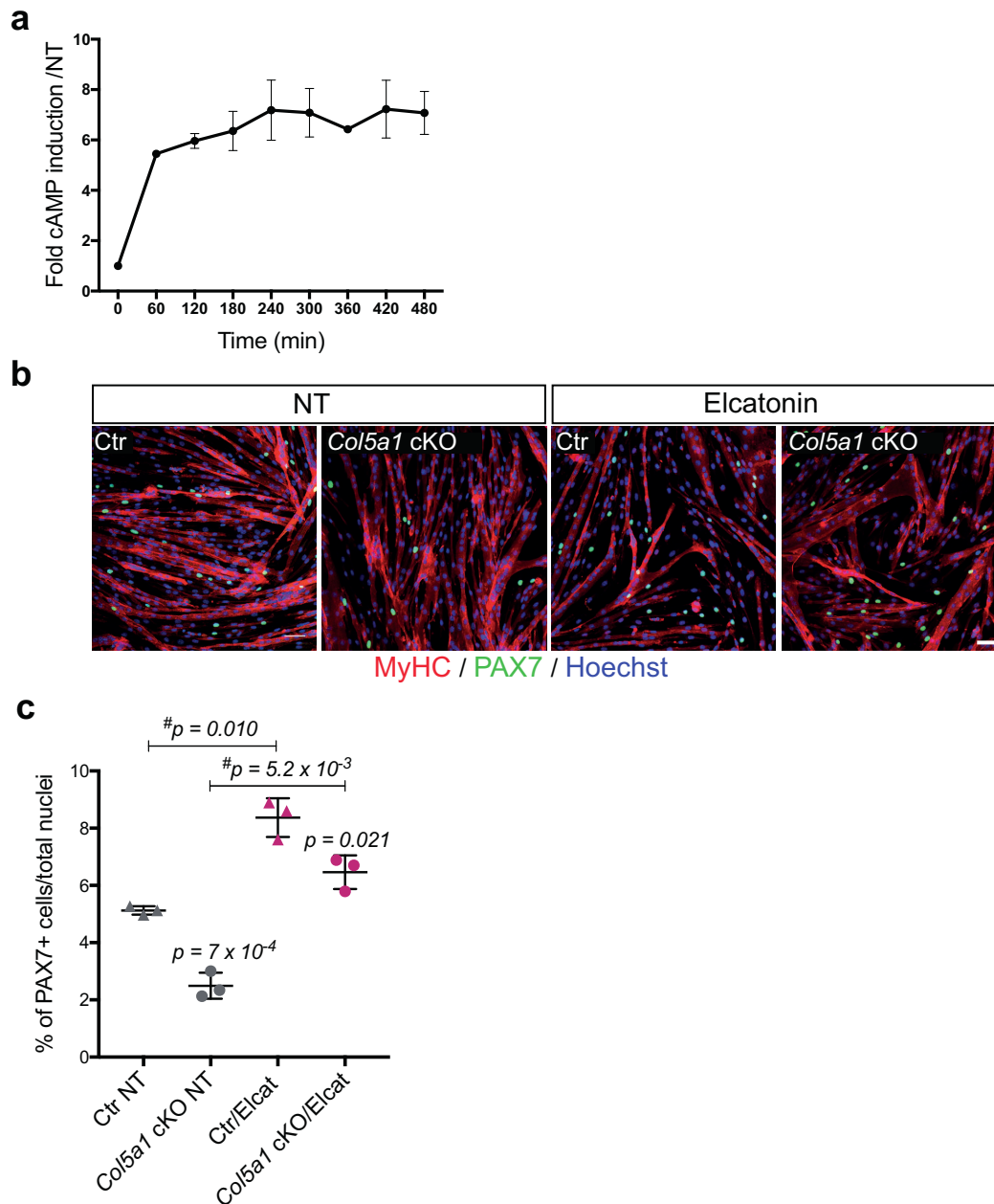


Extended Data Fig. 5 | See next page for caption.

Extended Data Fig. 5 | Screening for COLV receptor candidates

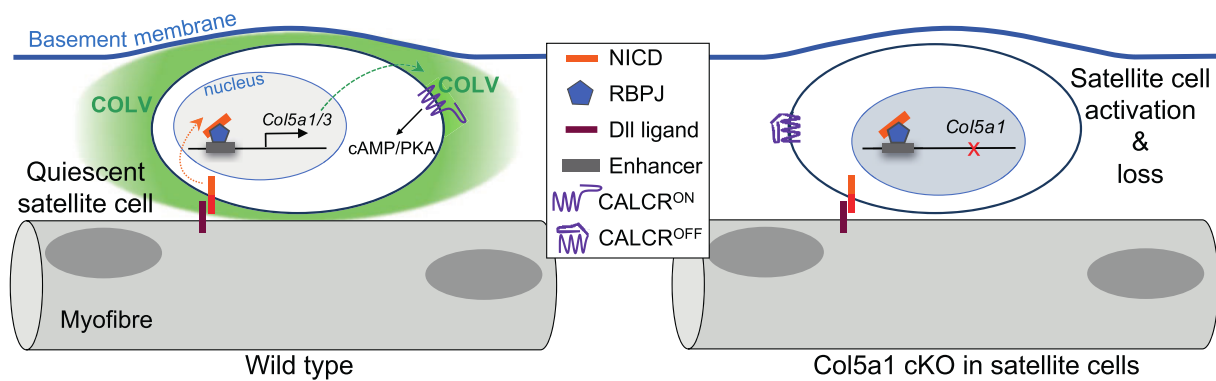
identifies CALCR. **a**, Screening for the COLV receptor: satellite cells from *Tg:Pax7-nGFP* mice were incubated for ten days with COLV and candidate receptors were targeted with respective inhibitors: 7rh for DDR1 (sub-panels C, D), the broad-spectrum Integrin-binding competitor RGDS peptide (sub-panels E, F), Obtustatin for Integrin $\alpha 1\beta 1$ (sub-panels G, H), TC-I 15 for Integrin $\alpha 2\beta 1$ (sub-panels I, J). DMSO solvent was used as a control for TC-I 15 and 7rh (sub-panels A, B). Satellite cell differentiation was assayed by MyHC immunostaining. **b**, EdU (2 h pulse) and CALCR staining of GFP⁺ C2C12 cells isolated by FACS and transduced with *Calcr*-GFP or mock-GFP retrovirus and cultured for 24 h with COLI (top) or COLV (bottom). Quantification of EdU⁺ *Calcr*-transduced C2C12 cells or mock-GFP cells treated for 24h with COLV or with the controls, COLI and HOAc ($n = 5$ independent experiments, ≥ 250 cells counted, 2 wells per condition). There was no significant difference between HOAc and COLI treated samples (data not shown). **c**, Experimental scheme of tamoxifen administration to control (Ctr) (*Calcr*^{+/+}) and cKO (*Calcr*^{fllox/fllox}) mice. FACS plot of satellite cells from *Pax7^{CreERT2/+}; Calcr^{fllox/fllox}; R26^{stop-YFP}* and *Pax7^{CreERT2/+}; Calcr^{+/+}; R26^{stop-YFP}* mice. Cells sorted based on YFP expression. **d**, Control and *Calcr* cKO satellite cells isolated by FACS, fixed immediately after sorting and immunostained for CALCR to confirm the absence of CALCR protein from recombined cells. For control (upper

panel), two fields from the same culture dish are shown, separated by a white line. Asterisk shows a non-recombined, CALCR⁺ cell in the cKO sample (lower panel). **e**, Quantification of PAX7⁺, Myogenin⁺ and EdU⁺ cells in *Calcr*-depleted satellite cells (*Pax7^{CT2/+}; Calcr^{fllox/fllox}; R26^{stop-YFP}*) isolated by FACS and treated for 32 h or 72 h with COLI or COLV ($n = 3$ mice, ≥ 250 cells counted, 2 wells per condition). **f**, Quantification of total PAX7⁺ (GFP), Myogenin⁺ and EdU⁺ myogenic cells isolated by FACS from *Tg:Pax7-nGFP* mice three days after cardiotoxin injury of tibialis anterior muscle, and incubated for 72 h in presence of COLI or COLV, or HOAc as a control, in the culture medium ($n = 3$ mice, ≥ 200 cells counted). **g**, CALCR protein in freshly isolated satellite cells, or satellite cells cultured for 12 h, from *Tg:Pax7-nGFP* mice, demonstrating that CALCR protein is still present when satellite cells are treated with different collagens (see Extended Data Fig. 2). **h**, Induction of *Calcr* transcript expression by RT-qPCR of *Tg:Pax7-nGFP* satellite cells isolated by FACS and cultured for 72 h in the presence of COLI or COLV. Results are normalized to *Tbp* ($n = 3$ mice). **i**, Immunostainings for CALCR protein of *Tg:Pax7-nGFP* satellite cells cultured for 72 h in presence of COLI or COLV ($n = 3$ mice, ≥ 50 cells, 2 wells per condition). Data are mean \pm s.d.; **b**, two-sided unpaired *t*-test; **c-i**, two-sided paired *t*-test. Scale bars, 25 μ m (**g**), 50 μ m (**a**, **b**, **d**, **i**).



Extended Data Fig. 6 | CALCR ligand elcatonin can substitute the depletion of the surrogate ligand COLV. **a**, Intracellular levels of cAMP in *Calcr*-transduced C2C12 cells treated with COLV for up to 480 min ($n = 4$ independent assays). **b**, Rescue of loss of COLV by elcatonin in an ex vivo self-renewal reserve-cell model, where PAX7⁺ non-proliferative cells return to quiescence (see Methods). MyHC and PAX7 staining of control (Ctr: *Tg:Pax7-CT2;Col5a1*^{+/+}; *R26*^{mTmG}) and *Col5a1*-null

(*Tg:Pax7-CT2;Col5a1*^{fllox/fllox}; *R26*^{mTmG}) cells, non-treated (NT) or treated with elcatonin. No GFP⁺EdU⁺ cells (12 h pulse) could be detected under any of the conditions, indicating GFP⁺ cells are quiescent (data not shown). **c**, Quantification of percentage of reserve cells (PAX7⁺ per total nuclei) ($n = 3$ mice per genotype and condition, ≥ 350 cells counted). Elcat, elcatonin. Data are mean \pm s.d.; two-sided paired *t*-test; #, *P* value calculated by two-sided unpaired *t*-test. Scale bar, 50 μ m.



Extended Data Fig. 7 | Schematic of Notch–COLV–CALCR axis in satellite cells. A Notch–COLV–CALCR signalling cascade actively maintains satellite cell quiescence. Satellite cells are in direct contact with the plasma membrane of the myofibre (black outline) and an overlying basement membrane (blue line). Activation of the Notch receptor is achieved by a ligand (probably DLL1 or DLL4) present on the muscle fibre. Induction of *Col5a1* and *Col5a3* (and also *Col6a1* and *Col6a2*) genes occurs via distal regulatory elements (grey box). Satellite-cell-produced

COLV is deposited under the basement membrane and acts as a surrogate ligand of the plasma membrane receptor CALCR, also expressed by the satellite cells, thereby propagating a cell-autonomous signalling system in the local niche. In the absence of COLV (deletion of *Col5a1*) the quiescent niche is disturbed, CALCR signalling is abrogated, and satellite cells spontaneously differentiate and fuse to myofibres, leading to exhaustion of the muscle stem cell pool.

Part II: Waking Up Muscle Stem Cells: PI3K Signalling is Ringing

Relaix & Machado. 2018

The EMBO Journal 37:e99297

Waking up muscle stem cells: PI3K signalling is ringing

Frederic Relaix^{1,2,3,4,5}  & Léo Machado^{1,2,3}

Adult skeletal muscle injury instructs endogenous quiescent stem cells to activate for repair. The pathways involved in this activation remain poorly understood. An elegant study by Wang *et al* (2018) combine mouse molecular genetics with muscle regeneration experiments, cell culture and transcriptomic analysis to show that early activation depends on a PI3K-mTORC1-Jun/FoxOs signalling axis.

The EMBO Journal (2018) e99297

See also: G Wang *et al*

Skeletal muscle is the most abundant tissue in amniotes and plays important roles in locomotion and metabolic regulation. Upon injury, skeletal muscle is able to regenerate in a few days via the activation of an endogenous stem cell population, called skeletal muscle stem cells (MuSCs) or satellite cells. These cells, located beneath the basal lamina of the muscle fibres, are maintained in a quiescent state in the adult. MuSCs are activated when muscle fibres are damaged through injury, exercise or in pathological situations. Once activated, MuSCs will enter the cell cycle, undergo a few rounds of division, then either differentiate and fuse to generate new muscle fibres, or self-renew the pool of quiescent stem cells by exiting the cell cycle (Relaix & Marcelle, 2009).

More than a decade ago, Jones *et al* (2005) have shown that phosphorylated p38 α / β MAPKs were induced in MuSCs on freshly isolated myofibres within the 15–20 min required for muscle harvest,

suggesting that this may be linked to quiescence exit. They hypothesized that fibre harvesting was essentially a massive injury and likely resulted in satellite cell activation. Recent studies using complementary strategies have shown that MuSC activation following dissociation is indeed a rapid process, with thousands of genes changing in a few hours, and that this early activation is associated with stress response transcriptional programmes (van den Brink *et al*, 2017; Machado *et al*, 2017; van Velthoven *et al*, 2017). This is in sharp contrast to the time required for the first division (around 24–36 h in response to muscle injury), probably reflecting the metabolic, epigenetic and cellular changes necessary to undergo a first cell division from a quiescent state. The extrinsic and intrinsic signalling pathways regulating exit from quiescence and the early activation are poorly understood. Wang *et al* (2018) take advantage of MuSC-specific deletion of p110 α , a catalytic subunit of phosphatidylinositol 3-kinase (PI3K) to demonstrate that this pathway is mandatory for MuSC activation (Fig 1). The PI3K-AKT-mTOR signalling pathway has been linked to MuSC quiescence and proliferation by previous studies (Gopinath *et al*, 2014; Yue *et al*, 2016, 2017) but the specific role of p110 α has not been investigated. Wang *et al* (2018) first observed that p110 α transcripts were highly expressed in freshly isolated satellite cells (Liu *et al*, 2013; Ryall *et al*, 2015), while the phosphorylated ribosomal S6 protein (p-S6), a marker for the activation of the PI3K/mTORC1 pathway, was detected in activated but not in quiescent MuSCs. With

the aim to evaluate the role of PI3K signalling in MuSC activation, Wang *et al* (2018) generated a MuSC-specific ablation of p110 α by crossing a conditional (*p110 α ^{fl/fl}*) allele with a tamoxifen-inducible *Pax7^{CreERT2}* mouse line. Following conditional ablation of p110 α in adult MuSCs, skeletal muscle repair was severely compromised, even a month after injury, demonstrating that PI3K signalling is required for skeletal muscle regeneration. Next, the authors analysed the consequence of conditionally ablating p110 α in MuSCs. By combining a lineage tracer (*R26R^{YFP}*) with *Pax7^{CreERT2}* and *p110 α ^{fl/fl}*, Wang *et al* (2018) observed that the number of YFP⁺ cells was unchanged, despite the loss of expression of two MuSC-specific markers, PAX7 and VCAM, likely via enhanced autophagy. Next, the authors showed that p110 α -null MuSCs fail to enter the cell cycle *in vitro* and *in vivo*, suggesting this might be due to a defective quiescence exit. Indeed, in contrast to control cells, freshly isolated mutant MuSCs showed many of the hallmarks of quiescent cells, such as smaller size, maintained G0 state, very low mRNA content, and a failure to express MyoD after activation.

In order to determine whether mTORC1 is a downstream component of PI3K signalling in MuSC early activation, Wang *et al* (2018) crossed *Pax7^{CreERT2}*; *p110 α ^{fl/fl}* mice with *Tsc1^{fl/fl}* mice. Ablation of *Tsc1*—a specific mTORC1 repressor—in p110 α -null MuSCs restored *Pax7* expression, as well as activation and proliferation of the mutant cells. Next, they used RNA-sequencing to

1 Inserm, IMRB U955-E10, Créteil, France. E-mail: frederic.reliax@inserm.fr

2 Faculté de Médecine, Université Paris Est Créteil, Créteil, France

3 Ecole Nationale Vétérinaire d'Alfort, Maisons-Alfort, France

4 Etablissement Français du Sang, Créteil, France

5 DHU Pepsy& Centre de Référence des Maladies Neuromusculaires GNMH, APHP, Hôpitaux Universitaires Henri Mondor, Créteil, France

DOI 10.15252/emj.201899297

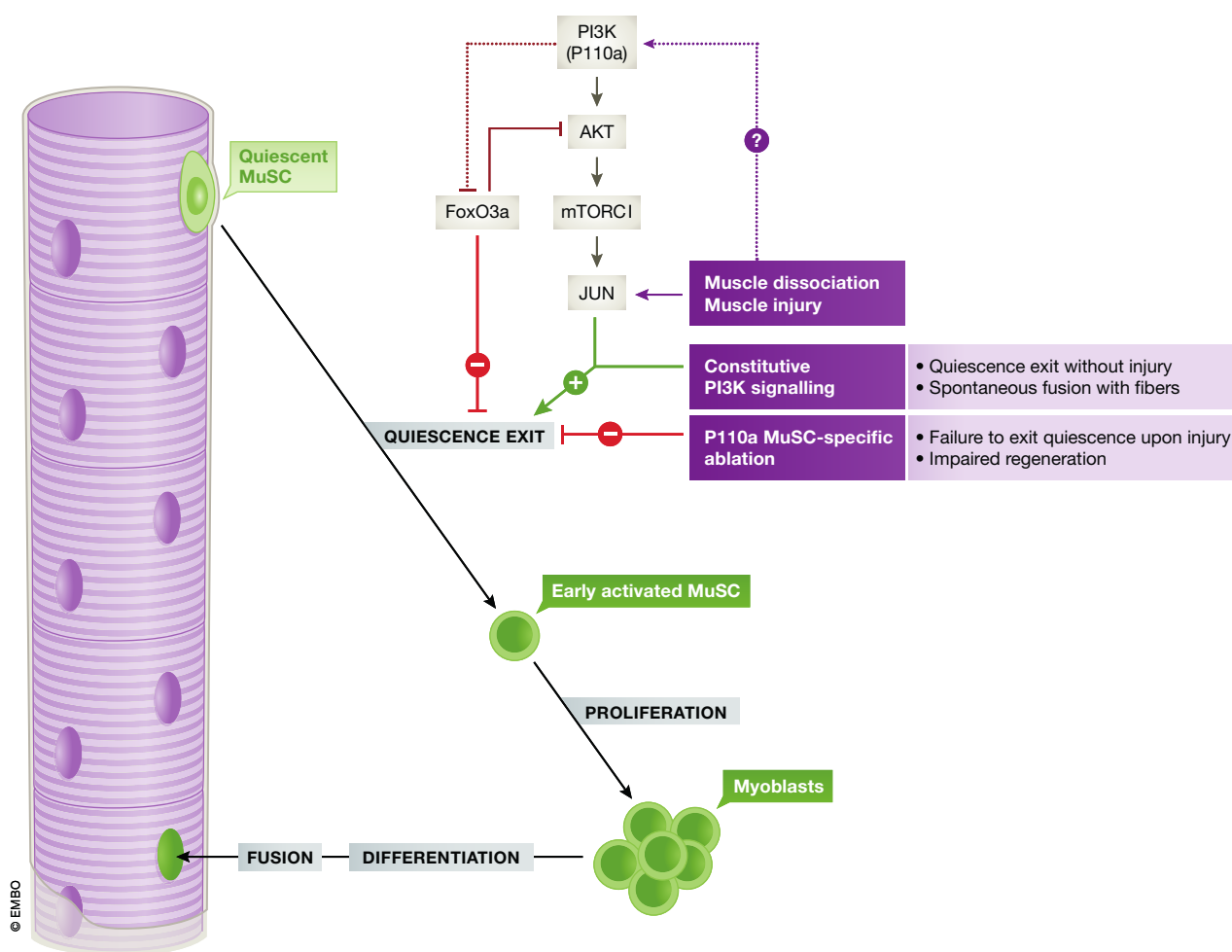


Figure 1. PI3K signalling controls skeletal muscle stem cell (MuSC) exit from quiescence.

Upon muscle dissociation or injury, skeletal muscle stem cells (MuSCs) exit quiescence, become activated, then proliferate and will eventually differentiate into fused myofibres. PI3K activation promotes quiescence exit through an AKT-mTORC1-Jun pathway. Constitutive PI3K signalling leads to activation and differentiation without injury while MuSCs fail to exit quiescence in a MuSC-specific PI3K mutant. FoxO3 is interacting with PI3K signalling to control quiescence exit. Altogether Wang *et al* (2018) identify a PI3K-mTORC1-Jun/FoxO3a signalling axis that is both required and sufficient to promote MuSC quiescence exit and early activation.

identify the genes downstream of PI3K during activation, comparing R26R^{YFP}-mediated lineage traced p110 α -null MuSCs to control MuSCs, isolated via flow cytometry. While *Pax7* and *Myf5* transcript remained unchanged, *MyoD* expression was downregulated, as expected. Interestingly, members of the AP-1 complex, such as *Jun*, *Fos* and *Fosb*, were decreased in p110 α -null MuSCs. These findings are consistent with the recent demonstration that mRNA levels of *MyoD* and of the members of the AP-1 family are specifically induced during the early activation of MuSCs (van den Brink *et al*, 2017; Machado *et al*, 2017; van Velthoven *et al*, 2017). Strikingly, combining rapamycin mTORC1 inhibition with MuSC-specific ablation of p110 α and *Tsc1* confirmed Jun as

downstream target of mTORC1, thereby defining a PI3K-mTORC1-Jun axis involved in controlling quiescence exit.

FoxOs are also important mediators of PI3K signalling and play important functions in myogenic cells, including cell proliferation, control of glycolytic and lipolytic flux, mitochondrial metabolism and autophagy. FoxO proteins localize in the cytoplasm of proliferating cells, while nuclear expression is observed in non-cycling cells. Wang *et al* (2018) used a variety of experiments, including knock-down and rescue experiments, to demonstrate that the PI3K-mTORC1-Jun axis induces FoxO3a nuclear exclusion. Reversely, the authors showed that FoxOs knock-down rescues the proliferative impairment of p110 α -null MuSCs

ex vivo, hinting at a mutual interplay between these factors.

Finally, to examine whether p110 α was sufficient to induce early activation, Wang and colleagues generated a MuSC-specific mouse line expressing inducible constitutively active p110 α mutant protein (p110 α ^{H1047R}), p110 α ca, combined with the R26R^{YFP} reporter. Induction of p110 α ca led to MuSC quiescence spontaneous exit, proliferation and differentiation, as revealed by lineage tracing of the YFP⁺ cells in muscle fibre myonuclei.

Altogether Wang *et al* (2018) convincingly identified a PI3K-mTORC1-Jun/FoxO3a signalling axis that is both required and sufficient to promote MuSC quiescence exit and early activation. It will be important to

assess the exact activity of the PI3K-mTOR-Jun axis in quiescent MuSCs as the conditional loss of P110 α in resting condition *in vivo* (where PI3K-mTOR-Jun axis is apparently inactive) leads to loss of PAX7 and VCAM proteins. The finding that PI3K signalling leads to a transcriptional response via AP-1 factors is novel and of particular interest. AP-1 expression has been identified as a major signature for early activation of MuSCs (van den Brink *et al*, 2017; Machado *et al*, 2017; van Velthoven *et al*, 2017). The precise role of this transcriptional complex with respect to the various aspects of MuSC activation needs to be investigated. Understanding how different signalling pathways are interconnected will be critical to fully comprehend MuSC quiescence exit. For example, Jones and colleagues had previously shown that phosphorylated p38 α / β MAPKs appear present in freshly isolated MuSCs, but the role of this pathway during early activation has remained elusive. p38 α is a repressor of Tsc1, thereby potentially connecting MAPK signalling to PI3K signalling. Recent studies have shown that Pten, an inhibitor of the PI3K pathway, regulates skeletal muscle stem cell quiescence, notably via FoxO1 and Notch signalling (Yue *et al*, 2016, 2017), and FoxO3 has been previously shown to promote MuSC quiescence (Gopinath *et al*, 2014). It will be of great importance to integrate these studies with the findings of Wang *et al* (2018). Finally, some of these results reminds the

systemic induction of the G_{alert} state, another model of mTORC1 activation in MuSCs (Rodgers *et al*, 2014). It is tempting to speculate that all these studies describe different parts of the same biological phenomena and underline a critical role for PI3K signalling in MuSC biology.

References

- van den Brink SC, Sage F, Vértesy Á, Spanjaard B, Peterson-Maduro J, Baron CS, Robin C, van Oudenaarden A (2017) Single-cell sequencing reveals dissociation-induced gene expression in tissue subpopulations. *Nat Methods* 14: 935–936
- Gopinath SD, Webb AE, Brunet A, Rando TA (2014) FOXO3 promotes quiescence in adult muscle stem cells during the process of self-renewal. *Stem Cell Reports* 2: 414–426
- Jones NC, Tyner KJ, Nibarger L, Stanley HM, Cornelison DDW, Fedorov YV, Olwin BB (2005) The p38 α / β MAPK functions as a molecular switch to activate the quiescent satellite cell. *J Cell Biol* 169: 105–116
- Liu L, Cheung TH, Charville GW, Hurgo BMC, Leavitt T, Shih J, Brunet A, Rando TA (2013) Chromatin modifications as determinants of muscle stem cell quiescence and chronological aging. *Cell Rep* 4: 189–204
- Machado L, Esteves de Lima J, Fabre O, Proux C, Legendre R, Szegedi A, Varet H, Ingerslev LR, Barrès R, Relaix F, Mourikis P (2017) *In situ* fixation redefines quiescence and early activation of skeletal muscle stem cells. *Cell Rep* 21: 1982–1993
- Relaix F, Marcelle C (2009) Muscle stem cells. *Curr Opin Cell Biol* 21: 748–753
- Rodgers JT, King KY, Brett JO, Cromie MJ, Charville GW, Maguire KK, Brunson C, Mastey N, Liu L, Tsai CR, Goodell MA, Rando TA (2014) mTORC1 controls the adaptive transition of quiescent stem cells from G0 to GAlert. *Nature* 510: 393–396
- Ryall JG, Dell'Orso S, Derfoul A, Juan A, Zare H, Feng X, Clermont D, Koulis M, Gutierrez-Cruz G, Fulco M, Sartorelli V (2015) The NAD⁺-dependent sirt1 deacetylase translates a metabolic switch into regulatory epigenetics in skeletal muscle stem cells. *Cell Stem Cell* 16: 171–183
- van Velthoven CTJ, de Morree A, Egner IM, Brett JO, Rando TA (2017) Transcriptional profiling of quiescent muscle stem cells *in vivo*. *Cell Rep* 21: 1994–2004
- Wang G, Zhu H, Situ C, Han L, Yu Y, Cheung TH, Liu K, Wu Z (2018) p110 α of PI3K is necessary and sufficient for quiescence exit in adult muscle satellite cells. *EMBO J* <https://doi.org/10.15252/emboj.201798239>
- Yue F, Bi P, Wang C, Li J, Liu X, Kuang S (2016) Conditional loss of pten in myogenic progenitors leads to postnatal skeletal muscle hypertrophy but age-dependent exhaustion of satellite cells. *Cell Rep* 17: 2340–2353
- Yue F, Bi P, Wang C, Shan T, Nie Y, Ratliff TL, Gavin TP, Kuang S (2017) Pten is necessary for the quiescence and maintenance of adult muscle stem cells. *Nat Commun* 8: 14328